LOCAL NICHE SOFTNESS-INDUCED NEGATIVE DUROTAXIS PROMOTES BRAIN METASTASIS WITHIN THE MECHANICALLY HETEROGENEOUS PRIMARY TUMOR

ZHENG YUFAN

PhD

The Hong Kong Polytechnic University

2025

The Hong Kong Polytechnic University

Department of Biomedical Engineering

Local niche softness-induced negative durotaxis promotes brain metastasis within the mechanically heterogeneous primary tumor

ZHENG Yufan

A thesis submitted in partial fulfilment of the requirements for the degree of Doctor of Philosophy

Dec. 2024

CERTIFICATE OF ORIGINALITY

I hereby declare that this thesis is my own work and that, to the best of my knowledge and belief, it reproduces no material previously published or written, nor material that has been accepted for the award of any other degree or diploma, except where due acknowledgement has been made in the text.

(Signed)

ZHENG Yufan (Name of student)

Abstract

Organotropism refers to the preferential but not random metastasis of tumor cells into specific organs, including brain. Brain metastasis is the most devastating cancer dissemination because of both the extremely poor patient survival and the perturbation of key neurological functions, such as cognition and sensation. Tumor microenvironment shapes metastatic organotropism, including brain tropism. Our previous study showed that long-term mechanical priming in soft niches in vitro shifted breast cancer organotropism to brain metastasis via the upregulation of histone deacetylase 3 (HDAC3) activity. However, it's unclear whether and how the long-term soft-priming process is achieved in the mechanically heterogenous primary tumor to promote the brain metastasis.

In this project, we developed a single-cell scale local niche softness biosensor, which enabled us to identify and separate tumor cells residing in local niches with different stiffnesses within tumor xenografts. With this biosensor, we found that local niche softness was not only correlated with the expressions of brain metastasis-related genes and HDAC3 activity, but also promoted the preferential metastasis of the resident cells into brain tissue. To unveil how soft niches impacted metastatic organotropism, we examined the influence of niche mechanics on cell mechanical behaviours, including durotaxis. Our results showed that soft-primed tumor cells and tumor cells isolated from local soft niches of xenografts were negative durotactic (i.e., migrating towards soft optimal microenvironment) and positive viscotactic (i.e., migrating towards microenvironment with high viscosity), both of which might ensure long-term residing of tumor cells in local soft niches of tumor xenografts. Importantly, soft niches promoted negative durotaxis via hyperactivation of integrin α10-Akt axis, which was required for niche softness-induced brain metastasis. Further, loss of brain metastatic potential abrogated negative durotaxis, indicating a reciprocal interaction between negative durotaxis and brain metastasis. We also uncovered a soft niche-specific cell competition that soft-primed tumor cells eliminated stiff-primed counterparts in an integrin α10-dependent manner. Besides, both soft-

primed cells and niche softness inactivate cancer-associated fibroblasts locally, which maintained local niche softness.

Collectively, we deciphered the crosstalk between local niche mechanics and tumor cells residing in the mechanically heterogenous primary tumor, elucidating that local soft niches enabled negative durotaxis of tumor cells to empower persistent priming and the acquisition of brain metastatic capability.

List of Publications

1. Zhang, B., Li, X., Tang, K., Xin, Y., Hu, G., **Zheng, Y**., Li, K., Zhang, C., & Tan, Y[*]. (2023). Adhesion to the Brain Endothelium Selects Breast Cancer Cells with Brain Metastasis Potential. International journal of molecular sciences, 24(8), 7087. https://doi.org/10.3390/ijms24087087
2. Tang, K.[#], **Zheng, Y.**[#], Hu, G., Xin, Y., Li, K., Zhang, C., Chen, X., Zhang, B., Li, X., Hu, B., Jia, Q., Zheng, Y. P., Yang, M., & Tan, Y. (2025). Local soft niches in mechanically heterogeneous primary tumors promote brain metastasis via mechanotransduction-mediated HDAC3 activity. *Science advances*, *11*(9), eadq2881. https://doi.org/10.1126/sciadv.adq2881

Presentations

1. Kai TANG[#], **Yufan ZHENG**[#], Youhua TAN*, Local soft niches in the primary breast tumor promote brain metastasis via mechanotransduction-mediated HDAC3 activity, MBI Conference 2023: Mechanobiology in Health and Disease, (2023), Poster
2. Kai TANG[#], **Yufan ZHENG**[#], Youhua TAN*, Local soft niches in the primary breast tumor promote brain metastasis via mechanotransduction-mediated HDAC3 activity, 2023 中国生物材料大会, (2023), Poster
3. **郑雨帆**，汤恺，李雪怡，张白，张存宇，茅仁伟，谭又华*，单细胞尺度的局部微环境软度传感器揭示肿瘤内软微环境促进乳腺癌细胞脑转移，第十四届全国生物力学大会，(2024), Poster
4. **郑雨帆**, Soft ECM-evoked negative-durotaxis mechanically organizes primary tumor and promotes brain metastasis，四川大学第十二届“全球青年学者论坛”, (2024), Oral

Acknowledgements

Human civilization is established on top of the accumulated explorations of nature, hopefully the journey towards Ph.D of mine brings new things to the academic society even indirectly save lives someday in the future. During this fascinating adventure, I did see a lot. I witnessed the refreshment of the understanding of life science every time I clicked the “refresh” button on computer, I experienced the driving force of Super Typhoon, a planetary-scale meteorological phenomenon, to me and, well, not to science but to graduation. However, things are not always bright and beautiful no matter in academic career or in daily life, I’m not sure if these are part of the prices that other people must pay to get the diploma, at least I’m glad that my research is not compromised in every sense.

Skipping the emotional craps, here I certainly would like to express my sincere thanks to many. I really appreciate the moral support and understanding from my family, especially my parents. All these years I didn’t receive even a single bit of pressure from my family members, the cultivation from them makes me who I am. And I would also like to say thanks to my girlfriend HE Meihong and the kitty “Twelve” we saved, well, or kidnapped. I did use a lot of company and love from one thousand kilometers away, which kept my inner peace and reminded me that every single creature’s life matters now and then.

Academically, first I want to thank my supervisor Dr. Youhua Tan, he showed me the intriguing research gap, led the exploration path of the study, not to mention the support of the grant and the stipend, all of which make the entire interesting project possible. Besides, I appreciate Prof. Yongping ZHENG, Prof. Mo YANG, Prof. Lei SUN, Dr Sharon Y. C. RUAN, Dr Chunyi WEN, Prof. Lin Bin and Dr. Leung King-chi, Franco for sharing the cell lines, reagents, equipment and research platforms. Moreover, I’d like to express my appreciation to all our group members, Dr. XIN Ying inspired me with the softness biosensor design, which is the most important milestone in my whole project; Dr. ZHANG Cunyu and Dr. MAO Renwei really discussed a lot with me; Dr. TANG Kai’s previous finding is my research background; HU Bing, ZHANG Bai and LI Xueyi also

cooperated with me in series experiments, which I believe relieved certain burdens from all of us. The rest of the group members: Dr. CHEN Xi, Dr. DU Pengyu, Dr.Wan Shaungshuang, Dr. Jiang Yefan, LI Keming, MENG Jianfeng, WU Chenghu, LIU Zejin, FAN Xiangli, HAN Xiaomei, LI Silu, and FANG Ziying, colleagues in our lab from other research groups: ZHANG Jing, HUANG Yingying, CHEN Jiareng and DU Wanting, as well as companions from other universities and institutions: ZHANG Shuwen, DONG Yijun from West China Center of Medical Sciences of Sichuan University, SHI Qiusheng from Beihang University, ZHANG Luqi from Technische Universität München, and Dr. TANG Xin's research group from University of Florida are all sincerely appreciated for the assistance, cooperation and valuable discussion.

At last, thank the staff members of dept. of BME, ULS, CAF, URFMS and Hong Kong Polytechnic University for providing the platform and dedicated service. All the research grants provided by Hong Kong Polytechnic University, Hong Kong government, Shenzhen government and China government are all generously appreciated.

Table of contents

List of Figures

Chapter II

Chapter IV

Chapter V

Chapter VI

List of abbreviations

Words/Phrases	abbreviations
a disintegrin and metalloproteinases	ADAM
atom force microscopy	AFM
ammonium persulfate	APS
autotaxin	ATX
brain-blood barrier	BBB
bright field	BF
basic fibroblast growth factor	bFGF
cancer-associated fibroblast	CAF
Ca^{2+}/calmodulin-dependent protein kinase II	CaMKII
central nervous system	CNS
cyclooxygenase-2	Cox-2
circulating tumor cells	CTC
C-X-C motif chemokine 1	CXCL1
C-X-C motif chemokine 12	CXCL12
C-X-C chemokine receptor type 4	CXCR4
Dichlorodimethylsilane	DCDMS
dickkopf-related protein 1	DKK1
extracellular matrix	ECM
Epithelial defense against cancer	EDAC
epithelial-to-mesenchymal transition	EMT
Epiregulin	EREG
fluorescence-activated cell sorting	FACS
fragments per kilobase million	FPKM
Gene Ontology	GO
granulocyte-colony stimulating factor	G-CSF
histone deacetylase 3	HDAC3
Heparin-binding EGF-like growth factor	HBEGF
immune fluorescence	IF
immune histological chemistry	IHC
interstitial fluid pressure	IFP

interleukin 13 receptor alpha 2	IL13Rα2
in vivo animal imaging system	ivis
Kyoto Encyclopedia of Genes and Genomes	KEGG
magnetic-activated cell sorting	MACS
matrix metalloproteinase	MMP
c-Jun N-terminal kinases	JNK
Latent Transforming Growth Factor Beta Binding Protein 1	LTBP1
lysophosphatidic acid	LPA
nuclear factor κ-light-chain-enhancer of activated B cells	NF-κB
phosphate-buffered saline	PBS
PBS containing 0.1% Tween 20	PBST
prostaglandin G/H synthase 2	PTGS2
rac Family Small GTPase 1	RAC1
N-Succinimidyl-6-(4-azido2-nitrophenyl-amino)hexanoate	SANPAH
stromal cell-derived factor 1	SDF-1
sulfated glycosaminoglycans	sGAGs
secreted protein acidic and rich in cysteine	SPARC
ST6 N-Acetylgalactosaminide Alpha-2,6-Sialyltransferase 5	ST6GALNAC5
secondary harmonic generation	SHG
Tetramethylethylenediamine	TEMED
transforming growth factor beta	TGF-β
tumor microenvironment	TME
triple negative breast cancer	TNBC
tumor-repopulating cells	TRC
ultra-violate	UV
Vascular cell adhesion protein 1	VCAM1

Chapter I: Introduction

1.1 Introduction

Metastasis is one of the hallmarks of cancer, about 90% of cancer patient deaths are caused by metastasis according to epidemiology [1]. Metastasis is a complex cascade first found to happen at the late stages of cancer. Hematogenous metastasis is the most common route of metastasis, and consists of multiple steps, such as cell detachment from the primary lesion, local invasion, intravasation, circulation via vasculature, extravasation, and target organ colonization [2].

Since the "seed and soil" theory was first established in 1989, it's well accepted that the cancer cell-intrinsic phenotype and the secondary organ microenvironment determine metastasis probability and efficiency [3]. "Seed" refers to the cancer cells with advanced metastatic potential to overcome all the limiting obstacles, while "Soil" means the suitable microenvironment for cancer cell outgrowth in secondary organs. However, recent advances point out that both cancer cell phenotype and organ microenvironment can be modified by different factors, the interaction between them has become a hotspot in oncology research but few of them have been well-identified yet.

For metastasis towards different organs, to achieve the steps mentioned above, cancer cells need a distinct series of signaling pathways or molecules, this leads to the fact that the metastasis process is not completely random to every organ but with a certain preference for different types of cancer cells. This explains why different cancer types or different subclones in the same cancer type show individual metastasis patterns, this organ-specific metastasizing phenomenon is called organotropism [4, 5]. Plenty of factors in the tumor microenvironment (TME) have been characterized to shift cancer cell organotropism, most of them are biochemical cues, such as gene alternations, cytokines, exosome, stroma cell interaction, pre-metastatic niche, immune defensive pattern, etc. [6-15].

Physical properties generally exist in all tissues and cells, many aspects are included in this concept. From macro to micro-/nano-meter scale: gravity is everywhere and fabricates our body in many ways [16, 17]; electromagnetic fields are sometimes artificially used in tissue engineering and regenerative medicine [18, 19]; Heart beat transport oxygen to whole body and blood flow exert shear

stress to vascular wall, blood cells and circulating tumor cells (CTC) [20, 21]; hydrostatic pressure directs self-organized animal development [22]; inside crowding tissues, solid stress describes the compression force from surrounding tissue [23-25]; interstitial fluid pressure (IFP) appeared in tumor is originated from local liquid crowdedness caused by leaked vascular system and solid stress-damaged liquid drainage system [26]; fluid viscosity educates cancer cells to metastasis [27]; normal/abnormal extracellular matrix (ECM) and viscoelasticity are the basis of cellular function/dysfunction [28-30]; besides mechanical properties, ECM component and architecture orchestrate modulating cell mechanotransduction reciprocally [31]; ECM tension directs cell migration through energy minimization [32]; geometry governs tissue development and symmetry breaking [33-36]; stretching and compressing cycling maintains cell hemostasis and sometimes induces inflammation [37, 38], cell-cell physical interaction inhibit transformation but also drive tumorigenesis [39-41] , focusing on (sub)cellular scale, external mechanical force can be directly/indirectly sensed by various mechanical sensitive membrane protein receptors (integrins, CD44, piezo channels, etc.) [42-45]; membrane tension/overall cancer cell stiffness determines cancer cell malignancy in many aspects [46-48]; PIP_2-ERM as linkers between membrane and cytoskeletons maintain the basic physical structure and function in most cells [49, 50]; three types of cytoskeletons collectively transmit force or generate force actively [42, 43]; the generated polarized cell contractility transmitted inside-out determines the pace that cell migrates [29, 51, 52], nucleus eventually receives the outside-in stress and responds by modulating transcription and epigenetics to reprogram the cellular phenotype [53-57]; aiming at the nanoscale biomechanics, molecular viscoelasticity matters in protein function [58]; molecular level protein polarized entropy emerge in evolution with actual physiological function or in coincidence [59, 60]; quantum mechanics effects like electron tunnelling have been identified to participate fundamental cellular signaling [61-63], which possibly cause cancer [64], could be used to treat cancer as well [65].

Specifically in tumors, the abnormal physical properties are identified as a hallmark of cancer [66, 67]. During or before cancer initiation, the tissue viscoelasticity, and ECM architecture have been altered, to sometimes support or limit cell transformation and cancer progression in different aspects [30, 68-70], uncontrolled cell proliferation generates solid stress inside the tumor, this compression-like force triggers symmetry breaking and promotes cancer progression and tissue damage [24, 71-73],

elevated IFP and interstitial flow caused by irregular and permeable vasculature structure exert shear stress and hydrostatic pressure to resident tumor cells and increase the cell invasiveness [74, 75], moreover, primary tumor fluid viscosity enhances tumor cell invasion [27, 76]. For the late stage cancer, in the cancer metastasis cascade, firstly the cancer cells need to invade the basement membrane, and surrounding tissue and intravasate the local microvasculature, these processes rely on the mechanical microenvironment, it also generates intense cellular or nuclear deformation, which damages cancer cell and educate cancer cell invasion at the same time [25, 77, 78], after successful intravasation before extravasation, circulating tumor cell endures shear stress in vascular system, which damage cancer cell and educate cancer cell invasion at the same time as well [46, 79, 80], after another nuclear deformation during extravasation, colonizing at targeting organ brings entirely distinct mechanical microenvironment, both mechanical adaptation and mechanical memory determine the outcome: dormancy, micrometastasis or macrometastasis [81, 82].

Despite the above-mentioned general cancer cell malignant behaviors, recently biophysical properties were identified to impact cancer cell organotropism as well, including circulating system pattern, organ-specific vascular structure, and matrix stiffness [5, 20, 83-86]. Following our previous research focusing on the role of matrix stiffness in metastatic organotropism, the existing research is limited. Most research claimed increased matrix stiffness facilitates the gain of metastasis potential regardless of targeting organs by up-regulating cellular contractile forces [84, 87-89], interestingly some research revealed contradictory phenomena, some suggest that some cancer cells exhibit more aggressive/invasive/malignant/metastatic on soft matrix [90-98], some states that the cellular response to matrix stiffness across cell lines or clones seems to be a predictive parameter of metastatic targeting organ [86, 99]. Our previous research revealed that long-term softness stimulation shifts breast cancer organotropism to brain-tropic, another project found medium stiffness priming could even reverse the bone-tropism of bone-targeting breast cancer cells to lung metastatic (both under review). However, all our previous findings were based on polyacrylamide hydrogel, there's no clue cancer cells follow the same trend in complicated TME.

Currently, for the mechanical model, most research about matrix stiffness in mechanobiology territory including ours, hydrogel models are used as tools to mimic the microenvironment in vivo

[41, 53, 84, 86-97, 99-103]. However, even though there are plenty of advanced innovations in hybrid biomaterials, coculture methods, or organoid culturing systems established recently, there's still a huge gap between artificial systems and real tissues. Thus, it's hard to judge controversial conclusions obtained from different vitro systems. Especially for TME where the mechanical microenvironment is heterogenous from large to single cell scale. Series contradictory phenomena are observed in different artificial systems, taking the role of matrix stiffness for example, besides the paradox that exists in how the above-mentioned metastatic organotropism or overall metastatic capacity is affected by tissue stiffness, there are more examples. From the beginning, some research supported that cancer initiation requires mechano-transduction supported by matrix stiffness [41, 68, 69], the opposite conclusion was obtained using an animal model, suggesting collagen I, the biggest tissue stiffness contributor, constrains cancer initiation [70]. Similar situations occurred when interrogating how stiffness/softness impacts cancer cell/cancer stem cell (CSC) stemness, soft [54, 95, 97, 104, 105] and stiff [55, 106-108] supporters both hold plenty of evidence.

1.2 Research gaps

Based on the existing conflict that has been mentioned in the above part, when investigating the role of mechanics in physiology or pathology, research in mechano-biology especially mechano-oncology sometimes lacks solidity. Despite the vitro systems based on biomaterials, currently the approach to confirm the correlation in vivo usually is to apply immunohistochemistry (IHC)/immunofluorescence (IF) staining to stain some well-identified markers to represent the cell phenotype and function, then analyze the collagen (fiber) density using picrosirius red staining/secondary harmonic generation (SHG) to represent ECM stiffness (few research paper directly applied atom force microscopy (AFM) to measure the elastic modulus [109]), and eventually check whether there is spatial co-localization. However, this simple method shows plenty of limitations:

1. Using collagens or other molecules to represent ECM stiffness is not convincing, ECM stiffness is a purely mechanical parameter, which could be affected by many variables including ECM type, structure, and residing cells [110, 111];

2. For the intratumoral mechanical microenvironment, the mechanical heterogeneity is from large scale to single cell scale [111-113], an unbiased method at single cell scale to separate cell populations from tumor is more convincing;
3. Simply using established biomarkers to assume the functional phenotype is not exclusive;
4. Current IF-based colocalization analysis is limited in limited scale, which is not comparable to the tumor size, this method is not unbiased.

Thus, we believe there is an urgent need to establish a new strategy to confirm the preliminary conclusions obtained based on simple mechanically homogeneous biomaterials, and this strategy cannot be another more advanced biomaterial, directly studying in vivo could be a promising direction. It's also unknown about the co-evolutional relationship between mechanical cues and residing cancer cells, so it's worth clarifying the crosstalk and interaction.

1.3 Objectives and scopes

Following on our previous project entitled "Local soft niches in mechanically heterogeneous primary tumors promote brain metastasis via mechanotransduction-mediated HDAC3 activity", the missing clue is the solid evidence that the correlation between tissue softness (and HDAC3) and brain metastasis potential indeed exists in local niches at single-cell scale in primary breast tumor. Thus, the specific research objectives are listed below:

1. Present a solid conclusion that our previous finding is also true in vivo;
2. Explain how this process is achieved in vivo.

Chapter II: Literature Review

2.1 Cancer

Cancer is the malignant disease that cell proliferates in an uncontrolled manner, currently there're three group of theories about cancer nature, one group claims that uncontrolled cancer cell proliferation is a result of random mutations (somatic mutation theory [114]), random mistakes made during DNA replication in stem cells (R-mutations), heritable (H-mutations) or caused by environmental carcinogens (E-mutations) (bad luck theory [115, 116]), another group of theories believe cancer is a tissue-targeting disease, neoplastic phenotypes are potentially reversible/inducible through interactions with healthy/neoplastic tissue (tissue organization field theory [117-128]), the third group compromises opinions from both sides, states cancer initiation is caused by the developmental phenotypic cell plasticity, which could be affected by external factors such as development, ageing and injury (ground state theory [129, 130]), or argues that disrupted ECM architecture or crosstalk as well as cellular oncogenic variation are both required for the successful cancer initiation (load-trigger mechanism [131]).

Except for uncontrolled and growth factor-independent cell proliferation, cancer has plenty of other hallmarks and representative behaviors, including growth suppression (cell-cell contact, senescence, lacking mechanical support, etc.) insensitivity, immune escape capacity, replicative immortality, pro-inflammation, angiogenesis, genome instability, cell death resistance, cellular metabolism reprograming and ability to invade and metastasize [132].

2.2 Cancer metastatic organotropism

Metastasis is a long process, for the most common hematogenous metastasis, cancer cells break through the basement membrane, invade the local tissue, intravasate into and circulate through the vascular system, be entrapped in the microcapillaries, extravasate out, (enter and exit dormancy) and colonize in the secondary organ. Even though cancer could occur to most proliferative cell types across all human organs, primary tumor growth is usually non-lethal and surgically removable. In clinical cases, metastasis and secondary colonization at distant organs account for about 90% of

cancer-associated patient death, which is the top two leading causes of premature deaths in multiple countries as the leading cause of death in populations < 65 years and 24% of all-cause of death in China during 2014-2018 [133].

For cancer metastasis, the common targeting organs include bone (typically an early or sometimes the only metastatic site), brain (typically the late metastatic site), liver, and lung [134]. However, since metastasis is such a complicated process, multiple signaling and molecules even biophysical processes are involved [135], so the overall metastasis outcome is not completely random, this cancer cell organ-selective dissemination is defined as metastatic organotropism [4-6, 10, 136]. Precisely, on the one hand, cancer dissemination organotropism pattern is primary organ-dependent, such as lung cancer prefers bone, liver, brain, and adrenal gland, while colorectal cancer prefers the liver and lung. More importantly, cancer cells are heterogeneous [24, 103, 112, 132, 137, 138], which brings specific advantage targeting a specific secondary site for different subpopulations [135]. Noting that another above-mentioned hallmark of cancer is plasticity, thus organotropism could also be modified and shifted along with the phenotypic reprogramming by the external stimulus and internal responses [5, 6, 11, 13-15, 83, 85].

Currently there have been lots of preliminary clues about the regulating mechanisms of metastatic organotropism, C-X-C motif chemokine 12 (CXCL12)/stromal cell-derived factor 1 (SDF-1) - C-X-C chemokine receptor type 4 (CXCR4) axis was identified as a bone metastasis regulator [139-141], CXCL12 pretreatment increased bone metastasis specific endothelial adhesion in vitro, CXCR4 blockage inhibited the invasion of prostate cancer [141], CXCR4 neutralizing antibody or specific blocking peptide skeletal metastasis burden in vivo [140]. Autotaxin (ATX) was routinely stored in α-granules of resting human platelets, cancer cell recruited and aggregated platelets, causing the releasement of ATX and the production of lysophosphatidic acid (LPA), which dominated the early dissemination of breast cancer bone colonization [142, 143]. Tumor cell-derived granulocyte-colony stimulating factor (G-CSF) directly remodeled the vascular endothelium, while the blockade of G-CSF reduced bone metastasis burden [144]. Tumor cell-secreted DKK1 regulated canonical WNT signaling of osteoblasts to promote bone metastasis, on the other hand, PTGS2-induced macrophage and neutrophil recruitment was suppressed by DKK1 via antagonizing cancer cell non-canonical

WNT/PCP-RAC1-JNK pathway in lung lesion, DKK1 also inhibited WNT/Ca^{2+}-CaMKII-NF-κB axis and reducing LTBP1-mediated TGF-β secretion of cancer cells [7]. Moreover, IL13Rα2, SPARC, and VCAM1 were identified as lung microenvironment-specific metastagenicity genes, while ID1, CXCL1, Cox-2, and MMP1 inhibited both primary and secondary lung lesion establishment [145]. Similarly, Cox-2, HBEGF, and EREG were found to regulate both lung and brain extravasation while ST6GALNAC5 was classified as a molecule specifically mediating brain-blood barrier (BBB) adhesion and transmigration capacity [146, 147]. Additionally, lipid metabolism was reported as a key regulator of brain metastasis [148-151].

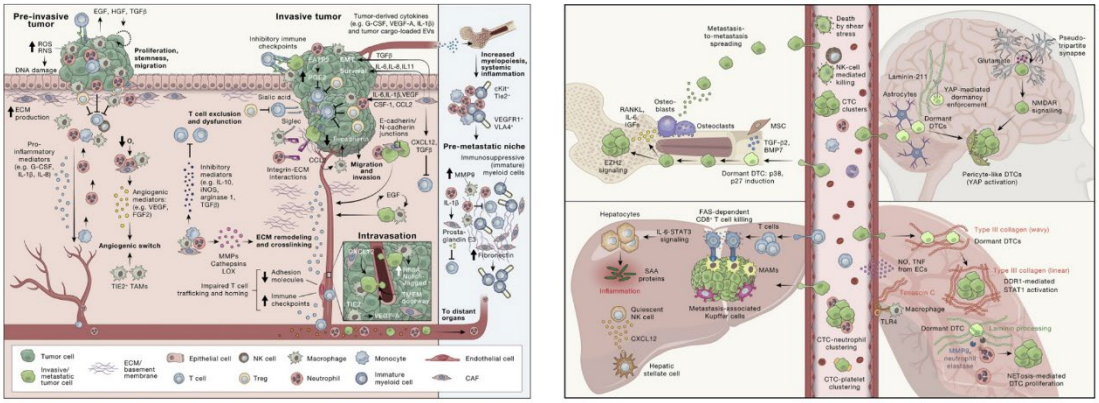

Fig. 2.1 Representative pathways in the invasion of primary tumor cells and metastasis at different distant organs [152]

2.3 Breast cancer metastasis

To study the regulating mechanism of internal or external cues in organotropism and understand the process of organ-specific metastasis, breast cancer is regarded as a good model because it can metastasize to all the major organs including the central nervous system (CNS) (10-30%), bone (70%), liver and lung, this multi-directional potential provides flexibility for researchers [136]. Breast cancer is a malignant disease that primarily occurs in the breast, it showed a peaky mortality in 1989 then gradually decreased by 42% till 2021, but it's still ranking No.1 in female cancer patient incidence and mortality [1]. There are four original major subtypes of breast cancer, luminal A (ER or PgR positive, or both, HER2 negative, low proliferation), luminal B (ER or PgR positive, or both, HER2 negative, high proliferation), HER2-enriched (HER2 positive and ER and PgR negative for

non-luminal, (HER2 positive and ER or PgR positive or both positive for luminal), and triple negative (sometimes called basal-like) breast cancer (TNBC) [153-155].

TNBC is the most aggressive breast cancer subtype, contributing > 85% of invasive breast cancer with BRCA1 germline mutations, irresponsive to endocrine therapy and HER2-targeting therapy, and extremely metastatic [156].

2.4 Breast cancer brain metastasis

Among all the metastatic targeting organs, brain metastasis in breast cancer, contributing to about 90% of the CNS lesions, is most devastating because of both the extremely poor patient survival and the perturbation of key neurological functions, such as cognition and sensory [157].

Brain metastasis is a complicated cascade of different types. Recent research discovers a new breast cancer leptomeninges metastasis pattern by abluminal migration along the blood vessels connecting calvarial or vertebral bone marrow and meninges by hijacking hematopoietic migration pathway, and mirror neurons under stress to recruit and co-opt macrophage to survive after arriving leptomeninges [158]. Except this, most brain metastasis cases are caused by colonization of trans-BBB-migrated cancer cells. In brain-targeting hematogenous metastasis cascade, firstly brain-tropic cells invade the local tissues and intravasate into the vascular system, which have not been found to be organ selective; then CTCs non-randomly circulate to brain micro-capillaries, which is determined by blood vessel architecture [83]; after that CTCs adhere to blood vessel endothelial cells, which requires the receptor of brain-specific blood vessel endothelial cell ligand [159]; next adhered cancer cells trans-migrate through BBB, which also selects brain-tropic cancer cells [146]; at last cancer cells invade brain parenchyma and colonize in the brain-specific viscoelastic microenvironment in different patterns [160-162].

2.5 Mechano-oncology

Recent advances in mechano-oncology suggest the crucial role of intrinsic cell mechanics and external mechanical microenvironmental cues in every stage of cancer progression, which will be introduced above respectively.

2.5.1 Cell mechanics in oncology

Cell stiffness is the most straightforward cell mechanics aspect. At cancer initiation or tumor cell transformation stage, cell stiffness transiently increased and dropped [163, 164]. Mature cancer cells are usually softer than normal counterparts except few counterexamples (some cervix squamous cancer, leukemia, and liver cancer cells [165-168]) [47, 48, 95, 97, 168-170], meanwhile, cancer cell softness often signified more malignant features, including metastatic phenotypes, with higher stemness or invasiveness and resistance to immune surveillance or chemo/radiotherapy [46, 171-178]. Manipulation of cancer cell stiffness by modulating cytoskeletons, ERM, cholesterol, and other molecules shifts stemness, invasiveness, and therapeutic and immune resistance [47-49, 97, 171, 172, 175, 179]. Interestingly, metastatic organotropism could also be affected by cytoskeleton polymerization and disruption [179].

Except for cell stiffness, another important concept in cancer cell mechanics is cell contractility or traction force, contractile force created by actomyosin machinery is generated in all cells to actively probe and adapt to their residing microenvironment features including the mechanical properties. Contractility empowers cell motility, however, if contractility is not in equilibrium because of some external cues, then cells would be “positively” dragged toward the winner direction, this phenomenon is called directional cell migration [29, 52, 102, 180, 181]. It’s generally accepted the traction force in cancer cells is higher than in normal cells despite some rare exceptions [96, 182, 183]. Similarly, contractility is required for plenty of cell behaviors, down-regulating contractility on soft microenvironment limits cell fundamental functions [184], cancer cell-intrinsic high contractility regardless of whatever external mechanical cues enables cancer cell extreme microenvironment adaptation capacity [183], using pharmacological agents or gene knock-down/off to perturbate contractility significantly restores cell normal behavior in both normal cells and cancer cells [183-188].

However, contractility or traction force in some special cell types is not monotonically increasing along with external microenvironment stiffness, for these specific cells, their best cell function performance may appear at an optimized stiffness [189-191].

2.5.2 Tissue mechanics in oncology

Tissue mechanics and cell mechanically sensitively responsive signaling are important parts that control cell behaviors in many ways during the whole lifespan of all living creatures [184, 192-194]. In neoplastic tissues and cancer cells, all these aspects are disturbed [53, 55, 78, 84, 88, 91, 102, 103, 105, 106, 108, 135, 177, 179, 183, 188]. The role of these mechanical cues, properties, or signaling is complicated, each individual factor could be a tumor suppressor, promoter, bi-functioned, or display as an opposite regulator in a distinct disease process. The details will be listed as follows.

Abnormal tissue mechanics is the most straightforward feature of cancerous tissue. Thousands of years ago, ancient doctors diagnosed cancer based on how tissue “feels”, even though at that time this “unknown disease” was believed to be incurable. Nowadays, precise physically defined parameters are applied to describe the physical properties of tissues, monitoring whether the tissue is in homeostatic order in this specific scale.

After cancer initiation and during cancer progression, due to the uncontrolled proliferation of malignant cancer cells, the room for cancer cells and adjacent healthy cells is limited, this is called solid stress in terminology. Basically, solid stress is a compression force, the direction of solid stress at the tumor periphery is tangential and it’s a tensile stretch-like force while the direction is radially inside at the tumor core [23, 195]. Solid stress accumulates along with the process that cancer grows, in relatively mild and less-invasive tumors, it is found compressive solid triggers so-called symmetry breaking by increasing cellular heterogeneity on epithelial-to-mesenchymal transition (EMT) level, creating both epithelial-like less-invasive and mesenchymal-like invasive cancer cells [24]. Moreover, these reprogrammed heterogeneous cell subpopulations would be sorted in a specific “mesenchymal at periphery, epithelial in core” residing order in both 2D and 3D culturing models,

generating an imbalanced stress gradient for a burst-like collective migration once solid stress is released [24, 33, 196]. In advanced-stage cancer, especially in the tumor periphery, extreme solid stress causes DNA damage but also educates cancer cells to be more invasive and malignant [25, 72, 73]. Interestingly, solid stress displays tumor suppressive manner by limiting proliferation and inducing apoptosis [25, 197-200]. Solid stress also affects tumor progression by influencing cancer-associated stroma cells, a well-identified example is cancer-associated fibroblast (CAF) [197, 201, 202].

Except for the solid stress, overcrowding scenario also impacts the vascular system function and integrity, resulting in hypoxia [113], acid-like immune suppressive [203-205], nutrition-deficient [206], drug unavailable [207], and high viscosity microenvironment, which promotes cancer cell migration and metastasis directly [27, 76]. Meanwhile, the body fluid leaks out of the circulating system and travels inside the tumoral tissue because of the irregular vessel system structure and integrity, generating elevated interstitial flow and IFP [26, 208, 209], IFP (or hydrostatic pressure) directly promotes cancer progress [74, 75, 210], luckily the elevated IFP could be partially rescued by anti-angiogenesis chemo-therapy [211, 212]. Besides IFP, interstitial flow (or shear stress) deteriorates cancer progression as well [213-216]. Nevertheless, primary tumor is not the only location where shear stress modifies cancer cells, after intravasation cancer cells circulate in blood vessels, intense shear stress damages cancer cells and induces an aggressive phenotype transition at the same time [46, 79, 80].

Tissue viscoelasticity describes how much energy is stored, released, and transferred into internal energy after deformation. Viscoelasticity can be generally comprehended with storage modulus (G') and loss modulus (G''), G' refers to the elastic part of the material feature, describing the difficulty the material is deformed in responses to compressive, stretching, or shear stress instantly, while G'' is the vicious property of material, describing a time-dependent resistance manner to deformation. The role of G' (elasticity or stiffness) will be discussed afterwards. The role of G'' (vicious component) in cancer tissue or cancer cells was identified recently [217-223], pioneer studies showed elevated G'' promoted cancer initiation and reprogrammed the interaction between cancer cells and CAF [30, 224].

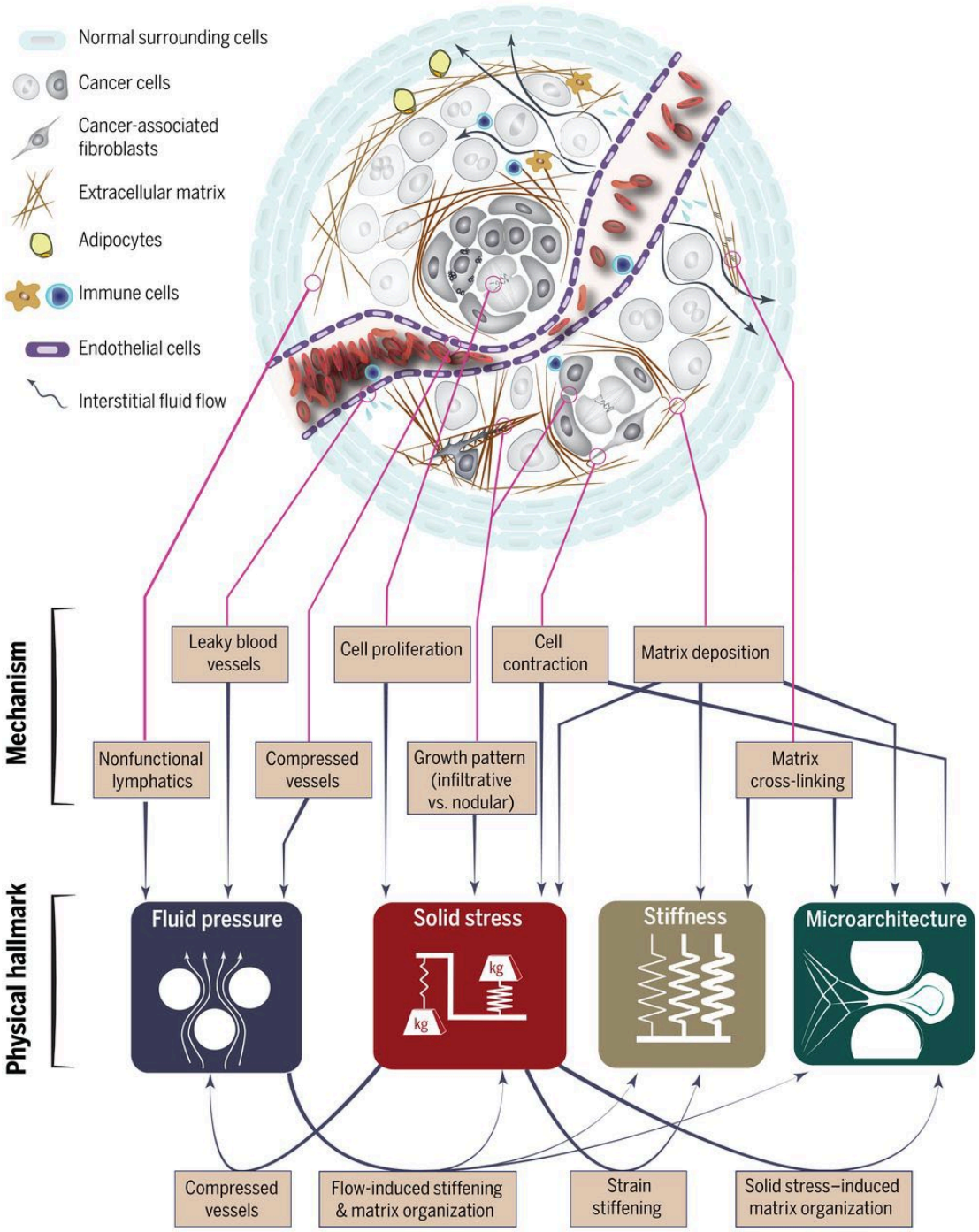

Fig. 2.2 Physical traits of cancer [66]

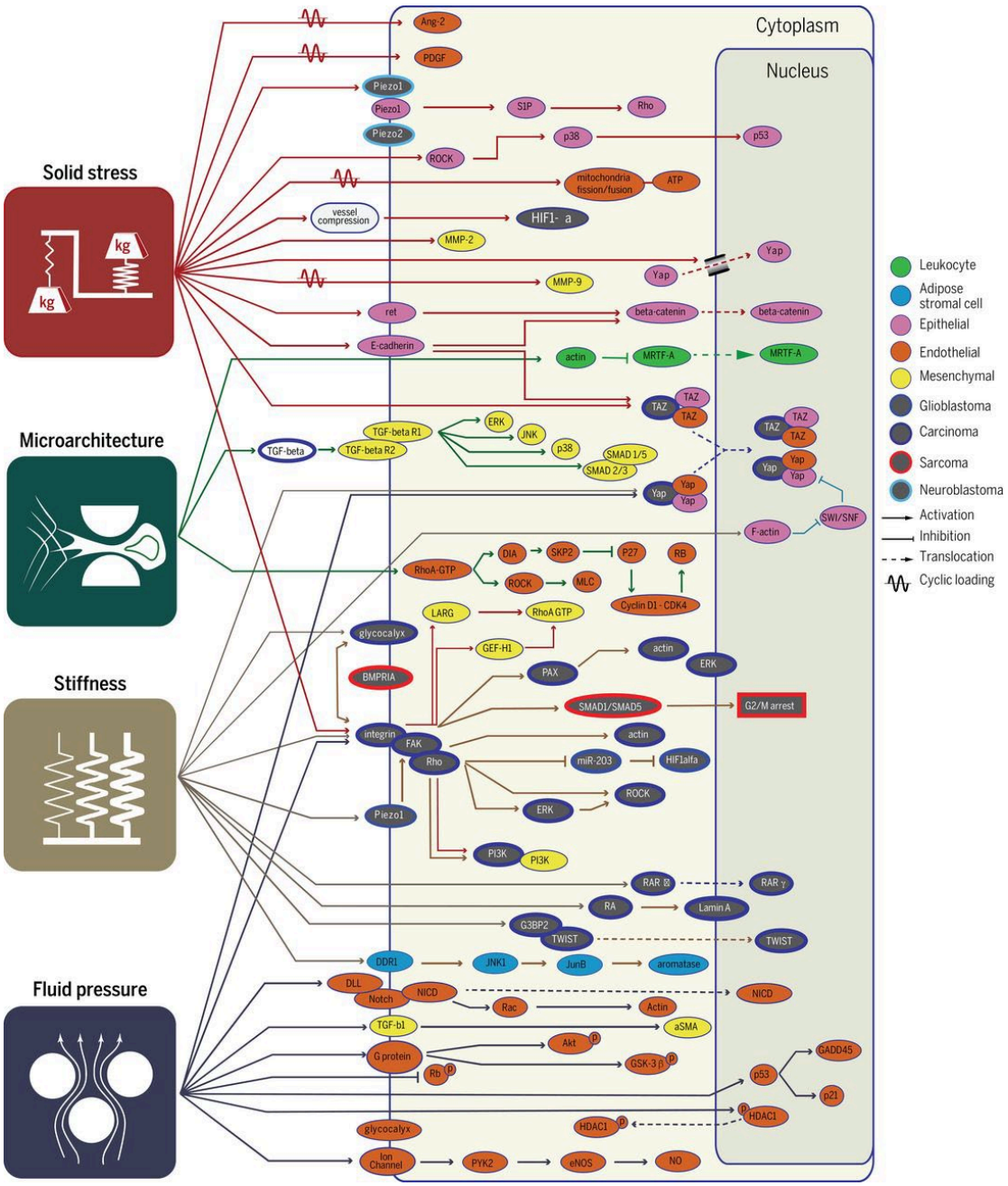

Fig. 2.3 Signaling responsive to physical traits of cancer [66]

2.6 ECM stiffness in cancer

For most solid tumors, increasement in ECM stiffness occurred along with tumor progression. This correlation has been used to diagnose cancer for decades. Plenty of processes have been identified and well-studied to be relevant to the overall stiffening effect in tumor tissue, especially the over-secretion of ECM components by cancer cells and CAFs as well as the aberrant ECM remodeling

such as realignment and crosslinking [32, 110, 202, 224-235]. However, because of the evolution of the technology of mechanical probing and sensing, researchers realized that the mechanical properties of tumor tissue are heterogeneous instead of relatively homogeneous, and this heterogeneity spectrum covers a wide range from tumor bulk scale to single-cell scale [84, 102, 103, 111, 112, 170, 217, 232, 236, 237].

As for how ECM stiffness impacts cancer cell behavior and overall cancer progression, current research exhibited controversial evidence based on the biomaterials selected as the research model. For cancer initiation or malignant transformation, several research claimed cellular malignant transformation requires specific ECM composition, stiffness, and mechanosensing, perturbating the focal adhesion, cytoskeleton, or contractility as well as unsupportive ECM type limited/reversed transformation [68, 69, 238]. Senescence was regarded as an anti-transformation cellular protection, it was reported senescence process is limited on stiffened ECM, which benefits the transformation [239]. In vivo conditions, there's another group of anti-cancer innate immune processes called cell competition. Epithelial defense against cancer (EDAC) is a typical cell competition process that surrounding normal cells positively extrudes out the "loser" transformed cells to maintain epithelial homeostasis, which was demonstrated to be ECM stiffness-dependent [41]. Interestingly, a new form of cell competition was discovered recently, transformed SmoM2-expressing basal cells win the competition by inducing differentiation and apoptosis in neighbors on collagen I-enriched back skin but failed cancer initiation [70]. For proliferation, it's generally accepted that elevated ECM stiffness promotes cancer cell proliferation across multiple cancer types [88, 94, 104, 240], but soft fibrin-selected tumor-repopulating cells (TRC) rapidly proliferated in soft matrices [95, 104, 241-243]. For cell motility, in most biomaterials including on stiff polyacrylamide hydrogel compared with soft, cancer cells showed enhanced migration and invasion [52, 78, 90, 102, 188, 244-246], but this conclusion was not consistent in all models [90, 92-98, 240, 247]. For cancer cell and cancer stem cell stemness, soft matrix especially softness stimulation in 3D culture was reported to enhance stemness in many different systems [54, 95, 97, 104, 105], but in 2D conditions or some evidence obtained from vivo, stiff polyacrylamide hydrogel maintained cell stemness [55, 106-108].

2.7 Stiffness modulation and ECM modification in tumor

For most major solid cancer types, the overall stiffening effect is dominant in most tumor tissues, three major processes are involved in this process, including 1. ECM synthesis and secretion; 2. ECM modification and remodeling; 3. ECM degradation.

ECM synthesis and (over)secretion result in ECM component deposition in tissue, laminin, and collagen IV construct basement membrane, fibronectin correlates with invasive EMT phenotype, collagen I limits cancer progression independent of matrix stiffness [248], non-enzymatic glycation and sulfation, creating AGEs and sGAGs [229, 249], which results in CAF activation, more malignant cancer cell phenotype transition and worse patient outcomes [249, 250]. Among various ECM types, fibrous collagen especially collagen I impacts stiffness most [67, 70, 113, 251, 252], many cell types in TME secret collagen (I), such as cancer cells [253], CAF [227, 231, 248], pericyte [252], etc.

There are two different ways of ECM modification and remodeling, one is through cellular mechanical force engagement, like “dragging” ECM fibers towards the cell [110, 254], or pushing the fibers away such as before and during mitosis [255, 256], the other is via biochemical reactions, such as enzymatic reaction or crosslinking by membrane protein, soluble proteins or exosome component [102, 105, 237]. Similarly, plenty of cell types participate in this process, including cancer cells and stroma cells [182, 235, 257]. Moreover, bone morphogenetic protein 1 and Tolloid-like proteinases synchronize matrix assembly, which displayed a correlation with worse clinical outcomes [258-260].

ECM degradation is mainly caused by enzymatic cleavage, the related enzyme could also be on the cell membrane, soluble, or in exosomes. (membrane-type) matrix metalloproteinases ((MT-)MMPs), disintegrin and metalloproteinases (ADAMs), and (disintegrin and metalloproteinases with thrombospondin motifs) ADAMTSs are major players in this process. Membrane-form MMPs and ADAMs mediate cancer cell invasion [261-263], and soluble or exosome-form MMPs, ADAMs and ADAMTS directly interact with ECM [264-266]. Both paths affect cancer progression. Besides, cathepsins are responsible for intracellular digestion and protein turnover of ECM components in lysosomes [260], hyaluronidase disorder is typically observed in cancer, resulting in hyaluronan

accumulation, on the other hand, tumoral uncanonical hyaluronidases transmembrane protein 2 (TMEM2) and CEMIP are often overexpressed in solid cancer, leading to increased hyaluronan turnover as well as excessive formation of hyaluronan fragments, both high molecular mass hyaluronan and bioactive hyaluronan fragments promotes cancer progression [267, 268].

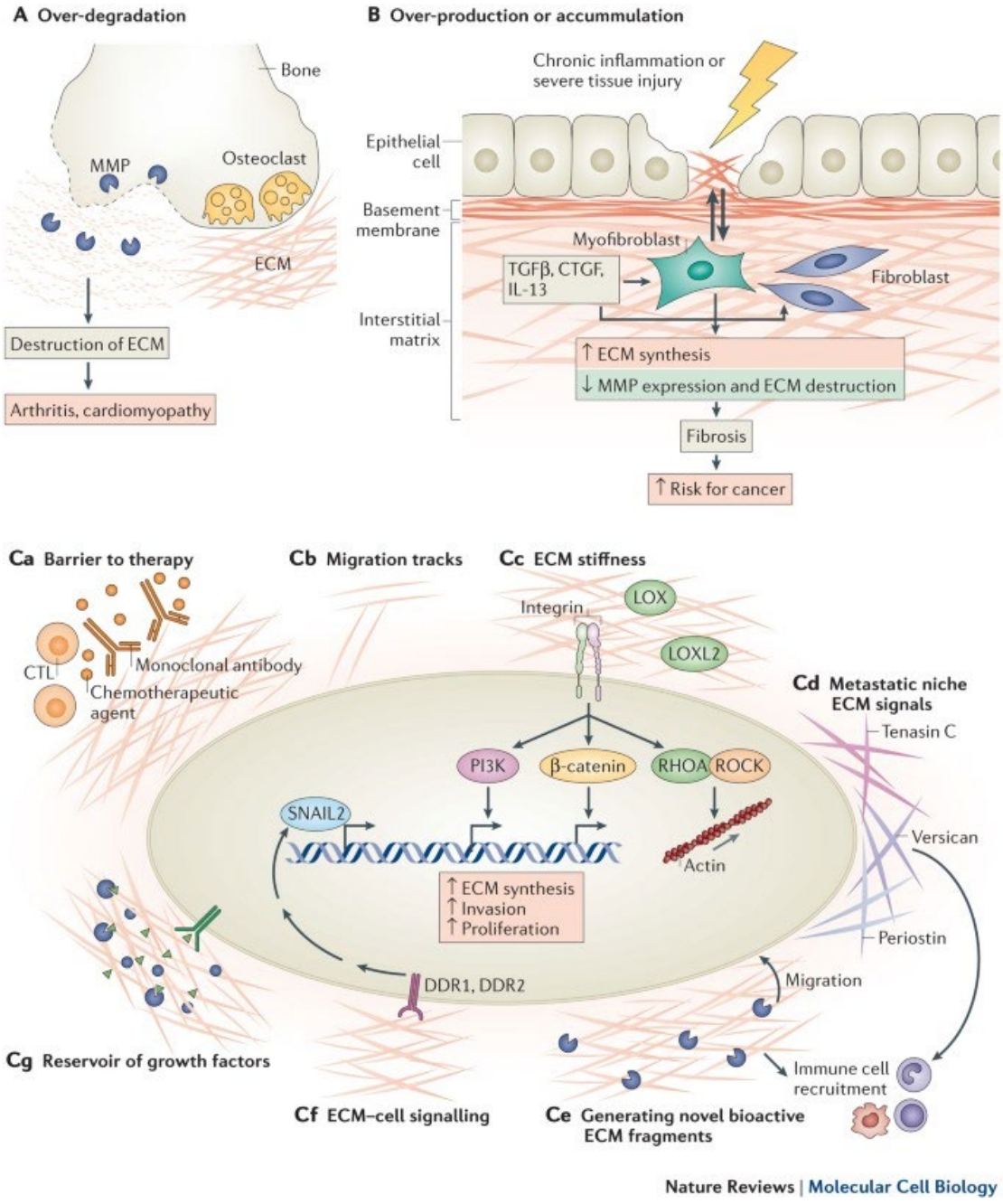

Fig. 2.4 Aberrant extracellular matrix remodeling in human diseases [269]

2.8 CAF in tumor

For most major solid cancer types, overall stiffening is relatively the leading effect. In all these cell contributors, CAFs are identified to be the strongest even dominant impactor to ECM stiffness [32, 110, 202, 224-235, 270-280].

Fibroblast dysfunction results in CAF generation, interestingly this process could occur even before neoplastic transformation [281]. However, fibroblast could display a distinct tumor suppressive role in the cancer initiation stage [282, 283] In later stages, the reprogramming of fibroblast towards CAF by cancer cells could be through TGFβ family receptors and the lipid mediator lysophosphatidic acid paracrine [284], which furtherly activate SMAD signaling and promotes cytoskeleton contractile activity and αSMA expression Cancer cell-fibroblast contact also induced CAF phenotype and deteriorate patient outcome via Notch/Jag1 signaling [285]. Inflammation-related cytokine such as IL1/6 promotes CAF transition through different ligand interactions and downstream pathways [286, 287]. All these stimuli induced an epigenetic switch on CAF phenotype [288, 289], which is also tissue and cell mechanics dependent [273, 290-294]. During cancer progression, CAFs are accumulatively recruited, mostly from local tissue instead of originating from circulating precursor cells [295]. CAF also proliferates along with tumor progress [270, 271]. At late-stage cancer, CAF exhibits a tumor-promoting manner, drives malignancy [296], suppresses immune surveillance or therapeutic efficiency [297, 298], leads collective migration [299], promotes cancer invasion [274, 278, 300], triggers metastasis [274, 301, 302], many of these protumor behaviors are achieved or promoted by the matrix depositing and remodeling capacity [197, 202, 225, 227, 231, 254, 258, 274, 276-280, 290, 291, 296, 300]. Currently, therapeutic strategies are developed to target CAFs. In some cases, depletion of CAFs significantly normalizes cancer stiffness [233], and pharmacologic inhibition or inactivation of the protumor CAF phenotype shows a similar outcome [234, 280]. Sometimes this strategy deteriorates clinical outcomes [282, 283].

2.9 Directional migration, durotaxis and viscotaxis

Cell motility and migration is a basic cell function, which is important in physiological homeostasis, developmental process as well as diseases, including cancer. In many cases, cell migration patterns are non-random but properly initiated and precisely guided, even in cancer cell migration, invasion, and metastasis, cancer cell still follows the cellular fundamental migration principles. This group of behaviors is classified as directed cell migration [180].

There are plenty of classes of directed cell migration behaviors, based on the signal type that the cell responds to and determines cell migration direction, chemotaxis (cell responds and follows chemical concentration gradient), haptotaxis (cell responds and follows ECM ligand gradient), topotaxis (cell responds and follows topological feature gradient), galvanotaxis (cell responds and follows electric potential gradient), durotaxis (cell responds and follows stiffness gradient) and viscotaxis (cell responds and follows material viscous behavior) are identified.

The first step of directed cell migration for the cell is to sense the signal gradient, for durotaxis and viscotaxis, the signaling sensing is mainly via the physical interaction between ECM ligand and mechano-sensitive membrane proteins. Integrins in focal adhesion and piezo1/2 channels could directly bind to different ECM proteins, which could act as candidates for the initiator of the mechanical gradient sensing stage [303]. Moreover, the membrane itself has been clarified as a mechanical sensor to trigger matrix-directed migration through membrane tension-caveolae-GEF Ect2-RhoA-actin polymerization-rear retraction mechanism [304, 305]. Here we'll skip the above-mentioned axis-independent manners to initiate the sensing stage [306], which are less related to this thesis [307].

After sensing the signal gradient, to accomplish directed cell migration, the establishment of cell polarity is critical. Currently, there are two proposed possible mechanisms, one is that piezo1/2 activation by stretching/curvature sensing could locally increase the concentration of second messengers such as intracellular calcium [308, 309], which could possibly establish the cellular signaling anisotropy and further form the cell polarity. CD44 and other direct mechanical sensors

show similar probability [307, 310-313], but it's not verified yet. The other well-identified mechanism is through clutch reinforcement, which has been extensively described in the motor-clutch model since first established in 1988 [189, 190, 314-319]. In brief, clutch reinforcement refers to the positive feedback between the external mechanical microenvironment and cell mechanotransduction, this loop initiates firstly by the confirmational change and the activation of integrins in nascent focal adhesions by external mechanical forces, which further activates p130cas [320], FAK, and recruits talin1/2, vinculin, paxillin, Zyxin and more integrins to form mature focal adhesion, and furtherly enhances mechanotransduction. Supposing a cell was residing on a stiffness gradient, distinct mechanical stimuli on different slides would trigger clutch reinforcement differently so that there would be more integrins recruited to bind with ECM ligands and generate force at the stiffer side, eventually the cells would be dragged towards the stiffer microenvironment, this is the classical motor-clutch model with clutch reinforcement to describe durotaxis [180].

For a long period, people believed durotaxis is the nature of all migrative cells. Recently the collective durotaxis evidence has been identified in vivo [29]. However, few cell types were identified to be adurotactic even negative-durotactic [189-191, 318, 321]. Firstly, it was found various mechano-targeting pharmacological agents showed the capacity to affect the durotaxis features [52], even being able to shift the optimal stiffness for cell migration or block the durotaxis behavior [189, 318]. People realized ECM-integrin catch bond-mediated lifetime matters in determining the durotaxis pattern in a stiffness biphasic manner, but normally this effect on bond lifetime was overridden by clutch reinforcement. Meanwhile, it's found retinal ganglion cell (RGC) axon growth is surprising towards a softer microenvironment [321]. After that, a pioneer study identified the first negative-durotactic cell line, U-251MG human glioblastoma cells, and clarified the reason why the biphasic response wasn't covered by clutch reinforcement was because the mechanotransduction signaling pathways were mechano-insensitive, adjusting the mechano-sensitivity based on this could alter durotaxis pattern [190]. And the next negative-durotactic cell type, acral melanoma cells, were identified afterward [191]. Although, currently there's completely no clue about why some special cells exhibit negative-durotaxis patterns, what signaling pathways accounted for this special behavior, and whether durotactic patterns could shift like phenotypic transition [322, 323].

Viscotaxis is the recently defined directed cell migration manner in response to material viscous behavior, it's reported that mesenchymal stem cell migrates towards a less viscous direction because of the focal adhesion and cell shape instability [324, 325]. Interestingly it's predicted that *Spiroplasma* and *Leptospira* dynamically change body shape to prevent them from drifting to low-viscosity regions where they swim poorly [326].

Cancer cells showed highly migrative and invasive capacity in vitro and in vivo, most cancer cells are claimed to be durotactic, and 231-WT cells have been addressed as a positive-durotactic cell type in plenty of research. The viscotaxis behavior of cancer cells is not addressed but is likely to follow the negative-viscotaxis pattern [324, 325]. But till now, the role of positive/negative-durotaxis/viscotaxis in cancer progression is completely unknown.

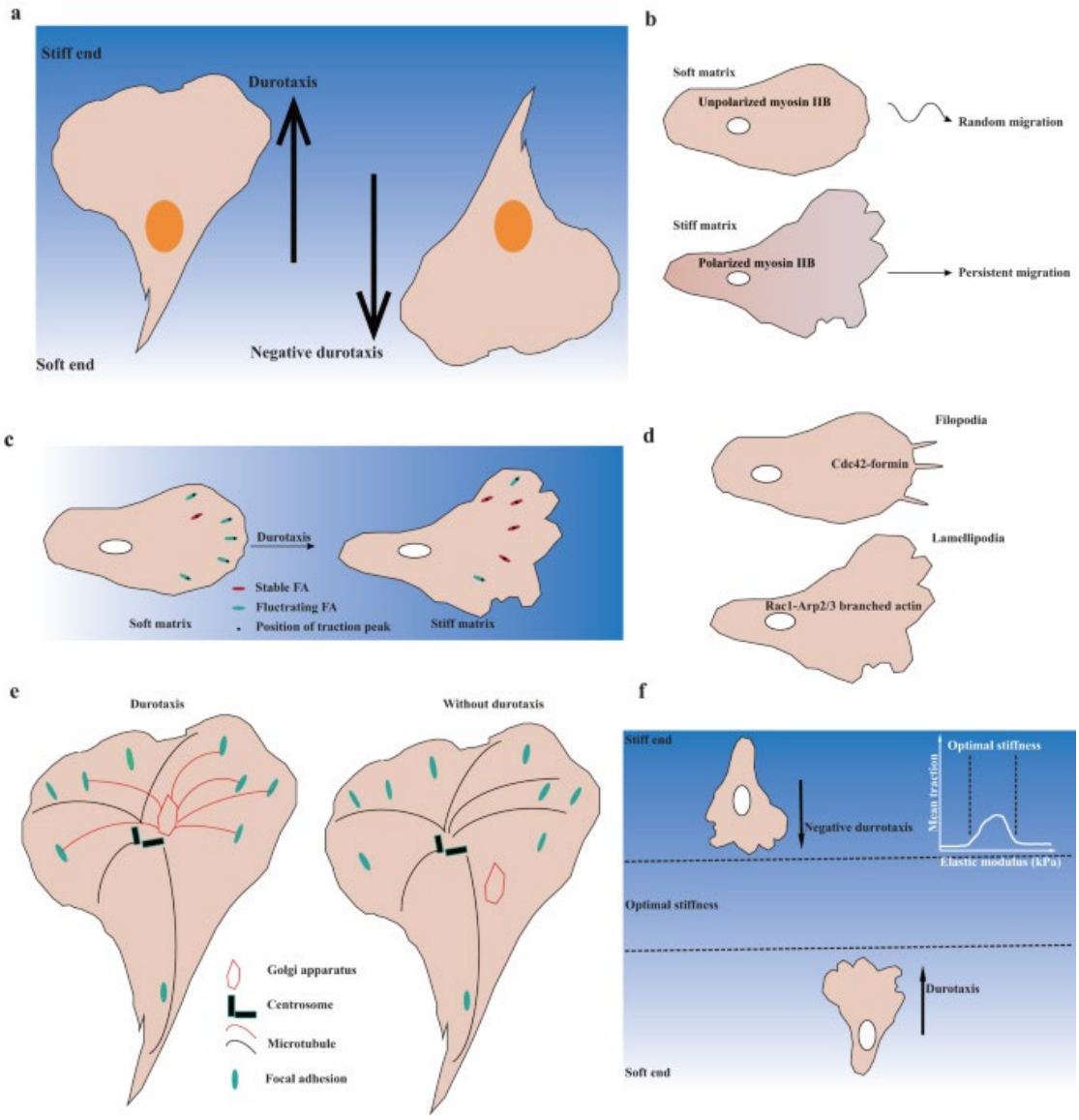

Fig. 2.5 Mechanisms of durotaxis and negative durotaxis [323]

2.10 Cell competition in cancer

Cell competition refers to a process in which one cell type or cell subclone (winner cell) outcompetes the other (loser cell) in the co-culture system or in vivo [327]. Currently, there have been a series of cell competition modes identified in development, homeostasis, and diseases, including cancer.

Cell competition has various types, if there's no gap in cellular fitness levels between competitor clones, this leads to stochastic replacement events in tissue to maintain the homeostasis in different

species, which is defined as neutral competition; if the one competitor somehow (such as inducing differentiation) exhibits proliferative advantage, the phenomenon is defined as biased competition; if one competitor positively eliminates the other, then the phenomenon is defined as active competition [327]. Cell competition functions differently in different stages of cancer, and many of them are proven or potentially mechanics-related.

In the cancer initiation stage, cancer cells compete with normal stroma cells, which could be neutral, cancer-suppressive, and cancer-promoting [327]. This cell competition pattern between stroma cells and cancer cells could be patient, organ type, cancer type, cancer cell number, stroma cell type, specific mutation even karyotypes dependent [328-334]. EDAC is well-known as a tumor-suppressive cell competition pattern in the cancer initiation stage, normal healthy epithelial layers can squeeze out transformed cells from tissue for maintaining homeostasis, which has been found in plenty of cancer types [335, 336]. Intercellular classical mechanical responsive molecule mutations (src [337], CDC42 [338], YAP [339]) trigger the neighbor EDAC against these cells. The EDAC process is found to be cell-cell physical interaction-related and dependent [340, 341]. Meanwhile, ECM mechanical property is also reported to regulate EDAC efficiency [41]. Clonal competition in the cancer initiation stage has also been identified [342, 343], notch signaling dominates whether the clonal competition is neutral or biased in stratified epithelia, while consistent biased competition causes lateral expansion of mutant clones and eventually leads to cancer initiation [343-345]. Notch signaling requires contact area-dependent cell-cell physical interactions [346], the required force magnitude is about 4 pN to 12 pN measured by DNA "Nano Yoyo" as the mechanical sensor [347], while it is found ROCK signaling as well as the actomyosin contractility in cell is required for notch signaling activation between cells [348-350]. The clonal competition in the haematopoietic bone marrow niche is a good example of continuous biased competition results in cancer initiation. The early expansion event of 'preleukaemic' HSCs is through clonal haematopoiesis, in this process both biased drift and active selection are involved [351-353], this competitive advantage is also found to enhance the physical adherence to the basement membrane niche [354-356]. In solid tissues, it's reported that mutant clones sometimes display a competitive advantage over adjacent normal cells, the competition could be biased or active and has been observed in carriers of many mutation types, including p53 [357], K-

Ras [358, 359], and plenty mechano-sensitive signaling, such as PI3K-Akt axis [359], notch signaling [359], Apc-β-catenin signaling [360-363], and Hippo-YAP signaling [330].

In established tumors, cell competition also exhibits bifunction. Cancer cells show extensive heterogeneity and rapid proliferation [12, 24, 99, 103, 137, 138, 231, 261, 364-366], meanwhile, series signaling pathways that drive developmental cell competition during embryogenesis are reactivated, thus a process referred to as 'cancer evolution' [367, 368]. This process largely increases the fitness of cancer to stimuli and deteriorates patient outcomes [364-366]. Here, YAP is found to be involved in competition between cancer cell clones as well, which promotes tumorigenesis [369], in normal cells or between stroma cells and cancerous cells similar role of YAP is observed [330, 362, 370-372]. The underlying mechanism of YAP-mediated cell competition is yet unknown, one hypothesis is YAP activation level reflects the cell's capacity to resist mechanical pressures [327].

Chapter III: Methods and Materials

3.1 Cell culture

HEK-293T human embryonic kidney cell line was a gift from Dr. RUAN Yechun (The Hong Kong Polytechnic University), SK-BR-3, 231-TGL, 231-BrM, and 231-WT human breast cancer cell lines were purchased from Memorial Sloan Kettering Cancer Center, all biomaterial-primed or virus transinfected variants, including 231-0.6, 231-35, pNDRG1-mCherry-fluc-231, pNDRG1-mCherry-fluc-231-scp1, pNDRG1-mCherry-fluc-231-scp1-0.6 and pNDRG1-mCherry-fluc-231-scp1-35 were generated in our lab. All these cells were cultured in High Glucose Dulbecco's Modified Eagle Medium (DMEM) (Gibco) supplemented with 10% (v/v) fetal bovine serum (FBS) (Gibco) and 1% penicillin/streptomycin (HyClone). Human Cerebral Microvascular Endothelial Cells (hCMEC/D3) were cultured with EndoGRO-MV complete culture media kit (Sigma-Aldrich), which was supplemented with 200 ng/mL human basic fibroblast growth factor (bFGF; Sigma-Aldrich) and 1% (v/v) penicillin/streptomycin. Human astrocytes, which were isolated from the cerebral cortex of the human brain, were kindly provided by Prof. YANG Mo (The Hong Kong Polytechnic University) and cultured in Astrocyte Medium (ScienCell). MCF-7 human breast cancer cell lines were purchased from Memorial Sloan Kettering Cancer Center and were cultured in RPMI-1640 medium (Gibco) with 10% (v/v) FBS and 1% (v/v) penicillin/streptomycin. The human umbilical vein endothelial cell (HUVEC) line was a generous gift from Prof. YANG Mo (The Hong Kong Polytechnic University). The HUVECs were cultured in Endothelial Cell Medium (ScienCell). NIH-3T3 murine fibroblast cell line was a generous gift from Dr. ZhaoXin (The Hong Kong Polytechnic University) and cultured in Minimum Essential Medium α (MEMα) with 10% (v/v) FBS and 1% (v/v) penicillin/streptomycin. Murine mesenchymal stem cell (shorted for mouse MSC) was generously provided by Dr. Wen Chunyi (The Hong Kong Polytechnic University), cultured ECM (Endothelial Culture Media) supplemented with 10% (v/v) FBS and 1% (v/v) penicillin/streptomycin. In some experiments, cells were treated with doxycycline, 20 μmol/mL LY294002 for 24 h, 10 μmol/mL SC79 for 24 h, 10 μmol/mL RGFP966 for 24 h, 10 μmol/mL fatostatin HBr for 24 h, or 5 μmol/mL docosahexaenoic acid for 24 h. 0.25% trypsin (for cells cultured on a petri dish) or Ethylene Diamine Tetraacetic Acid (EDTA) (Sigma) (only for cells cultured on hydrogel) was used to passage cells. All cell lines were cultured in a 5% CO_2 incubator at 37 °C.

3.2 Preparation of polyacrylamide hydrogel

Polyacrylamide (PA) hydrogel was prepared as previously described by Justin R. Tse et al.[373], generally, coverslip was treated with 0.1mol/L NaOH until evaporated, 3-Aminopropyltriethoxysilane (APES) for 5 min and 0.5% (v/v) glutaraldehyde in phosphate-buffered saline for 30 min, then acrylamide, bisacrylamide, 10% ammonium persulfate (APS), Tetramethylethylenediamine (TEMED) and ddH_2O were added with appropriate formula between treated coverslip and Dichlorodimethylsilane (DCDMS) hydrophobically modified glass slides, after fabrication 1 mmol/L N-Succinimidyl-6-(4-azido2-nitrophenyl-amino)hexanoate (SANPAH) was added to react under ultra-violate (UV) light, a thin layer of collagen-I was formed after overnight coating.

Elastic Modulus (kPa)	acrylamide (wt.%)	bis-acrylamide (wt.%)	APS (wt.%)	TEMED (wt.%)
0.6	3	0.06	1	0.1
2	4	0.1	1	0.1
5	5	0.15	1	0.1
15	10	0.15	1	0.1
35	10	0.3	1	0.1

Table 1.1 polyacrylamide hydrogel formula

3.3 Lentiviral transfection

pNDRG1-mCherry-puro and 3×FLAG-fluc-Neo vectors were synthesized by YanMing Biotech, Shenzhen, the design of shRNAs were: TLN1 target sequence: CCCAGAGTATTAACGCTCCAA; TLN2 target sequence: ACGATGCGTGTCGAGTCATTC; MYH10 target seq: CGGGATTCCTTCCTGAAAGAT; ITGA10: 5'-ACACACAAACAGACTGAAT-3'. The vectors were co-transfected with pMD.2G and psPAX2 vectors into HEK293 cells with Opti-MEM and lipo3000 Kits following the manufactory's instructions to package lentivirus, after 48 h, the

supernatant was collected, filtrated with PES membrane filter and treated with lentivirus concentration solution kit, the concentrated lentivirus was resuspended in Opti-MEM and added into corresponding cells, cells were treated with puromycin or G418 to purify the transfected populations with corresponding drug resistance. At last, single-cell cloning was conducted to enrich pNDRG1-mCherry-fluc-231 cells with the same sensor element copy number.

3.4 Reverse transcriptase quantitative polymerase chain reaction (RT-qPCR)

All primer nucleotide sequences used are listed in Table 1. below, including the primers used in the remaining chapters.

Target	Forward Primer	Reverse Primer
GAPDH	GCGACACCCACTCCTCCACCTTT	TGCTGTAGCCAAATTCGTTGTCATA
ANGPTL4	GTCCACCGACCTCCCGTTA	CCTCATGGTCTAGGTGCTTGT
Cox-2	CTGGCGCTCAGCCATACAG	CGCACTTATACTGGTCAAATCCC
EREG	GTGATTCCATCATGTATCCCAGG	GCCATTCATGTCAGAGCTACACT
HBEGF	ATCGTGGGGCTTCTCATGTTT	TTAGTCATGCCCAACTTCACTTT
ITGAV	ATCTGTGAGGTCGAAACAGGA	TGGAGCATACTCAACAGTCTTTG
ITGB3	GTGACCTGAAGGAGAATCTGC	CCGGAGTGCAATCCTCTGG
ITGA10	AACATCACCCACGCCTATTCC	GTTGGTAGTCACCTAAGTGGC
TLN1	GACGATGCAGTTTGAGCCG	GGGTCATCATCTGACAGAAAGAG
TLN2	GCGTGTCGAGTCATTCGGG	CCCTTTCCTCGGGTCTTCATC
Piezo2	ATGGCCTCAGAAGTGGTGTG	ATGTCCTTGCATCGTCGTTTT
PTEN	TGGATTCGACTTAGACTTGACCT	GGTGGGTTATGGTCTTCAAAAGG
SCNN1A	AGGGGAACAAGCGTGAGGA	GGTGGAACTCGATCAGGGC
SERPINB2	CAGCACCGAAGACCAGATGG	CCTGCAAAATCGCATCAGGATAA
ST6GALNAC5	CACTGGACGGATACCTCGGA	TCTGTCTGGTCAATCTGGGAG
MYH10	TGGTTTTGAGGCAGCTAGTATCA	AGTCCTGAATAGTAGCGATCCTT
PPL	CCGGAGCATCTCTAACAAGGA	GCATCCGCCTCTAGCACAT
BMF	GAGCCATCTCAGTGTGTGGAG	GCCAGCATTGCCATAAAAGAGTC
NDRG1	CTCCTGCAAGAGTTTGATGTCC	TCATGCCGATGTCATGGTAGG

Table 1.2 Primer nucleotide sequences.

The protocol of RT-qPCR has been extensively proved efficient. In detail, total mRNA was extracted using the E.Z.N.A.® Total RNA Kit (Omega) according to the manufacturer's instructions. The RevertAid First Strand cDNA Synthesis Kit (Thermo Fisher) was employed to synthesize cDNA from the extracted total RNA. Primers for quantitative RT-PCR were designed based on sequences from the National Center for Biotechnology Information (NCBI) database or Primer Bank (https://pga.mgh.harvard.edu/primerbank/index.html) and are listed in Table 1. Quantitative RT-PCR was performed using the Forget-Me-Not EvaGreen qPCR Master Mix with Rox (Biotium) and the CFX96 Real-Time System (Bio-Rad). Relative gene expression was calculated using the $2^{-\Delta\Delta CT}$ method and normalized to the expression of human glyceraldehyde 3-phosphate dehydrogenase (GAPDH).

3.5 Immune fluorescence (IF) staining

The protocol of IF was listed below: Cells or tumor cryostat sections were fixed with pre-chilled 4% PFA for 20 minutes at room temperature. Then samples were permeabilized with 0.3% Triton X-100 in PBS for 20 minutes and washed with PBS. After that, samples were blocked with 1% BSA and 22.52 mg/mL glycine in PBS containing 0.1% Tween 20 (PBST) for 1 hour at room temperature. Diluted primary antibodies in 1% BSA in PBST were incubated with the samples overnight at 4℃. The next day, samples were washed three times with PBST for 5 minutes each and incubated with diluted secondary antibodies in 1% BSA in PBST at room temperature for an hour. Then, decant the solution wash three times with PBST, and stain nuclei with DAPI. For F-actin staining, use the CytoPainter F-actin labeling kit (Abcam, # ab112125) or fluorescence-labeled phalloidin as per the user guidebook. Imaging was performed with a confocal microscope (Leica, TCS SPE) using 40× and 63× objectives to capture images. The fluorescence intensity results were analyzed with Fiji software.

The primary antibodies used in the study are listed below: HDAC3 (1:500; Abcam, cat. no. ab32369), Ki-67 (1:200, Abcam, cat. No. ab15580), Runx-2 (1:200; Abcam, # ab23981), SerpinB2 (1:200;

Abcam, # ab47742), mCherry (1:100; Invitrogen, # m11217) The secondary antibodies used in the study are Alexa Fluor 594 Goat Anti-Mouse IgG H&L (1:400, Abcam, # ab150116), TRITC Goat Anti-Rat IgG H+L (1:1000; Invitrogen, # 26-4826-82) and Alexa Fluor 647 Goat Anti-Mouse IgG H&L (1:400, Abcam, # ab15011).

3.6 AFM measurements

In this study, we utilized an atomic force microscope (AFM; BioScope Catalyst, Bruker) in conjunction with an inverted fluorescence microscope (Nikon) to visualize the probe and precisely control the cantilever tip and sample position in bright field (BF) while quantifying mCherry signaling excited by a 488 nm laser. Before measurement, cryostat-sectioned tumor slides were attached to coverslips pre-treated with poly-l-lysine. Silicon cantilevers (MLCT, Bruker) with a spring constant of 0.03 N/m were used for stiffness measurements of tissues and collagen gels in subsequent chapters. AFM software initialization, microscopy, cantilever setup, and calibration were performed according to the user manual. Specifically, we employed the contact mode and ScanAsyst in Fluid mode to measure tissue/hydrogel stiffness in PBS. Subsequently, laser position adjustment, AFM position adjustment, and cantilever calibration were conducted sequentially. To obtain Young's modulus of the tissue/hydrogel, the force (F) produced by the indentation between the probe and the cell was calculated using the formula

$$F = k \times \delta$$

, where (k) is the spring constant of the cantilever and (δ) is the indentation, which equals the sample height minus the deflection. Sneddon's modification of the Hertzian model was used to fit force-indentation curves generated by AFM for cantilevers with a pyramidal indenter. We calculated Young's modulus value using the formula

$$F = \frac{2}{\pi} \cdot \tan\alpha \cdot \frac{E}{1 - v^2} \cdot d^2$$

, where (d) represents the depth of indentation, (α) represents half the tip angle, and (v) equals 0.5. We set (d) below 500 nm to avoid sample damage. The elastic values of cells were obtained in the perinuclear area to minimize the effect of substrate-induced outliers. Force curves were randomly selected from cells without cell-cell contact or tissue sections to evaluate cell/tissue stiffness. To measure the viscous property of tissues, we used another AFM (JPK NanoWizard V BioScience

AFM, Bruker), the parameters for data collections were similar, and to calculate the dissipation area, JPK data processing 8.1 software was utilized.

3.7 Orthotopic injection

Nude/SCID female mice were used in this study. Mice were kept in cages under specific pathogen-free conditions. FACS assay, pNDRG1-mCherry-231-TGL/pNDRG1-mCherry-fluc-231-scp1 cells were cultured on a tissue culture plate in vitro for population expanding, then mice (4–8 weeks) were injected with 1,500,000 tumor cells with Matrigel into fat pad. The primary tumor growth process was monitored according to luminescence density until surgical resection. Analgesic buprenorphine was administrated through drinking water if signs of pain or discomfort were observed. The average time of this experiment would be about 4 – 8 weeks. At the endpoint of the study, mice were euthanized by carbon dioxide asphyxiation, primary tumor was harvested, minced, and digested in trypsin and collagenase, followed by FACS protocol to sort out cells into different groups.

3.8 Intracardiac injection

For metastasis assay in vivo, intracardiac injection was performed. The collected cells were resuspended in PBS and injected into Nude/SCID mice's left cardiac ventricle. To confirm a successful injection, the photon flux from the whole body of the mice was immediately measured using an IVIS Xenogen bioimager. The metastasis progression was monitored, and the luminescence was quantified at the indicated time points. The average time of the experiment is about 4 weeks. At the endpoint of the study, mice were euthanized by carbon dioxide asphyxiation, whole metastatic organs (brain, lung, and bone) were removed, incubated in DMEM medium with luciferin, and photon flux was measured afterwards. The tumor mass was minced, digested, or sliced for further biochemical analysis. Analgesic buprenorphine was administrated through drinking water if signs of pain or discomfort were observed. All animals were inspected, and their health condition was monitored daily throughout the experiment period.

3.9 Flow cytometry

Cells were harvested using trypsin or EDTA, and after washing with PBS, samples were filtered with a cell strainer. The percentage of each subpopulation was then detected by BD Accuri C6 flow cytometer (BD Biosciences) or BD FACSAria III Cell Sorter (BD Biosciences). Data was visualized using FlowJo software.

3.10 FACS

FACS was utilized to separate cell populations based on fluorescence level, for preparation, cell suspensions were filtered with cell strains into single cells, after that cell samples resuspended in PBS were loaded into BD FACSAria III Cell Sorter following the instruction of the instrument, sorted cells were collected into DMEM for lateral analysis. For some specific experiment designs, mCherryhi/lo pNDRG1-mCherry-231 cells harvested from TCP were defined as the 10% of the brightest/darkest mCherry populations; $mCherry^{+/-}$ pNDRG1-mCherry cells obtained from xenografts were gated based on the expression level of mCherry of the same clone harvested from 0.6/35 kPa polyacrylamide hydrogel gel.

3.11 MACS

MACS was adopted to select cancer cells from digested xenograft cells. Mouse Cell Depletion Kit (Miltenyibiotec) and MACS platform consisted of MidiMACS™ Separator, MACS® MultiStand, and LS columns were utilized strictly following the manufactory's instructions. In detail, centrifuged cell mixtures were resuspended in 0.5% BSA-contained PBS buffer, then mouse cell depletion cocktail was added in and incubated at 2~8°C, after incubation, cell mixtures were added into buffer-pre-rinsed LS columns installing on MACS Separator and MultiStand for isolation and collection.

3.12 HDAC3 activity assay

HDAC3 activity was measured as follows: To prepare the cell lysis, cells were washed with ice-cold PBS, and lysed cells in a non-denaturing lysis buffer (Solarbio, #R0030) supplemented with a protease inhibitor cocktail. To quantify protein, the protein concentrations were measured in the cell lysates using the bicinchoninic acid (BCA) assay to adjust protein concentrations to the same level across all samples for consistency. For immunoprecipitation, cell lysates were incubated with the HDAC3 primary antibody (Abcam, #ab13770) overnight at 4°C with gentle rotation. Then immunocomplexes were collected by incubating the lysates with protein-A/G beads (Abcam, #ab193262) for 2 hours, followed by four times washing to remove non-specific bindings beads. To measure the HDAC3 activity, the immunoprecipitated samples were tested using an HDAC fluorometric kit (Abcam, #ab156064).

3.13 Cryostat sectioning

Briefly, for the xenograft tissue cryostats section, the harvested tumor was washed with PBS, then embedded with optimal cutting temperature compound (Sakura), and snap frozen in liquid nitrogen. Leica CM1950 cryostats were utilized to cut frozen sample blocks into 10μm sections at -20°C, after that, tissue sections were transferred to poly-l-lysine-coated glass bottom dish or positively charged glass slides and immersed in PBS with 1% proteinase inhibitors (Beyotime) for following analysis.

3.14 B-Mode Ultrasound, and Shear Wave Elastography

The method of B-mode ultrasound, shear wave elastography on orthotopic xenograft was previously described [105], eight weeks after injection, mice were anesthetized, and ultrasound gel (AQUASONIC CLEAR) was smeared on the skin outside the primary lesion. Tumor margins were

determined by B-mode ultrasound, tumor stiffness was detected using shear wave elastography imaging with SL22-7lab detector (Superlinear) and Aixplorer model (SuperSonic Imagine, France).

3.15 In vitro BBB-transmigration assay

The protocol of BBB-transmigration assay was published in Nature Protocols [374]. Briefly, Human Cerebral Microvascular Endothelial Cells (hCMEC/D3) and Human Primary Astrocytes were prepared beforehand, for the preparation of 3 μm pore size transwell inserts (Corning, cat. No. 3415), the inserts were treated with 1 μg/ml poly-L-lysine (Sigma-Aldrich) overnight, then the inserts were washed for four times with PBS, followed by coating with 0.2% gelatin (Sigma-Aldrich) for 30 minutes. For plating astrocytes, the inserts were placed upside down in a 12-well plate. 1×10^5 primary human astrocytes were resuspended in 30 μl culture medium and plated on the membrane surface. The seeded astrocytes were fed every 15 minutes for 5 hours. Then flip the inserts and place them back in 24-well plates. Then, plate hCMEC/D3 cells, 5×10^4 hCMEC/D3 cells were seeded to the upper chamber of the inserts and incubated on the plate for 3 days without any disturbance. To label cancer cells, 1×10^5 cancer cells were collected and incubated with CellTracker Deep Red Dye (Invitrogen) according to the manufacturer's instructions. After labeling with fluorescence, the labeled cells were resuspended in a serum-free medium and added to the upper chamber of the above-mentioned transwell inserts with hCMEC/D3 and astrocyte. Cells were incubated for 48 hours for free migration towards serum gradient. At the endpoint of the incubation, non-invading cells were removed, and the chambers were washed with PBS and fixed with 4% PFA, after staining the cells with DAPI, immunofluorescence images of multiple fields from 3-6 inserts per experiment were captured with Nikon Eclipse Ti2-E Live-cell Fluorescence Imaging System and cell numbers were counted with Fiji software.

3.16 Preparation of gradient stiffness/viscous component polyacrylamide hydrogel

Gradient stiffness polyacrylamide hydrogel was prepared following Aleksi Isomursu's publication [190], which was similar procedures of PA hydrogel except the hydrophilic coverslip was switched into confocal dish and fluorescence beads-labeled 40 kPa unfabricated droplet and another 5 kPa unfabricated droplet on the other side was added and covered with hydrophobically treated coverslip. Gradient viscous component polyacrylamide hydrogel was prepared following Pallavi Uday Shirke's publication [324], the gradient gels were prepared using a two-drop diffusion technique as described earlier, and the formulations used were listed in the table below. After fabrication, the functionalization procedure was the same as introduced in 1.6.2.

G' (kPa)	G" (Pa)	acrylamide (wt.%)	bis-acrylamide (wt.%)	APS (wt.%)	TEMED (wt.%)
1.1	45	6.68	0.06	1	0.1
1.6	300.62	8	0.26	0.5	0.15

Table 1.3 polyacrylamide hydrogel formula

3.17 Single-cell trajectory

For single-cell trajectory, cells were labeled with fluorescence dye or transfected with fluorescence proteins, seeded in chips, gradient stiffness polyacrylamide hydrogels or gradient viscous component polyacrylamide hydrogels with low serum media, after cell attachment and fully spreading, cell locations were captured every 15 min with Nikon Ti2-E bioluminescence live cell imaging system (Nikon) and analyzed with Fiji and Chemotaxis and Migration Tool (ibid).

3.18 Vascular endothelial cell adhesion assay

For vascular endothelial cell adhesion assay, endothelial cells were pre-seeded into a 24-well plate, after achieving full confluency, cancer cells labeled with fluorescence dye or transfected with fluorescence proteins were added into the media and incubated for 10 min in a 5% CO_2 incubator at 37 °C. Then non-adhered cancer cells were washed out three times with PBS, after that the adhered cells were fixed with 4% PFA and imaged with Nikon Ti2-E bioluminescence live cell imaging system and analyzed with Fiji.

3.19 Bioinformatic analysis of scRNA-seq

For bioinformatic analysis of scRNA-seq, the Seurat package was used to process data, in the quality control procedure, only cells fulfilled 200 < nFeature_RNA < 7500 & percent.mt < 10 & percent.HB < 3 & nCount_RNA < 50000 were included. To determine the dimensionality of the dataset, ElbowPlot was used to choose the largest dimensionality with a strong enrichment of low p-value genes for downstream clustering. Clustering trees was used to determine the optimal resolution. PCA was conducted with the above-determined parameters and visualized with UMAP, and cell-type annotations were conducted with publicized makers. The statistical analysis was visualized by R and LoupeR.

3.20 Bioinformatic analysis of spatial transcriptomes

For bioinformatic analysis of spatial transcriptomes, Loupe Browser was used to show the gene transcriptional level, visualize the correlation transcriptional level between genes, filter the barcodes into different subgroups, and conduct the statistical analysis.

3.21 Brain slides co-culture assay

Brain slices from adult mouse brains were prepared following a previously reported method [375]. Brains were obtained from female BALB/c nude mice aged 6-8 weeks and embedded in preheated low-melting agarose at 42°C. The agarose-embedded brains were then sectioned into 250 μm slices using a vibratome (Leica, VT1200S). Subsequently, brain slices were transferred to 0.8 μm pore membranes (Millipore), and slice culture medium (DMEM supplemented with HBSS, 5% FBS, 1 mM L-glutamine, and 1% penicillin/streptomycin) was provided. After incubating the brain slices at 37°C with 5% CO_2 for 1 hour, 2 μL of medium containing 3 x 10^4 tumor cells were added to the surface of each slice and incubated for 48 hours. To assess tumor cell colonization on brain slices, the slices were gently washed with PBS once. Finally, 1 mL of 300 μg/mL D-luciferin (Abcam) was added to each well to cover the slice, and bioluminescence signals were measured.

Chapter IV: Intratumoral local niche softness correlates with breast cancer brain metastasis in vivo

4.1 Objectives and scopes

Besides the above-mentioned aspects that mediate metastatic organotropism in Chapters I and II, there have also been some clues about whether and how mechanical cues shift metastatic organotropism. Tissue architecture was proved to affect metastatic organotropism in zebrafish [83]. Exosomes with different subtypes of integrin remodeled target organs to establish the premetastatic niche, which determined organ-specific dissemination [85]. Accumulating evidence indicated that ECM stiffness, an important mechanical property of tumors, also regulated organotropic metastasis. A pioneer study showed how different single-cell clones proliferated on different substrates could be a parameter strongly correlating with metastatic organotropism [86]. Culturing TNBC cell line SUM159 on stiff polyacrylamide hydrogels for long term established a bone-targeting metastasis pattern [84]. Our previous project proved long-term soft-priming displayed a neuron-mimicking gene expression pattern and shifted the organotropism of TNBC cell line MDA-MB-231 to brain-tropism, which was dependent on the mechanotransduction-induced HDAC3 expression and activity.

Thus, this Chapter aims to prove that there is a correlation between tissue ECM mechanics and cancer cell brain metastasis capacity in vivo. The specific research contents are listed as follows:

1. Design a transcription-based single-cell scale local niche stiffness biosensor by screening the mechano-sensitive promoter candidate across multiple breast cancer cell lines;
2. Verify the effectiveness of the pNDRG1-mCherry stiffness biosensor using in vitro biomaterials with different stiffnesses and mechanical heterogeneous xenografts;
3. Based on this system, test the brain metastasis capacity of soft/stiff niche residing cells.

4.2 Results

4.2.1 Persistent priming in soft niches in vitro shifts breast cancer metastatic organotropism to brain-tropic

As the above-mentioned findings concluded, culturing human TNBC cell line MDA-MB-231 on 0.6 kPa polyacrylamide hydrogel gradually attenuates the bone-metastatic potential while

enhancing the brain-metastatic potential compared with 35 kPa culturing. This chapter aims to provide solid proof that this scenario, which we induced using biomaterials in vitro, indeed happened in vivo. Here, firstly we applied non-invasive ultrasonic elastography to measure the tissue stiffness range of the established orthotopically transplanted tumor xenograft using MDA-MB-231-TGL (shorted for 231-TGL), the results showed that the tumoral ECM stiffness ranges from 0.2 to 45 kPa while distributed randomly at large scale in tumor (Fig. 4.1a). This result is consistent with previous pioneer findings [111, 112, 170], meanwhile, this range well-covers the 0.6 kPa, 5 kPa, and 35 kPa that polyacrylamide hydrogels our previous projects applied.

Next, 231-TGL cells were seeded on 0.6 kPa and 35 kPa polyacrylamide hydrogel and stimulated for 30 days, these cells were named 231-0.6 and 231-35 afterwards. Just to double confirm the previous findings, we applied RT-qPCR to test the mRNA level of the classical brain/bone-metastatic gene markers of 231-0.6 and 231-35, which to find the brain-metastatic gene spectrum were up-regulating after soft-priming while bone-metastatic genes were down-regulated (Fig. 4.1b,c). The representativeness of brain metastasis gene Cox-2, SerpinB2, and bone metastasis gene Runx-2 was verified using IF by comparing 231-TGL and MDA231-BrM2-831 (shorted for 231-TGL), an MDA-MB-231-TGL variant selected/reprogrammed by multiple rounds of intracardially injection and brain lesion enrichment (Fig. 4.1d-f), and we measured the Cox-2, SerpinB2 level as well as Runx-2 n/c ratio in 231-0.6 and 231-35 (Fig. 4.1g-i). Additionally, we intracardially injected 231-0.6 and 231-35 into nude mouse fat pad, to find an increasement in brain metastasis intensity and incidence in the 231-0.6 group (Fig. 4.1j). In summary, soft-primed 231-0.6 showed advanced brain metastasis potential and limited bone metastasis potential, consistent with our previous finding.

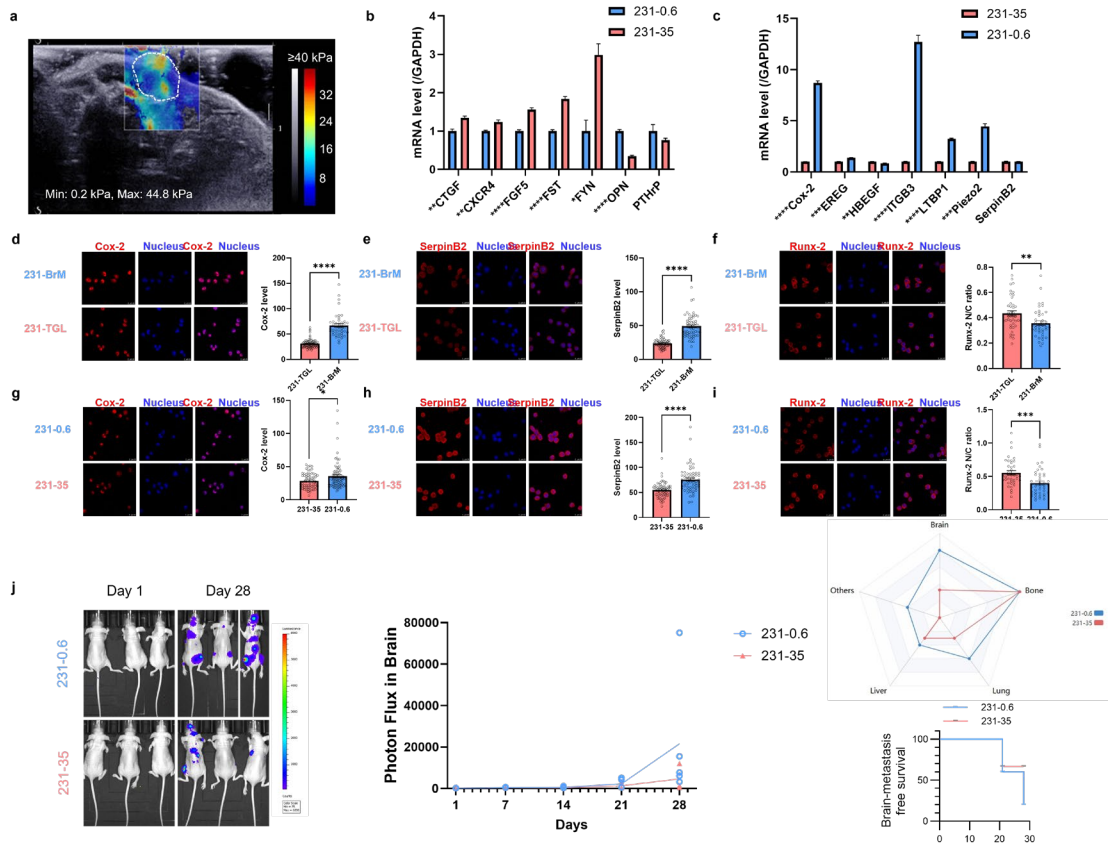

Fig. 4.1 Persistent priming in soft niches in vitro shifts breast cancer metastatic organotropism to brain-tropic. (a). Ultrasonic elastography graph of mouse fat pad orthotopic tumor xenograft. (b). mRNA transcriptional level and statistical analysis (with two-tailed Welch's t-test) of representative bone metastatic genes in 231-0.6 and 231-35. (c). mRNA transcriptional level and statistical analysis (with two-tailed Welch's t-test) of representative brain metastatic genes in 231-0.6 and 231-35 (n=3). (d-f). Representative confocal microscopy images and statistical analysis (with Mann-Whitney U test) of Cox-2 (n=76/43), SerpinB2 (n=66/61), and Runx-2 (n=42/41) in 231-TGL and 231-BrM. (g-i). Representative confocal microscopy images and statistical analysis (with Mann-Whitney U test) of Cox-2 (n= 64/82), SerpinB2 (n=64/61), and Runx-2 (n=40/42) in 231-35 and 231-0.6. (j). Representative bioluminescence images and statistical analysis of nude mice intracardiacally injected with 231-0.6 and 231-35 cells (n=5). (Error bars represent s.e.m., *: $P < 0.05$, **: $P < 0.01$, ***: $P < 0.001$, ****: $P < 0.0001$.)

4.2.2 Strategy to identify and separate subpopulations residing in local niches with different stiffnesses

Since we double-confirmed distinct overall mechanical stimulation on polyacrylamide hydrogel with different stiffness alters metastatic organotropism, especially what we focused on here, soft-priming enhanced brain metastatic capacity. Next, we asked whether, in the real tumor, this regulating process occurred as well, at least we are supposed to provide evidence there is a solid

correlation between tissue stiffness and brain metastatic gene expression, the mechanistic molecule (HDAC3 in previous finding) as well as brain metastatic related cellular functions.

Like what was mentioned in the background part, the intratumoral stiffness properties vary in a wide range and are distributed in a heterogenous pattern [103, 111, 112, 232], moreover, it's found cancer cells were able to sense stiffness at a certain distance away through fiber remodeling [182, 376], and cancer cells communicated with each other in tumor [330, 369, 377]. So, precisely clarifying our goal, we need to prove there's a solid correlation between intrinsic self-established spatiotemporally heterogeneous intratumoral tissue stiffness (softness) at the local niche scale and the (brain) metastatic potential of individual niche resident cancer cells.

To fulfill the requirement, the strategy we raised is to establish a single-cell scale local niche stiffness biosensor, this sensor should be fluorescence-based and well-functioning in live cells so that except staining the markers, we could also test the efficiency of the sensor using AFM in cryo-stats sections without PFA treatment, which has been proved to crosslink the ECM and impacts the tissue stiffness, we could even separate live cancer cell subpopulations harvested from tumor xenograft based on their previously residing local niche stiffness with magnetic-activated cell sorting (MACS) and fluorescence-activated cell sorting (FACS), then further analysis could be done.

4.2.3 The design of a single-cell scale local niche stiffness biosensor

Based on our ambition, here we summarized the features that our sensor should achieve:

1. Responding to ECM stiffness;
2. Fluorescence-based so that FACS could recognize;
3. Signal should be sensitive and monotonic within the intratumoral stiffness range (Fig. 4.1a);
4. Signal intensity MUST be strong, or the tissue autofluorescence may disturb the sensor signaling;
5. The response to external mechanical cues CANNOT be transient, or the tissue digestion, MACS, and FACS procedures may perturb the signal outcome.

Thus, here we established a sensor design consisting of fluorescence protein mCherry driven by an extremely mechano-sensitive promoter (Fig. 4.2a), which was inspired by the commonly used fluorescence reporter and a few previous projects [113, 377-379]. This sensor takes advantage of the intrinsic cell mechanosensing, which naturally functions at a single-cell scale, the external ECM mechanical features would be recognized by the cells, and the mechano-sensitive promoter would mechano-sensitively recruit transcription factors to produce mCherry mRNA for further protein synthesis. Meanwhile, mCherry is a very stable fluorescence protein with half a lifetime > 20 h [380].

4.2.4 Multiple transcriptome analysis screened pNDRG1 as the most mechanosensitive promoter across multiple human breast cancer cell lines

Following the above-mentioned design, here we would like to find the most mechanosensitive promoter in breast cancer, if ignoring the post-transcriptional modification, the mRNA level could fully represent the promoter transcriptional activity under a certain circumstance, thus we applied an RNA-seq to 231-0.6 and 231-35, we set two requirements for the premising candidate gene expression: high fold changes and high mRNA fragments per kilobase million (FPKM) to optimize the output signal quality and resolution; to avoid the cell-line dependency, we utilized the similar RNA-seq data (GSE1278887) in which SUM159 TNBC cell line was cultured on soft vs stiff polyacrylamide hydrogels published by Adam W. Watson's group and took the intersection part (Fig. 4.2b) [381]. Venn graph showed 4 genes fulfilled both requirements in both cell lines [382], NDRG1, PPL, KLRC2, and BMF were up-regulated on soft (Fig. 4.2c); while no candidate up-regulated on stiff was identified (data not shown).

Within these four candidate genes (promoters), NDRG1 showed localization at the top-right (Fig. 4.2d), indicating a good performance. Besides signaling sensitivity comparing 231-0.6 with 231-35, we expect signal monotonically responds within the intratumoral stiffness range (Fig. 4.1a), so we

seeded 231-TGL on 0.6 kPa, 5 kPa, 20 kPa, 35 kPa and TCP as positive control, check the mRNA transcriptional level of these genes, which to find only NDRG1 showed a smooth decrease in the whole interval (Fig. 4.2e). Thus, NDRG1 was finally selected to further construct the stiffness-responsive biosensor.

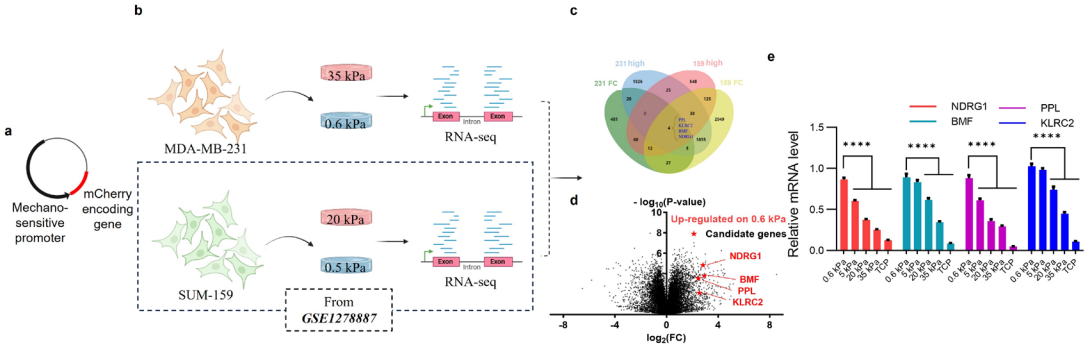

Fig. 4.2 Design and multiple transcriptome analysis screening of single-cell scale local niche stiffness biosensor lentiviral plasmid map consisting of the mechano-sensitive NDRG1 promoter-driven mCherry encoding gene (a). Lentiviral plasmid map of the sensor. (b). Workflow of multiple transcriptome analysis screening. (c). Venn graph for intersections of high fold changes and high mRNA FPKM in MDA-MB-231 and SUM159 cells on soft polyacrylamide hydrogel. (d). Volcano plot of transcriptomes of 231-0.6 and 231-35 cells. (e). mRNA transcriptional level and statistical analysis (with ordinary one-way ANOVA Tukey's multiple comparisons test) of NDRG1, PPL, KLRC2, and BMF in 231-TGL cells seeded on 0.6, 5, 20, 35 kPa polyacrylamide hydrogel and TCP (n=3). (Error bars represent s.e.m., ****: $P < 0.0001$.)

4.2.5 Verification of the effectiveness of pNDRG1-mCherry biosensor in vitro and in vivo

After successful stable transfection and selection of pNDRG1-mCherry and 3X FLAG-fluc plasmids into a 231-WT cell line. To test the effectiveness of the sensor in vitro, we seeded the transfected pNDRG1-mCherry-fluc-231 cell line on 0.6 kPa and 35 kPa polyacrylamide hydrogels (Fig. 4.3a), confocal microscopy proved the mCherry level of (short-term) soft-primed pNDRG1-mCherry-fluc-231 was significantly upregulated than stiff-primed (Fig. 4.3b). Flow cytometry confirmed the increasement trend, and the final positive ratio is about 13% (Fig. 4.3c).

More importantly, the pNDRG1-mCherry-fluc-231 cell line was orthotopically injected into the fat pad to form a mechanical heterogeneous tumor xenograft, then we cryo-stat sectioned the tumor (Fig. 2.3d). We conducted SHG to visualize the collagen fibers as stiffness indicator, we found in both tumor core and periphery mCherry^{-} cells co-localized with aligned collagen fibers while mCherry^{+} cells did not (Fig. 4.3e), then we directly measured the stiffness of the fresh cryo-stat sectioned tumor slides, the results showed mCherry only rose where Young's modulus was extremely low (~ 1000 Pa or less), while Young's modulus of other areas is ~10 kPa (Fig. 4.3e,f). These results substantiated the pNDRG1-mCherry biosensor well-functioned in vitro and in vivo with high efficiency, we would be able to identify and furtherly separate subpopulations residing on local niches with different stiffness.

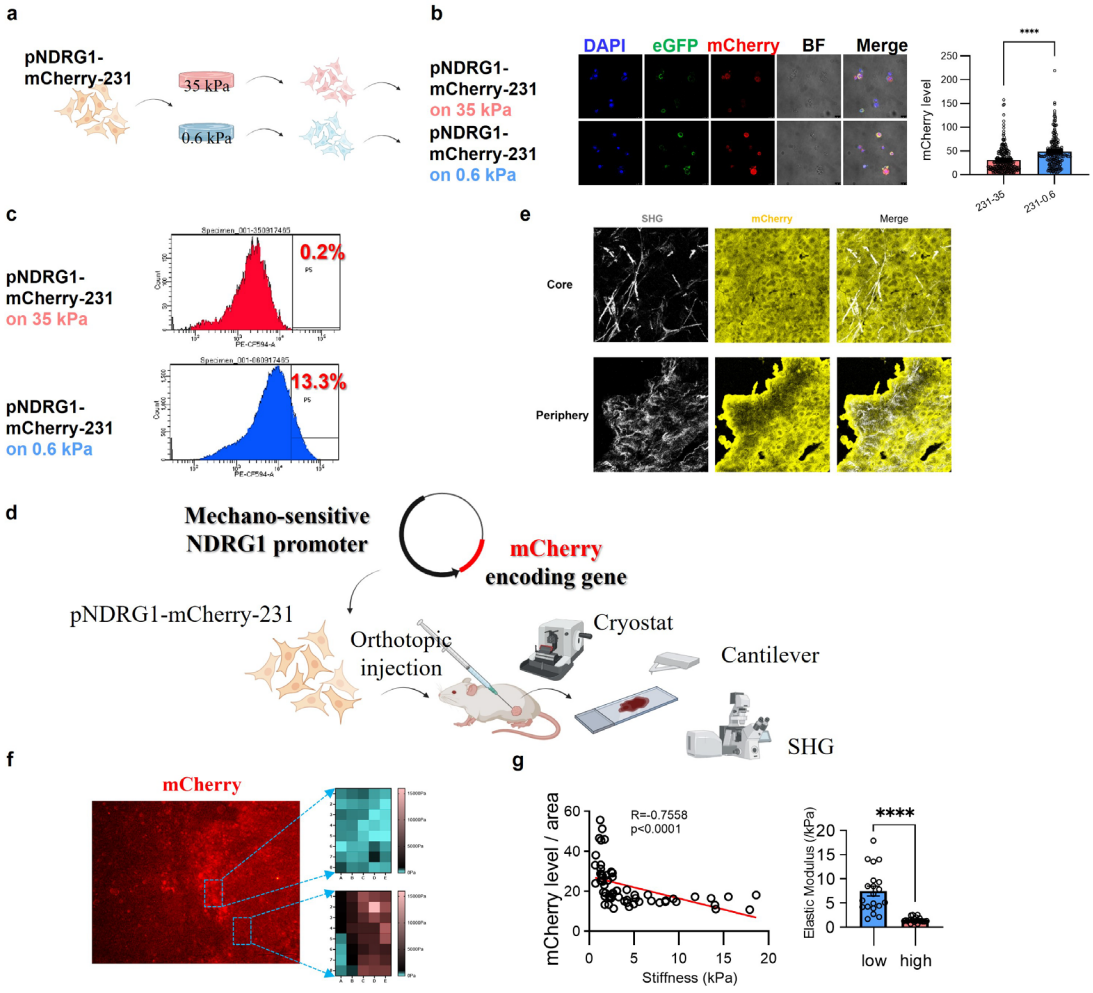

Fig. 4.3 Verification of the effectiveness of pNDRG1-mCherry biosensor in vitro and in vivo. (a) Workflow, (b) representative confocal microscopy images and statistical analysis (with Mann-Whitney U test) of pNDRG1-mCherry-231 cells seeded on 0.6 and 35 kPa polyacrylamide hydrogel

(n=228/189). (c). Flow cytometry graph of pNDRG1-mCherry-231 seeded on 0.6 and 35 kPa polyacrylamide hydrogel. (d) Workflow, (e-g) Multiphoton microscopy, fluorescence microscopy, atom force microscopy, and statistical analysis (with simple linear regression and two-tailed Welch's t-test) of elastic modulus mapping of mouse fat pad orthotopic tumor xenograft generated from pNDRG1-mCherry-231 cell line (n=60). (Error bars represent s.e.m., ****: $P < 0.0001$.)

4.2.6 Fidelity of the developed biosensor to represent the local niche stiffness in vivo

Before we start, there's a series of issues that need solving. Firstly, we exclude cell line dependency by testing the effectiveness of the pNDRG1-mCherry sensor in the MCF-7 and SK-BR-3 cell lines (Fig. 4.4a). Then, our previous finding showed that in long-term culture scenarios, some specific genes (such as brain metastasis genes, bone metastasis genes, inflammation-related genes, neuro-related genes, etc.) displayed a time-dependent increasing tendency, we hope our sensor signal to be stable and trustable, thus we cultured pNDRG1-mCherry-fluc-231 on 0.6 kPa and 35 kPa for 30 days (shorted for pNDRG1-mCherry-fluc-231-0.6/35), check whether the signal outcome showed an accumulative effect, flow cytometry results found the mCherry peak slightly shifted, however, the positive ratio remains stably comparing long-term culture with short-term culture (Fig. 4.4b), we suppose this will not influence our actions afterwards.

Next, we were concerned that the plasmid/lentivirus transfection process naturally introduced an extra variable, which is the copy number of the pNDRG1-mCherry element. mCherry signal outcome of pNDRG1-mCherry-fluc-231 cell line with imbalanced copy number cannot accurately reflect the local niche stiffness info, therefore, we conducted single cell clone technique and obtained pNDRG1-mCherry-fluc-231-scp1 cell line and check the sensor reporting performance. As a result, we observed a relatively narrow peak and a dramatic rise in the positive ratio in soft-primed pNDRG1-mCherry-fluc-231-scp1 vs stiff-primed (Fig. 4.4c). This clone was applied for the remainder of this study.

Next, regarding NDRG1, its role in tumor progression, especially metastasis, was controversial in

previous research. Plenty of evidence has demonstrated that NDRG1 functions as a metastasis suppressor, such as recent research showed metixene, an anti-Parkinson drug, directly up-regulates and phosphorylates NDRG1 to prevent breast cancer (231-BrM and other cell lines) brain metastasis [383], meanwhile, some research claimed NDRG1 regulates or at least correlates with brain metastatic potential or related signaling (like lipid metabolism [148, 149, 151, 384-386]) [387-391].

On the one hand, the possibility that the inserted pNDRG1-mCherry element would competitively inhibit the increasing trend of brain metastasis cannot be easily excluded. So, we used RT-qPCR to confirm our previous finding, luckily the promoting effect of soft-priming on brain-metastatic potential remained in pNDRG1-mCherry-fluc-231-scp1-0.6 (Fig. 4.4d)

Since we had excluded competitive inhibition, on the other hand, we wouldn't expect NDRG1 itself could function as a brain metastasis regulator independent of tissue mechanics, or the methodology to use mCherry/pNDRG1 transcription level as a ruler to represent the local niche softness, then looking for a positive correlation between mCherry(pNDRG1) and brain metastasis capacity could be an entire circular argument. Hence, we applied FACS to sort out the $mCherry^{hi}$ and $mCherry^{lo}$ (defined by highest/lowest 10% mCherry level) from TCP cultured pNDRG1-mCherry-fluc-231-scp1 (Fig. 4.4e), to check whether mCherry level naturally represented brain metastatic subpopulation independent of stiffness heterogeneity. Unexpectedly, we found $mCherry^{hi}$ group signified lower brain metastasis potential (Cox-2, SerpinB2 level) instead of higher (Fig. 4.4f,g), while had no impact on bone metastasis potential when stiffness was homogenous (Fig. 2.4h).

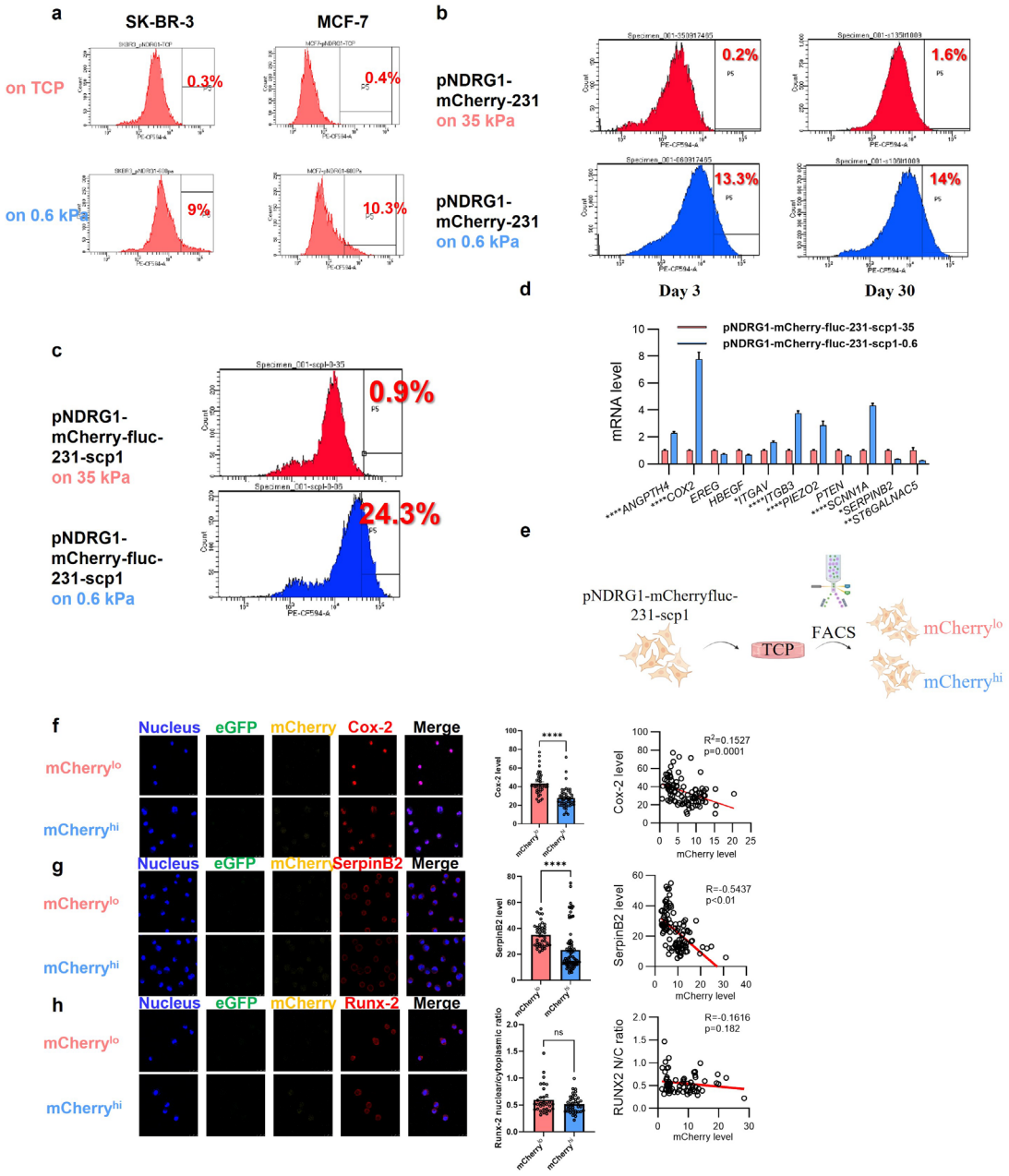

Fig. 4.4 Fidelity of the developed biosensor to represent the local niche stiffness in vivo. (a). Flow cytometry graph of pNDRG1-mCherry-SK-BR-3 and pNDRG1-mCherry-MCF-7 cells seeded on 0.6 kPa polyacrylamide hydrogel and TCP. (b). Flow cytometry graph of pNDRG1-mCherry-231 cells seeded on 0.6 and 35 kPa polyacrylamide hydrogel for 3 days and 30 days. (c). Flow cytometry graph of pNDRG1-mCherry-fluc-231-scp1 cells seeded on 0.6 and 35 kPa polyacrylamide hydrogel. (d). mRNA transcriptional level and statistical analysis (with two-tailed Welch's t-test) of representative brain metastatic genes in pNDRG1-mCherry-fluc-231-scp1-0.6 cells and pNDRG1-mCherry-fluc-231-scp1-35 (n=3). (e). Workflow, (f-h) representative confocal microscopy images and statistical analysis (with Mann-Whitney U test and simple linear regression) of mCherry^{hi} and mCherry^{lo} cells identified by FACS from pNDRG1-mCherry-fluc-231-scp1 cultured on TCP (n=40/53 for Cox-2, n=42/81 for SerpinB2, n=32/38 for Runx-2,). (Error bars represent s.e.m., ns: no significance, ****: P < 0.0001.)

4.2.7 Local niche softness within tumor xenografts correlated with breast cancer brain organotropism

After all the above-mentioned preparation, we could use the sensor system to interrogate the brain metastasis potential of soft/stiff local niche residing cancer cells in orthotopic xenograft.

First, we examined the brain metastasis potential of soft/stiff local niche residing cancer cells. Firstly, we conducted IF staining at cryo-stat sectioned tumor xenograft slides, and directly checked whether the brain metastatic gene positively correlated with mCherry softness-representing signal in situ (Fig. 4.5a). The results demonstrated compared with the previous result that brain metastatic genes negatively correlated with the mCherry signal without the presence of mechanical heterogeneity, which was the baseline (Fig. 4.5e-g), here the negative correlation between Cox-2 expression level and mCherry signal disappeared, meanwhile, the SerpinB2 level rose and displayed a significant positive correlation with mCherry level at single-cell scale (Fig. 4.5b and c), while Runx-2 N/C ratio (as bone-metastatic potential ruler [84]) showed a greatly negative correlation with mCherry signal at single-cell scale (Fig. 4.5d). We also stained F-actin (our previous study showed cytoskeletons are indicators of metastatic organotropism [179]) and HDAC3 (the mechanistic molecule we identified that softness induced to promote brain metastasis in vitro). We also noticed a positive/negative correlation between HDAC3 level as well as F-actin signaling and mCherry signal at single-cell scale (Fig. 4.5c and e). Noted that Runx-2 nuclear translocation and actin polymerization are both well-known direct mechanical responses, thus these results were another two proves that our single-cell scale pNDRG1-mCherry softness biosensor well-functioned in vivo as expected [192, 392-394].

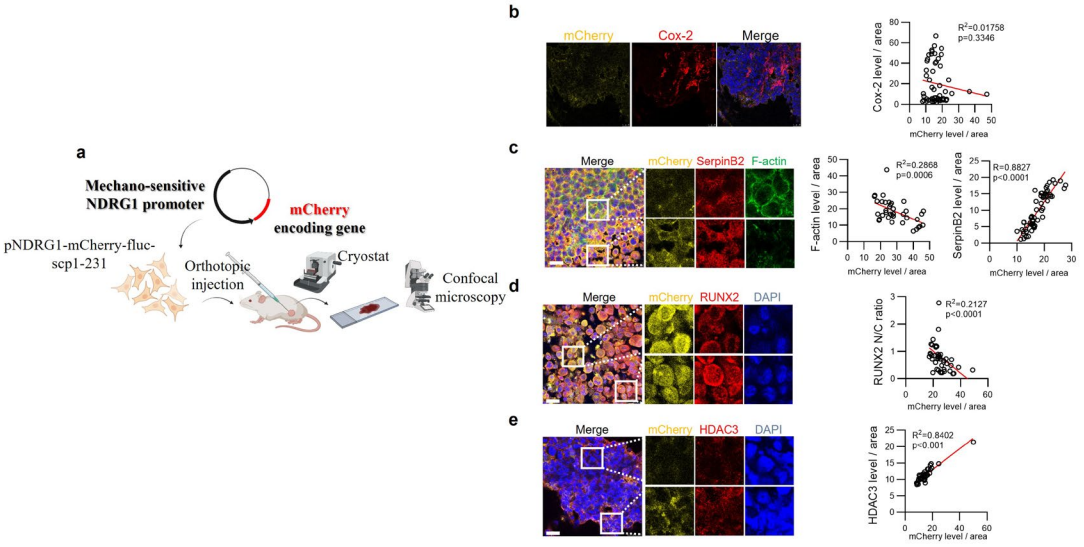

Fig. 4.5 Intratumoral local niche softness correlated with brain metastatic markers and HDAC3 level in situ. (a). Workflow, (b-e) representative confocal microscopy images and statistical analysis (with simple liner regression) of mCherry, Cox-2 (n=55), SerpinB2 (n=59), F-actin (n=59), Runx-2 (n=43), and HDAC3 (n=41) in mouse fat pad orthotopic tumor xenograft slides generated from pNDRG1-mCherry-fluc-231-scp1 cell line.

In-situ colocalization analysis straightly links local niche softness and brain metastasis potential, nevertheless, metastasis is a process started after cancer cells shed from the primary tumor, this is currently what only we could do based on the established stiffness sensor system. Here we designed a “gating-in-vitro and sorting-from-vivo” workflow (Fig. 4.6a), in detail, to separate the soft/stiff local niche resident subpopulations, firstly we should define the precise level of mCherry signal, above which we could assume that single cell was likely to be harvested from soft local niche, so we cultured the pNDRG1-mCherry-fluc-231-scp1 cell on 0.6 kPa and 35 kPa polyacrylamide hydrogels in vitro, and define the mCherry level that stiff-primed could hardly reach (ratio < 1%) in vitro as “mCherry^{+} gate”.

Next, the same pNDRG1-mCherry-fluc-231-scp1 clone was orthotopically injected into nude mouse fat pad. After the successful establishment of a pNDRG1-mCherry-fluc-231-scp1-based tumor xenograft with naturally self-established intrinsic mechanical heterogeneity, we harvested the tumor xenograft, minced the xenograft and digested it with trypsin and collagenase, the MACS procedure was applied to the digested tissue suspension with mouse cell depletion kit to exclude all non-cancer stroma cells afterwards, at last, we employed FACS to the collected cancer cell mixtures,

and the subpopulation with mCherry level above the "mCherry^{+} gate" was defined as mCherry^{+} cells, we assume it was located in soft local niches in the tumor, while others were defined as mCherry^{-} cells as a control. Please note that rigorously speaking, we can only guarantee mCherry^{+} cells were likely to have lived on soft niches in xenograft, however, we cannot be sure where mCherry^{-} group was harvested from. From the results we can tell, compared with polyacrylamide hydrogel-primed pNDRG1-mCherry-fluc-231-scp1 clone, xenograft-derived cell population showed a wide and skew distribution where mCherry positive ratio was ~5% or less (Fig. 4.6b), suggesting most cells were residing on stiff local niches in tumor xenograft, consistent with the generally accepted notion at most tumor is globally stiffened along with cancer progression [53, 55, 78, 84, 88, 91, 102, 103, 112].

We applied FACS to separate mCherry^{+} and mCherry^{-} cells and did a similar comparison, the result came out similar, Cox-2 level in mCherry^{+} group cells increased to the level that is comparable with mCherry^{-} group (Fig. 4.6c), SerpinB2 level in mCherry^{+} group increased and was even higher than mCherry^{-} group (Fig. 4.6d), meanwhile the Runx-2 N/C ratio was much higher in mCherry^{-} group than the counterpart in mCherry^{+} group (Fig. 4.6e). Besides, we detected the HDAC3 activity of mCherry^{+} and mCherry^{-} cells, and the results were consistent with our previous finding in vitro, soft local niche residing mCherry^{+} cells exhibited higher HDAC3 enzymatic activity (Fig. 4.6f). All the above results indicated that in the primary tumor, local niche softness/stiffness strongly correlated with brain/bone metastatic potential.

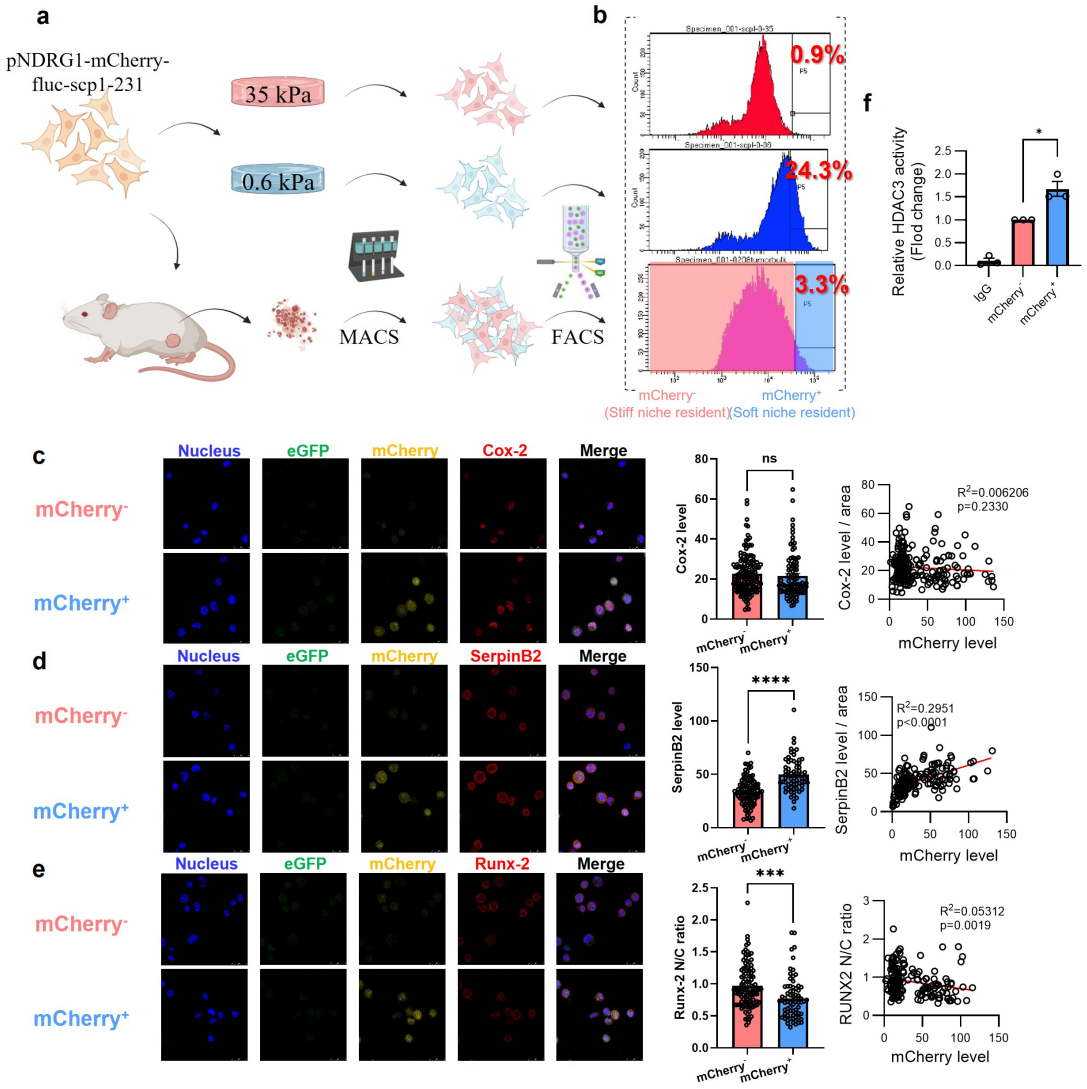

Fig. 4.6 Tumor cells residing in local soft niches of the xenografts displayed higher levels of brain metastasis markers and HDAC3 activity. (a). Workflow of "gating-in-vitro and sorting-from-vivo" and (b) flow cytometry graph of pNDRG1-mCherry-fluc-231-scp1 seeded on 0.6 and 35 kPa polyacrylamide hydrogel and the tumor cells harvested from pNDRG1-mCherry-fluc-231-scp1 mouse fat pad orthotopic tumor xenograft (n=3). (c-e). Representative confocal microscopy images and statistical analysis (with Mann-Whitney U test and simple linear regression) of mCherry, Cox-2 (n=139/92), SerpinB2 (n=99/67), and Runx-2 (n=108/72) in mCherry$^-$ and mCherry$^+$ cells. (f). HDAC3 activity of and statistical analysis (with two-tailed Welch's t-test) of mCherry$^-$ and mCherry$^+$ cells. (Error bars represent s.e.m., ns: no significance, *: $P < 0.05$, ***: $P < 0.001$, ****: $P < 0.0001$.)

After that, we tested the classical cancer cell brain metastatic functions of soft/stiff-residing mCherry$^+$/mCherry$^-$ cells obtained from tumor xenograft.

BBB is an integrated semi-permeable structure that selectively permits specific molecules or cell types to pass, it consists of three components: brain endothelial cell of the brain microcapillary,

astrocyte end-feet ensheathing the microcapillary, and pericyte to embed in the basement membrane of the brain microcapillary. BBB stops the passage of any harmful or unwanted pathogens, molecules, or cell types, cancer cells included. It's believed that BBB is one of the biggest barriers for cancer cells to establish brain metastasis. Here we used an in-vitro BBB-transmigration model to examine the BBB trans-migration ability of $mCherry^+$ and $mCherry^-$ cells, it was found $mCherry^+$ group showed a significant BBB trans-migration ability advantage over than $mCherry^-$ cells (Fig. 4.7a).

Next, we check the proliferation ability of $mCherry^+$ and $mCherry^-$ populations in a soft microenvironment. Both groups were seeded on 0.6 kPa and 35 kPa polyacrylamide hydrogels after FACS and applied Ki67 staining after 24 hours to interrogate their proliferation ability in different mechanical conditions, $mCherry^+$ group showed a higher proliferation ratio on 0.6 hydrogel and compromised proliferation ability on 35 kPa comparing with $mCherry^-$ group (Fig. 4.7b), indicating soft/stiff-local niche residing cells displayed proliferative advantage in niches with corresponded niches and held stronger clonal expanding ability on brain/bone-stiffness mimicking biomaterial. Interestingly, for both groups the above-mentioned proliferative advantage remained after 7-day culture on TCP right after FACS from tumor xenograft (Fig. 4.7c), reminiscent of the long metastatic journey in vivo and mechanical memory in organotropism maintaining [2, 4, 13, 20, 31, 80, 81, 84, 99, 134, 136, 157].

Then we validated the colonization ability of $mCherry^+$ and $mCherry^-$ populations in complex real brain microenvironment by seeding $mCherry^+$ and $mCherry^-$ cells on fresh vibratome sectioned brain tissue slides and co-culturing for 48h, then detected the bioluminescence intensity of cancer cells, which to find $mCherry^+$ group showed superior brain colonization capability (Fig. 4.7d).

These results indicated soft/stiff-local niche residing cells displayed advantages in each individual brain metastasis-related function, including transmigration through BBB to approach the brain, proliferation on niches with brain corresponded softness, and colonization in the complicated brain microenvironment.

At last, we tested the overall brain metastasis potential of mCherry$^+$ and mCherry$^-$ subpopulations in vivo, mCherry$^+$ and mCherry$^-$ cells were intracardiac injected into left ventricles of healthy nude mice and routinely monitored the organ-specific metastasis condition with in vivo animal imaging system (ivis) every week, the mCherry$^+$ cells exhibited superior brain macrometastasis establishment capacity than mCherry$^-$ cells (Fig. 4.7e). Moreover, the mouse brains were harvested after sacrificing, and ex-vivo luminescence imaging confirmed the metastasis advantage of mCherry$^+$ cells in brain tissue (Fig. 4.7f).

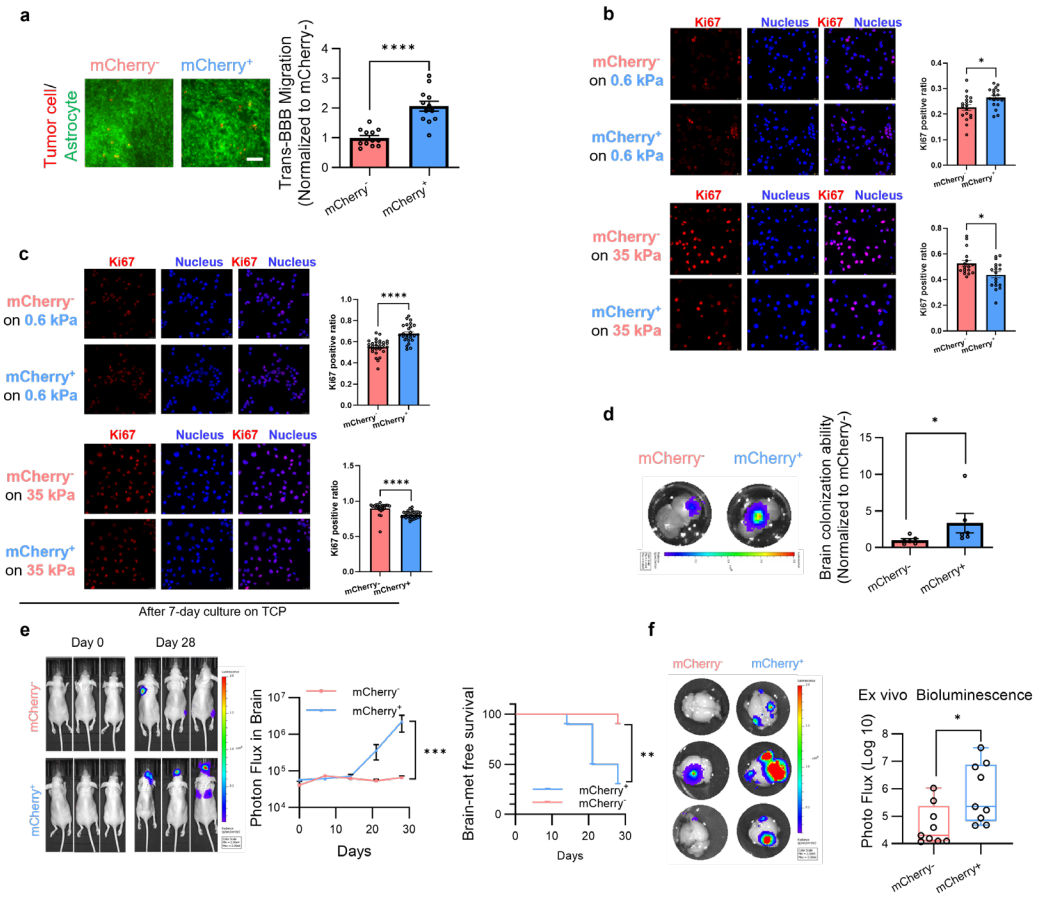

Fig. 4.7 Tumor cells residing in local soft niches of the xenografts exhibited brain metastatic capability in vitro and in vivo. (a). Representative fluorescence microscopy images and statistical analysis (with two-tailed Welch's t-test) of trans-BBB migration assay of mCherry$^-$ and mCherry$^+$ cells (n=12). (b). Representative confocal fluorescence microscopy images and statistical analysis (with two-tailed Welch's t-test) of Ki67 of mCherry$^-$ and mCherry$^+$ cells seeded on 0.6 (n=18) and 35 kPa (n=17/18) polyacrylamide hydrogel. (c). Representative confocal fluorescence microscopy images and statistical analysis (with two-tailed Welch's t-test) of Ki67 of mCherry$^-$ and mCherry$^+$ cells seeded on 0.6 (n=28/26) and 35 kPa (n=24/30) polyacrylamide hydrogel after 7-day culture on TCP. (d). Representative bioluminescence images and statistical analysis (with Mann-Whitney U test) of brain slide co-culture assay of mCherry$^-$ and mCherry$^+$ cells (n=6). (e). Representative bioluminescence images and statistical

analysis (with two-way ANOVA Šídák's multiple comparisons test and log-rank survival test) of nude mice intracardiacally injected with mCherry$^-$ and mCherry$^+$ cells (n=10). (f). Representative bioluminescence images and statistical analysis (with Mann-Whitney U test) of ex-vivo brains of nude mice intracardiacally injected with mCherry$^-$ and mCherry$^+$ cells (n=10). (Error bars represent s.e.m., *: $P < 0.05$, **: $P < 0.01$, ***: $P < 0.001$, ****: $P < 0.0001$.)

To fully understand the difference between mCherry$^+$ and mCherry$^-$ subpopulations harvested based on local niche stiffness, here we did an RNA-seq analysis of these two groups. Three independent orthotopic tumor xenografts were examined (Fig. 4.8a), the result showed that consistent with our previous RNA-seq finding in vitro, brain but not bone metastatic genes exhibited a broad spectrum of increasement in mCherry$^+$ group (Fig. 4.8b,c), meanwhile GO and KEGG analysis found series brain metastasis-related, neuron-related and inflammation-related terms and signaling pathways are enriched, suggesting mCherry$^+$ displayed a brain-tropic phenotype reprogramming in vivo (Fig. 4.8d,e).

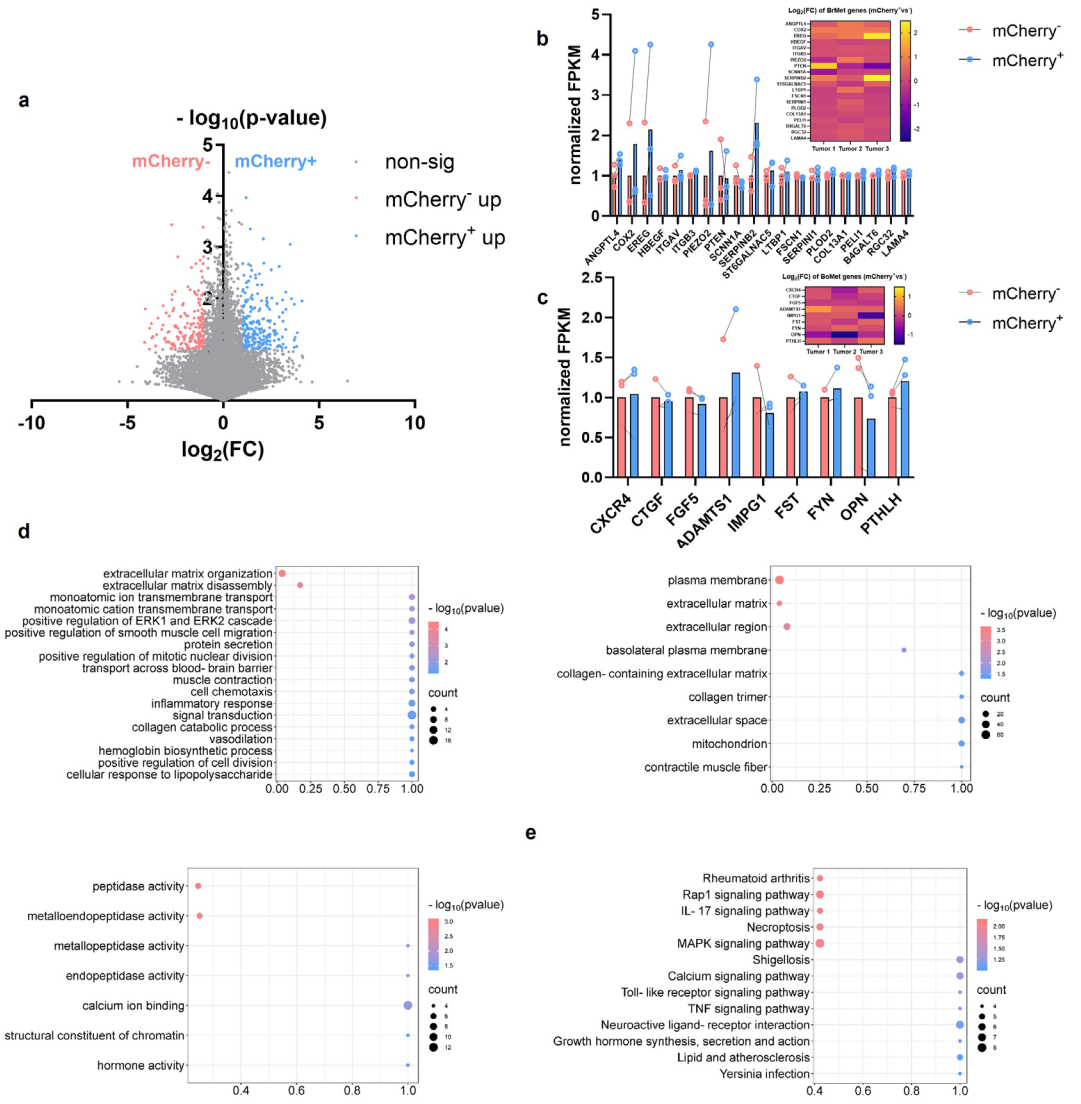

Fig. 4.8 Tumor cells residing in local soft niches of the xenografts exhibited brain metastatic phenotype and gene signature. (a). Volcano plot of transcriptomes of mCherry$^-$ and mCherry$^+$ cells. (b). mRNA transcriptional level and statistical analysis of representative bone metastatic genes in mCherry$^-$ and mCherry$^+$ cells (n=3). (c). mRNA transcriptional level and statistical analysis of representative brain metastatic genes in mCherry$^-$ and mCherry$^+$ cells (n=3). (d,e). Signaling pathways enriched in mCherry$^+$ cells with GO and KEGG enrichment.

Noted in this series of experiments, no additional mechanical intervention was included, all the mechanical stimulation to both mCherry$^+$ and mCherry$^-$ cells occurred in a self-organized naturally grown tumor xenograft (Fig. 4.5-3.8). All these results confirmed that the correlation between local niche softness, HDAC3, and brain-tropic metastasis potential truly existed without mechanical intervention in vivo.

Chapter V: Compromised ECM remodeling, negative-durotaxis, positive-viscotaxis and cell competition promote niche softness-induced brain metastasis

5.1 Objectives and scopes

In the last Chapter, we confirmed the findings that long-term soft-priming enhanced brain metastatic potential in vitro did occur in tumor xenografts. Since the acquisition of brain metastatic potential requires persistent priming in soft niches and cell migration in vivo is dynamic, it remains intriguing how this process is successfully achieved in vivo, where the microenvironment is mechanically heterogeneous.

In detail, three occasions should be well-explained:

1. Tumor cells do not constantly reside in the same location, jamming behaviors and cellular streams emerge inside a heterogenous tumor [169], most cancer cells were believed to be durotactic [52, 180], especially MDA-MB-231 breast cancer cells [52, 190], if these cancer cells follow similar principles in vivo, soft niche resident might migrate towards stiff niche, which cannot explain how the long-term mechanical stimuli were achieved. On the other hand, the mechanical microenvironment in tumor tissue is complicated, is there some other mechanical property that is strongly associated with tissue softness in the local niche scale, to induce soft-primed cells to migrate towards it?
2. In our previous finding, clonal selection and reprogramming co-exist on soft biomaterials, actually this process could be more complicated, as cancer cells compete with each other as well as the stroma cells [41, 70, 327, 330-335, 344, 358, 360-363, 369, 371, 372, 395]. Since the sensor outcome varies in three days and the short-term external mechanical dosing governed brain metastatic organotropism, there must be a mechanism controlling the population dominance in a corresponding niche, the proliferative advantage of soft-primed cells and $mCherry^+$ cells in the soft niche may partially explain the phenomenon, whether the cell competition between mechanically distinct local niche residing populations supports the clonal dominance remains unknown;
3. In primary tumor, tissue ECM is dynamically under synthesis, secretion, modification, and degradation [102, 105, 110, 202, 224, 225, 227, 230, 231, 233, 234], it's possible that for each cell, local niche stiffness gradually changes during tumor progression, is there a mechanism forbidding this possibility otherwise the long-term soft-priming cannot be guaranteed?

In summary, currently how cancer cells continuously accept similar mechanical signals in corresponding mechanical microenvironments in heterogenous tumor mass is unclear. How the mechanically heterogenous microenvironment is formed is also not understood.

To the best of our knowledge, the process of soft-priming in vivo is completely unknown. Uncovering the supporting mechanism of how mechanics-evoked organotropism is formed helps the academic society better understand the basic self-organization and co-evolution pattern of cancer cells and tissue mechanics in heterogeneous TME.

Thus, we raised the research question: what are the mechanisms supporting the long-term softness stimulations so that brain organotropism could be established eventually? To tackle this problem, here we focused on three main objectives:

1. Elucidate what makes soft-primed cells overcome durotaxis;
2. Test whether cell competition collaborates with proliferation advantage, jointly support the clonal dominance of soft-primed cells in soft local niche;
3. Clarify why the local niche around soft-primed cells is not stiffened.

5.2 Results

5.2.1 Soft-primed cells exhibit reduced mechanosensitivity to substrate rigidity-mediated YAP nuclear translocation and clutch reinforcement

As explained in Objectives and scopes, we hypothesized that tumor cells residing in local soft niches were negative durotaxis, which could enable persistent priming of tumor cells in soft microenvironments. As introduced in the Literature Review, current explanation of the behavior of negative durotaxis was the loss of clutch reinforcement and the generation of maximized

contractility on the substrate with optimal or relatively low stiffness[51, 322, 323]. Usually, the loss of clutch reinforcement meanwhile unsensitized cells to mechanical cues [51, 322, 323].

Firstly, we tested the mechano-sensitivity of soft-primed and stiff-primed cancer cells. The difference in proliferation rate is the most straightforward mechanical response, we noticed in Fig. 4.8, that no proliferation-related signaling was enriched. Here we analyzed the mCherry level of proliferating and non-proliferating cells to check the local niche stiffness of each group in tumor xenograft to confirm, consistently no significant difference was found between the two groups (Fig. 5.1a), suggesting soft niche residents were not in cell cycle arrest. YAP and focal adhesion mechano-sensitivity were reported to correlate with diverse positive/negative-durotaxis patterns [51], YAP was also found to regulate negative-durotaxis levels in melanoma [191]. Thus, we focused on YAP nuclear translocation and focal adhesion formation level on polyacrylamide hydrogels with different stiffness. We seed 231-0.6 and 231-35 on polyacrylamide hydrogels of 0.6, 2, 5, 15, 35 kPa and TCP, YAP nuclear translocation level of 231-0.6 was dramatically unsensitized in responsive to mechanical stimulation than 231-35 (Fig. 5.1b), meanwhile, 231-0.6 formed limited focal adhesion on 35 kPa polyacrylamide hydrogel compared with 231-35 (Fig. 5.1c), this flaw sustained even culturing on glass with super-physilogical stiffness (Fig. 5.1d). We collected $mCherry^+$ and $mCherry^-$ cells from tumor xenograft and seeded both groups on 0.6 and 35 kPa immediately, similar YAP nuclear translocation and focal adhesion formation mechano-insensitivity were detected (Fig. 5.1e). All these results implied that mechano-sensitivity was compromised in both soft hydrogel-primed cells in vitro and soft local niche residents in vivo.

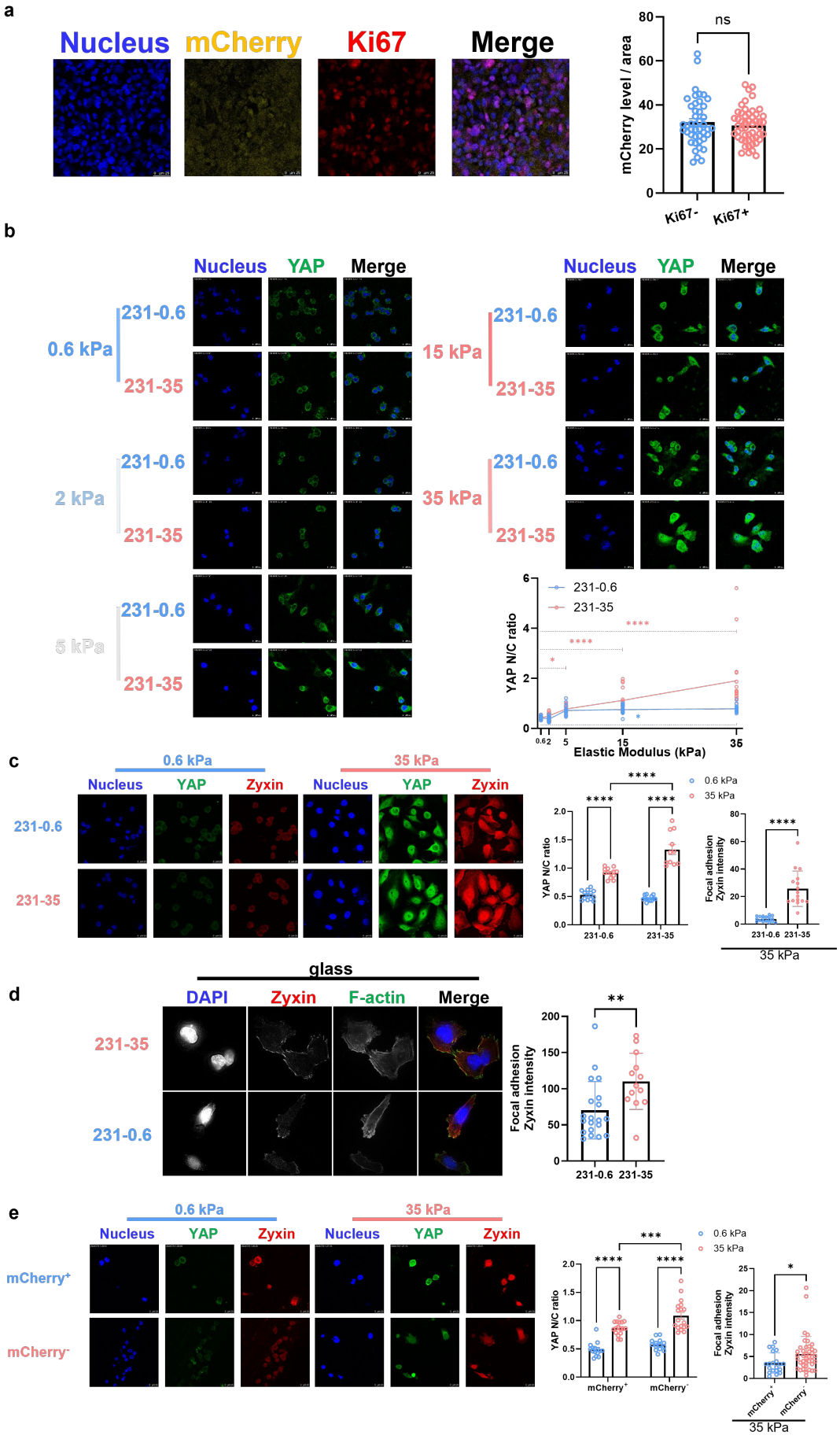
a
Nucleus
mCherry
Ki67
Merge
ns
mCherry level / area
Ki67-
Ki67+
b
Nucleus
YAP
Merge
0.6 kPa
2 kPa
5 kPa
15 kPa
35 kPa
231-0.6
231-35
YAP N/C ratio
Elastic Modulus (kPa)
c
0.6 kPa
35 kPa
Zyxin
Focal adhesion Zyxin intensity
d
glass
DAPI
F-actin
e
mCherry+
mCherry-

Fig. 5.1 Soft-primed cells are less sensitive to matrix rigidity-mediated YAP nuclear translocation and clutch reinforcement. (a) Representative confocal microscopy images and statistical analysis (with two-tailed Welch's t-test) of mCherry and Ki67 in mouse fat pad orthotopic tumor xenograft slides generated from pNDRG1-mCherry-fluc-231-scp1 cell line (n=44/51). (b) Representative confocal microscopy images and statistical analysis (with two-way ANOVA Šídák's multiple comparisons test) of YAP in 231-0.6 and 231-35 cells seeded on 0.6 (n=19/15), 2 (n=20/19), 5 (n=17/20), 15 (n=19/18) and 35 kPa (n=20/17) polyacrylamide hydrogel. (c) Representative confocal microscopy images and statistical analysis of YAP (with two-way ANOVA Šídák's multiple comparisons test) in 231-0.6 and 231-35 seeded on 0.6 (n=13/13), and 35 kPa (n=13/11) polyacrylamide hydrogel and zyxin (with Mann-Whitney U test) in 231-0.6 and 231-35 cells (n=18/16) seeded on 35 kPa polyacrylamide hydrogel. (d) Representative SIM super resolution microscopy images and statistical analysis of F-actin and zyxin (with Mann-Whitney U test) in 231-0.6 and 231-35 cells seeded on glass (n=17/20). (e) Representative confocal microscopy images and statistical analysis of YAP (with two-way ANOVA Šídák's multiple comparisons test) in $mCherry^-$ and $mCherry^+$ cells seeded on 0.6 (n=15/14), and 35 kPa (n=17/18) polyacrylamide hydrogel and zyxin (with Mann-Whitney U test) in $mCherry^-$ and $mCherry^+$ cells seeded on 35 kPa polyacrylamide hydrogel (n=20/41). (Error bars represent s.e.m., ns: no significance, *: $P < 0.05$, **: $P < 0.01$, ***: $P < 0.001$, ****: $P < 0.0001$.)

5.2.2 Tumor cells residing in local soft niches are negative durotactic

Mechano-insensitivity was often associated with negative durotaxis in theory and practice [51, 322, 323]. To determine whether soft priming indeed shifted cancer cell durotaxis pattern to negative-durotaxis, we established 5-35 kPa hybrid gradient stiffness polyacrylamide hydrogel as previously described in other research [51, 191]. To check the migration direction of soft-primed cells, we utilized gradient stiffness hydrogel, live cell imaging, and single-cell trajectory (Fig. 5.2a). We found that soft-primed cancer cells displayed a negative-durotaxis pattern distinct from the stiff-primed control group (Fig. 5.2b). To confirm the soft niche resident in tumor xenograft shared similar negative-durotaxis behavior, we did a similar experiment on $mCherry^+$ and $mCherry^-$ cells, the result demonstrated soft niche-residing cells were also negative-durotactic (Fig. 5.2c,d).

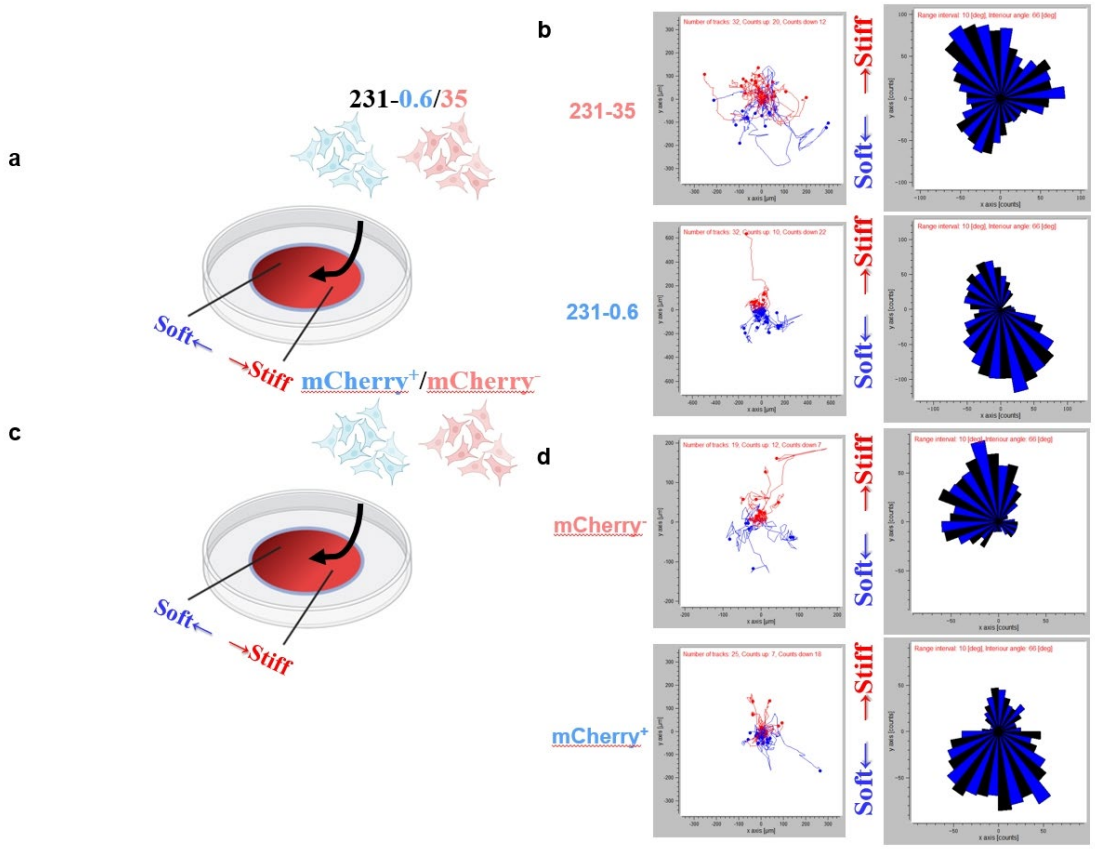

Fig. 5.2 Soft-primed cells are negative durotactic. (a). Workflow, (b) single cell trajectory and radar graph of 231-0.6 and 231-35 cells seeded on gradient stiffness polyacrylamide hydrogel. (c). Workflow, (d) single cell trajectory and radar graph of mCherry^{-} and mCherry^{+} cells seeded on gradient stiffness polyacrylamide hydrogel.

5.2.3 Soft priming shifts durotaxis pattern by hyperactivating integrin α10-Akt axis

Different from previous sporadic reports about some negative-durotactic cell types [51, 191, 321], here we found a way to shift the durotaxis behavior in the same cell type, this new finding makes it possible for us to interrogate the underlying signaling mechanism of durotaxis. Currently motor-clutch model without clutch reinforcement is the only explanation for negative-durotaxis behavior [190, 322, 323], the force between cells and substrate is generated by the ECM ligand-integrin bond. So we wonder if the negative-durotaxis and positive-viscotaxis behavior of 231-0.6 was caused by the down-regulation of some specific integrin subunit gene. Here we did an RNA-seq of 231-0.6 and 231-35 and checked the integrin and focal adhesion-related signaling using Gene Ontology (GO)

and Kyoto Encyclopedia of Genes and Genomes (KEGG) term enrichment, surprisingly we found several integrins, focal adhesion signaling, and PI3K-Akt axis as the downstream were enriched in 231-0.6 group (Fig. 5.3a). The volcano plot demonstrated integrin α10 encoding gene ITGA10 was the most impacted integrin gene in differentially expressed genes (DEGs) (Fig. 5.3b), suggesting the potential regulatory role. Existed research claimed that the Akt pathway was the dominant downstream of integrin α10 in many cellular functions in several cell types [396-399]. To confirm that the activation of the Akt signaling was mediated by integrin α10 in our case, we used small hairpin RNA (shRNA/Hairpin Vector) to knock down the ITGA10 gene before 30-day soft priming (Fig. 5.3c) (stable cell line shorted for 231-shITGA10-0.6) and applied IF staining and found p-Akt level were higher in 231-0.6 and rescued after shITGA10 treatment (Fig. 5.3d,e).

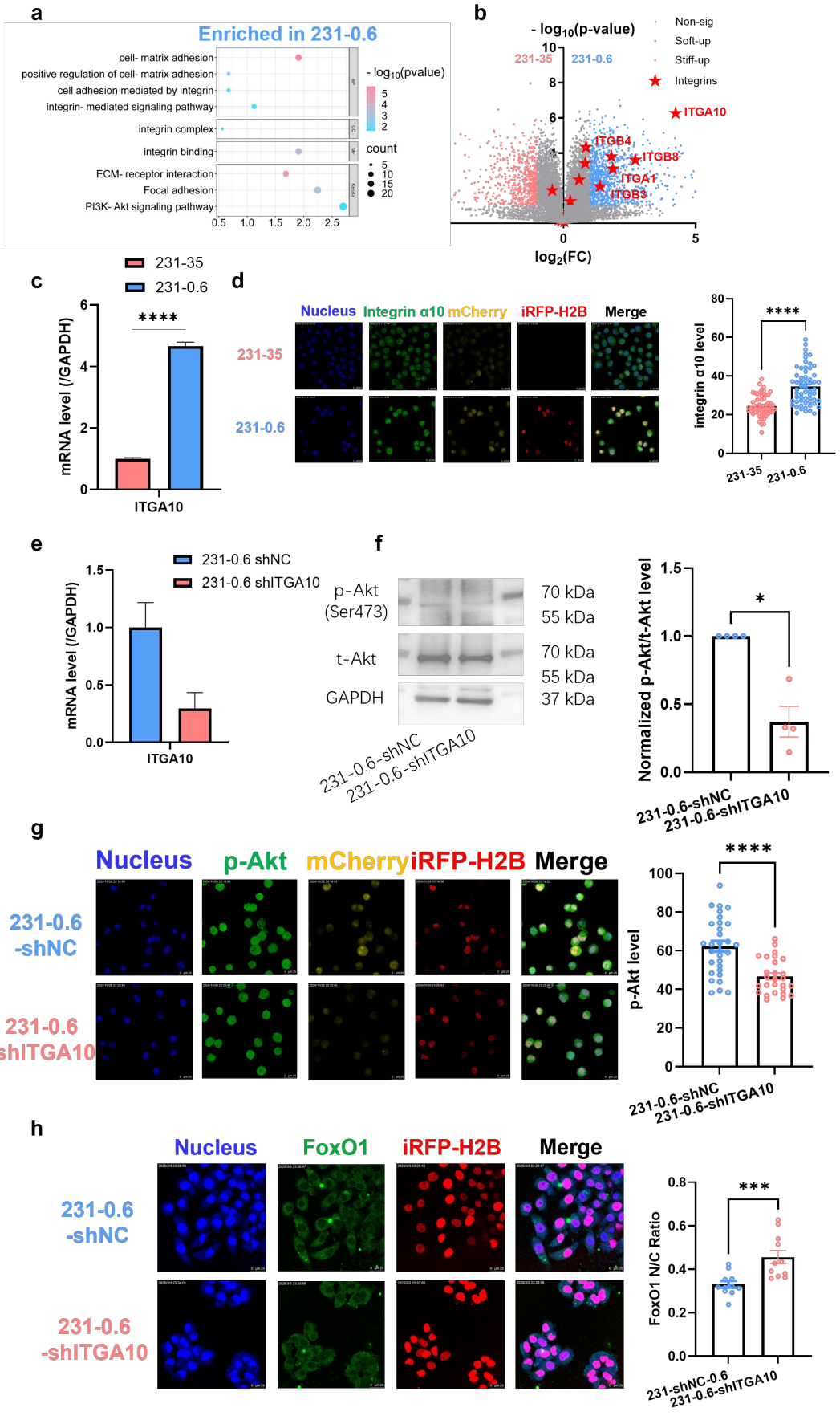
a
Enriched in 231-0.6
cell- matrix adhesion
positive regulation of cell- matrix adhesion
cell adhesion mediated by integrin
integrin- mediated signaling pathway
integrin complex
integrin binding
ECM- receptor interaction
Focal adhesion
PI3K- Akt signaling pathway
- log10(pvalue)
count
b
- log10(p-value)
231-35
231-0.6
Non-sig
Soft-up
Stiff-up
Integrins
ITGA10
ITGB4
ITGB8
ITGA1
ITGB3
log2(FC)
c
231-35
231-0.6
mRNA level (/GAPDH)
****
ITGA10
d
Nucleus
Integrin α10
mCherry
iRFP-H2B
Merge
231-35
231-0.6
integrin α10 level
****
231-35
231-0.6
e
231-0.6 shNC
231-0.6 shITGA10
mRNA level (/GAPDH)
ITGA10
f
p-Akt (Ser473)
t-Akt
GAPDH
70 kDa
55 kDa
70 kDa
55 kDa
37 kDa
231-0.6-shNC
231-0.6-shITGA10
Normalized p-Akt/t-Akt level
*
231-0.6-shNC
231-0.6-shITGA10
g
Nucleus
p-Akt
mCherry
iRFP-H2B
Merge
231-0.6 -shNC
231-0.6 -shITGA10
p-Akt level
****
231-0.6-shNC
231-0.6-shITGA10
h
Nucleus
FoxO1
iRFP-H2B
Merge
231-0.6 -shNC
231-0.6 -shITGA10
FoxO1 N/C Ratio
***
231-shNC-0.6
231-0.6-shITGA10

Fig. 5.3 Integrin α10-Akt signaling pathway was hyperactivated in soft-primed cells. (a). Integrins-PI3K-Akt-related signaling pathways enriched in 231-0.6 cells with GO and KEGG enrichment. (b). Volcano plot of transcriptomes of 231-0.6 and 231-35 cells. (c). mRNA transcriptional level of ITGA10 gene in 231-35 and 231-0.6 cells (n=3). (d) Representative confocal fluorescence microscopy images and statistical analysis (with Kruskal-Wallis one-way ANOVA and Dunn's multiple comparisons test) of integrin α10 of 231-35 and 231-0.6 cells (n=60). (e). mRNA transcriptional level of ITGA10 gene in 231-0.6 with shNC and 231-0.6 cells with shITGA10. (f) Representative western blotting images and statistical analysis (with Mann-Whitney U test) of p-Akt, t-Akt and GAPDH of 231-0.6 with shNC and 231-0.6 cells with shITGA10 (n=4). (g) Representative confocal fluorescence microscopy images and statistical analysis (with Mann-Whitney U test) of 231-0.6 with shNC and 231-0.6 cells with shITGA10 (n=30/27). (h) Representative confocal fluorescence microscopy images and statistical analysis (with Mann-Whitney U test) of FoxO1 of 231-0.6 with shNC and 231-0.6 cells with shITGA10 (n=11). (Error bars represent s.e.m., *: $P < 0.05$, **: $P < 0.01$, ****: $P < 0.0001$.)

After that, we examined if the up-regulation of integrin α10 was required for durotaxis pattern shifting from positive to negative in 231-0.6, which to find the YAP mechano-sensitivity and focal adhesion formation on the stiff substrate were rescued with ITGA10 gene knocking down (Fig. 5.4a,b), implicating the clutch reinforcement was normalized. Moreover, the single-cell trajectory results on gradient stiffness hydrogel showed the negative-durotaxis pattern shifting was reversed to positive after silencing ITGA10 (Fig. 5.4d). Then we checked if the integrin α10 downstream PI3K-Akt cascade impacted negative-durotaxis, we pharmacologically inhibited/activated the PI3K-Akt pathway with LY294002/sc79 in 231-0.6/35, surprisingly YAP mechano-sensitivity was not compromised by inhibition in 231-0.6 or enhanced by activation in 231-35 (Fig. 5.4a), but focal adhesion formation ability on 35 kPa polyacrylamide hydrogel or glass of 231-0.6 was normalized after inhibition similarly as knocking down ITGA10, and blocked in 231-35 after activation Akt (Fig. 5.4a,c). The direct single-cell trajectory analysis on gradient stiffness hydrogel demonstrated that the durotaxis pattern of 231-0.6 was reversed to positive after inhibiting the PI3K-Akt axis, and vice versa in 231-35 (Fig. 5.4d).

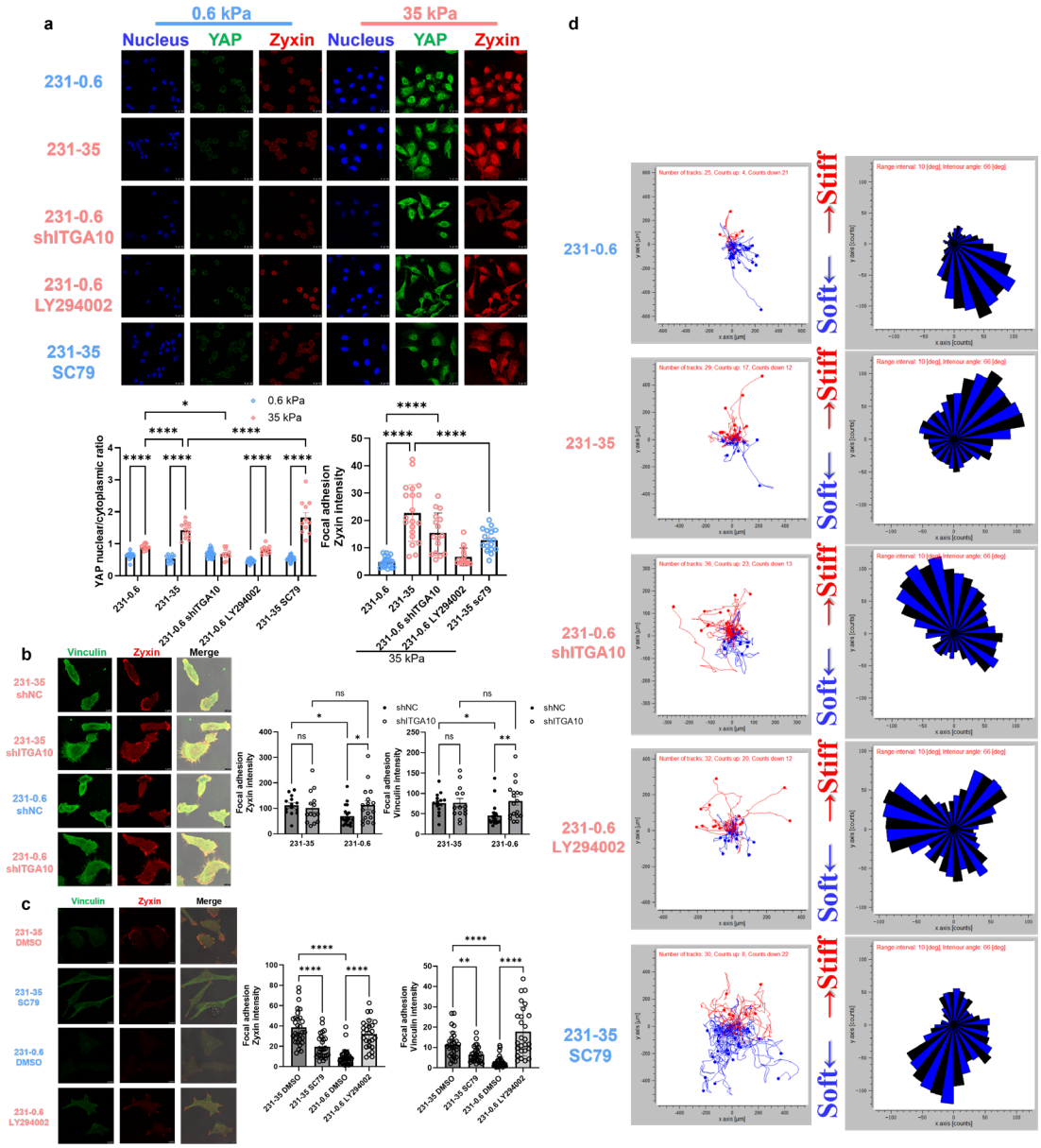

Fig. 5.4 Integrin α10-Akt signaling pathway was required for soft priming-induced negative durotaxis. (a) Representative confocal microscopy images and statistical analysis of YAP (with two-way ANOVA Šídák's multiple comparisons test) in 231-0.6 (n=15/13) , 231-35 (n=13/13), 231-0.6 with shITGA10 (n=30/11), 231-0.6 with LY294002 (n=28/12) and 231-35 cells with sc79 (n=25/11) seeded on 0.6, and 35 kPa polyacrylamide hydrogel and zyxin (with Kruskal-Wallis one-way ANOVA and Dunn's multiple comparisons test) in 231-0.6 (n=23), 231-35 (n=20), 231-0.6 with shITGA10 (n=16), 231-0.6 with LY294002 (n=15) and 231-35 cells with sc79 (n=17) cells seeded on 35 kPa polyacrylamide hydrogel. (b) Representative confocal microscopy images and statistical analysis of zyxin (with Kruskal-Wallis one-way ANOVA and Dunn's multiple comparisons test) in 231-0.6 (n=20/17), 231-35 (n=14/14) cells with shNC or shITGA10 seeded on glass. (c) Representative confocal microscopy images and statistical analysis of zyxin (with Kruskal-Wallis one-way ANOVA and Dunn's multiple comparisons test) in 231-0.6 (n=36), 231-35 (n=30), 231-0.6 with LY294002 (n=26) and 231-35 cells with sc79 (n=29) seeded on glass. (d) Single-cell trajectory and radar graph of 231-0.6, 231-35, 231-0.6 with shITGA10, 231-0.6

with LY294002, and 231-35 cells with sc79 seeded on gradient stiffness polyacrylamide hydrogel. (Error bars represent s.e.m., *: P < 0.05, **: P < 0.01, ****: P < 0.0001.)

At last, we interrogated if the proposed integrin α10-Akt cascade correlated with local niche softness in vivo, we co-stained mCherry and integrin α10/p-Akt in tumor xenograft slides generated from pNDRG1-mCherry-fluc-231-scp1 cell line, and significant positive correlations were observed between mCherry and integrin α10/p-Akt signaling (Fig. 5.5a), in addition, integrin α10 level was up-regulated in mCherry^{+} subpopulations separated in FACS (Fig. 5.5b).

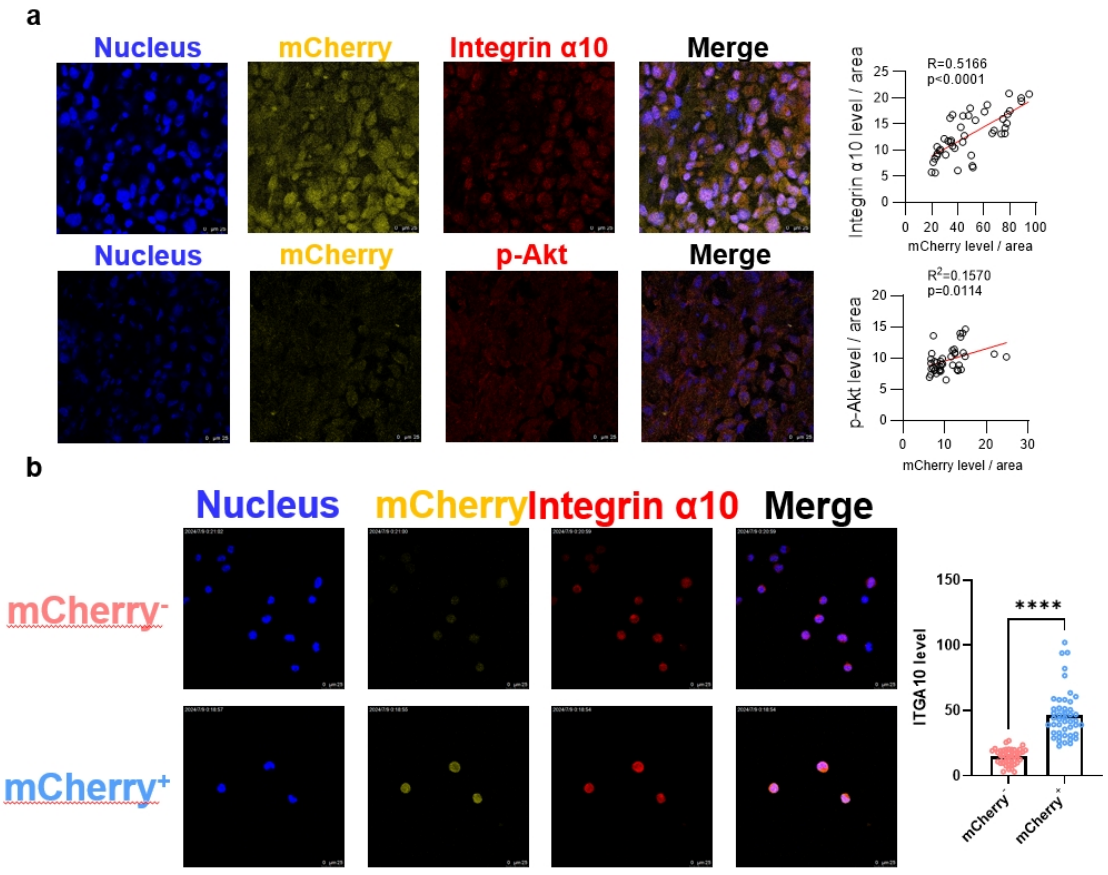

Fig. 5.5 Integrin α10-Akt signaling pathway was correlated with local niche softness in situ. (a) Representative confocal microscopy images and statistical analysis (with simple liner regression) of mCherry, integrin α10 (n=44) and p-Akt (n=40) in mouse fat pad orthotopic tumor xenograft slides generated from pNDRG1-mCherry-fluc-231-scp1 cell line. (b). Representative confocal microscopy images and statistical analysis (with Mann-Whitney U test) of mCherry and integrin α10 in mCherry^{-} and mCherry^{+} cells (n=43/46). (Error bars represent s.e.m., ****: P < 0.0001.)

In summary, we identified the key integrin α10-Akt cascade as the dominant signaling pathway in soft priming-evoked negative-durotaxis shifting.

5.2.4 Negative durotaxis is required for soft priming-induced brain metastatic organotropism

Considering all the above-mentioned results, especially in Chapter IV, we noticed that soft-primed cells were negative-durotactic and eventually, they metastasized to the brain for colonization, we naturally suspected that negative-durotaxis was required for brain metastatic organotropism triggered by soft mechanical stimulation. Here we stably transfected shRNA to silence ITGA10, and qPCR revealed a broad spectrum of down-regulation of brain metastasis genes with shITGA10 treatment than 231-0.6 control (Fig. 5.6a). We did a series of brain metastasis-related functional assays using multiple models. Following the metastasis journey, using an in-vitro endothelial cell monolayer assay, we found 231-shITGA10-0.6 displayed specifically compromised adhesion capacity on hCMEC/D3 brain endothelial cell but not HUVEC cell monolayer (Fig. 5.6b). Next, we applied an in-vitro BBB transmigration model, which found that the transmigration tended to be restrained in the 231-shITGA10-0.6 group (Fig. 5.6c). IF staining of Ki67 proved limited proliferation ability specific on 0.6 kPa polyacrylamide hydrogel but not glass (Fig. 5.6d). The overall brain colonization ability was measured by brain slide co-culture assay, which was dramatically repressed in the 231-shITGA10-0.6 group (Fig. 5.6e). The brain-tropic capability in vivo was tested using intracardiac injection, and the results discovered a huge reduction of brain metastasis on both intensity and incidence in 231-shITGA10-0.6 cells (Fig. 5.6f). To confirm our finding was clinically relevant, we compared the transcriptome of brain metastatic lesions and paired primary lesions in the same patient from GSE173661 in the GEO database, NCBI. We found ITGA10 gene transcriptional level was significantly enriched in brain metastatic subpopulations (Fig. 5.6g). In short, all these results illustrated that ITGA10-dependent negative-durotaxis was required for breast cancer brain metastasis.

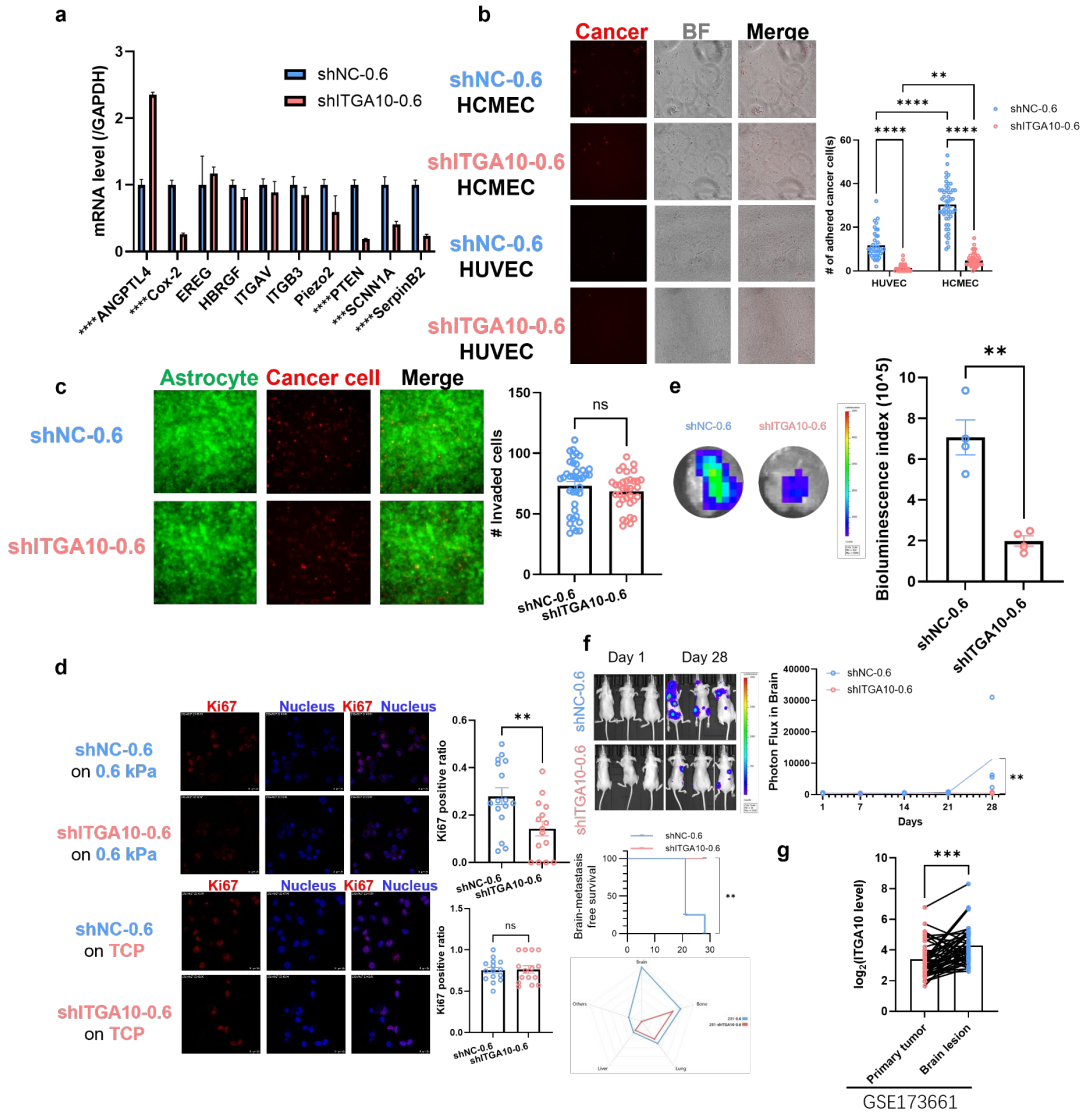

Fig. 5.6 Integrin α10-mediated negative durotaxis was required for soft priming-evoked brain metastasis in vitro and in vivo. (a). mRNA transcriptional level and statistical analysis (with two-tailed Welch's t-test) of representative brain metastatic genes in 231-shNC-0.6 and 231-shITGA10-0.6 cells (n=3). (b). Representative fluorescence microscopy images and statistical analysis (with two-way ANOVA Šídák's multiple comparisons test) of endothelial cell adhesion assay of 231-shNC-0.6 (n=39/50) and 231-shITGA10-0.6 cells (n=43/54). (c). Representative fluorescence microscopy images and statistical analysis (with two-tailed Welch's t-test) of trans-BBB migration assay of 231-shNC-0.6 and 231-shITGA10-0.6 cells (n=38/34). (d). Representative confocal fluorescence microscopy images and statistical analysis (with two-tailed Welch's t-test) of Ki67 of 231-shNC-0.6 and 231-shITGA10-0.6 cells seeded on 0.6 kPa polyacrylamide hydrogel (n=16/15) and glass (n=15). (e). Representative bioluminescence images and statistical analysis (with Mann-Whitney U test) of brain slice co-culture assay of 231-shNC-0.6 and 231-shITGA10-0.6 cells (n=4). (f). Representative bioluminescence images, statistical analysis (with two-way ANOVA Šídák's multiple comparisons test and log-rank survival test), and radar graph of nude mice intracardiacally injected with 231-shNC-0.6 and 231-shITGA10-0.6 cells (n=4/5). (g). ITGA10 gene transcription level and statistical analysis (with Mann-Whitney U test) of

paired primary tumor and brain lesion sample in GSE173661 (n=45). (Error bars represent s.e.m., ns: no significance, **: P < 0.01, ***: P < 0.001, ****: P < 0.0001.)

5.2.5 Niche mechanics dependent/independent negative durotaxis is sufficient to promote brain metastasis

Since negative-durotaxis was needed for brain organotropism, next we ask whether negative-durotaxis was enough to independently trigger brain tropism. We found overexpressing ITGA10 had no significant impact on negative-durotaxis (Fig. 5.7a), then we treated 231-35 with sc79 to activate PI3K-Akt signaling, qPCR results discovered PI3K-Akt activation increased most brain metastasis genes (Fig. 5.7b).

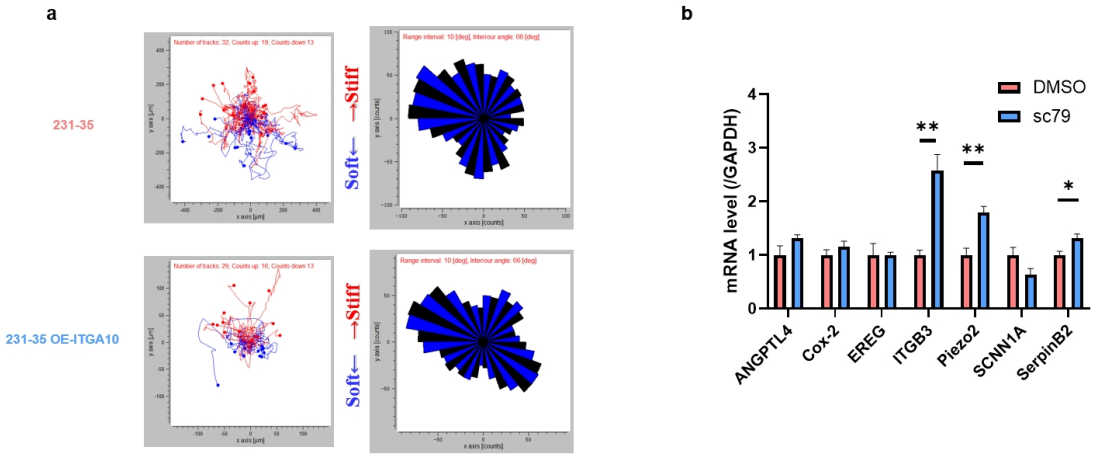

Fig. 5.7 AKT activation upregulates brain metastasis genes of breast cancer cells while overexpression of ITGA10 has no effects on the durotaxis pattern. (a) Single-cell trajectory and radar graph of 231-35 and 231-35 OE-ITGA10 seeded on gradient stiffness polyacrylamide hydrogel. (b) mRNA transcriptional level and statistical analysis (with two-tailed Welch's t-test) of representative brain metastatic genes in 231-WT with DMSO and 231-WT cells with sc79 (n=3). (Error bars represent s.e.m., *: P < 0.05, **: P < 0.01.)

However, the role of the PI3K-Akt pathway was exclusively reported including in breast cancer [400-404], we supposed the strategy that claimed to modulate negative-durotaxis by targeting Akt signaling and test brain metastasis was by no means convincing enough. Thus, we sought other ways, currently the only way to switch positive-durotaxis to negative ever reported was silencing TLN1

(encoding talin1) and TLN2 (encoding talin2) to forcibly delete clutch reinforcement [190, 322, 323], we established a doxycycline-induced 231-Tet-On-shTLN1-Tet-On-shTLN2-fluc cell line (Fig. 5.8a), we found short-term talin1 and talin2 deleting showed negligible influence on brain metastasis genes (Fig. 5.8b), then we mimicked the timeline of long-term priming, strikingly after 30-day doxycycline treatment, brain but not bone metastasis genes rose significantly, and immediately dropped even lower than the baseline control after we canceled the doxycycline induction for two days (Fig. 5.8c). Consistently, the YAP mechano-sensitivity and the focal adhesion formation ability dramatically decreased (Fig. 4.8d). This result encouraged the possibility that negative-durotaxis could independently provoke brain tropism. Pitiably, cancer cell basic cellular functions were seriously damaged by talin1+2-mediated focal adhesion maturation depletion, including collective migration (Fig. 5.8e), single-cell migration (Fig. 5.8f), proliferation (Fig. 5.8g) and substrate adhesion (Fig. 5.8h) [405, 406], we examined if silencing talin1+2 specifically enhanced the brain metastasis functions, including proliferation on soft matrix (Fig. 5.8i), BBB trans-migration (Fig. 5.8j) and adhesion to brain vascular endothelial cells (Fig. 5.8k), the results still appeared negative (Fig. 5.8i-k).

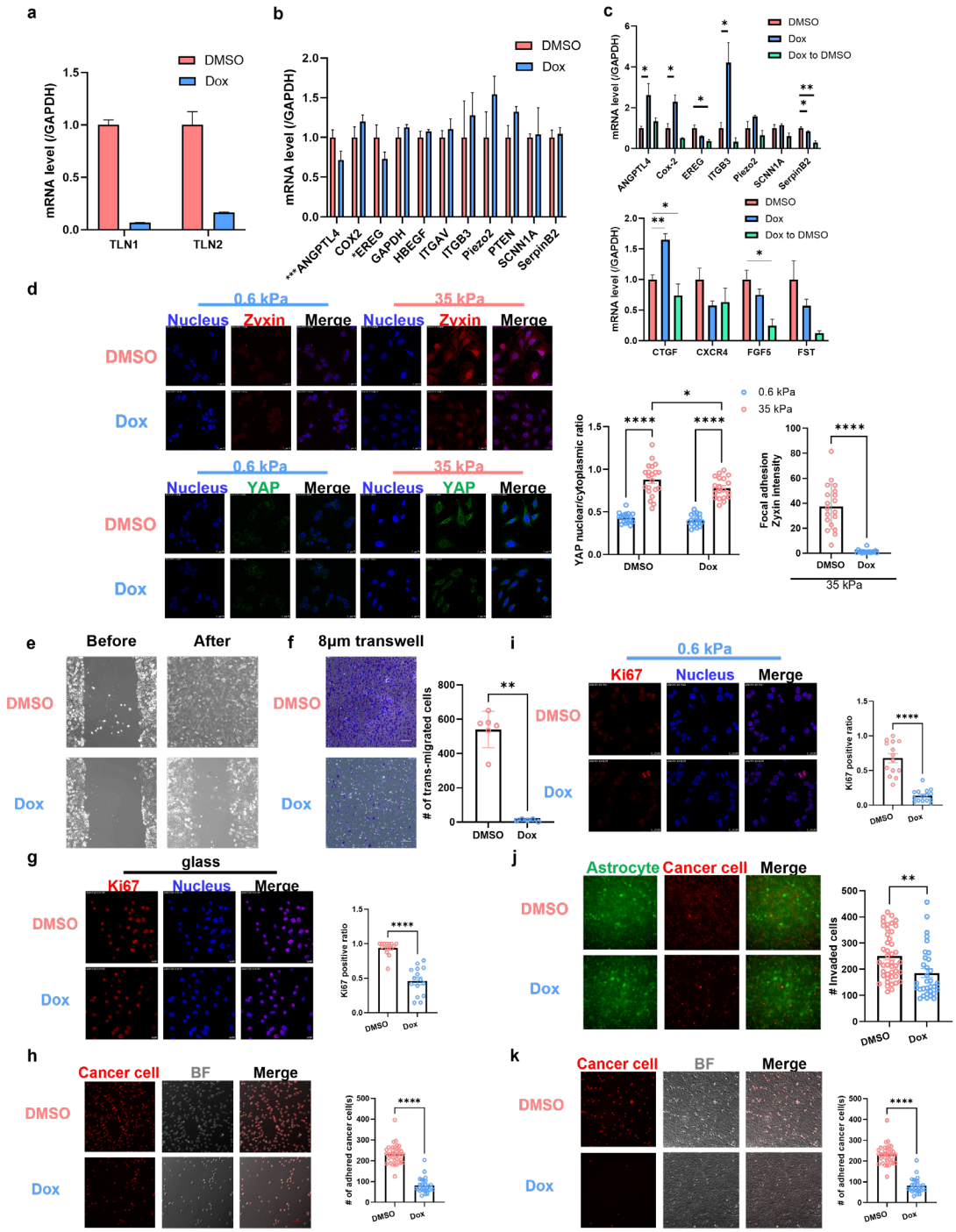

Fig. 5.8 Deletion of TLN1 and TLN2 for long term upregulates brain metastasis genes but not brain metastatic functions. (a). mRNA transcriptional level of TLN1 and TLN2 genes in 231-Tet-On-shTLN1-Tet-On-shTLN2-fluc cells with DMSO and with Dox for 3 days (n=3). (b). mRNA transcriptional level of representative brain metastatic genes in 231-Tet-On-shTLN1-Tet-On-shTLN2-fluc with DMSO and with Dox for 3 days (n=3). (c). mRNA transcriptional level of representative brain and bone metastatic genes in 231-Tet-On-shTLN1-Tet-On-shTLN2-fluc cells with DMSO, with Dox for 33 days and with 30-day Dox followed by 3-day DMSO (n=3). (d) Representative confocal microscopy images and statistical analysis of YAP (with two-way ANOVA Šídák's multiple comparisons test) in 231-Tet-On-shTLN1-Tet-On-shTLN2-fluc cells with DMSO (n=17/21) and with Dox (n=18/20) for 30 days seeded on 0.6 and 35 kPa polyacrylamide hydrogel and zyxin (with Mann-Whitney U test) in 231-Tet-On-

shTLN1-Tet-On-shTLN2-fluc cells with DMSO and with Dox for 30 days seeded on 35 kPa polyacrylamide hydrogel(n=19/18). (e). Representative bright field microscopy images and wound healing assay result of 231-Tet-On-shTLN1-Tet-On-shTLN2-fluc cells with DMSO and with Dox for 30 days. (f). Representative bright field microscopy images and statistical analysis (with two-tailed Welch's t-test) of transwell migration assay result of 231-Tet-On-shTLN1-Tet-On-shTLN2-fluc cells with DMSO and with Dox for 30 days (n=6). (g). Representative confocal fluorescence microscopy images and statistical analysis (with two-tailed Welch's t-test) of Ki67 of 231-Tet-On-shTLN1-Tet-On-shTLN2-fluc cells with DMSO and with Dox for 30 days seeded on glass (n=15). (h). Representative confocal fluorescence microscopy images and statistical analysis (with two-tailed Welch's t-test) of collagen monolayer adhesion assay result of 231-Tet-On-shTLN1-Tet-On-shTLN2-fluc cells with DMSO and with Dox for 30 days (n=37/27). (i). Representative confocal fluorescence microscopy images and statistical analysis (with two-tailed Welch's t-test) of Ki67 of 231-Tet-On-shTLN1-Tet-On-shTLN2-fluc cells with DMSO and with Dox for 30 days seeded on 0.6 kPa polyacrylamide hydrogel (n=14/15). (j). Representative confocal fluorescence microscopy images and statistical analysis (with two-tailed Welch's t-test) of trans-BBB migration assay result of 231-Tet-On-shTLN1-Tet-On-shTLN2-fluc cells with DMSO and with Dox for 30 days (n=44/32). (k). Representative confocal fluorescence microscopy images and statistical analysis (with two-tailed Welch's t-test) of HCMEC adhesion assay result of 231-Tet-On-shTLN1-Tet-On-shTLN2-fluc cells with DMSO and with Dox for 30 days (n=27/25). (Error bars represent s.e.m., *: $P < 0.05$, **: $P < 0.01$, ***: $P < 0.001$, ****: $P < 0.0001$.)

Since disrupting some specific segments in clutch reinforcement switches the durotaxis pattern to negative, limiting focal adhesion maturation and excessively damaged cellular function, we asked if disturbing mechano-transduction could be a compromised strategy as a third way to initiate negative-durotaxis. We searched clues from previous RNA-seq (Fig. 5.9a,b), and as expected we found series actomyosin-related signaling enriched in 231-35 (Fig. 5.9a), in addition, the volcano plot implied myosin IIb (encoded by MYH10) was the only myosin type significantly dropped after long-term soft priming (Fig. 5.9b). We asked if loss of myosin IIb independently altered the durotaxis pattern to negative. We knocked down the MYH10 gene in 231-WT (Fig. 5.9c). After shmMYH10 treatment, YAP mechano-sensitivity and focal adhesion formation capability considerably decreased (Fig. 5.9d). Meantime the durotaxis pattern changed into negative-durotaxis (Fig. 5.9e). However overexpression of MYH10 in 231-0.6 cannot reverse the compromised clutch reinforcement or negative-durotaxis (Fig. 5.9f,g).

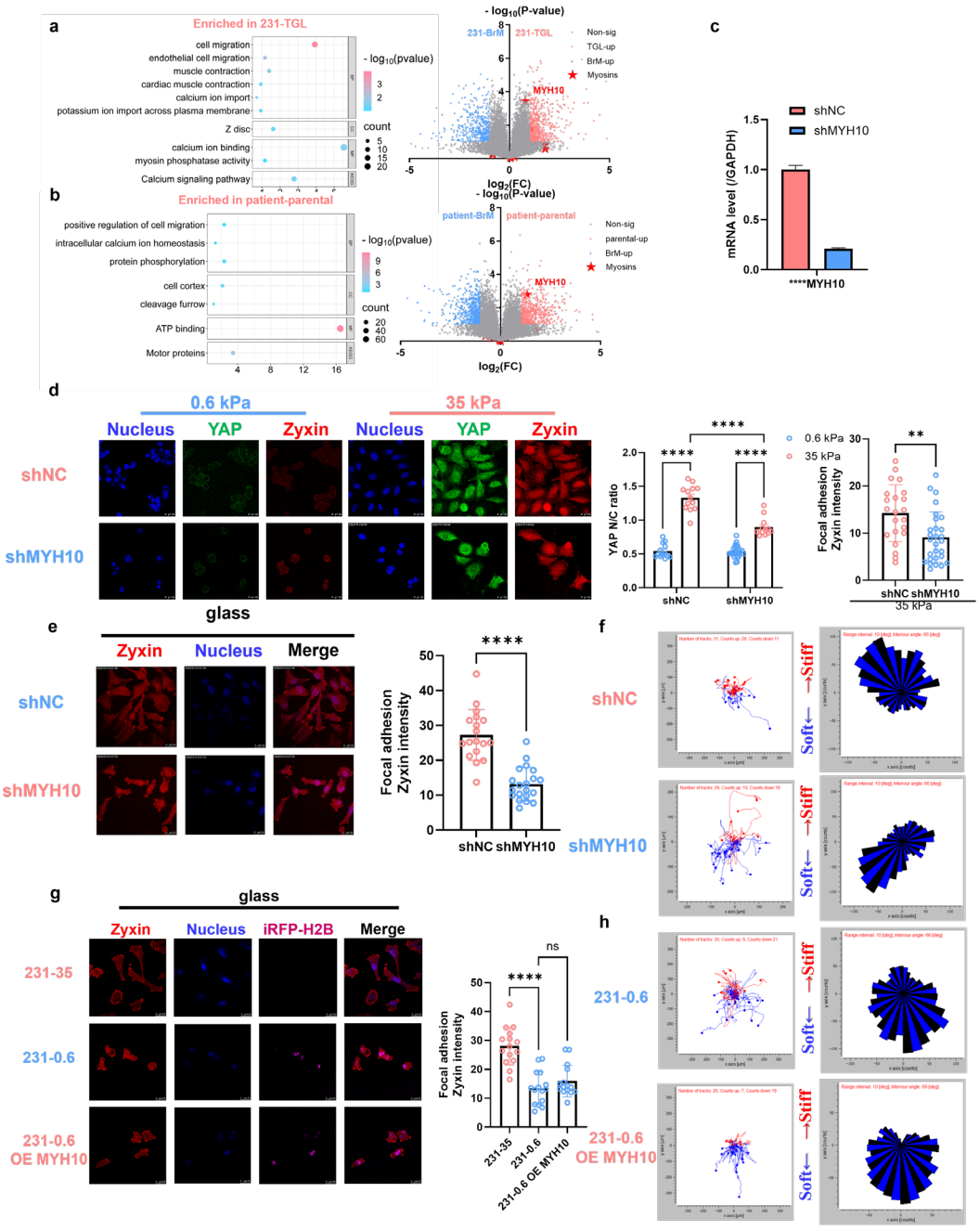

Fig. 5.9 Loss of Myosin IIb weakens mechanosensitivity and focal adhesion and induces negative durotaxis. (a). Migration, actomyosins, and motor protein-related signaling pathways enriched in 231-TGL cells with GO, KEGG enrichment, and Volcano plot of transcriptomes of 231-TGL and 231-BrM cells. (b). Migration, actomyosins, and motor proteins-related signaling pathways enriched in patient-TGL cells with GO, KEGG enrichment, and Volcano plot of transcriptomes of patient-WT and patient-BrM cells. (c). mRNA transcriptional level of MYH10 gene in 231-shNC and 231-shMYH10 cells (n=3). (d) Representative confocal microscopy images and statistical analysis of YAP (with two-way ANOVA Šídák's multiple comparisons test) in 231-shNC and 231-shMYH10 cells seeded on 0.6 (n=13/26) and 35 kPa (n=13/12) polyacrylamide hydrogel and zyxin (with Mann-Whitney U test) in 231-shNC and 231-shMYH10 cells seeded on 35 kPa polyacrylamide hydrogel (n=22/28). (e) Representative confocal

microscopy images and statistical analysis of zyxin (with Mann-Whitney U test) in 231-shNC and 231-shMYH10 cells seeded on glass (n=18/20). (f.) Single-cell trajectory and radar graph of 231-shNC and 231-shMYH10 cells seeded on gradient stiffness polyacrylamide hydrogel. (g) Representative confocal microscopy images and statistical analysis of zyxin (with Kruskal-Wallis one-way ANOVA and Dunn's multiple comparisons test) in 231-0.6, 231-0.6 OE-MYH10, and 231-35 cells seeded on glass (n=15). (h) Single-cell trajectory and radar graph of 231-0.6 and 231-0.6 OE-MYH10 cells seeded on gradient stiffness polyacrylamide hydrogel. (Error bars represent s.e.m., ns: no significance, **: $P < 0.01$, ****: $P < 0.0001$.)

Next, we asked if brain tropism was established after interfering MYH10 gene, we tested the brain metastasis gene expression level, and qPCR results found a notable improvement (Fig. 5.10a). Similarly, we examined critical functional assays during brain metastasis, and we found after interfering MYH10 gene, cancer cell adhesion ability to brain vascular endothelial cells but not HUVEC increased (Fig. 5.10b), BBB transmigration ability also enhanced (Fig. 5.10c), MYH10 silenced cancer cell displayed significant proliferative advantage on 0.6 kPa soft microenvironment but not on glass (Fig. 5.10d), and brain slide co-culture assay uncovered stronger brain colonization capacity (Fig. 5.10e). The brain metastasis capability in vivo was examined by intracardiac injection of 231-fluc-shMYH10 cell line and control, which to find both the brain metastasis intensity and incidence greatly enhanced (Fig. 5.10f). To verify if our finding was clinically relevant, we utilized paired brain and primary lesion transcriptome data in GSE173661 again. We noticed MYH10 gene expression level was significantly lower in brain metastatic subpopulations (Fig. 5.10g).

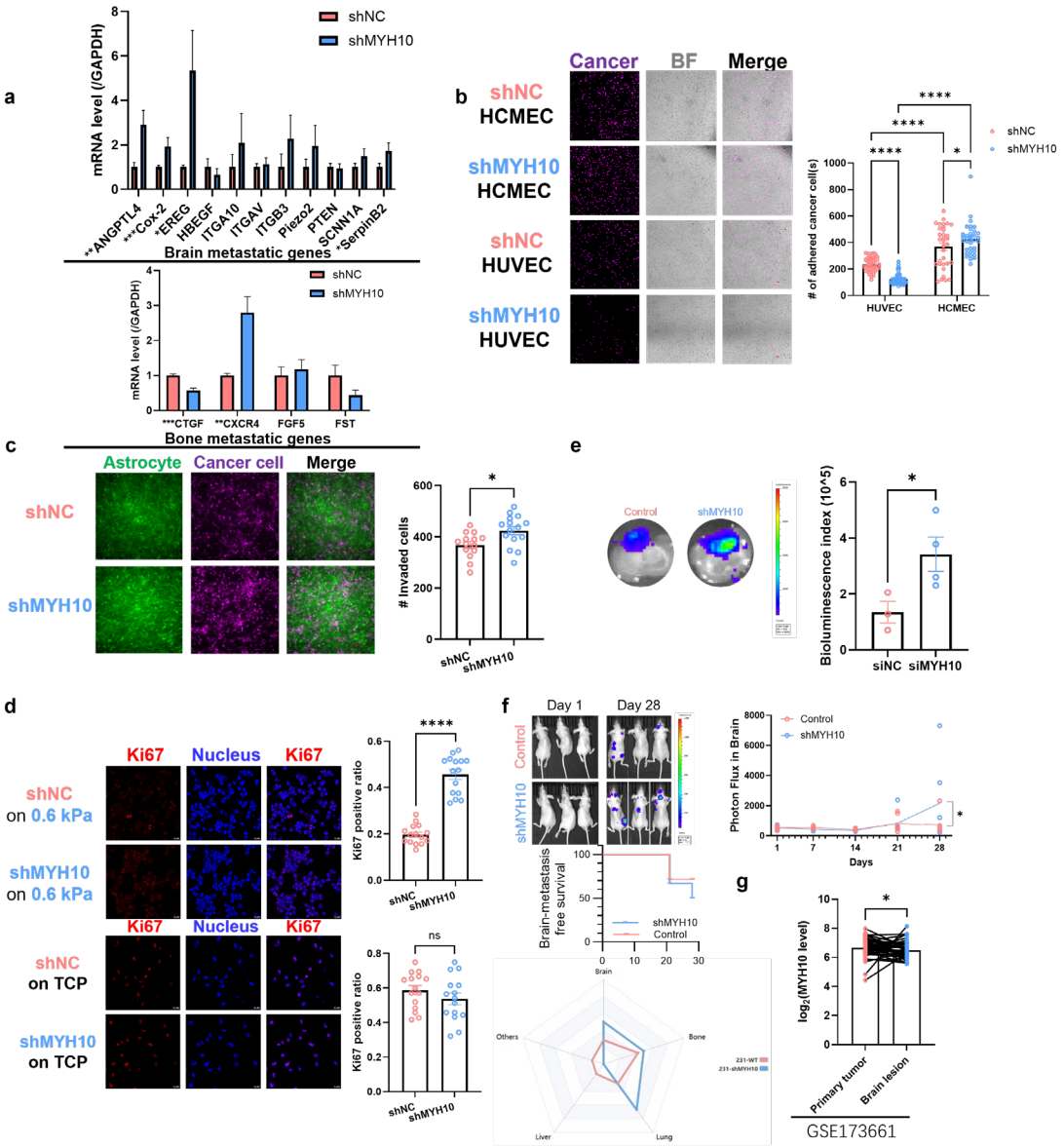

Fig. 5.10 Loss of Myosin IIb promotes brain metastatic capacity in vitro and in vivo. (a). mRNA transcriptional level and statistical analysis (with two-tailed Welch's t-test) of representative brain and bone metastatic genes in 231-shNC and 231-shMYH10 cells (n=3). (b). Representative fluorescence microscopy images and statistical analysis (with two-way ANOVA Šídák's multiple comparisons test) of endothelial cell adhesion assay of 231-shNC (n=43/33) and 231-shMYH10 cells (n=43/35). (c). Representative fluorescence microscopy images and statistical analysis (with two-tailed Welch's t-test) of trans-BBB migration assay of 231-shNC and 231-shMYH10 cells (n=14/15). (d). Representative confocal fluorescence microscopy images and statistical analysis (with Mann-Whitney U test) of Ki67 of 231-shNC and 231-shMYH10 cells seeded on 0.6 kPa polyacrylamide hydrogel (n=15) and glass (n=15). (e). Representative bioluminescence images and statistical analysis (with Mann-Whitney U test) of brain slide co-culture assay of 231-shNC and 231-shMYH10 cells (n=4). (f). Representative bioluminescence images, statistical analysis (with two-way ANOVA Šídák's multiple comparisons test and log-rank survival test), and radar graph of nude mice intracardiacally injected with 231-shNC and 231-shMYH10 cells (n=7/6). (g). MYH10 gene transcription level and statistical analysis (with Mann-

Whitney U test) of paired primary tumor and brain lesion sample in GSE173661 (n=45). (Error bars represent s.e.m., ns: no significance, *: $P < 0.05$, **: $P < 0.01$, ***: $P < 0.001$, ****: $P < 0.0001$.)

In summary, we used three different ways to convert durotaxis pattern dependent/independent of external mechanics, under all circumstances the brain metastasis potential was affected responsively, proposing negative-durotaxis was an independent trigger for brain-targeting metastasis.

5.2.6 Brain metastatic potential affects durotaxis pattern in a positive feedback loop

We have demonstrated negative durotaxis was both required and sufficient for brain metastasis. Nevertheless, it's unclear if brain metastasis potential was also able to reverse the durotaxis pattern. To tackle this question, we first focused on 231-BrM, as a brain-tropic variant selected and reprogrammed in the brain microenvironment from parental 231-WT [146], it represented the brain-tropic subpopulation selected or reprogrammed from 231-WT. We found that 231-BrM performed similar YAP mechano-sensitivity but reduced focal adhesion formation than 231-WT (Fig. 5.11a,b). More importantly, the single-cell trajectory revealed 231-BrM cell line was negative-durotactic (Fig. 5.11c).

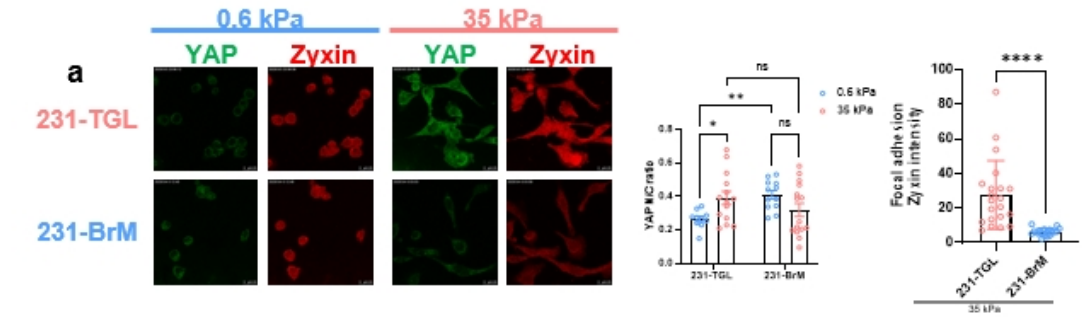
a
0.6 kPa
35 kPa
YAP
Zyxin
YAP
Zyxin
231-TGL
231-BrM
ns
**
*
ns
0.6 kPa
35 kPa
YAP N/C ratio
231-TGL
231-BrM
****
Focal adhesion Zyxin intensity
231-TGL
231-BrM
35 kPa

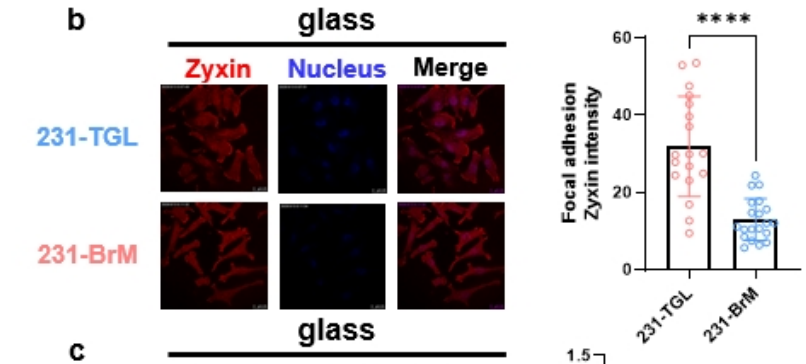
b
glass
Zyxin
Nucleus
Merge
231-TGL
231-BrM
****
Focal adhesion Zyxin intensity
231-TGL
231-BrM
c
glass
YAP
Nucleus
Merge
231-TGL
231-BrM
****
YAP N/C ratio
231-TGL
231-BrM

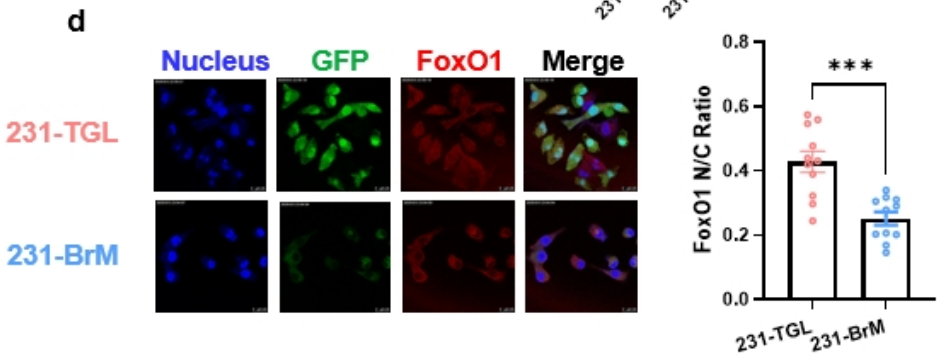
d
Nucleus
GFP
FoxO1
Merge
231-TGL
231-BrM
***
FoxO1 N/C Ratio
231-TGL
231-BrM

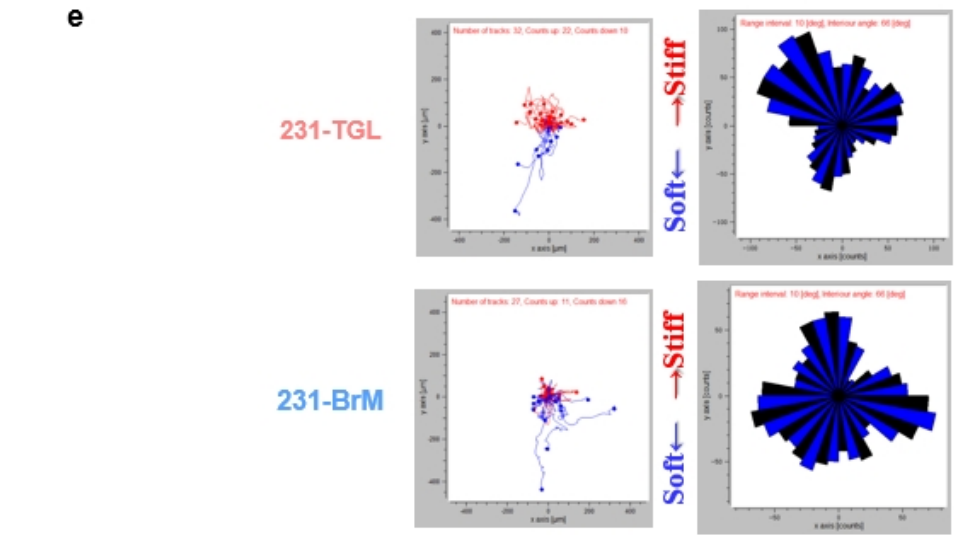
e
231-TGL
Stiff
Soft
231-BrM
Stiff
Soft

Fig. 5.11 Brain-tropic variant 231-BrM was negative durotactic. (a) Representative confocal microscopy images and statistical analysis of YAP (with two-way ANOVA Šídák's multiple comparisons test) in 231-TGL (n=10/14) and 231-BrM (n=12/15) cells seeded on 0.6, and 35 kPa polyacrylamide hydrogel and zyxin (with Mann-Whitney U test) in 231-shNC and 231-shMYH10 cells seeded on 35 kPa polyacrylamide hydrogel (n=21/18). (b) Representative confocal microscopy images and statistical analysis of zyxin (with Mann-Whitney U test) in 231-shNC and 231-shMYH10 cells seeded on glass (n=18/20). (c) Representative confocal microscopy images and statistical analysis of YAP (with two-way ANOVA Šídák's multiple comparisons test) in 231-TGL and 231-BrM cells seeded on glass (n=15/14). (d) Representative confocal microscopy images and statistical analysis of FoxO1 (with Mann-Whitney U test) in 231-TGL and 231-BrM cells seeded on glass (n=11). (e) Single-cell trajectory and radar graph of 231-TGL and 231-BrM cells seeded on gradient stiffness polyacrylamide hydrogel. (Error bars represent s.e.m., ns: no significance, ****: $P < 0.0001$.)

Our previous research uncovered soft-primed cancer cells up-regulated the expression and enzymatic activity of HDAC3 to enhance brain tropism, the correlation of which was further confirmed in Chapter IV in vivo, we blocked the HDAC3 with RGFP966 in 231-0.6 to specifically inhibit brain organotropism, interestingly we noticed the YAP mechano-sensitivity and focal adhesion formation capacity increased after HDAC3 inhibition (Fig. 5.12a), at the same time the durotaxis pattern of 231-0.6 switched from negative to positive (Fig. 5.12b).

It's well-known that lipid metabolism is required for brain-specific metastasis and brain tumor progression [148-151, 386, 407]. Here we applied pharmacological agents fatostatin HBr and docosahexaenoic acid to blockade SREBF1 and CD36 respectfully, which governed the lipid intercellular de novo synthesis and extracellular uptake [408, 409]. Both ways to inhibit lipid metabolism dramatically strengthened YAP mechano-sensitivity and focal adhesion formation in 231-0.6 (Fig. 5.12a-c), moreover, fatostatin HBr treatment reversed the negative-durotaxis of 231-0.6 to positive (Fig. 5.12d). Similar results were obtained from BrM-brain metastatic variant system, with Akt, HDAC3 and SREBF1 inhibition (Fig. 5.13).

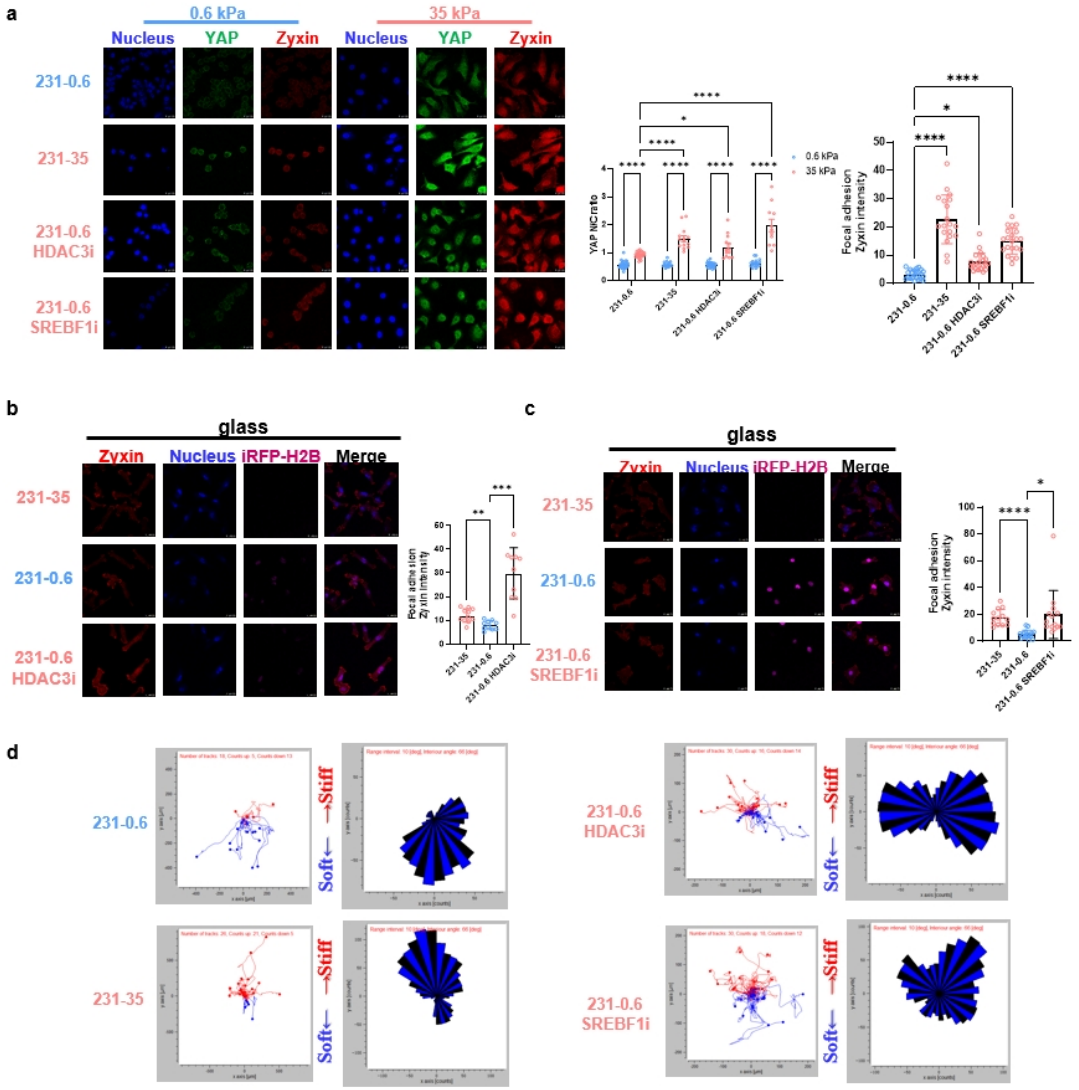

Fig. 5.12 Reduction of brain metastatic potential in soft-primed cells by inhibiting HDAC3 activity and lipid metabolism enhances mechanosensitivity and focal adhesion and shifts the migration pattern to positive durotaxis. (a) Representative confocal microscopy images and statistical analysis of YAP (with two-way ANOVA Šídák's multiple comparisons test) in 231-0.6 (n=25/24), 231-35 (n=15/14), 231-0.6 cells with RGFP966 (n=25/13) and fatostatin HBr (n=18/11) seeded on 0.6, and 35 kPa polyacrylamide hydrogel and zyxin (with Kruskal-Wallis one-way ANOVA and Dunn's multiple comparisons test) in 231-0.6 (n=23), 231-35 (n=19), and 231-0.6 cells with RGFP966 (n=21) and fatostatin HBr (n=21) seeded on 35 kPa polyacrylamide hydrogel. (b) Representative confocal microscopy images and statistical analysis of zyxin (with Kruskal-Wallis one-way ANOVA and Dunn's multiple comparisons test) in 231-0.6 (n=11), 231-35 (n=10), and 231-0.6 cells with RGFP966 (n=10) seeded on glass. (c) Representative confocal microscopy images and statistical analysis of zyxin (with Kruskal-Wallis one-way ANOVA and Dunn's multiple comparisons test) in 231-0.6 (n=13), 231-35 (n=17) and 231-0.6 cells fatostatin HBr (n=14) seeded on glass. (d) Single-cell trajectory and radar graph of 231-TGL and 231-BrM cells seeded on gradient stiffness polyacrylamide hydrogel. (Error bars represent s.e.m., *: $P < 0.05$, **: $P < 0.01$, ****: $P < 0.0001$.)

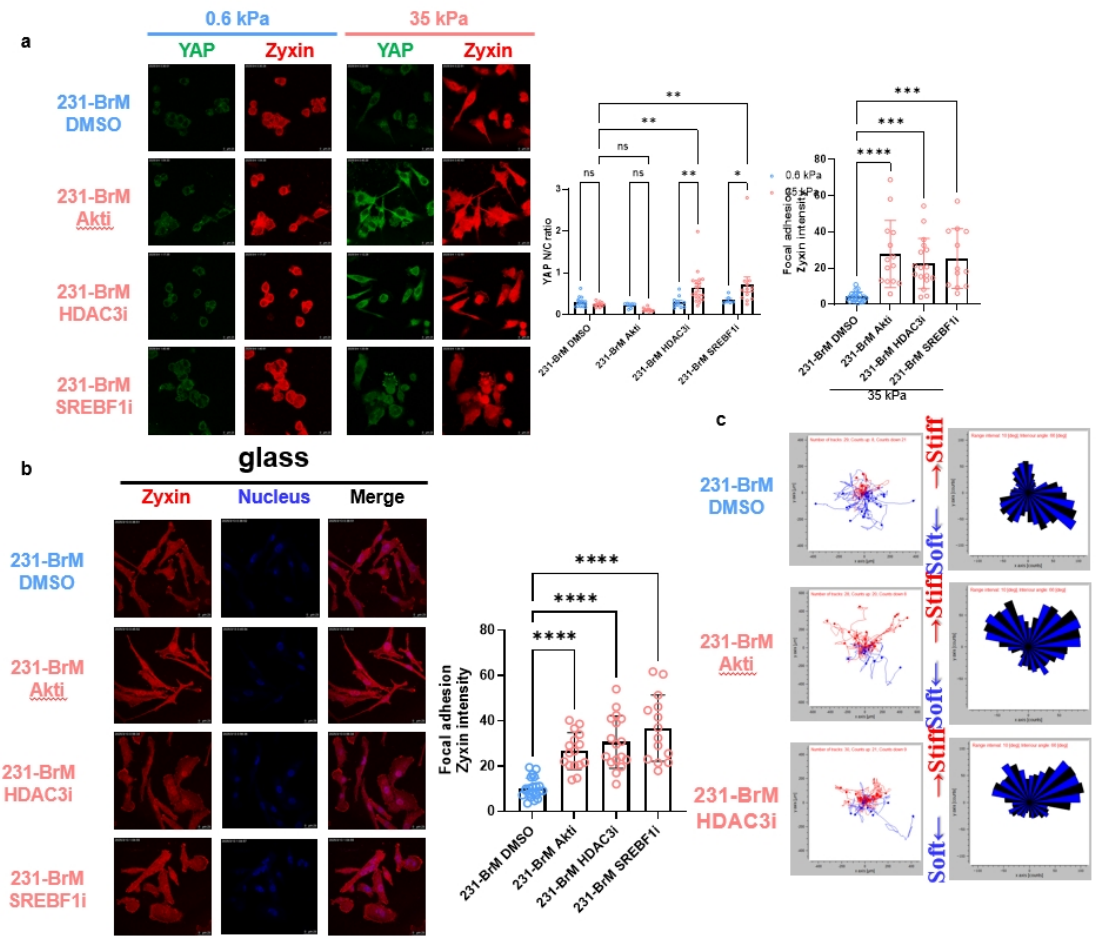

Fig. 5.13 Reduction of brain metastatic potential in 231-BrM variant by inhibiting Akt, HDAC3 activity and lipid metabolism enhances mechanosensitivity and focal adhesion and shifts the migration pattern to positive durotaxis. (a) Representative confocal microscopy images and statistical analysis of YAP (with two-way ANOVA Šídák's multiple comparisons test) in 231-BrM cells with DMSO (n=14/12), LY294002 (n=7/11), RGFP966 (n=11/19) and fatostatin HBr (n=6/13) seeded on 0.6, and 35 kPa polyacrylamide hydrogel and zyxin (with Kruskal-Wallis one-way ANOVA and Dunn's multiple comparisons test) in 231-BrM cells with DMSO (n=20), LY294002 (n=14), RGFP966 (n=17) and fatostatin HBr (n=12) seeded on 35 kPa polyacrylamide hydrogel. (b) Representative confocal microscopy images and statistical analysis of zyxin (with Kruskal-Wallis one-way ANOVA and Dunn's multiple comparisons test) in 231-BrM cells with DMSO (n=21), LY294002 (n=16), RGFP966 (n=17) and fatostatin HBr (n=14) seeded on glass. (c) Single-cell trajectory and radar graph of 231-BrM cells with DMSO, LY294002, RGFP966 and fatostatin HBr seeded on gradient stiffness polyacrylamide hydrogel. (Error bars represent s.e.m., *: $P < 0.05$, **: $P < 0.01$, ****: $P < 0.0001$.)

Collectively, three distinct ways to modulate brain organotropism were conducted, all of which strongly impacted the durotaxis pattern, implying a general positive feedback loop.

5.2.7 Negative durotactic cells are positive viscotactic

All tissues are viscoelastic [162], viscous properties and elasticity are usually associated across organs, soft organs usually exhibit stronger viscous behavior [162]. The viscous property in tumors is found to emerge in the tumor's early stage and has been reported to promote cancer initiation, cancer stroma cell interaction, cancer cell proliferation, and collective invasion [30, 224, 410, 411]. However, currently, no research has considered the viscous behavior of tumor ECM as also heterogenous because of intratumoral heterogeneity. We considered if the viscous property and elasticity in different local niches in the tumor were also associated. Here we used AFM to measure the elasticity and viscous properties of randomly selected areas in cryo-stat tumor slides, which to find hysteresis areas were higher in the lower elasticity region (Fig. 5.13a)

Since we showed soft local niche in the tumor also displayed stronger viscous behavior, and loss of clutch reinforcement could possibly explain focal adhesion dynamics/instability-induced positive-viscotaxis as well [324], we asked if soft-primed cancer cells were positive-viscotactic to keep locating in corresponding local niche. Here we prepared a polyacrylamide hydrogel with a gradient on the viscous property but consistent elasticity (Fig. 5.13b) [324]. We found soft-primed 231-0.6 group was positive-viscotactic while the stiff-primed 231-35 cells were negative-viscotactic (Fig. 5.13c). Moreover, we observed the shifting from positive- to negative-viscotaxis of soft-primed 231-0.6 cells after the ITGA10 gene interfering (Fig. 5.13d). Also, after MYH10 gene silencing, 231-WT cells become positive-viscotactic (Fig. 5.13e). We also separated $mCherry^+$ and $mCherry^-$ cells from xenograft and did similar tests, which found $mCherry^+$ cells were positive-viscotactic and $mCherry^-$ cells were negative-viscotactic (Fig. 5.13f). All these findings suggested that negative-durotaxis and positive-viscotaxis were closely associated.

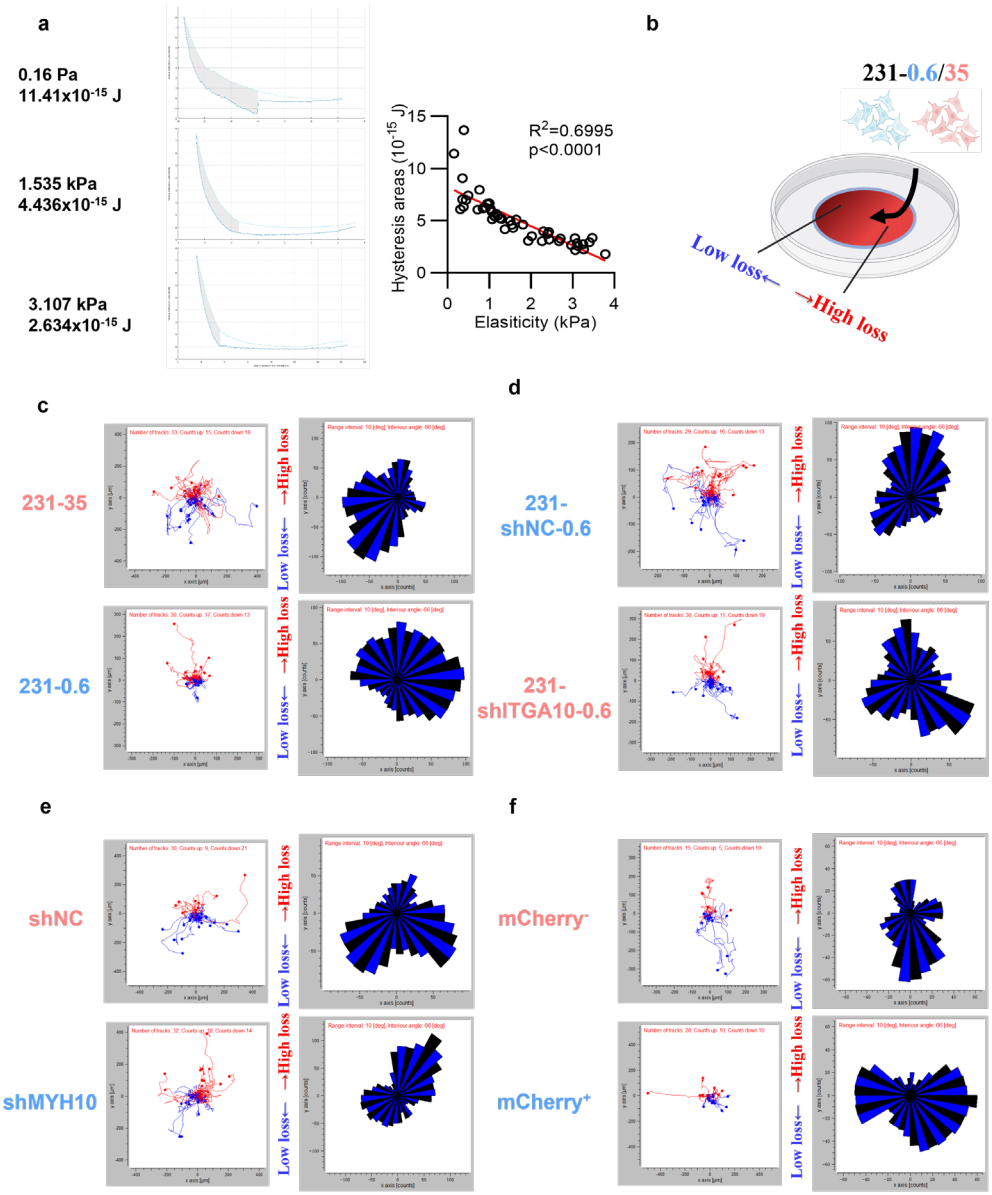

Fig. 5.14 Local soft niches were highly viscous and soft-primed tumor cells were both negative durotactic and positive viscotactic. (a) Representative force curves of atom force microscopy and statistical analysis (with simple liner regression) of hysteresis areas and elastic modulus of mouse fat pad orthotopic tumor xenograft generated from pNDRG1-mCherry-231 cell line (n=50). (b). Workflow, (c) single cell trajectory and radar graph of 231-0.6 and 231-35 cells seeded on gradient viscous property polyacrylamide hydrogel. (d) Single-cell trajectory and radar graph of 231-shNC-0.6 and 231-shITGA10-0.6 cells seeded on gradient viscous property polyacrylamide hydrogel. (e) Single-cell trajectory and radar graph of 231-shNC and 231-shMYH10 cells seeded on gradient viscous property polyacrylamide hydrogel. (f) Single-cell trajectory and radar graph of $mCherry^-$ and $mCherry^+$ cells seeded on gradient viscous property polyacrylamide hydrogel.

We hypothesized that the negative-durotaxis and positive-viscotaxis behaviors both were the reasons why soft-primed cancer cells were able to keep residing in soft niches. To confirm the negative-durotaxis truly dominated the local soft niche distribution of soft-primed cancer cells in tumors. We established two groups from the same pNDRG1-mCherry-fluc-scp1 clone, one group transfected iRFP-H2B and long-term primed with 0.6 kPa microenvironment, the other long-term primed with 35 kPa microenvironment, now that negative-durotactic and positive-viscotactic subpopulation were permanently labeled, then two groups were 1:1 mixed and orthotopically injected into mouse mammary fat pad to self-organize a tumor, after successful tumor establishment, we collected the cancer cells with MACS, using flow cytometry to check the mCherry expression level (representing the residing local niche softness) of $iRFP^+$ and $iRFP^-$ populations (Fig. 5.14a), the result showed the total cell number of $iRFP^+$ and $iRFP^-$ group remained 1:1 after tumor establishment (Fig. 5.14b). Meanwhile, the overall mCherry expression level was similar in the $iRFP^+$ negative-durotactic and positive-viscotactic group compared with $iRFP^-$ cells (Fig. 5.14c). However, we noticed $iRFP^+$ cells contributed significantly more to the $mCherry^+$ subpopulation (the same gate defined in Chapter IV), and most $mCherry^+$ subpopulations originated from iRFP-labeled cells (Fig. 4.14d), meaning that in the soft niche in tumor, the predominant cells were pre-induced negative-durotactic and positive-viscotactic cells. All these results indicated that negative/positive-durotaxis and positive/negative-viscotaxis of cancer cells played a major role in the self-establishment of intratumoral mechanical microenvironment especially determining the soft local niche resident identification, which guaranteed the long-term soft priming of soft niche residents.

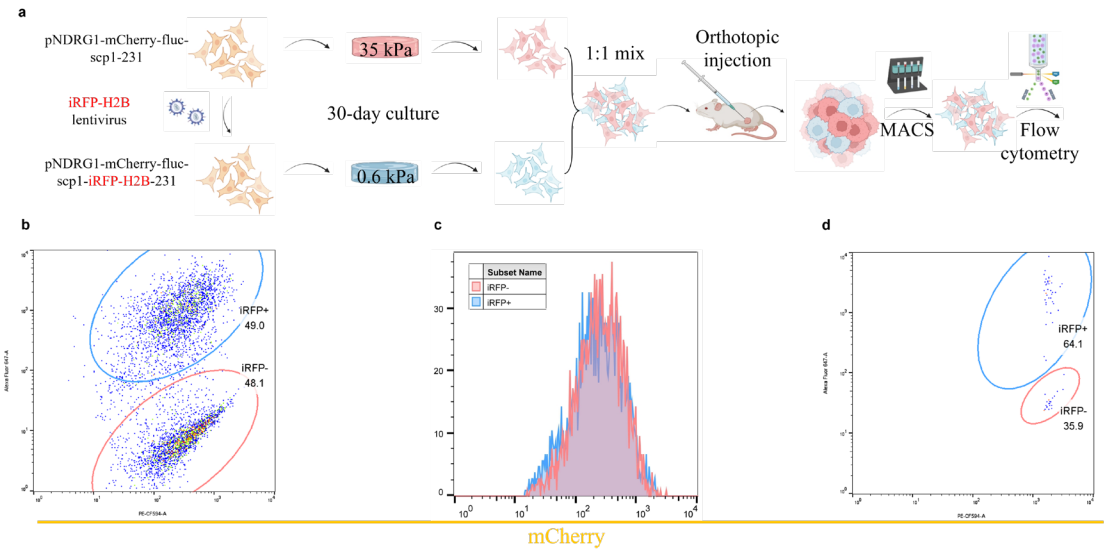

Fig. 5.15 Soft-primed tumor cells predominantly resided in local soft niches of tumor xenografts, which might be related to negative durotactic and viscotactic ability. (a) Workflow and (b-e) flow cytometry results of cancer cells harvested from orthotopic xenograft generated from 1:1 mixed pNDRG1-mCherry-fluc-scp1-35 and pNDRG1-mCherry-fluc-scp1-iRFP-H2B-0.6 cells

5.2.8 Soft-primed cells outcompete stiff-primed cells via ITGA10

Soft-primed cells maintained local niche softness and kept residing on the local soft niche, meanwhile, soft-primed cells showed proliferative advantage on the soft local niche (Fig. 4.7b,c), which helped soft-primed cells to keep the clonal dominance in one way, we asked if cell competition was involved to achieve the same goal. Here we labeled the 231-0.6 with iRFP-H2B and dyed 231-35 with a green cell tracker, mixed and seeded on different stiffness polyacrylamide hydrogel with different cell densities supplied with low serum. In this design, low-density groups represented the baseline that cell competition was not involved, and in high-density groups, both cell types shared similar proliferation but were also influenced by cell competition caused by cell-cell contact, then we could compare the low-density group with the high-density group to visualize the impact from pure cell competition (Fig. 5.15a). The results discovered that on 35 kPa polyacrylamide hydrogel, the ratio of 231-0.6 and 231-35 was the same with or without cell competition, interestingly on 0.6 kPa this ratio significantly increased in the cell competition group than control (Fig. 5.15b). In addition, we conducted a live cell imaging to capture the moment 231-35 cells were eliminated (Fig. 5.15c), weirdly some double positive cells were observed, which

could be caused by cytosol or membrane transmission (Fig. 5.15d). Negative-durotactic 231-0.6 positively migrated towards a softer microenvironment, meanwhile, 231-0.6 was the competition winner specifically a soft microenvironment, we wonder if negative-durotaxis was associated with cell competition superiority. Surprisingly, we found the competition advantage disappeared after silencing the ITGA10 gene in 231-0.6 specifically on 0.6 kPa but not 35 kPa polyacrylamide hydrogel (Fig. 5.15e). In summary, we discovered an unknown soft microenvironment-special and negative-durotaxis-dependent cell competition manner, which along with proliferative advantage both explained the clonal dominance in soft local niche.

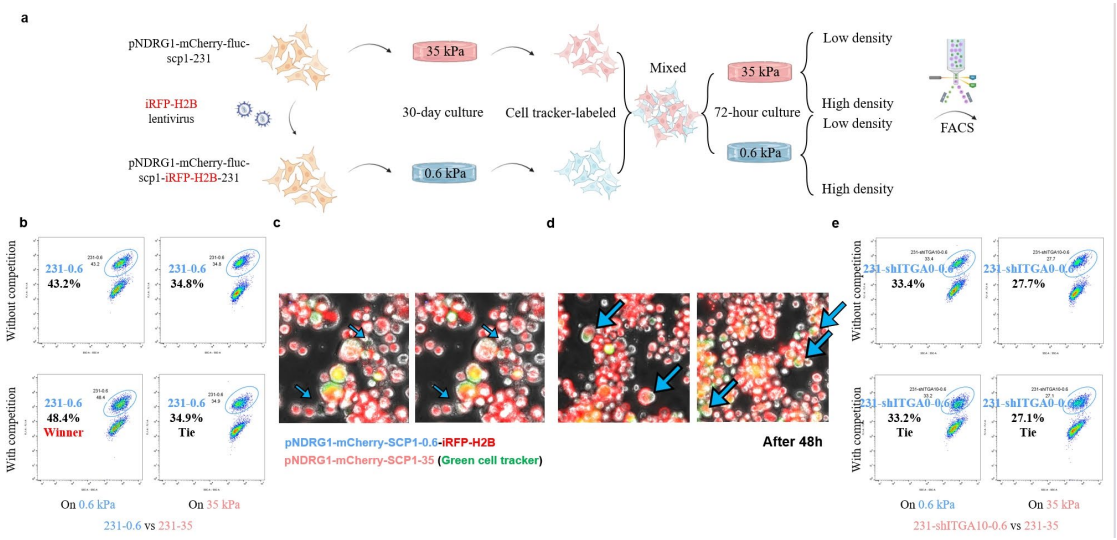

Fig. 5.16 Soft-primed cells eliminated stiff-primed cells in an ITGA10-dependent manner. (a). Workflow and (b) flow cytometry results of 1:1 mixed green cell tracker-labeled pNDRG1-mCherry-fluc-scp1-35 and pNDRG1-mCherry-fluc-scp1-iRFP-H2B-0.6 cells cultured on 0.6, and 35 kPa polyacrylamide hydrogel with low and high cell density. (c). Representative live cell image of eliminated loser cells of 1:1 mixed green cell tracker-labeled pNDRG1-mCherry-fluc-scp1-35 and pNDRG1-mCherry-fluc-scp1-iRFP-H2B-0.6 cells cultured on 0.6 kPa polyacrylamide hydrogel with high cell density. (d). Representative live cell image of hybrid cells of 1:1 mixed green cell tracker-labeled pNDRG1-mCherry-fluc-scp1-35 and pNDRG1-mCherry-fluc-scp1-iRFP-H2B-0.6 cells cultured on 0.6 kPa polyacrylamide hydrogel with high cell density. (d) Flow cytometry results of 1:1 mixed green cell tracker-labeled pNDRG1-mCherry-fluc-scp1-35 and pNDRG1-mCherry-fluc-scp1-iRFP-H2B-shITGA10-0.6 cells cultured on 0.6, and 35 kPa polyacrylamide hydrogel with low and high cell density.

5.2.9 Soft-primed cells display compromised CAF activation to maintain local niche softness

To answer the third question we raised in this Chapter, explaining how brain-tropic cells maintain a nearby local soft niche, we tested whether CAF, the strongest ECM modifier [32, 110, 202, 224-235, 270-280], was activated differently by 231-0.6 and 231-35 in the corresponding local niche.

Firstly, we applied microchannel chemotaxis assay to NIH-3T3 fibroblast with 231-0.6/231-35 condition media (CM) in the left/right compartment to check if soft-primed cell showed limited fibroblast recruitment ability (Fig. 5.16a), single cell trajectory results showed there was no difference between 231-0.6 and 231-35 CM (Fig. 5.16b). Even though 231-35 didn't actively recruit more fibroblast, we applied single-cell trajectory on gradient stiffness hydrogel to find fibroblast itself is durotactic, still, there would likely be more fibroblast in the stiff local niche (Fig. 5.16c,d). Next, we seeded NIH-3T3 cells on 0.6/35 kPa hydrogel and supplied 0.6/231-35 CM to mimic different local niche microenvironments with both cancer cell paracrine and ECM stiffness, which to find 231-35 CM on 35 kPa gel group fibroblast was activated more, represented by αSMA as a CAF marker (Fig. 5.16e). Here there were two variables, while it's well known that fibroblast or other stroma cell to CAF transition requires mechano-transduction [412-414], which was double-confirmed by Fig. 5.16g,h. We also asked whether 231-0.6/35 CM functioned differently independent of stiffness, we seeded NIH-3T3 on the glass to provide sufficient mechano-transduction support, then provided 231-0.6/35 CM, 231-35 CM group fibroblast still showed activation advantage (Fig. 5.16i,j), suggesting that 231-0.6/35 instinct CAF activation abilities are different.

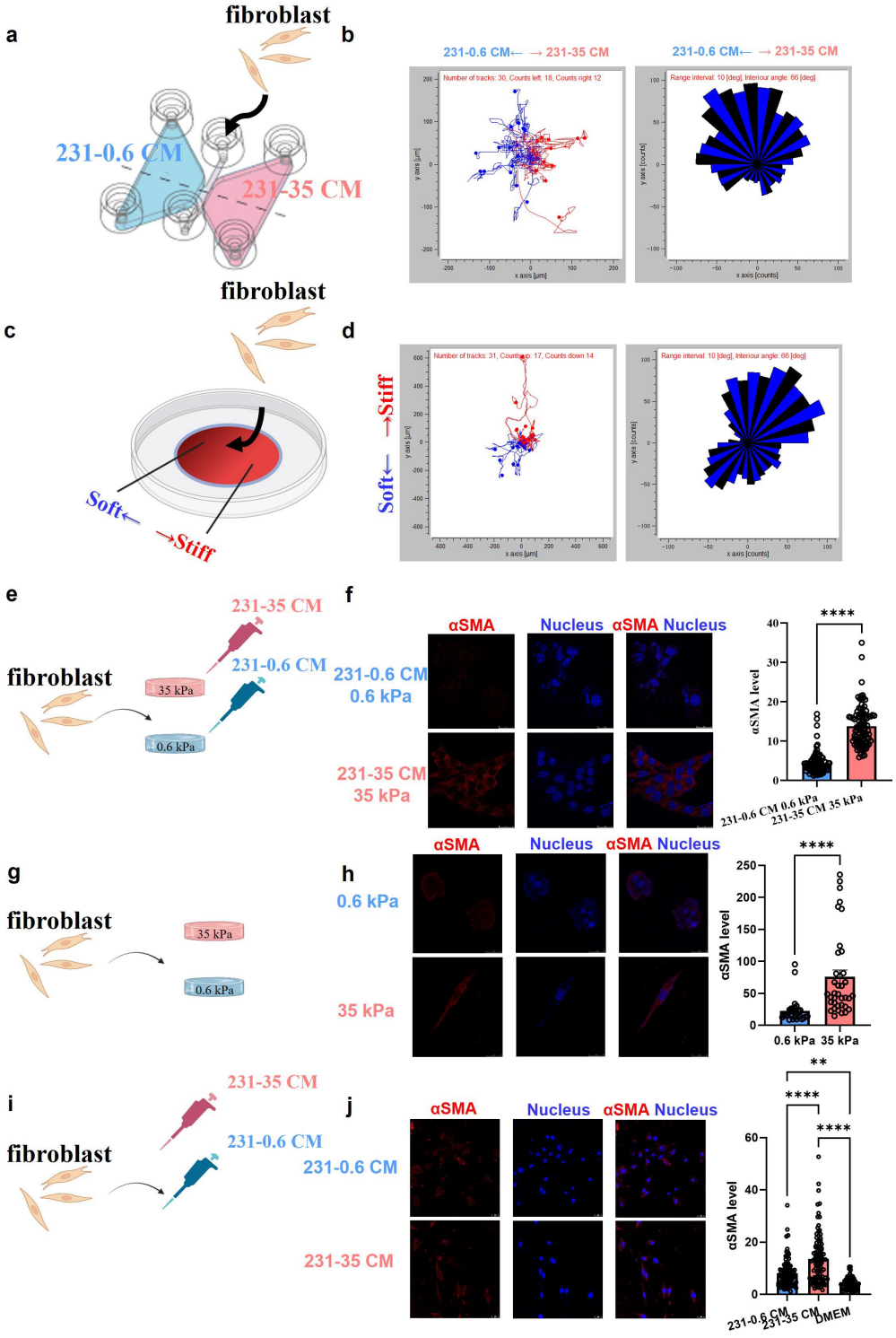

Fig. 5.17 CAF recruitment was limited by niche softness, CAF activation was compromised by both soft niche and soft niche resident paracrine. (a). Workflow, (b) single cell trajectory and radar graph of fibroblast NIH-3T3 cells seeded in chemotaxis chip supplied with 231-0.6 CM on the left and 231-35 CM on the right. (c). Workflow, (d) single cell trajectory and radar graph of fibroblast NIH-3T3 cells seeded on gradient stiffness polyacrylamide hydrogel. (e). Workflow, (f) representative confocal fluorescence microscopy images and statistical analysis (with Mann-Whitney U test) of αSMA of NIH-3T3 cells seeded on 0.6 and 35 kPa polyacrylamide hydrogel supplied with 231-0.6 CM and 231-35 CM

respectfully. (g). Workflow, (h) representative confocal fluorescence microscopy images and statistical analysis (with Mann-Whitney U test) of αSMA of NIH-3T3 cells seeded on 0.6 and 35 kPa polyacrylamide hydrogel. (i). Workflow, (j) representative confocal fluorescence microscopy images, and statistical analysis (with Kruskal-Wallis one-way ANOVA and Dunn's multiple comparisons test) of αSMA of NIH-3T3 cells seeded on glass supplied with 231-0.6 CM on left and 231-35 CM. (Error bars represent s.e.m., **: $P < 0.01$, ****: $P < 0.0001$.)

In the previous study, we found long-term culture is required to develop organotropism, here we'd like to guarantee it is long-term but not short-term stiffness stimulation contributes to this CAF activation promoting manner, we seeded TGL shortly on 0.6/35 kPa hydrogel to collect CM, as expected short-term culture did not alter the CAF activation ability (Fig. 5.17a). Since 231-0.6 and 231-35 displayed distinct metastatic organotropism (Chapter IV), next, we asked whether cells with different tropism could activate CAF differently independent of stiffness, thus we compared the CAF activation potential of BoM with BrM CM (BoM/BrM are 231-TGL-derived variants with bone/brain metastatic organotropism and routinely maintained on TCP for culturing), and we found there was no significant difference (Fig. 5.17b), all these data suggested both stiffness and long-term stimulation were critical. It's known CAF has multiple sources in vivo [230, 414, 415]. To avoid cell line dependency, we repeated all the above-mentioned experiments with a mouse MSC cell line, and all phenomena remained (Fig. 5.17c-h).

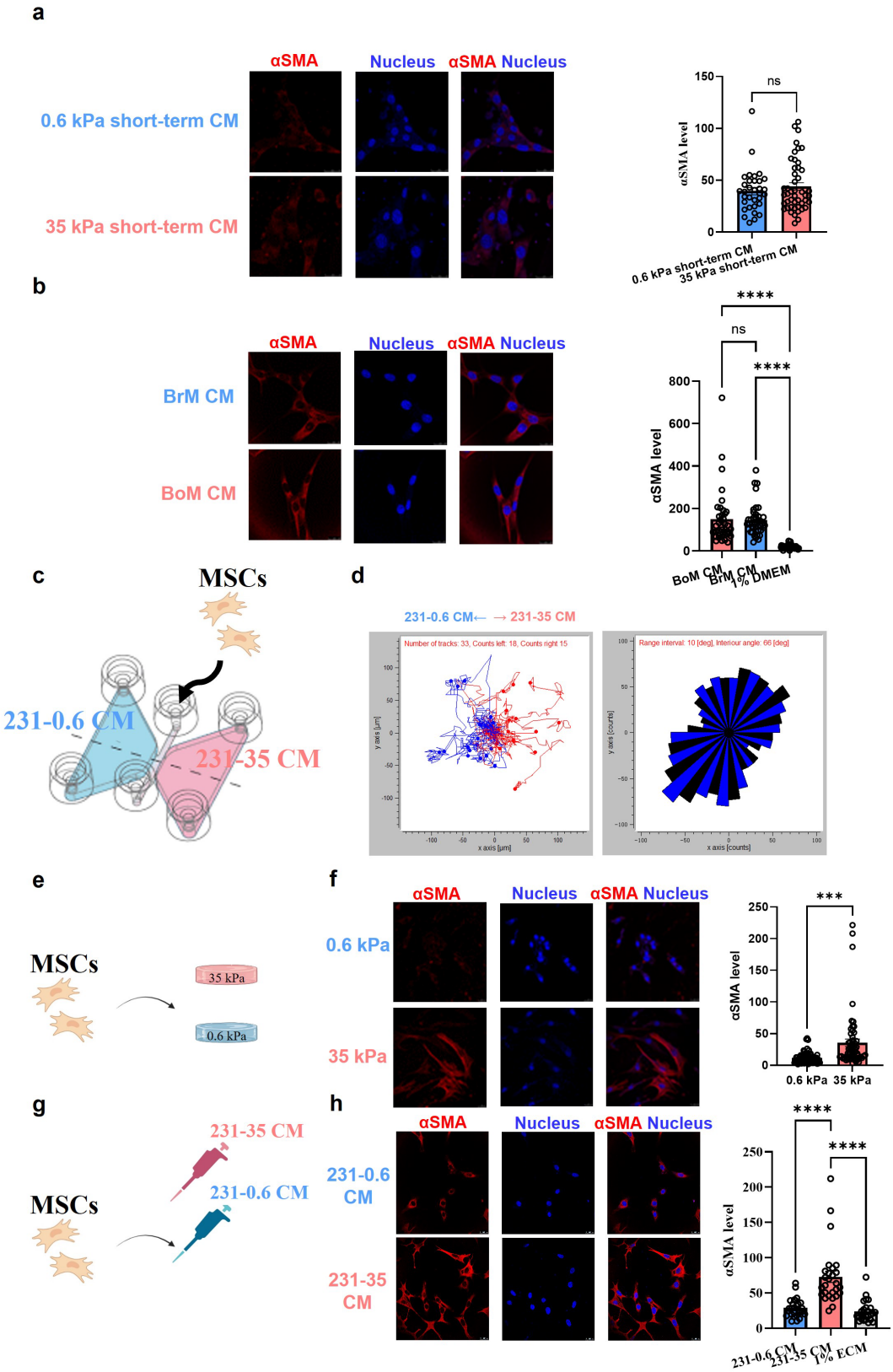

Fig. 5.18 Compromised CAF activation was not caused by short-term soft-primed resident paracrine, or organotropism and independent of the cell origin of CAF. (a) Representative confocal fluorescence microscopy images and statistical analysis (with Mann-Whitney U test) of αSMA of NIH-3T3 cells seeded on glass supplied with CM of 231-WT cells short-termly cultured on 0.6 and 35 kPa

polyacrylamide hydrogel. (b) Representative confocal fluorescence microscopy images and statistical analysis (with Kruskal-Wallis one-way ANOVA and Dunn's multiple comparisons test) of αSMA of NIH-3T3 cells seeded on glass supplied with CM of 231-BrM and 231-BoM cells. (c). Workflow, (d) single cell trajectory and radar graph of mouse MSCs seeded in chemotaxis chip supplied with 231-0.6 CM on the left and 231-35 CM on the right. (e). Workflow, (f) representative confocal fluorescence microscopy images and statistical analysis (with Mann-Whitney U test) of αSMA of mouse MSCs seeded on 0.6 and 35 kPa polyacrylamide hydrogel. (g). Workflow, (h) representative confocal fluorescence microscopy images and statistical analysis (with Kruskal-Wallis one-way ANOVA and Dunn's multiple comparisons test) of αSMA of mouse MSCs seeded on glass supplied with 231-0.6 CM on left and 231-35 CM. (Error bars represent s.e.m., ns: no significance, ***: $P < 0.001$, ****: $P < 0.0001$.)

Considering CAF populations are also heterogeneous, the definition of CAF subpopulation depended on the clustering process in scRNA-seq and specific marker selection, but it has been reported some subpopulations showed limited ECM-related function but mainly secreted cytokines [230, 231, 261, 270, 276]. To guarantee the CAF induced by CM indeed remodeling ECM, we seeded 0.6/231-35 CM induced NIH-3T3-derived CAF in 3D collagen gel to evaluate their ECM remodeling capacity (Fig. 5.18a), then SHG with multi-photon microscopy were conducted, showing 231-35 CM-induced CAF generated more collagen alignment than 231-0.6 CM (Fig. 5.18b), to check the impact of the remodeling on ECM stiffness, we seeded 0.6/231-35 CM induced NIH-3T3-derived CAF on the top of 2D collagen gel, and applied AFM to measure the stiffness next to the induced CAFs (Fig. 5.18c), which to found the 231-0.6 CM induced NIH-3T3-derived CAF less stiffened the local collagen gel than 231-35 group (Fig. 5.18d). Moreover, the 231-0.6 population itself exhibited similarly compromised ECM remodeling ability (Fig. 5.18e,f).

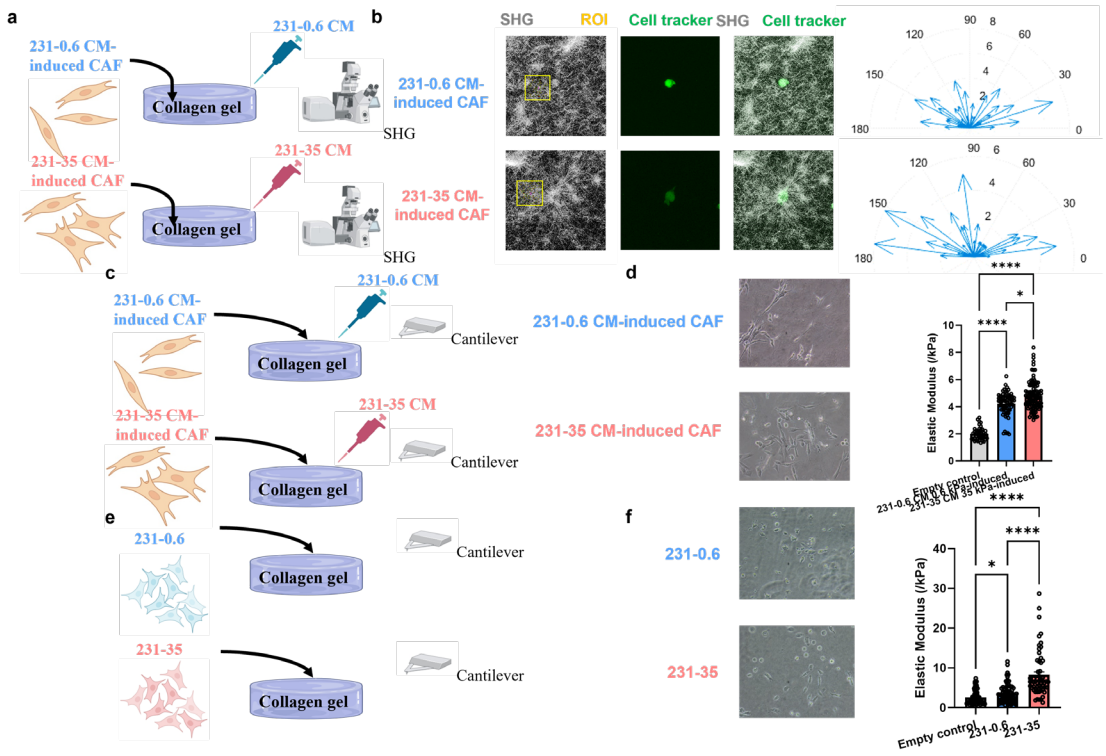

Fig. 5.19 Soft-primed cells and the conditioned CAF showed limited ECM stiffening ability. (a). Workflow, (b) representative multiphoton microscopy images and radar graph of collagen fibers of collagen gels embedded with 231-0.6 CM and 231-35 CM induced NIH-3T3 cells supplied with 231-0.6 CM and 231-35 CM. (c). Workflow, (d) representative bright field microscopy images and statistical analysis (with Kruskal-Wallis one-way ANOVA and Dunn's multiple comparisons test) of elastic modulus of collagen gels seeded with 231-0.6 CM and 231-35 CM induced NIH-3T3 cells on the top supplied with 231-0.6 CM and 231-35 CM respectfully. (e). Workflow, (f) representative bright field microscopy images and statistical analysis (with Kruskal-Wallis one-way ANOVA and Dunn's multiple comparisons test) of elastic modulus of collagen gels seeded with 231-0.6 and 231-35 cells. (g) Workflow and (h) representative multiphoton microscopy images of mCherry and collagen fibers in mouse fat pad orthotopic tumor xenograft slides generated from pNDRG1-mCherry-fluc-231-scp1 cell line. (Error bars represent s.e.m., *: $P < 0.05$, ****: $P < 0.0001$.)

5.2.10 Local niche softness, brain metastasis potential, and negative durotaxis pattern are clinically correlated

The correlation between local niche softness, brain metastasis potential, and negative-durotaxis pattern has been exclusively proved in vitro in the work above, meanwhile, we showed integrin α10 was up-regulated in soft niche residents and brain metastatic subpopulations (Fig. 5.6g). However,

this study focused on intratumoral heterogeneity, information at single-cell scale and spatial distribution were lost in bulk RNA-seq.

To elucidate if our finding displayed clinical relevance at a single-cell scale, we analyzed the single-cell RNA-seq data of GSM7782698 of GSE243275 in the GEO database. Whole-cell population cell type annotation was conducted to exclude non-cancer cells (Fig. 5.19a), focusing on cancer cells, we identified NDRG1 as a single-cell scale breast cancer local niche softness ruler across cell lines (Fig. 4.1-4.4), thus we discovered a positive correlation between NDRG1, brain metastasis gene signature, integrin α10-PI3K-Akt signature (Fig. 5.19b), individual brain metastasis-related genes (Fig. 5.19c) and individual integrin α10-PI3K-Akt related genes (Fig. 5.19d) in the UMAP distribution. Moreover, we separated cancer cells into NDRG1+ and NDRG1- groups, both brain metastasis signature and integrin α10-PI3K-Akt signature are enhanced in NDRG1+ subgroup (Fig. 5.19e,f). Another patient sample scRNA-seq GSM7782697 of GSE243275 in the GEO database was also analyzed, which showed similar results (data not shown).

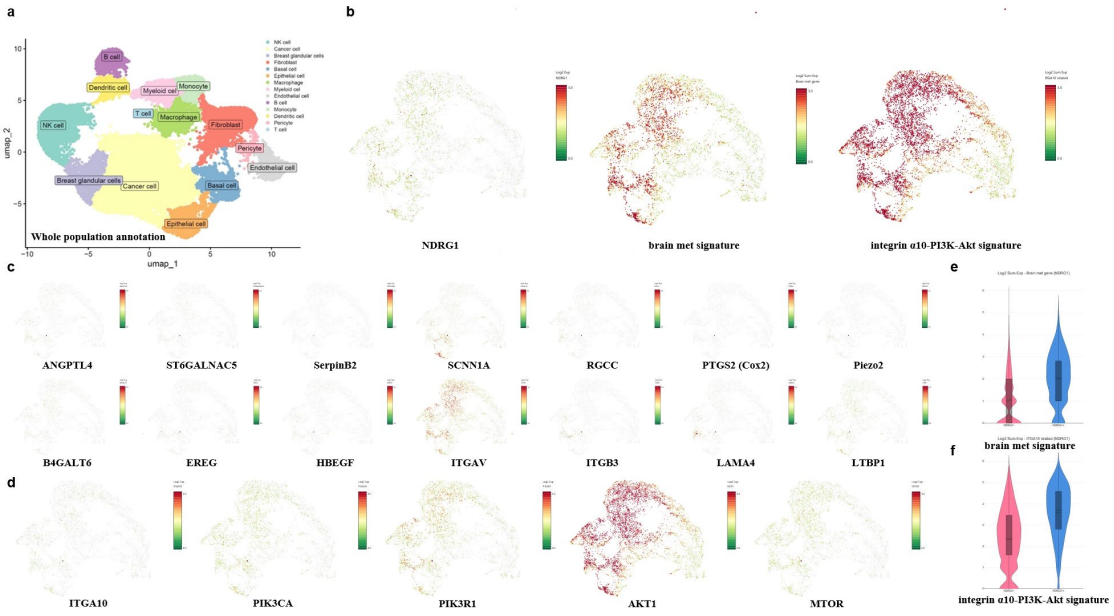

Fig. 5.20 NDRG1, brain metastasis potential, and negative durotaxis manner are positively correlated at single-cell scale in the patient sample. (a). UMAP visualization of whole population cell type annotation. (b-d) UMAP visualization of cancer cells overlaid with the expression of indicated genes and gene sets. (e,f) Violin plot of indicated gene set level of NDRG1- and NDRG1+ subpopulations.

To clarify whether our finding exhibited clinical relevance at spatial distribution in tumors, we analyzed the spatial transcriptomics data of the Human Whole Transcriptome Probe Set sample (sample ID: Visium_FFPE_Human_Breast_Cancer) in 10x Genomics. The spatial distribution NDRG1, brain metastasis gene signature, and integrin α10-PI3K-Akt signature were demonstrated (Fig. 5.20a), the expression of which at single barcode resolution showed a positive correlation between each two (Fig. 5.20b), we separate the barcodes into NDRG1- and NDRG1+ groups (Fig. 5.20c), brain metastasis gene signature, integrin α10-PI3K-Akt signature and individual brain metastasis genes and integrin α10-PI3K-Akt genes were up-regulated in NDRG1+ subgroup barcodes (Fig. 5.20d,e). Another two patient spatial transcriptome samples (sample ID: Visium_Human_Breast_Cancer, Parent_Visium_Human_BreastCancer) in 10x Genomics were also analyzed, which exhibited similar positive correlations (data not shown).

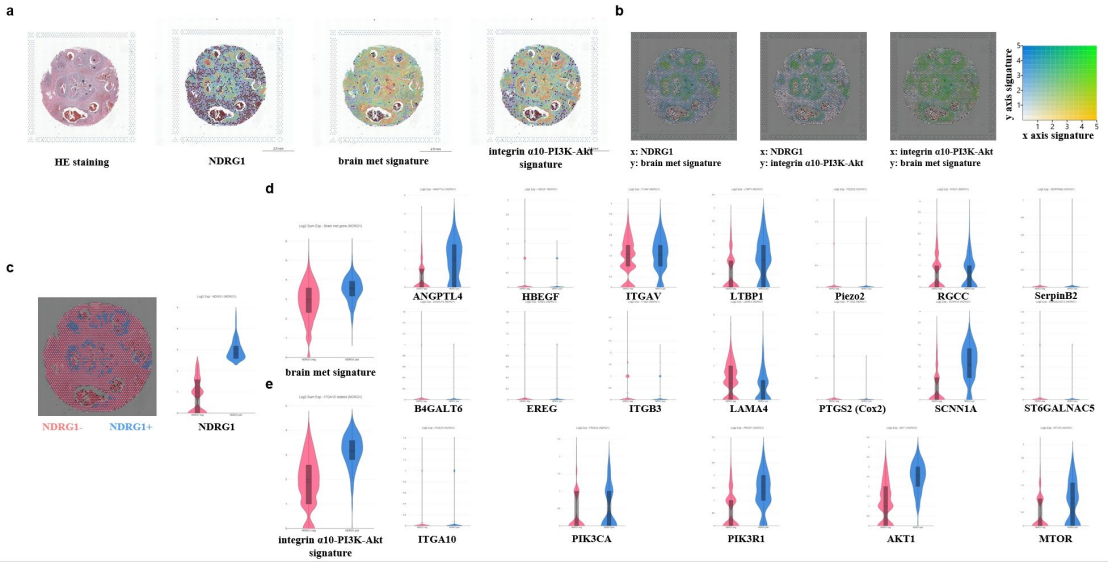

Fig. 5.21 NDRG1, brain metastasis potential, and negative durotaxis manner are spatially correlated in the patient sample. (a). HE staining and heatmap of indicated genes in spatial transcriptome at single-barcode resolution. (b) Visualization of correlation of indicated genes and gene sets in spatial transcriptome at single-barcode resolution. (c) NDRG1 distribution and violin plot of NDRG1- and NDRG1+ subgroup barcodes. (d,e). Violin plot of indicated gene set and individual level of NDRG1- and NDRG1+ subgroup barcodes.

Collectively, scRNA-seq and spatial transcriptome confirmed the brain that the local niche softness, brain metastasis potential, and negative-durotaxis pattern are correlated in clinical patient samples.

5.2.11 Local niche softness and CAF are negatively correlated in clinical samples

CAF activation was limited by softness and soft niche residents in vitro, if it was still true in vivo and in clinic remained unknown. Similar to 3.2.10, we checked the spatial distribution of related signatures in the tumor, and we analyzed the spatial transcriptomics data of the Human Whole Transcriptome Probe Set sample (sample ID: Visium_FFPE_Human_Breast_Cancer) in 10x Genomics. The spatial distribution NDRG1 and CAF signature were demonstrated (Fig. 5.21a), the expression of which at single barcode resolution showed a negative correlation between each two (Fig. 5.21b), we separate the barcodes into NDRG1- and NDRG1+ groups (Fig. 5.21c), CAF signature and individual CAF marker genes were down-regulated in NDRG1+ subgroup barcodes (Fig. 5.21d,e). Another two patient spatial transcriptome samples (sample ID: Visium_Human_Breast_Cancer, Parent_Visium_Human_BreastCancer) in 10x Genomics were also analyzed, which exhibited similar negative correlations (data not shown).

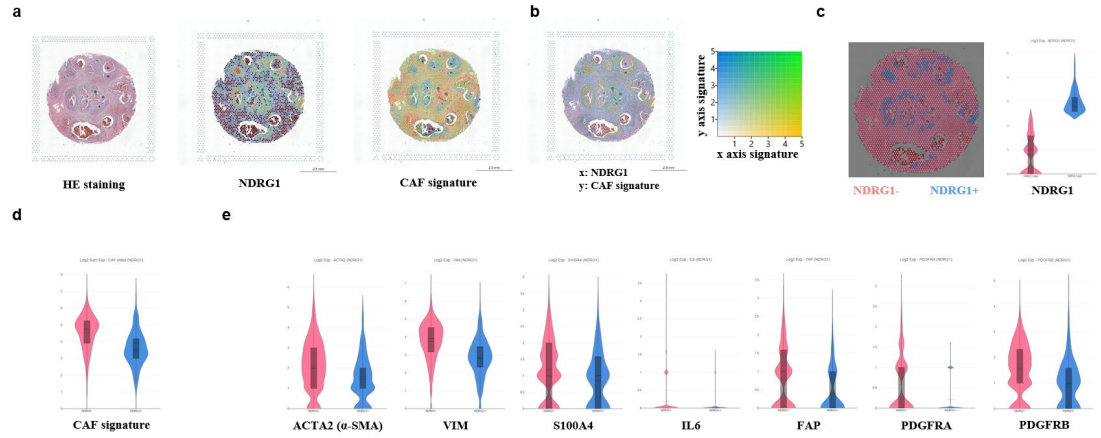

Fig. 5.22 NDRG1 and CAF activation are negatively spatially correlated in the patient sample. (a). HE staining and heatmap of indicated genes in spatial transcriptome at single-barcode resolution. (b) Visualization of correlation of indicated genes and gene sets in spatial transcriptome at single-barcode resolution. (c) NDRG1 distribution and violin plot of NDRG1- and NDRG1+ subgroup barcodes. (d,e). Violin plot of indicated gene set and individual level of NDRG1- and NDRG1+ subgroup barcodes.

In short, we demonstrated CAF and local niche softness displayed a negative correlation spatially, which confirmed our finding in vivo and in clinic.

Chapter VI: Discussions and Limitations

6.1 Conclusion

In the first chapter of the present thesis, we established a single-cell scale local niche softness biosensor and exclusively verified the efficiency in vitro and in vivo. With the new sensor, we identified a soft local niche, separated cancer cells from tumor xenograft based on residing niche stiffness for each cell, and proved the soft local niche residents were brain metastatic in xenograft. (Fig. 6.1)

In the second chapter of the proposed study, we explained how soft niche and soft niche resident were kept long-term correlated: Firstly, we demonstrated soft primed cells were integrin α10-PI3K-Akt hyperactivation-dependent negative-durotactic and positive-viscotactic thereby they preferred kept residing in soft and viscous-like niche. Secondly, we discovered a soft niche-specific cell competition manner in that soft niche residing cells eliminated outsiders to guarantee clonal dominance. Thirdly, we revealed soft niche residents showed limited CAF activation and ECM remodeling ability so that soft niche wouldn't be stiffened. All this guaranteed long-term soft-priming and promoted brain metastasis. Interestingly, negative-durotaxis independently enhanced brain metastasis potential with a positive feedback loop (Fig. 6.1).

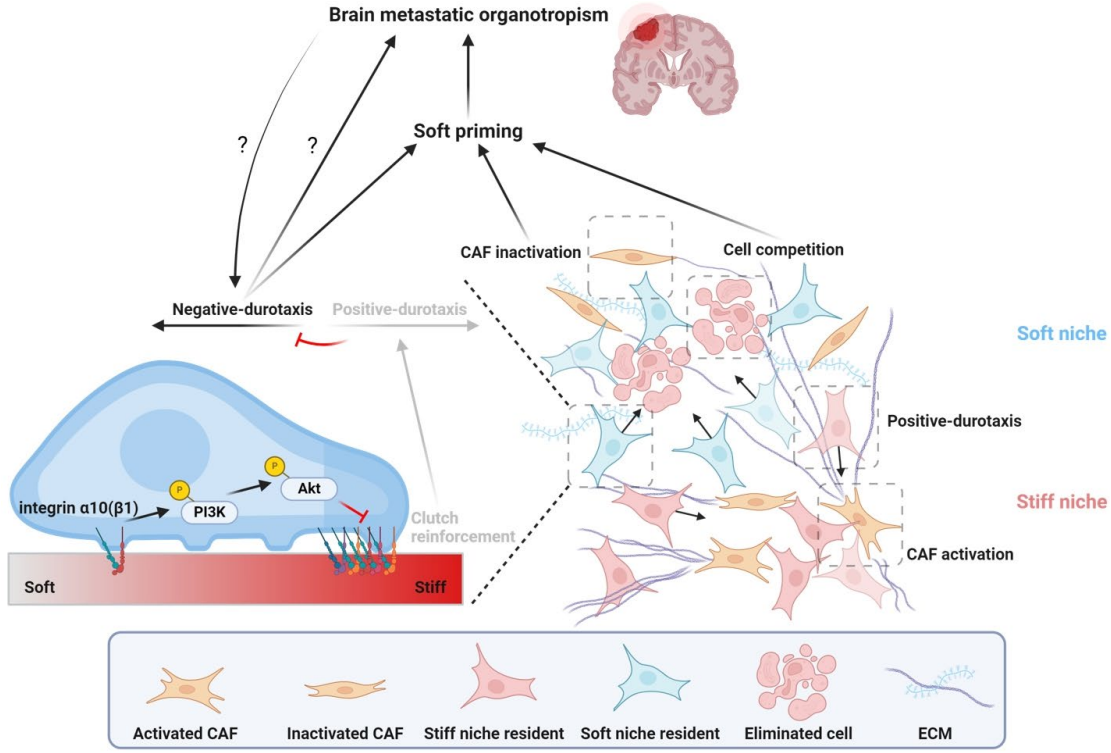

Fig. 6.1 Graphic Illustration of the present study

6.2 Significance

Metastatic organotropism determines the ending of some cancer patients in a certain sense. Brain metastasis is the most devastating and is sometimes regarded as the last metastasis [157]. In the previous research we found in-vitro soft priming on biomaterials enhanced brain metastasis, especially BBB trans-migration and brain colonization ability. This previously unappreciated role of ECM softness was surprising, however, it lacked clinical relevance, and we had no clue whether softness plays the same role in tumors where the mechanical properties were heterogenous [111, 112, 246].

Under this circumstance, as suggested in a recent perspective [386], establishing a local niche mechanics biosensor to focus on local niche mechanics is needed. In Chapter IV, we developed the pNDRG1-mCherry sensor, it provided a tool for us to separate populations based on cell residing microenvironment. The "responsive promoter" strategy could be extended even beyond mechano-oncology, researchers could imitate the design and the workflow to separate other subpopulations from vivo at a single-cell scale, for instance, separating cells enduring other mechanical stimulations using corresponding mechano-sensitive promoter, separating cells surviving immune attack with corresponding immune attack-responsive promoter or separating host cell parasitized by specific pathogens with cell-autonomous immunity-related promoter.

With this sensor, we exclusively provided in-vivo evidence that soft-residing cells were brain metastatic. Besides, because the in-situ correlation data was mutually bidirectional, we could also conclude brain metastatic seeds were residing in relatively softer niches. This external mechano-stimulation-free proof was unprecedentedly stronger than any other studies conducted based on in-vitro biomaterials.

The good correlation in vivo proved the clinical relevance of our finding in vitro, but an intriguing

problem emerged: How is the correlation maintained so that soft niche could long-termly educate the residents to become brain metastatic? Then we explored the answer in Chapter V.

Soft priming cannot be achieved if soft niche residents migrated away, therefore we inspected what kept soft primed cells residing in the soft niche. Some rare negative-durotactic cell types were recently identified [51, 191, 321], but little was known about the specific molecular mechanism or whether the durotaxis pattern could be reprogrammed [322, 323]. We uncovered soft priming switched from positive-durotaxis manner to negative, we also identified the integrin α10-PI3K-Akt signaling pathway was required for negative-durotaxis shifting. In addition, we found negative-durotaxis not only guaranteed long-term soft priming but also contributed to brain metastasis capacity independently of microenvironment mechanics with a positive feedback loop. Further, tissues are viscoelastic, if there are certain viscous properties in soft local niche, meanwhile it attracts soft-primed cells, the process should be more convincing. We uncovered the soft local niches were more viscous-like in tumors, meanwhile negative-durotaxis manner was associated with positive-viscotaxis and vice versa (verified by soft priming/shITGA10/shMYH10), both of which help the self-organization of cancer mechano-heterogeneity. It was the first time that the pathological meaning and the underlying mechanism of negative-durotaxis and positive-viscotaxis were identified, which was an innovation of both concepts.

Soft priming cannot be reached without clonal dominance, we found a soft niche-specific soft-primed cell competence superiority, which was correlated with a cytosol/membrane transmission, interestingly integrin α10 in 231-0.6 was required in this process, this phenomenon and the precise mechanism were completely unknown, but it well-explained the clonal dominance of soft-primed cell in the soft local niche.

Soft priming cannot be accomplished without soft niches, thus we investigated the reason why the soft local niche is not stiffened. CAFs contribute most to ECM modification [32, 110, 202, 224-235, 270-280], it's reported that soft microenvironment limited CAF activation [250, 290, 414], here we found soft niche residents displayed compromised CAF activation capacity as well, both of which resulted in restricted local niche stiffening effect, which explained how the local niche softness was maintained.

6.3 Limitations and Perspectives

In Chapter IV, we designed a novel pNDRG1-mCherry local niche softness biosensor, this sensor could be extensively used to confirm correlations in vivo without any additional mechanical application, however, there were several limitations in the sensor design. The key limitation was that the effectiveness of the pNDRG1-mCherry sensor relied on mechano-transduction-mediated transcriptional mechano-sensitivity, sometimes mechano-transduction could be disturbed, and then the sensor signals lost meaning. Meanwhile, any genomic or pharmacological manipulation possibly impacting the mechano-transduction could bias the sensor outcome, so the pNDRG1-mCherry sensor could only establish correlations but not causal relationships. Another problem was because basically pNDRG1-mCherry was the transcriptional reporter of NDRG1, and NDRG1 was a functional protein, circular argument was always a potential confounding to exclude. Moreover, the usage of the sensor required precise control of the virus transfection copy number, or the competitive inhibitor would be an issue. Even though we applied single-cell clones to unify, when separating $mCherry^+$ populations from xenograft, polyploid cells were collected as well, which were identified as more metastatic and malignant subpopulations [416, 417]. To solve this problem, we might need another opposite local niche stiffness (versus softness) biosensor for equilibrium. Currently, we have not found a qualified candidate representing local niche stiffness but irrelevant to organotropism.

In Chapter V, about the negative-durotaxis of soft-primed 231-0.6, here we proved the durotaxis pattern was not an intrinsic feature for each cell type or cell line, the durotaxis pattern could be manipulated. We identified the softness-integrin α10-PI3K-Akt axis as the key regulator in softness-evoked negative-durotaxis, however, there's still a gap between Akt phosphorylation and clutch reinforcement. The cycle of $PI(3,4)P_2$, PI_4P, $PI(4,5)P_2$ PIP_3, PTEN, and mitochondrial trafficking might be involved in this process [418, 419]. After that we found negative-durotaxis was a prerequisite of brain metastasis with a positive feedback loop, this correlation seemed to be correct: negative-durotaxis was a seeking-for-softness behavior meanwhile the softest organ in body was brain, recent finding suggesting there're two (at least) modes of brain metastatic colonization [161], the stiffness

gap between brain vasculature and parenchyma promoted brain metastatic infiltration in TNBC and lung adenocarcinoma (LUAD), which formed perivascular sheaths with diffusive contact with astrocytes and microglia [160], brain metastasis was an vasculature-to-parenchyma (stiff-to-soft, non-viscous-to-viscous) process, if the stiffness and viscous property gradient explained the importance of negative-durotaxis and positive-viscotaxis in brain metastasis remained unclear; the PI3K-Akt signaling mediated negative-durotaxis and was the hallmark of brain metastatic phenotype meanwhile [400-404], melanoma was negative-durotactic meanwhile exhibited the highest brain metastasis risk across all cancer types [12, 191]. Even though we extensively provided evidence that these two behaviors could hardly be decoupled, it remained intriguing how there were casual relationships between the two unrelated phenomena, further studies were required to understand the intrinsic connection between brain tropism and negative-durotaxis.

The correlation between viscous behavior and low elasticity was a new finding, we demonstrated that negative-durotaxis and positive-viscotaxis collectively guaranteed long-term soft priming. Negative-viscotaxis was believed because of membrane/integrin-ECM ligand bond instability in high loss microenvironment so that low loss directional won the force competition [324], thus we hypothesized and proved that if soft-primed cells displayed compromised clutch reinforcement anyway, logically negative-viscotaxis should be reversed. However, this explanation was too abstractive, so we planned to cooperate with external experts to establish a theoretical model to illustrate the positive-viscotaxis process of the negative-durotactic subpopulation.

Little is known about the new form of cell competition we discovered since it's integrin α10-dependent, current mechanical signaling (YAP, ERK, Notch, etc.)-related cell competition types were worth considering, [361, 369-372, 395].

Besides, we claimed compromised CAF inactivation participated in the positive feedback loop to maintain the local niche softness, here we only considered the ECM secretion and modification, it's possible that 231-0.6 and 231-0.6-induced CAF phenotype positively degrade local ECM to soften the local niche, it's worth exploring by further research.

Reference List

[1] R.L. Siegel, A.N. Giaquinto, A. Jemal, Cancer statistics, 2024, CA Cancer J Clin 74(1) (2024) 12-49.

[2] S. Gerstberger, Q. Jiang, K. Ganesh, Metastasis, Cell 186(8) (2023) 1564-1579.

[3] S. Paget, The distribution of secondary growths in cancer of the breast, The Lancet 133(3421) (1889) 571-573.

[4] Y. Gao, I. Bado, H. Wang, W. Zhang, J.M. Rosen, X.H.F. Zhang, Metastasis Organotropism: Redefining the Congenial Soil, Dev Cell 49(3) (2019) 375-391.

[5] U.F. Azubuike, K. Tanner, Biophysical determinants of cancer organotropism, Trends Cancer 9(3) (2023) 188-197.

[6] F. Urabe, K. Patil, G.A. Ramm, T. Ochiya, C. Soekmadji, Extracellular vesicles in the development of organ-specific metastasis, J Extracell Vesicles 10(9) (2021) e12125.

[7] X. Zhuang, H. Zhang, X. Li, X. Li, M. Cong, F. Peng, J. Yu, X. Zhang, Q. Yang, G. Hu, Differential effects on lung and bone metastasis of breast cancer by Wnt signalling inhibitor DKK1, Nat Cell Biol 19(10) (2017) 1274-1285.

[8] G. Li, X. Yi, S. Du, L. Gong, Q. Wu, J. Cai, S. Sun, Y. Cao, L. Chen, L. Xu, Z. Wang, Tumour-derived exosomal piR-25783 promotes omental metastasis of ovarian carcinoma by inducing the fibroblast to myofibroblast transition, Oncogene 42(6) (2023) 421-433.

[9] H. Zhang, T. Deng, R. Liu, M. Bai, L. Zhou, X. Wang, S. Li, X. Wang, H. Yang, J. Li, T. Ning, D. Huang, H. Li, L. Zhang, G. Ying, Y. Ba, Exosome-delivered EGFR regulates liver microenvironment to promote gastric cancer liver metastasis, Nat Commun 8 (2017) 15016.

[10] H.B. Lengel, B. Mastrogiacomo, J.G. Connolly, K.S. Tan, Y. Liu, C.N. Fick, E.G. Dunne, D. He, M.B. Lankadasari, B.A. Satravada, Y. Sun, R. Kundra, C. Fong, S. Smith, G.J. Riely, C.M. Rudin, D.R. Gomez, D.B. Solit, M.F. Berger, B.T. Li, M.W. Mayo, I. Matei, D.C. Lyden, P.S. Adusumilli, N. Schultz, F. Sanchez-Vega, D.R. Jones, Genomic mapping of metastatic organotropism in lung adenocarcinoma, Cancer cell 41(5) (2023).

[11] M. Rogava, T.J. Aprati, W.-Y. Chi, J.C. Melms, C. Hug, S.H. Davis, E.M. Earlie, C. Chung, S.K. Deshmukh, S. Wu, G. Sledge, S. Tang, P. Ho, A.D. Amin, L. Caprio, C. Gurjao, S. Tagore, B. Ngo, M.J. Lee, G. Zanetti, Y. Wang, S. Chen, W. Ge, L.M.N. Melo, G. Allies, J. Rösler, G.T. Gibney, O.J. Schmitz, M. Sykes, R.J. Creusot, T. Tüting, D. Schadendorf, M. Röcken, T.K. Eigentler, A. Molotkov, A. Mintz, S.F. Bakhoum, S. Beyaz, L.C. Cantley, P.K. Sorger, S.W. Meckelmann, A. Tasdogan, D. Liu, A.M. Laughney, B. Izar, Loss of Pip4k2c confers liver-metastatic organotropism through insulin-dependent PI3K-AKT pathway activation, Nat Cancer 5(3) (2024) 433-447.

[12] X. Wang, Y. Chen, B. Lan, Y. Wang, W. Lin, X. Jiang, J. Ye, B. Shang, C. Feng, J. Liu, J. Zhai, M. Xu, Q. Li, L. Lin, M. Hu, F. Zheng, L. Chen, C. Shao, Y. Wang, Y. Shi, Heterogeneity of tyrosine-based melanin anabolism regulates pulmonary and cerebral organotropic colonization microenvironment of melanoma cells, Theranostics 12(5) (2022) 2063-2079.

[13] C. Wang, D. Luo, The metabolic adaptation mechanism of metastatic organotropism, Exp Hematol Oncol 10(1) (2021) 30.

[14] X. Lu, Y. Kang, Efficient acquisition of dual metastasis organotropism to bone and lung through stable spontaneous fusion between MDA-MB-231 variants, Proc Natl Acad Sci U S A 106(23) (2009) 9385-9390.

[15] K. Kos, M.A. Aslam, R. van de Ven, M.D. Wellenstein, W. Pieters, A. van Weverwijk, D.E.M. Duits,

K. van Pul, C.-S. Hau, K. Vrijland, D. Kaldenbach, E.A.M. Raeven, S.A. Quezada, R. Beyaert, H. Jacobs, T.D. de Gruijl, K.E. de Visser, Tumor-educated Tregs drive organ-specific metastasis in breast cancer by impairing NK cells in the lymph node niche, Cell Rep 38(9) (2022) 110447.
[16] K.E. Hupfeld, H.R. McGregor, P.A. Reuter-Lorenz, R.D. Seidler, Microgravity effects on the human brain and behavior: Dysfunction and adaptive plasticity, Neurosci Biobehav Rev 122 (2021) 176-189.
[17] L. Vico, P. Collet, A. Guignandon, M.H. Lafage-Proust, T. Thomas, M. Rehaillia, C. Alexandre, Effects of long-term microgravity exposure on cancellous and cortical weight-bearing bones of cosmonauts, Lancet 355(9215) (2000) 1607-1611.
[18] J.S. Khaw, R. Xue, N.J. Cassidy, S.H. Cartmell, Electrical stimulation of titanium to promote stem cell orientation, elongation and osteogenesis, Acta Biomater 139 (2022) 204-217.
[19] A.V. Van Huizen, J.M. Morton, L.J. Kinsey, D.G. Von Kannon, M.A. Saad, T.R. Birkholz, J.M. Czajka, J. Cyrus, F.S. Barnes, W.S. Beane, Weak magnetic fields alter stem cell-mediated growth, Sci Adv 5(1) (2019) eaau7201.
[20] G. Follain, D. Herrmann, S. Harlepp, V. Hyenne, N. Osmani, S.C. Warren, P. Timpson, J.G. Goetz, Fluids and their mechanics in tumour transit: shaping metastasis, Nature reviews. Cancer 20(2) (2020) 107-124.
[21] X. Wang, Y. Shen, M. Shang, X. Liu, L.L. Munn, Endothelial mechanobiology in atherosclerosis, Cardiovasc Res 119(8) (2023) 1656-1675.
[22] M. Bagnat, B. Daga, S. Di Talia, Morphogenetic Roles of Hydrostatic Pressure in Animal Development, Annu Rev Cell Dev Biol 38 (2022) 375-394.
[23] H.T. Nia, H. Liu, G. Seano, M. Datta, D. Jones, N. Rahbari, J. Incio, V.P. Chauhan, K. Jung, J.D. Martin, V. Askoxylakis, T.P. Padera, D. Fukumura, Y. Boucher, F.J. Hornicek, A.J. Grodzinsky, J.W. Baish, L.L. Munn, R.K. Jain, Solid stress and elastic energy as measures of tumour mechanopathology, Nature biomedical engineering 1 (2016).
[24] X. Zhao, J. Hu, Y. Li, M. Guo, Volumetric compression develops noise-driven single-cell heterogeneity, Proc. Natl. Acad. Sci. U. S. A. 118(51) (2021).
[25] G.P.d.F. Nader, S. Agüera-Gonzalez, F. Routet, M. Gratia, M. Maurin, V. Cancila, C. Cadart, A. Palamidessi, R.N. Ramos, M. San Roman, M. Gentili, A. Yamada, A. Williart, C. Lodillinsky, E. Lagoutte, C. Villard, J.-L. Viovy, C. Tripodo, J. Galon, G. Scita, N. Manel, P. Chavrier, M. Piel, Compromised nuclear envelope integrity drives TREX1-dependent DNA damage and tumor cell invasion, Cell 184(20) (2021).
[26] M.A. Swartz, A.W. Lund, Lymphatic and interstitial flow in the tumour microenvironment: linking mechanobiology with immunity, Nature reviews. Cancer 12(3) (2012) 210-219.
[27] K. Bera, A. Kiepas, I. Godet, Y. Li, P. Mehta, B. Ifemembi, C.D. Paul, A. Sen, S.A. Serra, K. Stoletov, J. Tao, G. Shatkin, S.J. Lee, Y. Zhang, A. Boen, P. Mistriotis, D.M. Gilkes, J.D. Lewis, C.-M. Fan, A.P. Feinberg, M.A. Valverde, S.X. Sun, K. Konstantopoulos, Extracellular fluid viscosity enhances cell migration and cancer dissemination, Nature 611(7935) (2022) 365-373.
[28] A. Elosegui-Artola, A. Gupta, A.J. Najibi, B.R. Seo, R. Garry, C.M. Tringides, I. de Lázaro, M. Darnell, W. Gu, Q. Zhou, D.A. Weitz, L. Mahadevan, D.J. Mooney, Matrix viscoelasticity controls spatiotemporal tissue organization, Nat Mater 22(1) (2023) 117-127.
[29] A. Shellard, R. Mayor, Collective durotaxis along a self-generated stiffness gradient in vivo, Nature 600(7890) (2021) 690-694.
[30] W. Fan, K. Adebowale, L. Váncza, Y. Li, M.F. Rabbi, K. Kunimoto, D. Chen, G. Mozes, D.K.-C. Chiu, Y. Li, J. Tao, Y. Wei, N. Adeniji, R.L. Brunsing, R. Dhanasekaran, A. Singhi, D. Geller, S.H. Lo,

L. Hodgson, E.G. Engleman, G.W. Charville, V. Charu, S.P. Monga, T. Kim, R.G. Wells, O. Chaudhuri, N.J. Török, Matrix viscoelasticity promotes liver cancer progression in the pre-cirrhotic liver, Nature 626(7999) (2024) 635-642.
[31] J.J.F. Sleeboom, G.S. van Tienderen, K. Schenke-Layland, L.J.W. van der Laan, A.A. Khalil, M.M.A. Verstegen, The extracellular matrix as hallmark of cancer and metastasis: From biomechanics to therapeutic targets, Sci Transl Med 16(728) (2024) eadg3840.
[32] M.R. Zanotelli, J.P. Miller, W. Wang, I. Ortiz, E. Tahon, F. Bordeleau, C.A. Reinhart-King, Tension directs cancer cell migration over fiber alignment through energy minimization, Biomaterials 311 (2024) 122682.
[33] F. Lin, Y. Zhou, X. Duan, X. Fang, Q. Zhang, Y. Zhang, P. Wang, J. Huang, Spontaneous formation and spatial self-organization of mechanically induced mesenchymal-like cells within geometrically confined cancer cell monolayers, Biomaterials 281 (2022) 121337.
[34] M. Bao, J. Xie, N. Katoele, X. Hu, B. Wang, A. Piruska, W.T.S. Huck, Cellular Volume and Matrix Stiffness Direct Stem Cell Behavior in a 3D Microniche, ACS Appl Mater Interfaces 11(2) (2019) 1754-1759.
[35] L.F. Lorenzo-Martín, T. Hübscher, A.D. Bowler, N. Broguiere, J. Langer, L. Tillard, M. Nikolaev, F. Radtke, M.P. Lutolf, Spatiotemporally resolved colorectal oncogenesis in mini-colons ex vivo, Nature 629(8011) (2024) 450-457.
[36] M. Nikolaev, O. Mitrofanova, N. Broguiere, S. Geraldo, D. Dutta, Y. Tabata, B. Elci, N. Brandenberg, I. Kolotuev, N. Gjorevski, H. Clevers, M.P. Lutolf, Homeostatic mini-intestines through scaffold-guided organoid morphogenesis, Nature 585(7826) (2020) 574-578.
[37] D.C. Bagley, T. Russell, E. Ortiz-Zapater, S. Stinson, K. Fox, P.F. Redd, M. Joseph, C. Deering-Rice, C. Reilly, M. Parsons, C. Brightling, J. Rosenblatt, Bronchoconstriction damages airway epithelia by crowding-induced excess cell extrusion, Science (New York, N.Y.) 384(6691) (2024) 66-73.
[38] M.M. Nava, Y.A. Miroshnikova, L.C. Biggs, D.B. Whitefield, F. Metge, J. Boucas, H. Vihinen, E. Jokitalo, X. Li, J.M. García Arcos, B. Hoffmann, R. Merkel, C.M. Niessen, K.N. Dahl, S.A. Wickström, Heterochromatin-Driven Nuclear Softening Protects the Genome against Mechanical Stress-Induced Damage, Cell 181(4) (2020).
[39] R. Guo, D. Han, X. Song, Y. Gao, Z. Li, X. Li, Z. Yang, Z. Xu, Context-dependent regulation of Notch signaling in glial development and tumorigenesis, Science advances 9(45) (2023) eadi2167.
[40] A.M. Mendonsa, T.-Y. Na, B.M. Gumbiner, E-cadherin in contact inhibition and cancer, Oncogene 37(35) (2018) 4769-4780.
[41] S.P. Pothapragada, P. Gupta, S. Mukherjee, T. Das, Matrix mechanics regulates epithelial defence against cancer by tuning dynamic localization of filamin, Nature communications 13(1) (2022) 218.
[42] P. Kanchanawong, D.A. Calderwood, Organization, dynamics and mechanoregulation of integrin-mediated cell-ECM adhesions, Nat Rev Mol Cell Biol 24(2) (2023) 142-161.
[43] A. Saraswathibhatla, D. Indana, O. Chaudhuri, Cell-extracellular matrix mechanotransduction in 3D, Nat Rev Mol Cell Biol 24(7) (2023) 495-516.
[44] C. Chen, S. Zhao, A. Karnad, J.W. Freeman, The biology and role of CD44 in cancer progression: therapeutic implications, J Hematol Oncol 11(1) (2018) 64.
[45] Y. Jiang, X. Yang, J. Jiang, B. Xiao, Structural Designs and Mechanogating Mechanisms of the Mechanosensitive Piezo Channels, Trends Biochem Sci 46(6) (2021) 472-488.
[46] Y. Xin, X. Chen, X. Tang, K. Li, M. Yang, W.C.-S. Tai, Y. Liu, Y. Tan, Mechanics and Actomyosin-Dependent Survival/Chemoresistance of Suspended Tumor Cells in Shear Flow, Biophys J 116(10) (2019)

1803-1814.
[47] X. Chen, Z. Xu, K. Tang, G. Hu, P. Du, J. Wang, C. Zhang, Y. Xin, K. Li, Q. Zhang, J. Hu, Z. Zhang, M. Yang, G. Wang, Y. Tan, The Mechanics of Tumor Cells Dictate Malignancy via Cytoskeleton-Mediated APC/Wnt/β-Catenin Signaling, Research (Wash D C) 6 (2023) 0224.
[48] J. Wang, B. Zhang, X. Chen, Y. Xin, K. Li, C. Zhang, K. Tang, Y. Tan, Cell mechanics regulate the migration and invasion of hepatocellular carcinoma cells via JNK signaling, Acta Biomater 176 (2024) 321-333.
[49] S. Conti, V. Venturini, A. Cañellas-Socias, C. Cortina, J.F. Abenza, C. Stephan-Otto Attolini, E. Middendorp Guerra, C.K. Xu, J.H. Li, L. Rossetti, G. Stassi, P. Roca-Cusachs, A. Diz-Muñoz, V. Ruprecht, J. Guck, E. Batlle, A. Labernadie, X. Trepat, Membrane to cortex attachment determines different mechanical phenotypes in LGR5+ and LGR5- colorectal cancer cells, Nat Commun 15(1) (2024) 3363.
[50] P. Verdys, J. Rey Barroso, A. Girel, J. Vermeil, M. Bergert, T. Sanchez, A. Métais, T. Mangeat, E. Bellard, C. Bigot, C. Astarie-Dequeker, A. Labrousse, J.-P. Girard, I. Maridonneau-Parini, C. Vérollet, F. Lagarrigue, A. Diz-Muñoz, J. Heuvingh, M. Piel, O. du Roure, V. Le Cabec, S. Carréno, R. Poincloux, Ezrin, radixin, and moesin are dispensable for macrophage migration and cellular cortex mechanics, EMBO J (2024).
[51] A. Isomursu, K.-Y. Park, J. Hou, B. Cheng, M. Mathieu, G.A. Shamsan, B. Fuller, J. Kasim, M.M. Mahmoodi, T.J. Lu, G.M. Genin, F. Xu, M. Lin, M.D. Distefano, J. Ivaska, D.J. Odde, Directed cell migration towards softer environments, Nature Materials 21(9) (2022) 1081-1090.
[52] B.J. DuChez, A.D. Doyle, E.K. Dimitriadis, K.M. Yamada, Durotaxis by Human Cancer Cells, Biophys J 116(4) (2019) 670-683.
[53] M. Jang, J. An, S.W. Oh, J.Y. Lim, J. Kim, J.K. Choi, J.-H. Cheong, P. Kim, Matrix stiffness epigenetically regulates the oncogenic activation of the Yes-associated protein in gastric cancer, Nat Biomed Eng 5(1) (2021) 114-123.
[54] Y. Chang, J. Zhang, X. Huo, X. Qu, C. Xia, K. Huang, F. Xie, N. Wang, X. Wei, Q. Jia, Substrate rigidity dictates colorectal tumorigenic cell stemness and metastasis via CRAD-dependent mechanotransduction, Cell reports 38(7) (2022) 110390.
[55] X. Liu, Y. Ye, L. Zhu, X. Xiao, B. Zhou, Y. Gu, H. Si, H. Liang, M. Liu, J. Li, Q. Jiang, J. Li, S. Yu, R. Ma, S. Su, J.Y. Liao, Q. Zhao, Niche stiffness sustains cancer stemness via TAZ and NANOG phase separation, Nature communications 14(1) (2023) 238.
[56] S. Dupont, S.A. Wickström, Mechanical regulation of chromatin and transcription, Nat Rev Genet 23(10) (2022) 624-643.
[57] S. Jiao, C. Li, F. Guo, J. Zhang, H. Zhang, Z. Cao, W. Wang, W. Bu, M. Lin, J. Lü, Z. Zhou, SUN1/2 controls macrophage polarization via modulating nuclear size and stiffness, Nat Commun 14(1) (2023) 6416.
[58] N. Mittal, E.B. Michels, A.E. Massey, Y. Qiu, S.P. Royer-Weeden, B.R. Smith, A.X. Cartagena-Rivera, S.J. Han, Myosin-independent stiffness sensing by fibroblasts is regulated by the viscoelasticity of flowing actin, Commun Mater 5 (2024).
[59] R.G. Gaudet, S. Zhu, A. Halder, B.-H. Kim, C.J. Bradfield, S. Huang, D. Xu, A. Mamiñska, T.N. Nguyen, M. Lazarou, E. Karatekin, K. Gupta, J.D. MacMicking, A human apolipoprotein L with detergent-like activity kills intracellular pathogens, Science (New York, N.Y.) 373(6552) (2021).
[60] F.L. Sendker, Y.K. Lo, T. Heimerl, S. Bohn, L.J. Persson, C.-N. Mais, W. Sadowska, N. Paczia, E. Nußbaum, M. Del Carmen Sánchez Olmos, K. Forchhammer, D. Schindler, T.J. Erb, J.L.P. Benesch, E.G.

Marklund, G. Bange, J.M. Schuller, G.K.A. Hochberg, Emergence of fractal geometries in the evolution of a metabolic enzyme, Nature 628(8009) (2024) 894-900.
[61] D. DeVault, J.H. Parkes, B. Chance, Electron tunnelling in cytochromes, Nature 215(5101) (1967) 642-644.
[62] D.S. Wuttke, M.J. Bjerrum, J.R. Winkler, H.B. Gray, Electron-tunneling pathways in cytochrome C, Science 256(5059) (1992) 1007-1009.
[63] H. Xin, W.J. Sim, B. Namgung, Y. Choi, B. Li, L.P. Lee, Quantum biological tunnel junction for electron transfer imaging in live cells, Nat Commun 10(1) (2019) 3245.
[64] L. Slocombe, M. Sacchi, J. Al-Khalili, An open quantum systems approach to proton tunnelling in DNA, Communications Physics 5(1) (2022) 109.
[65] A. Jain, J. Gosling, S. Liu, H. Wang, E.M. Stone, S. Chakraborty, P.-S. Jayaraman, S. Smith, D.B. Amabilino, M. Fromhold, Y.-T. Long, L. Pérez-García, L. Turyanska, R. Rahman, F.J. Rawson, Wireless electrical-molecular quantum signalling for cancer cell apoptosis, Nat Nanotechnol 19(1) (2024) 106-114.
[66] H.T. Nia, L.L. Munn, R.K. Jain, Physical traits of cancer, Science 370(6516) (2020).
[67] Y. Xin, K. Li, M. Huang, C. Liang, D. Siemann, L. Wu, Y. Tan, X. Tang, Biophysics in tumor growth and progression: from single mechano-sensitive molecules to mechanomedicine, Oncogene 42(47) (2023) 3457-3490.
[68] T. Panciera, A. Citron, D. Di Biagio, G. Battilana, A. Gandin, S. Giulitti, M. Forcato, S. Bicciato, V. Panzetta, S. Fusco, L. Azzolin, A. Totaro, A.P. Dei Tos, M. Fassan, V. Vindigni, F. Bassetto, A. Rosato, G. Brusatin, M. Cordenonsi, S. Piccolo, Reprogramming normal cells into tumour precursors requires ECM stiffness and oncogene-mediated changes of cell mechanical properties, Nature Materials 19(7) (2020) 797-806.
[69] O. Chaudhuri, S.T. Koshy, C. Branco da Cunha, J.-W. Shin, C.S. Verbeke, K.H. Allison, D.J. Mooney, Extracellular matrix stiffness and composition jointly regulate the induction of malignant phenotypes in mammary epithelium, Nat Mater 13(10) (2014) 970-978.
[70] N. Bansaccal, P. Vieugue, R. Sarate, Y. Song, E. Minguijon, Y.A. Miroshnikova, D. Zeuschner, A. Collin, J. Allard, D. Engelman, A.-L. Delaunois, M. Liagre, L. de Groote, E. Timmerman, D. Van Haver, F. Impens, I. Salmon, S.A. Wickström, A. Sifrim, C. Blanpain, The extracellular matrix dictates regional competence for tumour initiation, Nature 623(7988) (2023) 828-835.
[71] G. Seano, H.T. Nia, K.E. Emblem, M. Datta, J. Ren, S. Krishnan, J. Kloepper, M.C. Pinho, W.W. Ho, M. Ghosh, V. Askoxylakis, G.B. Ferraro, L. Riedemann, E.R. Gerstner, T.T. Batchelor, P.Y. Wen, N.U. Lin, A.J. Grodzinsky, D. Fukumura, P. Huang, J.W. Baish, T.P. Padera, L.L. Munn, R.K. Jain, Solid stress in brain tumours causes neuronal loss and neurological dysfunction and can be reversed by lithium, Nature biomedical engineering 3(3) (2019) 230-245.
[72] M.E. Fernández-Sánchez, S. Barbier, J. Whitehead, G. Béalle, A. Michel, H. Latorre-Ossa, C. Rey, L. Fouassier, A. Claperon, L. Brullé, E. Girard, N. Servant, T. Rio-Frio, H. Marie, S. Lesieur, C. Housset, J.-L. Gennisson, M. Tanter, C. Ménager, S. Fre, S. Robine, E. Farge, Mechanical induction of the tumorigenic β-catenin pathway by tumour growth pressure, Nature 523(7558) (2015) 92-95.
[73] J.M. Tse, G. Cheng, J.A. Tyrrell, S.A. Wilcox-Adelman, Y. Boucher, R.K. Jain, L.L. Munn, Mechanical compression drives cancer cells toward invasive phenotype, Proc Natl Acad Sci U S A 109(3) (2012) 911-916.
[74] Y.C. Kao, J.R. Jheng, H.J. Pan, W.Y. Liao, C.H. Lee, P.L. Kuo, Elevated hydrostatic pressure enhances the motility and enlarges the size of the lung cancer cells through aquaporin upregulation

mediated by caveolin-1 and ERK1/2 signaling, Oncogene 36(6) (2017) 863-874.
[75] M. Hofmann, M. Guschel, A. Bernd, J. Bereiter-Hahn, R. Kaufmann, C. Tandi, H. Wiig, S. Kippenberger, Lowering of tumor interstitial fluid pressure reduces tumor cell proliferation in a xenograft tumor model, Neoplasia 8(2) (2006) 89-95.
[76] J. Gonzalez-Molina, X. Zhang, M. Borghesan, J. Mendonça da Silva, M. Awan, B. Fuller, N. Gavara, C. Selden, Extracellular fluid viscosity enhances liver cancer cell mechanosensing and migration, Biomaterials 177 (2018) 113-124.
[77] N. Koushki, A. Ghagre, L.K. Srivastava, C. Molter, A.J. Ehrlicher, Nuclear compression regulates YAP spatiotemporal fluctuations in living cells, Proc. Natl. Acad. Sci. U. S. A. 120(28) (2023) e2301285120.
[78] W. Wang, P.V. Taufalele, M. Millet, K. Homsy, K. Smart, E.D. Berestesky, C.T. Schunk, M.M. Rowe, F. Bordeleau, C.A. Reinhart-King, Matrix stiffness regulates tumor cell intravasation through expression and ESRP1-mediated alternative splicing of MENA, Cell reports 42(4) (2023) 112338.
[79] Z. Xu, K. Li, Y. Xin, K. Tang, M. Yang, G. Wang, Y. Tan, Fluid shear stress regulates the survival of circulating tumor cells via nuclear expansion, J Cell Sci 135(10) (2022).
[80] Y. Xin, K. Li, M. Yang, Y. Tan, Fluid Shear Stress Induces EMT of Circulating Tumor Cells via JNK Signaling in Favor of Their Survival during Hematogenous Dissemination, Int J Mol Sci 21(21) (2020).
[81] E. Cambria, M.F. Coughlin, M.A. Floryan, G.S. Offeddu, S.E. Shelton, R.D. Kamm, Linking cell mechanical memory and cancer metastasis, Nature reviews. Cancer 24(3) (2024) 216-228.
[82] S. Bakhshandeh, C. Werner, P. Fratzl, A. Cipitria, Microenvironment-mediated cancer dormancy: Insights from metastability theory, Proc. Natl. Acad. Sci. U. S. A. 119(1) (2022).
[83] C.D. Paul, K. Bishop, A. Devine, E.L. Paine, J.R. Staunton, S.M. Thomas, J.R. Thomas, A.D. Doyle, L.M. Miller Jenkins, N.Y. Morgan, R. Sood, K. Tanner, Tissue Architectural Cues Drive Organ Targeting of Tumor Cells in Zebrafish, Cell Syst 9(2) (2019).
[84] A.W. Watson, A.D. Grant, S.S. Parker, S. Hill, M.B. Whalen, J. Chakrabarti, M.W. Harman, M.R. Roman, B.L. Forte, C.C. Gowan, R. Castro-Portuguez, L.K. Stolze, C. Franck, D.A. Cusanovich, Y. Zavros, M. Padi, C.E. Romanoski, G. Mouneimne, Breast tumor stiffness instructs bone metastasis via maintenance of mechanical conditioning, Cell Rep 35(13) (2021) 109293.
[85] A. Hoshino, B. Costa-Silva, T.-L. Shen, G. Rodrigues, A. Hashimoto, M. Tesic Mark, H. Molina, S. Kohsaka, A. Di Giannatale, S. Ceder, S. Singh, C. Williams, N. Soplop, K. Uryu, L. Pharmer, T. King, L. Bojmar, A.E. Davies, Y. Ararso, T. Zhang, H. Zhang, J. Hernandez, J.M. Weiss, V.D. Dumont-Cole, K. Kramer, L.H. Wexler, A. Narendran, G.K. Schwartz, J.H. Healey, P. Sandstrom, K.J. Labori, E.H. Kure, P.M. Grandgenett, M.A. Hollingsworth, M. de Sousa, S. Kaur, M. Jain, K. Mallya, S.K. Batra, W.R. Jarnagin, M.S. Brady, O. Fodstad, V. Muller, K. Pantel, A.J. Minn, M.J. Bissell, B.A. Garcia, Y. Kang, V.K. Rajasekhar, C.M. Ghajar, I. Matei, H. Peinado, J. Bromberg, D. Lyden, Tumour exosome integrins determine organotropic metastasis, Nature 527(7578) (2015) 329-335.
[86] A. Kostic, C.D. Lynch, M.P. Sheetz, Differential matrix rigidity response in breast cancer cell lines correlates with the tissue tropism, PLoS One 4(7) (2009) e6361.
[87] D.J. McGrail, Q.M.N. Kieu, J.A. Iandoli, M.R. Dawson, Actomyosin tension as a determinant of metastatic cancer mechanical tropism, Phys Biol 12(2) (2015) 026001.
[88] R.V. Kondapaneni, S.S. Rao, Matrix stiffness and cluster size collectively regulate dormancy versus proliferation in brain metastatic breast cancer cell clusters, Biomater Sci 8(23) (2020) 6637-6646.
[89] S.C. Wei, L. Fattet, J.H. Tsai, Y. Guo, V.H. Pai, H.E. Majeski, A.C. Chen, R.L. Sah, S.S. Taylor, A.J. Engler, J. Yang, Matrix stiffness drives epithelial-mesenchymal transition and tumour metastasis through

a TWIST1-G3BP2 mechanotransduction pathway, Nat Cell Biol 17(5) (2015) 678-688.
[90] E.C. Filipe, S. Velayuthar, A. Philp, M. Nobis, S.L. Latham, A.L. Parker, K.J. Murphy, K. Wyllie, G.S. Major, O. Contreras, E.T.Y. Mok, R.F. Enriquez, S. McGowan, K. Feher, L.-E. Quek, S.E. Hancock, M. Yam, E. Tran, Y.F.I. Setargew, J.N. Skhinas, J.L. Chitty, M. Phimmachanh, J.Z.R. Han, A.L. Cadell, M. Papanicolaou, H. Mahmodi, B. Kiedik, S. Junankar, S.E. Ross, N. Lam, R. Coulson, J. Yang, A. Zaratzian, A.M. Da Silva, M. Tayao, I.L. Chin, A. Cazet, M. Kansara, D. Segara, A. Parker, A.J. Hoy, R.P. Harvey, O. Bogdanovic, P. Timpson, D.R. Croucher, E. Lim, A. Swarbrick, J. Holst, N. Turner, Y.S. Choi, I.V. Kabakova, A. Philp, T.R. Cox, Tumor Biomechanics Alters Metastatic Dissemination of Triple Negative Breast Cancer via Rewiring Fatty Acid Metabolism, Adv Sci (Weinh) 11(23) (2024) e2307963.
[91] A. Sohrabi, A.E.Y.T. Lefebvre, M.J. Harrison, M.C. Condro, T.M. Sanazzaro, G. Safarians, I. Solomon, S. Bastola, S. Kordbacheh, N. Toh, H.I. Kornblum, M.A. Digman, S.K. Seidlits, Microenvironmental stiffness induces metabolic reprogramming in glioblastoma, Cell Rep 42(10) (2023) 113175.
[92] P. Romani, N. Nirchio, M. Arboit, V. Barbieri, A. Tosi, F. Michielin, S. Shibuya, T. Benoist, D. Wu, C.C.T. Hindmarch, M. Giomo, A. Urciuolo, F. Giamogante, A. Roveri, P. Chakravarty, M. Montagner, T. Calì, N. Elvassore, S.L. Archer, P. De Coppi, A. Rosato, G. Martello, S. Dupont, Mitochondrial fission links ECM mechanotransduction to metabolic redox homeostasis and metastatic chemotherapy resistance, Nat Cell Biol 24(2) (2022) 168-180.
[93] W.A. Lam, L. Cao, V. Umesh, A.J. Keung, S. Sen, S. Kumar, Extracellular matrix rigidity modulates neuroblastoma cell differentiation and N-myc expression, Mol Cancer 9 (2010) 35.
[94] J. Schrader, T.T. Gordon-Walker, R.L. Aucott, M. van Deemter, A. Quaas, S. Walsh, D. Benten, S.J. Forbes, R.G. Wells, J.P. Iredale, Matrix stiffness modulates proliferation, chemotherapeutic response, and dormancy in hepatocellular carcinoma cells, Hepatology 53(4) (2011) 1192-1205.
[95] J. Liu, Y. Tan, H. Zhang, Y. Zhang, P. Xu, J. Chen, Y.-C. Poh, K. Tang, N. Wang, B. Huang, Soft fibrin gels promote selection and growth of tumorigenic cells, Nat Mater 11(8) (2012) 734-741.
[96] D.J. McGrail, Q.M.N. Kieu, M.R. Dawson, The malignancy of metastatic ovarian cancer cells is increased on soft matrices through a mechanosensitive Rho-ROCK pathway, J Cell Sci 127(Pt 12) (2014) 2621-2626.
[97] Y. Tan, A. Tajik, J. Chen, Q. Jia, F. Chowdhury, L. Wang, J. Chen, S. Zhang, Y. Hong, H. Yi, D.C. Wu, Y. Zhang, F. Wei, Y.-C. Poh, J. Seong, R. Singh, L.-J. Lin, S. Doğanay, Y. Li, H. Jia, T. Ha, Y. Wang, B. Huang, N. Wang, Matrix softness regulates plasticity of tumour-repopulating cells via H3K9 demethylation and Sox2 expression, Nat Commun 5 (2014) 4619.
[98] X. Tang, T.B. Kuhlenschmidt, Q. Li, S. Ali, S. Lezmi, H. Chen, M. Pires-Alves, W.W. Laegreid, T.A. Saif, M.S. Kuhlenschmidt, A mechanically-induced colon cancer cell population shows increased metastatic potential, Mol Cancer 13 (2014) 131.
[99] Z. Liu, L. Wang, H. Xu, Q. Du, L. Li, L. Wang, E.S. Zhang, G. Chen, Y. Wang, Heterogeneous Responses to Mechanical Force of Prostate Cancer Cells Inducing Different Metastasis Patterns, Adv Sci (Weinh) 7(15) (2020) 1903583.
[100] R.S. Stowers, A. Shcherbina, J. Israeli, J.J. Gruber, J. Chang, S. Nam, A. Rabiee, M.N. Teruel, M.P. Snyder, A. Kundaje, O. Chaudhuri, Matrix stiffness induces a tumorigenic phenotype in mammary epithelium through changes in chromatin accessibility, Nat Biomed Eng 3(12) (2019) 1009-1019.
[101] B. Wu, D.-A. Liu, L. Guan, P.K. Myint, L. Chin, H. Dang, Y. Xu, J. Ren, T. Li, Z. Yu, S. Jabban, G.B. Mills, J. Nukpezah, Y.H. Chen, E.E. Furth, P.A. Gimotty, R.G. Wells, V.M. Weaver, R. Radhakrishnan, X.W. Wang, W. Guo, Stiff matrix induces exosome secretion to promote tumour growth,

Nat Cell Biol 25(3) (2023) 415-424.
[102] S. Patwardhan, P. Mahadik, O. Shetty, S. Sen, ECM stiffness-tuned exosomes drive breast cancer motility through thrombospondin-1, Biomaterials 279 (2021) 121185.
[103] C. Liu, M. Li, Z.-X. Dong, D. Jiang, X. Li, S. Lin, D. Chen, X. Zou, X.-D. Zhang, G.D. Luker, Heterogeneous microenvironmental stiffness regulates pro-metastatic functions of breast cancer cells, Acta Biomater 131 (2021) 326-340.
[104] C. Li, S. Qiu, X. Liu, F. Guo, J. Zhai, Z. Li, L. Deng, L. Ge, H. Qian, L. Yang, B. Xu, Extracellular matrix-derived mechanical force governs breast cancer cell stemness and quiescence transition through integrin-DDR signaling, Signal transduction and targeted therapy 8(1) (2023) 247.
[105] K.-Y. Ng, Q.T. Shea, T.-L. Wong, S.T. Luk, M. Tong, C.-M. Lo, K. Man, J.-P. Yun, X.-Y. Guan, T.K. Lee, Y.-P. Zheng, S. Ma, Chemotherapy-Enriched THBS2-Deficient Cancer Stem Cells Drive Hepatocarcinogenesis through Matrix Softness Induced Histone H3 Modifications, Adv Sci (Weinh) 8(5) (2021) 2002483.
[106] J.J. Northey, M.-K. Hayward, Y. Yui, C. Stashko, F. Kai, J.K. Mouw, D. Thakar, J.N. Lakins, A.J. Ironside, S. Samson, R.A. Mukhtar, E.S. Hwang, V.M. Weaver, Mechanosensitive hormone signaling promotes mammary progenitor expansion and breast cancer risk, Cell Stem Cell 31(1) (2024).
[107] S.H.D. Wong, B. Yin, Z. Li, W. Yuan, Q. Zhang, X. Xie, Y. Tan, N. Wong, K. Zhang, L. Bian, Mechanical manipulation of cancer cell tumorigenicity via heat shock protein signaling, Science advances 9(27) (2023) eadg9593.
[108] D. Pankova, Y. Jiang, M. Chatzifrangkeskou, I. Vendrell, J. Buzzelli, A. Ryan, C. Brown, E. O'Neill, RASSF1A controls tissue stiffness and cancer stem-like cells in lung adenocarcinoma, EMBO J 38(13) (2019) e100532.
[109] W. Qian, T. Hadi, M. Silvestro, X. Ma, C.F. Rivera, A. Bajpai, R. Li, Z. Zhang, H. Qu, R.S. Tellaoui, A. Corsica, A.L. Zias, K. Garg, T. Maldonado, B. Ramkhelawon, W. Chen, Microskeletal stiffness promotes aortic aneurysm by sustaining pathological vascular smooth muscle cell mechanosensation via Piezo1, Nature communications 13(1) (2022) 512.
[110] A.A. Khalil, D. Smits, P.D. Haughton, T. Koorman, K.A. Jansen, M.P. Verhagen, M. van der Net, K. van Zwieten, L. Enserink, L. Jansen, A.G. El-Gammal, D. Visser, M. Pasolli, M. Tak, D. Westland, P.J. van Diest, C.B. Moelans, M.G. Roukens, S. Tavares, A.-M. Fortier, M. Park, R. Fodde, M. Gloerich, F.J.T. Zwartkruis, P.W. Derksen, J. de Rooij, A YAP-centered mechanotransduction loop drives collective breast cancer cell invasion, Nature communications 15(1) (2024) 4866.
[111] M. Plodinec, M. Loparic, C.A. Monnier, E.C. Obermann, R. Zanetti-Dallenbach, P. Oertle, J.T. Hyotyla, U. Aebi, M. Bentires-Alj, R.Y. Lim, C.A. Schoenenberger, The nanomechanical signature of breast cancer, Nature nanotechnology 7(11) (2012) 757-65.
[112] Z. Hajjarian, E.F. Brachtel, D.M. Tshikudi, S.K. Nadkarni, Mapping Mechanical Properties of the Tumor Microenvironment by Laser Speckle Rheological Microscopy, Cancer research 81(18) (2021) 4874-4885.
[113] T. Samuel, S. Rapic, C. O'Brien, M. Edson, Y. Zhong, R.S. DaCosta, Quantitative intravital imaging for real-time monitoring of pancreatic tumor cell hypoxia and stroma in an orthotopic mouse model, Science advances 9(23) (2023) eade8672.
[114] T. Boveri, M. Boveri, The Origin of Malignant Tumors, Williams & Wilkins1929.
[115] C. Tomasetti, B. Vogelstein, Cancer etiology. Variation in cancer risk among tissues can be explained by the number of stem cell divisions, Science (New York, N.Y.) 347(6217) (2015) 78-81.
[116] C. Tomasetti, L. Li, B. Vogelstein, Stem cell divisions, somatic mutations, cancer etiology, and

cancer prevention, Science (New York, N.Y.) 355(6331) (2017) 1330-1334.
[117] A.M. Soto, C. Sonnenschein, The tissue organization field theory of cancer: a testable replacement for the somatic mutation theory, Bioessays 33(5) (2011) 332-340.
[118] M.V. Maffini, J.M. Calabro, A.M. Soto, C. Sonnenschein, Stromal regulation of neoplastic development: age-dependent normalization of neoplastic mammary cells by mammary stroma, Am J Pathol 167(5) (2005) 1405-1410.
[119] K.D. McCullough, W.B. Coleman, G.J. Smith, J.W. Grisham, Age-dependent induction of hepatic tumor regression by the tissue microenvironment after transplantation of neoplastically transformed rat liver epithelial cells into the liver, Cancer research 57(9) (1997) 1807-1813.
[120] M.J.C. Hendrix, E.A. Seftor, R.E.B. Seftor, J. Kasemeier-Kulesa, P.M. Kulesa, L.-M. Postovit, Reprogramming metastatic tumour cells with embryonic microenvironments, Nature reviews. Cancer 7(4) (2007) 246-255.
[121] K. Illmensee, B. Mintz, Totipotency and normal differentiation of single teratocarcinoma cells cloned by injection into blastocysts, Proc. Natl. Acad. Sci. U. S. A. 73(2) (1976) 549-553.
[122] L. Li, M.C. Connelly, C. Wetmore, T. Curran, J.I. Morgan, Mouse embryos cloned from brain tumors, Cancer research 63(11) (2003) 2733-2736.
[123] M.H. Barcellos-Hoff, S.A. Ravani, Irradiated mammary gland stroma promotes the expression of tumorigenic potential by unirradiated epithelial cells, Cancer research 60(5) (2000) 1254-1260.
[124] M.V. Maffini, A.M. Soto, J.M. Calabro, A.A. Ucci, C. Sonnenschein, The stroma as a crucial target in rat mammary gland carcinogenesis, J Cell Sci 117(Pt 8) (2004) 1495-1502.
[125] V.M. Weaver, O.W. Petersen, F. Wang, C.A. Larabell, P. Briand, C. Damsky, M.J. Bissell, Reversion of the malignant phenotype of human breast cells in three-dimensional culture and in vivo by integrin blocking antibodies, The Journal of cell biology 137(1) (1997) 231-245.
[126] D.C. Radisky, D.D. Levy, L.E. Littlepage, H. Liu, C.M. Nelson, J.E. Fata, D. Leake, E.L. Godden, D.G. Albertson, M.A. Nieto, Z. Werb, M.J. Bissell, Rac1b and reactive oxygen species mediate MMP-3-induced EMT and genomic instability, Nature 436(7047) (2005) 123-127.
[127] M.D. Sternlicht, A. Lochter, C.J. Sympson, B. Huey, J.P. Rougier, J.W. Gray, D. Pinkel, M.J. Bissell, Z. Werb, The stromal proteinase MMP3/stromelysin-1 promotes mammary carcinogenesis, Cell 98(2) (1999) 137-146.
[128] A. Lochter, A. Srebrow, C.J. Sympson, N. Terracio, Z. Werb, M.J. Bissell, Misregulation of stromelysin-1 expression in mouse mammary tumor cells accompanies acquisition of stromelysin-1-dependent invasive properties, The Journal of biological chemistry 272(8) (1997) 5007-5015.
[129] L. Zhu, D. Finkelstein, C. Gao, L. Shi, Y. Wang, D. López-Terrada, K. Wang, S. Utley, S. Pounds, G. Neale, D. Ellison, A. Onar-Thomas, R.J. Gilbertson, Multi-organ Mapping of Cancer Risk, Cell 166(5) (2016).
[130] A. Jassim, E.P. Rahrmann, B.D. Simons, R.J. Gilbertson, Cancers make their own luck: theories of cancer origins, Nature reviews. Cancer 23(10) (2023) 710-724.
[131] J.J. Evans, M.M. Alkaisi, P.H. Sykes, Tumour Initiation: a Discussion on Evidence for a "Load-Trigger" Mechanism, Cell Biochem Biophys 77(4) (2019) 293-308.
[132] D. Hanahan, Hallmarks of Cancer: New Dimensions, Cancer discovery 12(1) (2022) 31-46.
[133] D. Jiang, L. Zhang, W. Liu, Y. Ding, J. Yin, R. Ren, Q. Li, Y. Chen, J. Shen, X. Tan, H. Zhang, G. Cao, Trends in cancer mortality in China from 2004 to 2018: A nationwide longitudinal study, Cancer communications (London, England) 41(10) (2021) 1024-1036.
[134] K. Ganesh, J. Massagué, Targeting metastatic cancer, Nature medicine 27(1) (2021) 34-44.

[135] Z. Yuan, Y. Li, S. Zhang, X. Wang, H. Dou, X. Yu, Z. Zhang, S. Yang, M. Xiao, Extracellular matrix remodeling in tumor progression and immune escape: from mechanisms to treatments, Mol Cancer 22(1) (2023) 48.
[136] W. Chen, A.D. Hoffmann, H. Liu, X. Liu, Organotropism: new insights into molecular mechanisms of breast cancer metastasis, NPJ Precis Oncol 2(1) (2018) 4.
[137] J.G. Reiter, M. Baretti, J.M. Gerold, A.P. Makohon-Moore, A. Daud, C.A. Iacobuzio-Donahue, N.S. Azad, K.W. Kinzler, M.A. Nowak, B. Vogelstein, An analysis of genetic heterogeneity in untreated cancers, Nature reviews. Cancer 19(11) (2019) 639-650.
[138] I. Vitale, E. Shema, S. Loi, L. Galluzzi, Intratumoral heterogeneity in cancer progression and response to immunotherapy, Nature medicine 27(2) (2021) 212-224.
[139] J. Wang, R. Loberg, R.S. Taichman, The pivotal role of CXCL12 (SDF-1)/CXCR4 axis in bone metastasis, Cancer Metastasis Rev 25(4) (2006) 573-87.
[140] Y.X. Sun, A. Schneider, Y. Jung, J. Wang, J. Dai, J. Wang, K. Cook, N.I. Osman, A.J. Koh-Paige, H. Shim, K.J. Pienta, E.T. Keller, L.K. McCauley, R.S. Taichman, Skeletal localization and neutralization of the SDF-1(CXCL12)/CXCR4 axis blocks prostate cancer metastasis and growth in osseous sites in vivo, J Bone Miner Res 20(2) (2005) 318-29.
[141] R.S. Taichman, C. Cooper, E.T. Keller, K.J. Pienta, N.S. Taichman, L.K. McCauley, Use of the stromal cell-derived factor-1/CXCR4 pathway in prostate cancer metastasis to bone, Cancer research 62(6) (2002) 1832-7.
[142] R. Leblanc, S.C. Lee, M. David, J.C. Bordet, D.D. Norman, R. Patil, D. Miller, D. Sahay, J. Ribeiro, P. Clézardin, G.J. Tigyi, O. Peyruchaud, Interaction of platelet-derived autotaxin with tumor integrin αVβ3 controls metastasis of breast cancer cells to bone, Blood 124(20) (2014) 3141-50.
[143] A. Boucharaba, C.M. Serre, S. Grès, J.S. Saulnier-Blache, J.C. Bordet, J. Guglielmi, P. Clézardin, O. Peyruchaud, Platelet-derived lysophosphatidic acid supports the progression of osteolytic bone metastases in breast cancer, The Journal of clinical investigation 114(12) (2004) 1714-25.
[144] R.K.H. Yip, J.S. Rimes, B.D. Capaldo, F. Vaillant, K.A. Mouchemore, B. Pal, Y. Chen, E. Surgenor, A.J. Murphy, R.L. Anderson, G.K. Smyth, G.J. Lindeman, E.D. Hawkins, J.E. Visvader, Mammary tumour cells remodel the bone marrow vascular microenvironment to support metastasis, Nat Commun 12(1) (2021) 6920.
[145] A.J. Minn, G.P. Gupta, P.M. Siegel, P.D. Bos, W. Shu, D.D. Giri, A. Viale, A.B. Olshen, W.L. Gerald, J. Massagué, Genes that mediate breast cancer metastasis to lung, Nature 436(7050) (2005) 518-24.
[146] P.D. Bos, X.H.F. Zhang, C. Nadal, W. Shu, R.R. Gomis, D.X. Nguyen, A.J. Minn, M.J. van de Vijver, W.L. Gerald, J.A. Foekens, J. Massagué, Genes that mediate breast cancer metastasis to the brain, Nature 459(7249) (2009) 1005-1009.
[147] G. Chang, L. Shi, Y. Ye, H. Shi, L. Zeng, S. Tiwary, J.T. Huse, L. Huo, L. Ma, Y. Ma, S. Zhang, J. Zhu, V. Xie, P. Li, L. Han, C. He, S. Huang, YTHDF3 Induces the Translation of m(6)A-Enriched Gene Transcripts to Promote Breast Cancer Brain Metastasis, Cancer Cell 38(6) (2020) 857-871.e7.
[148] Y.-Q. Li, F.-Z. Sun, C.-X. Li, H.-N. Mo, Y.-T. Zhou, D. Lv, J.-T. Zhai, H.-L. Qian, F. Ma, RARRES2 regulates lipid metabolic reprogramming to mediate the development of brain metastasis in triple negative breast cancer, Mil Med Res 10(1) (2023) 34.
[149] P.K. Parida, M. Marquez-Palencia, S. Ghosh, N. Khandelwal, K. Kim, V. Nair, X.-Z. Liu, H.S. Vu, L.G. Zacharias, P.I. Gonzalez-Ericsson, M.E. Sanders, B.C. Mobley, J.G. McDonald, A. Lemoff, Y. Peng, C. Lewis, G. Vale, N. Halberg, C.L. Arteaga, A.B. Hanker, R.J. DeBerardinis, S. Malladi, Limiting

mitochondrial plasticity by targeting DRP1 induces metabolic reprogramming and reduces breast cancer brain metastases, Nat Cancer 4(6) (2023) 893-907.
[150] P.K. Parida, M. Marquez-Palencia, V. Nair, A.K. Kaushik, K. Kim, J. Sudderth, E. Quesada-Diaz, A. Cajigas, V. Vemireddy, P.I. Gonzalez-Ericsson, M.E. Sanders, B.C. Mobley, K. Huffman, S. Sahoo, P. Alluri, C. Lewis, Y. Peng, R.M. Bachoo, C.L. Arteaga, A.B. Hanker, R.J. DeBerardinis, S. Malladi, Metabolic diversity within breast cancer brain-tropic cells determines metastatic fitness, Cell Metab 34(1) (2022) 90-105.e7.
[151] G.B. Ferraro, A. Ali, A. Luengo, D.P. Kodack, A. Deik, K.L. Abbott, D. Bezwada, L. Blanc, B. Prideaux, X. Jin, J.M. Posada, J. Chen, C.R. Chin, Z. Amoozgar, R. Ferreira, I.X. Chen, K. Naxerova, C. Ng, A.M. Westermark, M. Duquette, S. Roberge, N.I. Lindeman, C.A. Lyssiotis, J. Nielsen, D.E. Housman, D.G. Duda, E. Brachtel, T.R. Golub, L.C. Cantley, J.M. Asara, S.M. Davidson, D. Fukumura, V.A. Dartois, C.B. Clish, R.K. Jain, M.G. Vander Heiden, FATTY ACID SYNTHESIS IS REQUIRED FOR BREAST CANCER BRAIN METASTASIS, Nat Cancer 2(4) (2021) 414-428.
[152] K.E. de Visser, J.A. Joyce, The evolving tumor microenvironment: From cancer initiation to metastatic outgrowth, Cancer Cell 41(3) (2023) 374-403.
[153] N. Harbeck, M. Gnant, Breast cancer, Lancet (London, England) 389(10074) (2017) 1134-1150.
[154] C.M. Perou, T. Sørlie, M.B. Eisen, M. van de Rijn, S.S. Jeffrey, C.A. Rees, J.R. Pollack, D.T. Ross, H. Johnsen, L.A. Akslen, O. Fluge, A. Pergamenschikov, C. Williams, S.X. Zhu, P.E. Lønning, A.L. Børresen-Dale, P.O. Brown, D. Botstein, Molecular portraits of human breast tumours, Nature 406(6797) (2000) 747-752.
[155] T. Sørlie, C.M. Perou, R. Tibshirani, T. Aas, S. Geisler, H. Johnsen, T. Hastie, M.B. Eisen, M. van de Rijn, S.S. Jeffrey, T. Thorsen, H. Quist, J.C. Matese, P.O. Brown, D. Botstein, P.E. Lønning, A.L. Børresen-Dale, Gene expression patterns of breast carcinomas distinguish tumor subclasses with clinical implications, Proc. Natl. Acad. Sci. U. S. A. 98(19) (2001) 10869-10874.
[156] F. Derakhshan, J.S. Reis-Filho, Pathogenesis of Triple-Negative Breast Cancer, Annu Rev Pathol 17 (2022) 181-204.
[157] Y. Wang, F. Ye, Y. Liang, Q. Yang, Breast cancer brain metastasis: insight into molecular mechanisms and therapeutic strategies, Br J Cancer 125(8) (2021) 1056-1067.
[158] A.E. Whiteley, D. Ma, L. Wang, S.Y. Yu, C. Yin, T.T. Price, B.G. Simon, K.R. Xu, K.A. Marsh, M.L. Brockman, T.M. Prioleau, K.I. Zhou, X. Cui, P.E. Fecci, W.R. Jeck, C.M. McCall, J.L. Neff, D.A. Sipkins, Breast cancer exploits neural signaling pathways for bone-to-meninges metastasis, Science 384(6702) (2024) eadh5548.
[159] B. Zhang, X. Li, K. Tang, Y. Xin, G. Hu, Y. Zheng, K. Li, C. Zhang, Y. Tan, Adhesion to the Brain Endothelium Selects Breast Cancer Cells with Brain Metastasis Potential, Int J Mol Sci 24(8) (2023).
[160] M. Uroz, A.E. Stoddard, B.P. Sutherland, O. Courbot, R. Oria, L. Li, C.R. Ravasio, M.T. Ngo, J. Yang, J.B.J.N.C.B. Tefft, Differential stiffness between brain vasculature and parenchyma promotes metastatic infiltration through vessel co-option, (2024) 1-10.
[161] S. Gan, D.G. Macalinao, S.H. Shahoei, L. Tian, X. Jin, H. Basnet, C. Bibby, J.T. Muller, P. Atri, E.J.C.C. Seffar, Distinct tumor architectures and microenvironments for the initiation of breast cancer metastasis in the brain, (2024).
[162] O. Chaudhuri, J. Cooper-White, P.A. Janmey, D.J. Mooney, V.B. Shenoy, Effects of extracellular matrix viscoelasticity on cellular behaviour, Nature 584(7822) (2020) 535-546.
[163] L.-S.Z. Rathje, N. Nordgren, T. Pettersson, D. Rönnlund, J. Widengren, P. Aspenström, A.K.B. Gad, Oncogenes induce a vimentin filament collapse mediated by HDAC6 that is linked to cell stiffness,

Proc Natl Acad Sci U S A 111(4) (2014) 1515-1520.
[164] H.K. Matthews, S. Ganguli, K. Plak, A.V. Taubenberger, Z. Win, M. Williamson, M. Piel, J. Guck, B. Baum, Oncogenic Signaling Alters Cell Shape and Mechanics to Facilitate Cell Division under Confinement, Dev Cell 52(5) (2020).
[165] G. Zhang, M. Long, Z.Z. Wu, W.Q. Yu, Mechanical properties of hepatocellular carcinoma cells, World journal of gastroenterology 8(2) (2002) 243-6.
[166] Y.X. Ding, Y. Cheng, Q.M. Sun, Y.Y. Zhang, K. You, Y.L. Guo, D. Han, L. Geng, Mechanical characterization of cervical squamous carcinoma cells by atomic force microscopy at nanoscale, Medical oncology (Northwood, London, England) 32(3) (2015) 71.
[167] M.J. Rosenbluth, W.A. Lam, D.A. Fletcher, Force microscopy of nonadherent cells: a comparison of leukemia cell deformability, Biophysical journal 90(8) (2006) 2994-3003.
[168] S. Iyer, R.M. Gaikwad, V. Subba-Rao, C.D. Woodworth, I. Sokolov, Atomic force microscopy detects differences in the surface brush of normal and cancerous cells, Nat Nanotechnol 4(6) (2009) 389-393.
[169] T. Fuhs, F. Wetzel, A.W. Fritsch, X. Li, R. Stange, S. Pawlizak, T.R. Kießling, E. Morawetz, S. Grosser, F. Sauer, J. Lippoldt, F. Renner, S. Friebe, M. Zink, K. Bendrat, J. Braun, M.H. Oktay, J. Condeelis, S. Briest, B. Wolf, L.-C. Horn, M. Höckel, B. Aktas, M.C. Marchetti, M.L. Manning, A. Niendorf, D. Bi, J.A. Käs, Rigid tumours contain soft cancer cells, Nature Physics 18(12) (2022) 1510-1519.
[170] S.E. Cross, Y.-S. Jin, J. Rao, J.K. Gimzewski, Nanomechanical analysis of cells from cancer patients, Nat Nanotechnol 2(12) (2007) 780-783.
[171] J. Lv, Y. Liu, F. Cheng, J. Li, Y. Zhou, T. Zhang, N. Zhou, C. Li, Z. Wang, L. Ma, M. Liu, Q. Zhu, X. Liu, K. Tang, J. Ma, H. Zhang, J. Xie, Y. Fang, H. Zhang, N. Wang, Y. Liu, B. Huang, Cell softness regulates tumorigenicity and stemness of cancer cells, EMBO J 40(2) (2021) e106123.
[172] Y. Zhou, D. Wang, L. Zhou, N. Zhou, Z. Wang, J. Chen, R. Pang, H. Fu, Q. Huang, F. Dong, H. Cheng, H. Zhang, K. Tang, J. Ma, J. Lv, T. Cheng, R. Fiskesund, X. Zhang, B. Huang, Cell softness renders cytotoxic T lymphocytes and T leukemic cells resistant to perforin-mediated killing, Nat Commun 15(1) (2024) 1405.
[173] J. Lv, X. Liu, Y. Zhou, F. Cheng, H. Chen, S. Li, D. Wang, L. Zhou, Z. Wang, N. Zhou, J. Chen, B. Huang, YAP Inactivation by Soft Mechanotransduction Relieves MAFG for Tumor Cell Dedifferentiation, Research (Wash D C) 6 (2023) 0215.
[174] X. Chen, K. Tang, X. Li, C. Zhang, Y. Xin, K. Li, Y. Tan, Biomechanics of cancer stem cells, Essays Biochem 66(4) (2022) 359-369.
[175] Y. Liu, T. Zhang, H. Zhang, J. Li, N. Zhou, R. Fiskesund, J. Chen, J. Lv, J. Ma, H. Zhang, K. Tang, F. Cheng, Y. Zhou, X. Zhang, N. Wang, B. Huang, Cell Softness Prevents Cytolytic T-cell Killing of Tumor-Repopulating Cells, Cancer research 81(2) (2021) 476-488.
[176] Y.L. Han, A.F. Pegoraro, H. Li, K. Li, Y. Yuan, G. Xu, Z. Gu, J. Sun, Y. Hao, S.K. Gupta, Y. Li, W. Tang, X. Tang, L. Teng, J.J. Fredberg, M. Guo, Cell swelling, softening and invasion in a three-dimensional breast cancer model, Nature Physics 16(1) (2020) 101-108.
[177] V. Swaminathan, K. Mythreye, E.T. O'Brien, A. Berchuck, G.C. Blobe, R. Superfine, Mechanical stiffness grades metastatic potential in patient tumor cells and in cancer cell lines, Cancer research 71(15) (2011) 5075-5080.
[178] K. Lei, A. Kurum, M. Kaynak, L. Bonati, Y. Han, V. Cencen, M. Gao, Y.-Q. Xie, Y. Guo, M.T.M. Hannebelle, Y. Wu, G. Zhou, M. Guo, G.E. Fantner, M.S. Sakar, L. Tang, Cancer-cell stiffening via

cholesterol depletion enhances adoptive T-cell immunotherapy, Nat Biomed Eng 5(12) (2021) 1411-1425.
[179] K. Tang, Y. Xin, K. Li, X. Chen, Y. Tan, Cell Cytoskeleton and Stiffness Are Mechanical Indicators of Organotropism in Breast Cancer, Biology (Basel) 10(4) (2021).
[180] S. SenGupta, C.A. Parent, J.E. Bear, The principles of directed cell migration, Nature reviews. Molecular cell biology 22(8) (2021) 529-547.
[181] R. Poincloux, O. Collin, F. Lizárraga, M. Romao, M. Debray, M. Piel, P. Chavrier, Contractility of the cell rear drives invasion of breast tumor cells in 3D Matrigel, Proc Natl Acad Sci U S A 108(5) (2011) 1943-1948.
[182] C. Walter, J. Mathur, A. Pathak, Reciprocal intra- and extra-cellular polarity enables deep mechanosensing through layered matrices, Cell Rep 42(4) (2023) 112362.
[183] B. Yang, H. Wolfenson, V.Y. Chung, N. Nakazawa, S. Liu, J. Hu, R.Y.-J. Huang, M.P. Sheetz, Stopping transformed cancer cell growth by rigidity sensing, Nat Mater 19(2) (2020) 239-250.
[184] H. Wolfenson, G. Meacci, S. Liu, M.R. Stachowiak, T. Iskratsch, S. Ghassemi, P. Roca-Cusachs, B. O'Shaughnessy, J. Hone, M.P. Sheetz, Tropomyosin controls sarcomere-like contractions for rigidity sensing and suppressing growth on soft matrices, Nat Cell Biol 18(1) (2016) 33-42.
[185] M. Unbekandt, D.R. Croft, D. Crighton, M. Mezna, D. McArthur, P. McConnell, A.W. Schüttelkopf, S. Belshaw, A. Pannifer, M. Sime, J. Bower, M. Drysdale, M.F. Olson, A novel small-molecule MRCK inhibitor blocks cancer cell invasion, Cell Commun Signal 12 (2014) 54.
[186] L. Liu, C. Chen, P. Liu, J. Li, Z. Pang, J. Zhu, Z. Lin, H. Zhou, Y. Xie, T. Lan, Z.-S. Chen, Z. Zeng, W. Fang, MYH10 Combines with MYH9 to Recruit USP45 by Deubiquitinating Snail and Promotes Serous Ovarian Cancer Carcinogenesis, Progression, and Cisplatin Resistance, Adv Sci (Weinh) 10(14) (2023) e2203423.
[187] N.O. Alieva, A.K. Efremov, S. Hu, D. Oh, Z. Chen, M. Natarajan, H.T. Ong, A. Jégou, G. Romet-Lemonne, J.T. Groves, M.P. Sheetz, J. Yan, A.D. Bershadsky, Myosin IIA and formin dependent mechanosensitivity of filopodia adhesion, Nat Commun 10(1) (2019) 3593.
[188] Y. Peng, Z. Chen, Y. He, P. Li, Y. Chen, X. Chen, Y. Jiang, X. Qin, S. Li, T. Li, C. Wu, H. Yang, F. You, Y. Liu, Non-muscle myosin II isoforms orchestrate substrate stiffness sensing to promote cancer cell contractility and migration, Cancer Lett 524 (2022) 245-258.
[189] B. Yeoman, G. Shatkin, P. Beri, A. Banisadr, P. Katira, A.J. Engler, Adhesion strength and contractility enable metastatic cells to become adurotactic, Cell Rep 34(10) (2021) 108816.
[190] A. Isomursu, K.Y. Park, J. Hou, B. Cheng, M. Mathieu, G.A. Shamsan, B. Fuller, J. Kasim, M.M. Mahmoodi, T.J. Lu, G.M. Genin, F. Xu, M. Lin, M.D. Distefano, J. Ivaska, D.J. Odde, Directed cell migration towards softer environments, Nat Mater 21(9) (2022) 1081-1090.
[191] Y. Huang, J. Su, J. Liu, X. Yi, F. Zhou, J. Zhang, J. Wang, X. Meng, L. Si, C. Wu, YAP Activation in Promoting Negative Durotaxis and Acral Melanoma Progression, Cells 11(22) (2022).
[192] A.J. Engler, S. Sen, H.L. Sweeney, D.E. Discher, Matrix elasticity directs stem cell lineage specification, Cell 126(4) (2006) 677-89.
[193] K.H. Vining, D.J. Mooney, Mechanical forces direct stem cell behaviour in development and regeneration, Nat Rev Mol Cell Biol 18(12) (2017) 728-742.
[194] M. Segel, B. Neumann, M.F.E. Hill, I.P. Weber, C. Viscomi, C. Zhao, A. Young, C.C. Agley, A.J. Thompson, G.A. Gonzalez, A. Sharma, S. Holmqvist, D.H. Rowitch, K. Franze, R.J.M. Franklin, K.J. Chalut, Niche stiffness underlies the ageing of central nervous system progenitor cells, Nature 573(7772) (2019) 130-134.
[195] T. Stylianopoulos, J.D. Martin, V.P. Chauhan, S.R. Jain, B. Diop-Frimpong, N. Bardeesy, B.L.

Smith, C.R. Ferrone, F.J. Hornicek, Y. Boucher, L.L. Munn, R.K. Jain, Causes, consequences, and remedies for growth-induced solid stress in murine and human tumors, Proc Natl Acad Sci U S A 109(38) (2012) 15101-15108.
[196] G. Cai, X. Li, S.-S. Lin, S.J. Chen, N.C. Rodgers, K.M. Koning, D. Bi, A.P. Liu, Matrix confinement modulates 3D spheroid sorting and burst-like collective migration, Acta biomaterialia 179 (2024) 192-206.
[197] J. Barbazan, C. Pérez-González, M. Gómez-González, M. Dedenon, S. Richon, E. Latorre, M. Serra, P. Mariani, S. Descroix, P. Sens, X. Trepat, D.M. Vignjevic, Cancer-associated fibroblasts actively compress cancer cells and modulate mechanotransduction, Nat Commun 14(1) (2023) 6966.
[198] G. Cheng, J. Tse, R.K. Jain, L.L. Munn, Micro-environmental mechanical stress controls tumor spheroid size and morphology by suppressing proliferation and inducing apoptosis in cancer cells, PLoS One 4(2) (2009) e4632.
[199] M. Delarue, F. Montel, D. Vignjevic, J. Prost, J.-F. Joanny, G. Cappello, Compressive stress inhibits proliferation in tumor spheroids through a volume limitation, Biophys J 107(8) (2014) 1821-1828.
[200] G. Helmlinger, P.A. Netti, H.C. Lichtenbeld, R.J. Melder, R.K. Jain, Solid stress inhibits the growth of multicellular tumor spheroids, Nat Biotechnol 15(8) (1997) 778-783.
[201] M. Kalli, P. Papageorgis, V. Gkretsi, T. Stylianopoulos, Solid Stress Facilitates Fibroblasts Activation to Promote Pancreatic Cancer Cell Migration, Ann Biomed Eng 46(5) (2018) 657-669.
[202] B.G. Kim, J.S. Sung, Y. Jang, Y.J. Cha, S. Kang, H.H. Han, J.H. Lee, N.H. Cho, Compression-induced expression of glycolysis genes in CAFs correlates with EMT and angiogenesis gene expression in breast cancer, Commun Biol 2 (2019) 313.
[203] B.A. Webb, M. Chimenti, M.P. Jacobson, D.L. Barber, Dysregulated pH: a perfect storm for cancer progression, Nat Rev Cancer 11(9) (2011) 671-677.
[204] A.H. Morrison, K.T. Byrne, R.H. Vonderheide, Immunotherapy and Prevention of Pancreatic Cancer, Trends Cancer 4(6) (2018) 418-428.
[205] E. Boedtkjer, S.F. Pedersen, The Acidic Tumor Microenvironment as a Driver of Cancer, Annu Rev Physiol 82 (2020) 103-126.
[206] R.K. Jain, J.D. Martin, T. Stylianopoulos, The role of mechanical forces in tumor growth and therapy, Annu Rev Biomed Eng 16 (2014) 321-346.
[207] V.P. Chauhan, J.D. Martin, H. Liu, D.A. Lacorre, S.R. Jain, S.V. Kozin, T. Stylianopoulos, A.S. Mousa, X. Han, P. Adstamongkonkul, Z. Popović, P. Huang, M.G. Bawendi, Y. Boucher, R.K. Jain, Angiotensin inhibition enhances drug delivery and potentiates chemotherapy by decompressing tumour blood vessels, Nat Commun 4 (2013) 2516.
[208] L.M.K. Hansem, R. Huang, C.S. Wegner, T.G. Simonsen, J.-V. Gaustad, A. Hauge, E.K. Rofstad, Intratumor Heterogeneity in Interstitial Fluid Pressure in Cervical and Pancreatic Carcinoma Xenografts, Transl Oncol 12(8) (2019) 1079-1085.
[209] H.D. Roh, Y. Boucher, S. Kalnicki, R. Buchsbaum, W.D. Bloomer, R.K. Jain, Interstitial hypertension in carcinoma of uterine cervix in patients: possible correlation with tumor oxygenation and radiation response, Cancer research 51(24) (1991) 6695-6698.
[210] T. Yu, K. Liu, Y. Wu, J. Fan, J. Chen, C. Li, G. Zhu, Z. Wang, L. Li, High interstitial fluid pressure promotes tumor cell proliferation and invasion in oral squamous cell carcinoma, Int J Mol Med 32(5) (2013) 1093-1100.
[211] C.G. Willett, Y. Boucher, E. di Tomaso, D.G. Duda, L.L. Munn, R.T. Tong, D.C. Chung, D.V. Sahani, S.P. Kalva, S.V. Kozin, M. Mino, K.S. Cohen, D.T. Scadden, A.C. Hartford, A.J. Fischman, J.W.

Clark, D.P. Ryan, A.X. Zhu, L.S. Blaszkowsky, H.X. Chen, P.C. Shellito, G.Y. Lauwers, R.K. Jain, Direct evidence that the VEGF-specific antibody bevacizumab has antivascular effects in human rectal cancer, Nature medicine 10(2) (2004) 145-147.
[212] A.G. Taghian, R. Abi-Raad, S.I. Assaad, A. Casty, M. Ancukiewicz, E. Yeh, P. Molokhia, K. Attia, T. Sullivan, I. Kuter, Y. Boucher, S.N. Powell, Paclitaxel decreases the interstitial fluid pressure and improves oxygenation in breast cancers in patients treated with neoadjuvant chemotherapy: clinical implications, J Clin Oncol 23(9) (2005) 1951-1961.
[213] Q. Huang, X. Hu, W. He, Y. Zhao, S. Hao, Q. Wu, S. Li, S. Zhang, M. Shi, Fluid shear stress and tumor metastasis, Am J Cancer Res 8(5) (2018) 763-777.
[214] C.L. Yankaskas, K. Bera, K. Stoletov, S.A. Serra, J. Carrillo-Garcia, S. Tuntithavornwat, P. Mistriotis, J.D. Lewis, M.A. Valverde, K. Konstantopoulos, The fluid shear stress sensor TRPM7 regulates tumor cell intravasation, Sci Adv 7(28) (2021).
[215] W.J. Polacheck, A.E. German, A. Mammoto, D.E. Ingber, R.D. Kamm, Mechanotransduction of fluid stresses governs 3D cell migration, Proc Natl Acad Sci U S A 111(7) (2014) 2447-2452.
[216] J.D. Shields, M.E. Fleury, C. Yong, A.A. Tomei, G.J. Randolph, M.A. Swartz, Autologous chemotaxis as a mechanism of tumor cell homing to lymphatics via interstitial flow and autocrine CCR7 signaling, Cancer Cell 11(6) (2007) 526-538.
[217] M. Hadzipasic, S. Zhang, Z. Huang, R. Passaro, M.S. Sten, G.M. Shankar, H.T. Nia, Emergence of nanoscale viscoelasticity from single cancer cells to established tumors, Biomaterials 305 (2024) 122431.
[218] T. Vicar, J. Chmelik, J. Navratil, R. Kolar, L. Chmelikova, V. Cmiel, J. Jagos, I. Provaznik, M. Masarik, J. Gumulec, Cancer cell viscoelasticity measurement by quantitative phase and flow stress induction, Biophys J 121(9) (2022) 1632-1642.
[219] Y. Abidine, A. Giannetti, J. Revilloud, V.M. Laurent, C. Verdier, Viscoelastic Properties in Cancer: From Cells to Spheroids, Cells 10(7) (2021).
[220] B. Zhou, Y. Hao, Z. Wang, P. Wei, L. Du, Q. Xia, Dynamical and noninvasive monitoring of curcumin effect on the changes in the viscoelasticity of human breast cancer cells: A novel model to assess cell apoptosis, Talanta 236 (2022) 122899.
[221] A.N. Ketene, E.M. Schmelz, P.C. Roberts, M. Agah, The effects of cancer progression on the viscoelasticity of ovarian cell cytoskeleton structures, Nanomedicine 8(1) (2012).
[222] Y. Teng, K. Zhu, C. Xiong, J. Huang, Electrodeformation-Based Biomechanical Chip for Quantifying Global Viscoelasticity of Cancer Cells Regulated by Cell Cycle, Anal Chem 90(14) (2018) 8370-8378.
[223] A.A. Bhirde, B.V. Chikkaveeraiah, A. Srivatsan, G. Niu, A.J. Jin, A. Kapoor, Z. Wang, S. Patel, V. Patel, A.M. Gorbach, R.D. Leapman, J.S. Gutkind, A.R. Hight Walker, X. Chen, Targeted therapeutic nanotubes influence the viscoelasticity of cancer cells to overcome drug resistance, ACS Nano 8(5) (2014) 4177-4189.
[224] F.-Y. Lin, C.-Y. Chang, H. Nguyen, H. Li, M.L. Fishel, C.-C. Lin, Viscoelastic hydrogels for interrogating pancreatic cancer-stromal cell interactions, Mater Today Bio 19 (2023) 100576.
[225] M. Egeblad, M.G. Rasch, V.M. Weaver, Dynamic interplay between the collagen scaffold and tumor evolution, Curr Opin Cell Biol 22(5) (2010) 697-706.
[226] R. Kalluri, M. Zeisberg, Fibroblasts in cancer, Nature Reviews Cancer 6(5) (2006) 392-401.
[227] M. Najafi, B. Farhood, K. Mortezaee, Extracellular matrix (ECM) stiffness and degradation as cancer drivers, J Cell Biochem 120(3) (2019) 2782-2790.

[228] H.E. Barker, J. Chang, T.R. Cox, G. Lang, D. Bird, M. Nicolau, H.R. Evans, A. Gartland, J.T. Erler, LOXL2-mediated matrix remodeling in metastasis and mammary gland involution, Cancer research 71(5) (2011) 1561-72.
[229] W. Wang, L.A. Hapach, L. Griggs, K. Smart, Y. Wu, P.V. Taufalele, M.M. Rowe, K.M. Young, M.E. Bates, A.C. Johnson, N.J. Ferrell, A. Pozzi, C.A. Reinhart-King, Diabetic hyperglycemia promotes primary tumor progression through glycation-induced tumor extracellular matrix stiffening, Sci Adv 8(46) (2022) eabo1673.
[230] D. Lavie, A. Ben-Shmuel, N. Erez, R. Scherz-Shouval, Cancer-associated fibroblasts in the single-cell era, Nature cancer 3(7) (2022) 793-807.
[231] A. Costa, Y. Kieffer, A. Scholer-Dahirel, F. Pelon, B. Bourachot, M. Cardon, P. Sirven, I. Magagna, L. Fuhrmann, C. Bernard, C. Bonneau, M. Kondratova, I. Kuperstein, A. Zinovyev, A.M. Givel, M.C. Parrini, V. Soumelis, A. Vincent-Salomon, F. Mechta-Grigoriou, Fibroblast Heterogeneity and Immunosuppressive Environment in Human Breast Cancer, Cancer cell 33(3) (2018) 463-479.e10.
[232] H.T. Nia, L.L. Munn, R.K. Jain, Physical traits of cancer, Science 370(6516) (2020).
[233] A. Nicolás-Boluda, J. Vaquero, G. Laurent, G. Renault, R. Bazzi, E. Donnadieu, S. Roux, L. Fouassier, F. Gazeau, Photothermal Depletion of Cancer-Associated Fibroblasts Normalizes Tumor Stiffness in Desmoplastic Cholangiocarcinoma, ACS Nano 14(5) (2020) 5738-5753.
[234] T. Iida, Y. Mizutani, N. Esaki, S.M. Ponik, B.M. Burkel, L. Weng, K. Kuwata, A. Masamune, S. Ishihara, H. Haga, K. Kataoka, S. Mii, Y. Shiraki, T. Ishikawa, E. Ohno, H. Kawashima, Y. Hirooka, M. Fujishiro, M. Takahashi, A. Enomoto, Pharmacologic conversion of cancer-associated fibroblasts from a protumor phenotype to an antitumor phenotype improves the sensitivity of pancreatic cancer to chemotherapeutics, Oncogene 41(19) (2022) 2764-2777.
[235] O. Maller, A.P. Drain, A.S. Barrett, S. Borgquist, B. Ruffell, I. Zakharevich, T.T. Pham, T. Gruosso, H. Kuasne, J.N. Lakins, I. Acerbi, J.M. Barnes, T. Nemkov, A. Chauhan, J. Gruenberg, A. Nasir, O. Bjarnadottir, Z. Werb, P. Kabos, Y.-Y. Chen, E.S. Hwang, M. Park, L.M. Coussens, A.C. Nelson, K.C. Hansen, V.M. Weaver, Tumour-associated macrophages drive stromal cell-dependent collagen crosslinking and stiffening to promote breast cancer aggression, Nat Mater 20(4) (2021) 548-559.
[236] M. Li, X. Zhang, M. Wang, Y. Wang, J. Qian, X. Xing, Z. Wang, Y. You, K. Guo, J. Chen, D. Gao, Y. Zhao, L. Zhang, R. Chen, J. Cui, Z. Ren, Activation of Piezo1 contributes to matrix stiffness-induced angiogenesis in hepatocellular carcinoma, Cancer communications (London, England) 42(11) (2022) 1162-1184.
[237] B. Wu, D.A. Liu, L. Guan, P.K. Myint, L. Chin, H. Dang, Y. Xu, J. Ren, T. Li, Z. Yu, S. Jabban, G.B. Mills, J. Nukpezah, Y.H. Chen, E.E. Furth, P.A. Gimotty, R.G. Wells, V.M. Weaver, R. Radhakrishnan, X.W. Wang, W. Guo, Stiff matrix induces exosome secretion to promote tumour growth, Nature cell biology 25(3) (2023) 415-424.
[238] M.J. Paszek, N. Zahir, K.R. Johnson, J.N. Lakins, G.I. Rozenberg, A. Gefen, C.A. Reinhart-King, S.S. Margulies, M. Dembo, D. Boettiger, D.A. Hammer, V.M. Weaver, Tensional homeostasis and the malignant phenotype, Cancer Cell 8(3) (2005) 241-254.
[239] G. Santinon, I. Brian, A. Pocaterra, P. Romani, E. Franzolin, C. Rampazzo, S. Bicciato, S. Dupont, dNTP metabolism links mechanical cues and YAP/TAZ to cell growth and oncogene-induced senescence, EMBO J 37(11) (2018).
[240] A. Sohrabi, A. Lefebvre, M.J. Harrison, M.C. Condro, T.M. Sanazzaro, G. Safarians, I. Solomon, S. Bastola, S. Kordbacheh, N. Toh, H.I. Kornblum, M.A. Digman, S.K. Seidlits, Microenvironmental stiffness induces metabolic reprogramming in glioblastoma, Cell reports 42(10) (2023) 113175.

[241] Y. Liu, J. Lv, X. Liang, X. Yin, L. Zhang, D. Chen, X. Jin, R. Fiskesund, K. Tang, J. Ma, H. Zhang, W. Dong, S. Mo, T. Zhang, F. Cheng, Y. Zhou, J. Xie, N. Wang, B. Huang, Fibrin Stiffness Mediates Dormancy of Tumor-Repopulating Cells via a Cdc42-Driven Tet2 Epigenetic Program, Cancer research 78(14) (2018) 3926-3937.
[242] Y. Tan, A.R. Wood, Q. Jia, W. Zhou, J. Luo, F. Yang, J. Chen, J. Chen, J. Sun, J. Seong, A. Tajik, R. Singh, N. Wang, Soft matrices downregulate FAK activity to promote growth of tumor-repopulating cells, Biochem Biophys Res Commun 483(1) (2017) 456-462.
[243] M. Zhang, C. Xu, H.-Z. Wang, Y.-N. Peng, H.-O. Li, Y.-J. Zhou, S. Liu, F. Wang, L. Liu, Y. Chang, Q. Zhao, J. Liu, Soft fibrin matrix downregulates DAB2IP to promote Nanog-dependent growth of colon tumor-repopulating cells, Cell Death Dis 10(3) (2019) 151.
[244] Y. Peng, Z. Chen, Y. Chen, S. Li, Y. Jiang, H. Yang, C. Wu, F. You, C. Zheng, J. Zhu, Y. Tan, X. Qin, Y. Liu, ROCK isoforms differentially modulate cancer cell motility by mechanosensing the substrate stiffness, Acta biomaterialia 88 (2019) 86-101.
[245] Y.A. Miroshnikova, J.K. Mouw, J.M. Barnes, M.W. Pickup, J.N. Lakins, Y. Kim, K. Lobo, A.I. Persson, G.F. Reis, T.R. McKnight, E.C. Holland, J.J. Phillips, V.M. Weaver, Tissue mechanics promote IDH1-dependent HIF1α-tenascin C feedback to regulate glioblastoma aggression, Nature cell biology 18(12) (2016) 1336-1345.
[246] C. Stashko, M.-K. Hayward, J.J. Northey, N. Pearson, A.J. Ironside, J.N. Lakins, R. Oria, M.-A. Goyette, L. Mayo, H.G. Russnes, E.S. Hwang, M.L. Kutys, K. Polyak, V.M. Weaver, A convolutional neural network STIFMap reveals associations between stromal stiffness and EMT in breast cancer, Nature communications 14(1) (2023) 3561.
[247] Z. Gu, F. Liu, E.A. Tonkova, S.Y. Lee, D.J. Tschumperlin, M.B. Brenner, Soft matrix is a natural stimulator for cellular invasiveness, Mol Biol Cell 25(4) (2014) 457-469.
[248] S. Bhattacharjee, F. Hamberger, A. Ravichandra, M. Miller, A. Nair, S. Affo, A. Filliol, L. Chin, T.M. Savage, D. Yin, N.M. Wirsik, A. Mehal, N. Arpaia, E. Seki, M. Mack, D. Zhu, P.A. Sims, R. Kalluri, B.Z. Stanger, K.P. Olive, T. Schmidt, R.G. Wells, I. Mederacke, R.F. Schwabe, Tumor restriction by type I collagen opposes tumor-promoting effects of cancer-associated fibroblasts, The Journal of clinical investigation 131(11) (2021).
[249] A. Kuşoğlu, D. Örnek, A. Dansık, C. Uzun, S. Nur Özkan, S. Sarıca, K. Yangın, Ş. Özdinç, D.T. Sorhun, N. Solcan, E.C. Doğanalp, Ø. Arlov, K. Cunningham, I.C. Karaoğlu, S. Kizilel, I. Solaroğlu, P. Bulutay, P. Fırat, S. Erus, S. Tanju, Ş. Dilege, G. Vunjak-Novakovic, N. Tuncbag, E. Öztürk, Extracellular Matrix Sulfation in the Tumor Microenvironment Stimulates Cancer Stemness and Invasiveness, Adv Sci (Weinh) (2024) e2309966.
[250] M. Jang, S.W. Oh, Y. Lee, J.Y. Kim, E.S. Ji, P. Kim, Targeting extracellular matrix glycation to attenuate fibroblast activation, Acta biomaterialia 141 (2022) 255-263.
[251] K.R. Levental, H. Yu, L. Kass, J.N. Lakins, M. Egeblad, J.T. Erler, S.F.T. Fong, K. Csiszar, A. Giaccia, W. Weninger, M. Yamauchi, D.L. Gasser, V.M. Weaver, Matrix crosslinking forces tumor progression by enhancing integrin signaling, Cell 139(5) (2009) 891-906.
[252] X. Li, J. Pan, T. Liu, W. Yin, Q. Miao, Z. Zhao, Y. Gao, W. Zheng, H. Li, R. Deng, D. Huang, S. Qiu, Y. Zhang, Q. Qi, L. Deng, M. Huang, P.M.-K. Tang, Y. Cao, M. Chen, W. Ye, D. Zhang, Novel TCF21high pericyte subpopulation promotes colorectal cancer metastasis by remodelling perivascular matrix, Gut 72(4) (2023) 710-721.
[253] Y. Chen, S. Yang, J. Tavormina, D. Tampe, M. Zeisberg, H. Wang, K.K. Mahadevan, C.-J. Wu, H. Sugimoto, C.-C. Chang, R.R. Jenq, K.M. McAndrews, R. Kalluri, Oncogenic collagen I homotrimers

from cancer cells bind to α3β1 integrin and impact tumor microbiome and immunity to promote pancreatic cancer, Cancer Cell 40(8) (2022).
[254] W.-H. Jung, N. Yam, C.-C. Chen, K. Elawad, B. Hu, Y. Chen, Force-dependent extracellular matrix remodeling by early-stage cancer cells alters diffusion and induces carcinoma-associated fibroblasts, Biomaterials 234 (2020) 119756.
[255] S. Nam, Y.-H. Lin, T. Kim, O. Chaudhuri, Cellular Pushing Forces during Mitosis Drive Mitotic Elongation in Collagen Gels, Adv Sci (Weinh) 8(4) (2021) 2000403.
[256] V.K. Gupta, O. Chaudhuri, Mechanical regulation of cell-cycle progression and division, Trends Cell Biol 32(9) (2022) 773-785.
[257] R. Li, Y. Wang, X. Zhang, M. Feng, J. Ma, J. Li, X. Yang, F. Fang, Q. Xia, Z. Zhang, M. Shang, S. Jiang, Exosome-mediated secretion of LOXL4 promotes hepatocellular carcinoma cell invasion and metastasis, Mol Cancer 18(1) (2019) 18.
[258] S. Torres, R.A. Bartolomé, M. Mendes, R. Barderas, M.J. Fernandez-Aceñero, A. Peláez-García, C. Peña, M. Lopez-Lucendo, R. Villar-Vázquez, A.G. de Herreros, F. Bonilla, J.I. Casal, Proteome profiling of cancer-associated fibroblasts identifies novel proinflammatory signatures and prognostic markers for colorectal cancer, Clin Cancer Res 19(21) (2013) 6006-6019.
[259] X. Wu, T. Liu, O. Fang, L.J. Leach, X. Hu, Z. Luo, miR-194 suppresses metastasis of non-small cell lung cancer through regulating expression of BMP1 and p27(kip1), Oncogene 33(12) (2014) 1506-1514.
[260] T.R. Cox, The matrix in cancer, Nat Rev Cancer 21(4) (2021) 217-238.
[261] J.M. Houthuijzen, R. de Bruijn, E. van der Burg, A.P. Drenth, E. Wientjens, T. Filipovic, E. Bullock, C.S. Brambillasca, E.M. Pulver, M. Nieuwland, I. de Rink, F. van Diepen, S. Klarenbeek, R. Kerkhoven, V.G. Brunton, C.L.G.J. Scheele, M.C. Boelens, J. Jonkers, CD26-negative and CD26-positive tissue-resident fibroblasts contribute to functionally distinct CAF subpopulations in breast cancer, Nat Commun 14(1) (2023) 183.
[262] T. Tapia, R. Ottman, R. Chakrabarti, LIM kinase1 modulates function of membrane type matrix metalloproteinase 1: implication in invasion of prostate cancer cells, Mol Cancer 10 (2011) 6.
[263] Y. Li, C. Kuscu, A. Banach, Q. Zhang, A. Pulkoski-Gross, D. Kim, J. Liu, E. Roth, E. Li, K.R. Shroyer, P.I. Denoya, X. Zhu, L. Chen, J. Cao, miR-181a-5p Inhibits Cancer Cell Migration and Angiogenesis via Downregulation of Matrix Metalloproteinase-14, Cancer research 75(13) (2015) 2674-2685.
[264] Y. Hassona, N. Cirillo, K. Heesom, E.K. Parkinson, S.S. Prime, Senescent cancer-associated fibroblasts secrete active MMP-2 that promotes keratinocyte dis-cohesion and invasion, Br J Cancer 111(6) (2014) 1230-1237.
[265] Y.-L. Che, S.-J. Luo, G. Li, M. Cheng, Y.-M. Gao, X.-M. Li, J.-M. Dai, H. He, J. Wang, H.-J. Peng, Y. Zhang, W.-Y. Li, H. Wang, B. Liu, H. Linghu, The C3G/Rap1 pathway promotes secretion of MMP-2 and MMP-9 and is involved in serous ovarian cancer metastasis, Cancer Lett 359(2) (2015) 241-249.
[266] G. Bergers, R. Brekken, G. McMahon, T.H. Vu, T. Itoh, K. Tamaki, K. Tanzawa, P. Thorpe, S. Itohara, Z. Werb, D. Hanahan, Matrix metalloproteinase-9 triggers the angiogenic switch during carcinogenesis, Nat Cell Biol 2(10) (2000) 737-744.
[267] R. Stern, Hyaluronidases in cancer biology, Semin Cancer Biol 18(4) (2008) 275-280.
[268] M.A. Jacobetz, D.S. Chan, A. Neesse, T.E. Bapiro, N. Cook, K.K. Frese, C. Feig, T. Nakagawa, M.E. Caldwell, H.I. Zecchini, M.P. Lolkema, P. Jiang, A. Kultti, C.B. Thompson, D.C. Maneval, D.I. Jodrell, G.I. Frost, H.M. Shepard, J.N. Skepper, D.A. Tuveson, Hyaluronan impairs vascular function

and drug delivery in a mouse model of pancreatic cancer, Gut 62(1) (2013) 112-120.
[269] C. Bonnans, J. Chou, Z. Werb, Remodelling the extracellular matrix in development and disease, Nature Reviews Molecular Cell Biology 15(12) (2014) 786-801.
[270] D. Öhlund, A. Handly-Santana, G. Biffi, E. Elyada, A.S. Almeida, M. Ponz-Sarvise, V. Corbo, T.E. Oni, S.A. Hearn, E.J. Lee, I.I.C. Chio, C.-I. Hwang, H. Tiriac, L.A. Baker, D.D. Engle, C. Feig, A. Kultti, M. Egeblad, D.T. Fearon, J.M. Crawford, H. Clevers, Y. Park, D.A. Tuveson, Distinct populations of inflammatory fibroblasts and myofibroblasts in pancreatic cancer, The Journal of Experimental Medicine 214(3) (2017) 579-596.
[271] D.A. Beacham, E. Cukierman, Stromagenesis: the changing face of fibroblastic microenvironments during tumor progression, Semin Cancer Biol 15(5) (2005) 329-341.
[272] J.J. Tomasek, G. Gabbiani, B. Hinz, C. Chaponnier, R.A. Brown, Myofibroblasts and mechano-regulation of connective tissue remodelling, Nat Rev Mol Cell Biol 3(5) (2002) 349-363.
[273] R. Malik, T. Luong, X. Cao, B. Han, N. Shah, J. Franco-Barraza, L. Han, V.B. Shenoy, P.I. Lelkes, E. Cukierman, Rigidity controls human desmoplastic matrix anisotropy to enable pancreatic cancer cell spread via extracellular signal-regulated kinase 2, Matrix Biol 81 (2019) 50-69.
[274] J.G. Goetz, S. Minguet, I. Navarro-Lérida, J.J. Lazcano, R. Samaniego, E. Calvo, M. Tello, T. Osteso-Ibáñez, T. Pellinen, A. Echarri, A. Cerezo, A.J.P. Klein-Szanto, R. Garcia, P.J. Keely, P. Sánchez-Mateos, E. Cukierman, M.A. Del Pozo, Biomechanical remodeling of the microenvironment by stromal caveolin-1 favors tumor invasion and metastasis, Cell 146(1) (2011) 148-163.
[275] J.Z. Kechagia, J. Ivaska, P. Roca-Cusachs, Integrins as biomechanical sensors of the microenvironment, Nat Rev Mol Cell Biol 20(8) (2019) 457-473.
[276] C. Zeltz, I. Primac, P. Erusappan, J. Alam, A. Noel, D. Gullberg, Cancer-associated fibroblasts in desmoplastic tumors: emerging role of integrins, Semin Cancer Biol 62 (2020) 166-181.
[277] E.V. Nguyen, B.A. Pereira, M.G. Lawrence, X. Ma, R.J. Rebello, H. Chan, B. Niranjan, Y. Wu, S. Ellem, X. Guan, J. Wu, J.N. Skhinas, T.R. Cox, G.P. Risbridger, R.A. Taylor, N.L. Lister, R.J. Daly, Proteomic Profiling of Human Prostate Cancer-associated Fibroblasts (CAF) Reveals LOXL2-dependent Regulation of the Tumor Microenvironment, Mol Cell Proteomics 18(7) (2019) 1410-1427.
[278] X. Tang, Y. Hou, G. Yang, X. Wang, S. Tang, Y.E. Du, L. Yang, T. Yu, H. Zhang, M. Zhou, S. Wen, L. Xu, M. Liu, Stromal miR-200s contribute to breast cancer cell invasion through CAF activation and ECM remodeling, Cell Death Differ 23(1) (2016) 132-145.
[279] H. Mohammadi, E. Sahai, Mechanisms and impact of altered tumour mechanics, Nat Cell Biol 20(7) (2018) 766-774.
[280] C.D. Madsen, J.T. Pedersen, F.A. Venning, L.B. Singh, E. Moeendarbary, G. Charras, T.R. Cox, E. Sahai, J.T. Erler, Hypoxia and loss of PHD2 inactivate stromal fibroblasts to decrease tumour stiffness and metastasis, EMBO Rep 16(10) (2015) 1394-1408.
[281] D.S.R. Lockwood, T.M. Yeadon, A.D. Clouston, D.G. Crawford, J. Fawcett, S.A. Callaghan, D.C. Gotley, Tumor progression in hepatocellular carcinoma: relationship with tumor stroma and parenchymal disease, J Gastroenterol Hepatol 18(6) (2003) 666-672.
[282] A.D. Rhim, P.E. Oberstein, D.H. Thomas, E.T. Mirek, C.F. Palermo, S.A. Sastra, E.N. Dekleva, T. Saunders, C.P. Becerra, I.W. Tattersall, C.B. Westphalen, J. Kitajewski, M.G. Fernandez-Barrena, M.E. Fernandez-Zapico, C. Iacobuzio-Donahue, K.P. Olive, B.Z. Stanger, Stromal elements act to restrain, rather than support, pancreatic ductal adenocarcinoma, Cancer Cell 25(6) (2014) 735-747.
[283] B.C. Özdemir, T. Pentcheva-Hoang, J.L. Carstens, X. Zheng, C.-C. Wu, T.R. Simpson, H. Laklai, H. Sugimoto, C. Kahlert, S.V. Novitskiy, A. De Jesus-Acosta, P. Sharma, P. Heidari, U. Mahmood, L.

Chin, H.L. Moses, V.M. Weaver, A. Maitra, J.P. Allison, V.S. LeBleu, R. Kalluri, Depletion of carcinoma-associated fibroblasts and fibrosis induces immunosuppression and accelerates pancreas cancer with reduced survival, Cancer Cell 25(6) (2014) 719-734.
[284] O. De Wever, Q.-D. Nguyen, L. Van Hoorde, M. Bracke, E. Bruyneel, C. Gespach, M. Mareel, Tenascin-C and SF/HGF produced by myofibroblasts in vitro provide convergent pro-invasive signals to human colon cancer cells through RhoA and Rac, FASEB J 18(9) (2004) 1016-1018.
[285] C. Strell, J. Paulsson, S.-B. Jin, N.P. Tobin, A. Mezheyeuski, P. Roswall, C. Mutgan, N. Mitsios, H. Johansson, S.M. Wickberg, J. Svedlund, M. Nilsson, P. Hall, J. Mulder, D.C. Radisky, K. Pietras, J. Bergh, U. Lendahl, F. Wärnberg, A. Östman, Impact of Epithelial-Stromal Interactions on Peritumoral Fibroblasts in Ductal Carcinoma in Situ, Journal of the National Cancer Institute 111(9) (2019) 983-995.
[286] N. Erez, M. Truitt, P. Olson, S.T. Arron, D. Hanahan, Cancer-Associated Fibroblasts Are Activated in Incipient Neoplasia to Orchestrate Tumor-Promoting Inflammation in an NF-kappaB-Dependent Manner, Cancer Cell 17(2) (2010) 135-147.
[287] V. Sanz-Moreno, C. Gaggioli, M. Yeo, J. Albrengues, F. Wallberg, A. Viros, S. Hooper, R. Mitter, C.C. Féral, M. Cook, J. Larkin, R. Marais, G. Meneguzzi, E. Sahai, C.J. Marshall, ROCK and JAK1 signaling cooperate to control actomyosin contractility in tumor cells and stroma, Cancer Cell 20(2) (2011) 229-245.
[288] J. Albrengues, T. Bertero, E. Grasset, S. Bonan, M. Maiel, I. Bourget, C. Philippe, C. Herraiz Serrano, S. Benamar, O. Croce, V. Sanz-Moreno, G. Meneguzzi, C.C. Feral, G. Cristofari, C. Gaggioli, Epigenetic switch drives the conversion of fibroblasts into proinvasive cancer-associated fibroblasts, Nat Commun 6 (2015) 10204.
[289] J. Albrengues, I. Bourget, C. Pons, V. Butet, P. Hofman, S. Tartare-Deckert, C.C. Feral, G. Meneguzzi, C. Gaggioli, LIF mediates proinvasive activation of stromal fibroblasts in cancer, Cell Rep 7(5) (2014) 1664-1678.
[290] F. Calvo, N. Ege, A. Grande-Garcia, S. Hooper, R.P. Jenkins, S.I. Chaudhry, K. Harrington, P. Williamson, E. Moeendarbary, G. Charras, E. Sahai, Mechanotransduction and YAP-dependent matrix remodelling is required for the generation and maintenance of cancer-associated fibroblasts, Nat Cell Biol 15(6) (2013) 637-646.
[291] C.T. Foster, F. Gualdrini, R. Treisman, Mutual dependence of the MRTF-SRF and YAP-TEAD pathways in cancer-associated fibroblasts is indirect and mediated by cytoskeletal dynamics, Genes Dev 31(23-24) (2017) 2361-2375.
[292] F. Calvo, R. Ranftl, S. Hooper, A.J. Farrugia, E. Moeendarbary, A. Bruckbauer, F. Batista, G. Charras, E. Sahai, Cdc42EP3/BORG2 and Septin Network Enables Mechano-transduction and the Emergence of Cancer-Associated Fibroblasts, Cell Rep 13(12) (2015) 2699-2714.
[293] M.D. Amatangelo, D.E. Bassi, A.J.P. Klein-Szanto, E. Cukierman, Stroma-derived three-dimensional matrices are necessary and sufficient to promote desmoplastic differentiation of normal fibroblasts, Am J Pathol 167(2) (2005) 475-488.
[294] C.A. Fordyce, K.T. Patten, T.B. Fessenden, R. DeFilippis, E.S. Hwang, J. Zhao, T.D. Tlsty, Cell-extrinsic consequences of epithelial stress: activation of protumorigenic tissue phenotypes, Breast Cancer Res 14(6) (2012) R155.
[295] A. Arina, C. Idel, E.M. Hyjek, M.-L. Alegre, Y. Wang, V.P. Bindokas, R.R. Weichselbaum, H. Schreiber, Tumor-associated fibroblasts predominantly come from local and not circulating precursors, Proc Natl Acad Sci U S A 113(27) (2016) 7551-7556.
[296] R. Scherz-Shouval, S. Santagata, M.L. Mendillo, L.M. Sholl, I. Ben-Aharon, A.H. Beck, D. Dias-

Santagata, M. Koeva, S.M. Stemmer, L. Whitesell, S. Lindquist, The reprogramming of tumor stroma by HSF1 is a potent enabler of malignancy, Cell 158(3) (2014) 564-578.
[297] S. Mariathasan, S.J. Turley, D. Nickles, A. Castiglioni, K. Yuen, Y. Wang, E.E. Kadel, H. Koeppen, J.L. Astarita, R. Cubas, S. Jhunjhunwala, R. Banchereau, Y. Yang, Y. Guan, C. Chalouni, J. Ziai, Y. Şenbabaoğlu, S. Santoro, D. Sheinson, J. Hung, J.M. Giltnane, A.A. Pierce, K. Mesh, S. Lianoglou, J. Riegler, R.A.D. Carano, P. Eriksson, M. Höglund, L. Somarriba, D.L. Halligan, M.S. van der Heijden, Y. Loriot, J.E. Rosenberg, L. Fong, I. Mellman, D.S. Chen, M. Green, C. Derleth, G.D. Fine, P.S. Hegde, R. Bourgon, T. Powles, TGFβ attenuates tumour response to PD-L1 blockade by contributing to exclusion of T cells, Nature 554(7693) (2018) 544-548.
[298] D.V.F. Tauriello, S. Palomo-Ponce, D. Stork, A. Berenguer-Llergo, J. Badia-Ramentol, M. Iglesias, M. Sevillano, S. Ibiza, A. Cañellas, X. Hernando-Momblona, D. Byrom, J.A. Matarin, A. Calon, E.I. Rivas, A.R. Nebreda, A. Riera, C.S.-O. Attolini, E. Batlle, TGFβ drives immune evasion in genetically reconstituted colon cancer metastasis, Nature 554(7693) (2018) 538-543.
[299] C. Gaggioli, S. Hooper, C. Hidalgo-Carcedo, R. Grosse, J.F. Marshall, K. Harrington, E. Sahai, Fibroblast-led collective invasion of carcinoma cells with differing roles for RhoGTPases in leading and following cells, Nat Cell Biol 9(12) (2007) 1392-1400.
[300] S. Hooper, C. Gaggioli, E. Sahai, A chemical biology screen reveals a role for Rab21-mediated control of actomyosin contractility in fibroblast-driven cancer invasion, Br J Cancer 102(2) (2010) 392-402.
[301] N. Dumont, B. Liu, R.A. Defilippis, H. Chang, J.T. Rabban, A.N. Karnezis, J.A. Tjoe, J. Marx, B. Parvin, T.D. Tlsty, Breast fibroblasts modulate early dissemination, tumorigenesis, and metastasis through alteration of extracellular matrix characteristics, Neoplasia 15(3) (2013) 249-262.
[302] A. Calon, E. Espinet, S. Palomo-Ponce, D.V.F. Tauriello, M. Iglesias, M.V. Céspedes, M. Sevillano, C. Nadal, P. Jung, X.H.F. Zhang, D. Byrom, A. Riera, D. Rossell, R. Mangues, J. Massagué, E. Sancho, E. Batlle, Dependency of colorectal cancer on a TGF-β-driven program in stromal cells for metastasis initiation, Cancer Cell 22(5) (2012) 571-584.
[303] P. Nordenfelt, T.I. Moore, S.B. Mehta, J.M. Kalappurakkal, V. Swaminathan, N. Koga, T.J. Lambert, D. Baker, J.C. Waters, R. Oldenbourg, T. Tani, S. Mayor, C.M. Waterman, T.A. Springer, Direction of actin flow dictates integrin LFA-1 orientation during leukocyte migration, Nat Commun 8(1) (2017) 2047.
[304] J.H.R. Hetmanski, H. de Belly, I. Busnelli, T. Waring, R.V. Nair, V. Sokleva, O. Dobre, A. Cameron, N. Gauthier, C. Lamaze, J. Swift, A. Del Campo, T. Starborg, T. Zech, J.G. Goetz, E.K. Paluch, J.-M. Schwartz, P.T. Caswell, Membrane Tension Orchestrates Rear Retraction in Matrix-Directed Cell Migration, Dev Cell 51(4) (2019).
[305] F. Baschieri, S. Dayot, N. Elkhatib, N. Ly, A. Capmany, K. Schauer, T. Betz, D.M. Vignjevic, R. Poincloux, G. Montagnac, Frustrated endocytosis controls contractility-independent mechanotransduction at clathrin-coated structures, Nat Commun 9(1) (2018) 3825.
[306] T. Lämmermann, B.L. Bader, S.J. Monkley, T. Worbs, R. Wedlich-Söldner, K. Hirsch, M. Keller, R. Förster, D.R. Critchley, R. Fässler, M. Sixt, Rapid leukocyte migration by integrin-independent flowing and squeezing, Nature 453(7191) (2008) 51-55.
[307] N. Pal, M. Wu, H.P. Lu, Probing conformational dynamics of an enzymatic active site by an in situ single fluorogenic probe under piconewton force manipulation, Proc Natl Acad Sci U S A 113(52) (2016) 15006-15011.
[308] C.D. Cox, N. Bavi, B. Martinac, Biophysical Principles of Ion-Channel-Mediated Mechanosensory Transduction, Cell Rep 29(1) (2019).

[309] X. Yang, C. Lin, X. Chen, S. Li, X. Li, B. Xiao, Structure deformation and curvature sensing of PIEZO1 in lipid membranes, Nature 604(7905) (2022) 377-383.
[310] A. Chopra, M.E. Murray, F.J. Byfield, M.G. Mendez, R. Halleluyan, D.J. Restle, D. Raz-Ben Aroush, P.A. Galie, K. Pogoda, R. Bucki, C. Marcinkiewicz, G.D. Prestwich, T.I. Zarembinski, C.S. Chen, E. Puré, J.Y. Kresh, P.A. Janmey, Augmentation of integrin-mediated mechanotransduction by hyaluronic acid, Biomaterials 35(1) (2014) 71-82.
[311] B.J. DeOre, P.P. Partyka, F. Fan, P.A. Galie, CD44 mediates shear stress mechanotransduction in an in vitro blood-brain barrier model through small GTPases RhoA and Rac1, FASEB J 36(5) (2022) e22278.
[312] Y. Kim, S. Kumar, CD44-mediated adhesion to hyaluronic acid contributes to mechanosensing and invasive motility, Mol Cancer Res 12(10) (2014) 1416-1429.
[313] G. Safarians, A. Sohrabi, I. Solomon, W. Xiao, S. Bastola, B.W. Rajput, M. Epperson, I. Rosenzweig, K. Tamura, B. Singer, J. Huang, M.J. Harrison, T. Sanazzaro, M.C. Condro, H.I. Kornblum, S.K. Seidlits, Glioblastoma Spheroid Invasion through Soft, Brain-Like Matrices Depends on Hyaluronic Acid-CD44 Interactions, Adv Healthc Mater 12(14) (2023) e2203143.
[314] T. Mitchison, M. Kirschner, Cytoskeletal dynamics and nerve growth, Neuron 1(9) (1988) 761-772.
[315] A. Elosegui-Artola, R. Oria, Y. Chen, A. Kosmalska, C. Pérez-González, N. Castro, C. Zhu, X. Trepat, P. Roca-Cusachs, Mechanical regulation of a molecular clutch defines force transmission and transduction in response to matrix rigidity, Nat Cell Biol 18(5) (2016) 540-548.
[316] C.E. Chan, D.J. Odde, Traction dynamics of filopodia on compliant substrates, Science 322(5908) (2008) 1687-1691.
[317] B.L. Bangasser, S.S. Rosenfeld, D.J. Odde, Determinants of maximal force transmission in a motor-clutch model of cell traction in a compliant microenvironment, Biophys J 105(3) (2013) 581-592.
[318] B.L. Bangasser, G.A. Shamsan, C.E. Chan, K.N. Opoku, E. Tüzel, B.W. Schlichtmann, J.A. Kasim, B.J. Fuller, B.R. McCullough, S.S. Rosenfeld, D.J. Odde, Shifting the optimal stiffness for cell migration, Nat Commun 8 (2017) 15313.
[319] M. Lerche, A. Elosegui-Artola, J.Z. Kechagia, C. Guzmán, M. Georgiadou, I. Andreu, D. Gullberg, P. Roca-Cusachs, E. Peuhu, J. Ivaska, Integrin Binding Dynamics Modulate Ligand-Specific Mechanosensing in Mammary Gland Fibroblasts, iScience 23(3) (2020) 100907.
[320] Y. Sawada, M. Tamada, B.J. Dubin-Thaler, O. Cherniavskaya, R. Sakai, S. Tanaka, M.P. Sheetz, Force sensing by mechanical extension of the Src family kinase substrate p130Cas, Cell 127(5) (2006) 1015-1026.
[321] D.E. Koser, A.J. Thompson, S.K. Foster, A. Dwivedy, E.K. Pillai, G.K. Sheridan, H. Svoboda, M. Viana, L.d.F. Costa, J. Guck, C.E. Holt, K. Franze, Mechanosensing is critical for axon growth in the developing brain, Nature Neuroscience 19(12) (2016) 1592-1598.
[322] M. Mathieu, A. Isomursu, J. Ivaska, Positive and negative durotaxis - mechanisms and emerging concepts, J Cell Sci 137(8) (2024).
[323] C. Ji, Y. Huang, Durotaxis and negative durotaxis: where should cells go?, Commun Biol 6(1) (2023) 1169.
[324] P.U. Shirke, H. Goswami, V. Kumar, D. Shah, S. Beri, S. Das, J. Bellare, S. Mayor, K.V. Venkatesh, J.R. Seth, A. Majumder, "Viscotaxis"- directed migration of mesenchymal stem cells in response to loss modulus gradient, Acta biomaterialia 135 (2021) 356-367.
[325] P. Saez, P.U. Shirke, J.R. Seth, J. Alegre-Cebollada, A.J.A.a.S. Majumder, Competing elastic and

viscous gradients determine directional cell migration, (2023).
[326] B. Liebchen, P. Monderkamp, B. Ten Hagen, H. Löwen, Viscotaxis: Microswimmer Navigation in Viscosity Gradients, Phys Rev Lett 120(20) (2018) 208002.
[327] S.M. van Neerven, L. Vermeulen, Cell competition in development, homeostasis and cancer, Nature reviews. Molecular cell biology 24(3) (2023) 221-236.
[328] S.J. Pfau, R.E. Silberman, K.A. Knouse, A. Amon, Aneuploidy impairs hematopoietic stem cell fitness and is selected against in regenerating tissues in vivo, Genes Dev 30(12) (2016) 1395-1408.
[329] B. Vogelstein, N. Papadopoulos, V.E. Velculescu, S. Zhou, L.A. Diaz, K.W. Kinzler, Cancer genome landscapes, Science (New York, N.Y.) 339(6127) (2013) 1546-1558.
[330] I.M. Moya, S.A. Castaldo, L. Van den Mooter, S. Soheily, L. Sansores-Garcia, J. Jacobs, I. Mannaerts, J. Xie, E. Verboven, H. Hillen, A. Algueró-Nadal, R. Karaman, M. Van Haele, W. Kowalczyk, M. De Waegeneer, S. Verhulst, P. Karras, L. van Huffel, L. Zender, J.-C. Marine, T. Roskams, R. Johnson, S. Aerts, L.A. van Grunsven, G. Halder, Peritumoral activation of the Hippo pathway effectors YAP and TAZ suppresses liver cancer in mice, Science 366(6468) (2019) 1029-1034.
[331] L. Ballesteros-Arias, V. Saavedra, G. Morata, Cell competition may function either as tumour-suppressing or as tumour-stimulating factor in Drosophila, Oncogene 33(35) (2014) 4377-4384.
[332] A. Sasaki, T. Nagatake, R. Egami, G. Gu, I. Takigawa, W. Ikeda, T. Nakatani, J. Kunisawa, Y. Fujita, Obesity Suppresses Cell-Competition-Mediated Apical Elimination of RasV12-Transformed Cells from Epithelial Tissues, Cell reports 23(4) (2018) 974-982.
[333] H. Watanabe, K. Ishibashi, H. Mano, S. Kitamoto, N. Sato, K. Hoshiba, M. Kato, F. Matsuzawa, Y. Takeuchi, T. Shirai, S. Ishikawa, Y. Morioka, T. Imagawa, K. Sakaguchi, S. Yonezawa, S. Kon, Y. Fujita, Mutant p53-Expressing Cells Undergo Necroptosis via Cell Competition with the Neighboring Normal Epithelial Cells, Cell reports 23(13) (2018) 3721-3729.
[334] D. Fernandez-Antoran, G. Piedrafita, K. Murai, S.H. Ong, A. Herms, C. Frezza, P.H. Jones, Outcompeting p53-Mutant Cells in the Normal Esophagus by Redox Manipulation, Cell Stem Cell 25(3) (2019).
[335] W. Hill, A. Zaragkoulias, B. Salvador-Barbero, G.J. Parfitt, M. Alatsatianos, A. Padilha, S. Porazinski, T.E. Woolley, J.P. Morton, O.J. Sansom, C. Hogan, EPHA2-dependent outcompetition of KRASG12D mutant cells by wild-type neighbors in the adult pancreas, Curr. Biol. 31(12) (2021) 2550-2560.e5.
[336] S. Porazinski, J. de Navascués, Y. Yako, W. Hill, M.R. Jones, R. Maddison, Y. Fujita, C. Hogan, EphA2 Drives the Segregation of Ras-Transformed Epithelial Cells from Normal Neighbors, Current Biology : CB 26(23) (2016) 3220-3229.
[337] M. Kajita, C. Hogan, A.R. Harris, S. Dupre-Crochet, N. Itasaki, K. Kawakami, G. Charras, M. Tada, Y. Fujita, Interaction with surrounding normal epithelial cells influences signalling pathways and behaviour of Src-transformed cells, J Cell Sci 123(Pt 2) (2010) 171-80.
[338] A.G. Grieve, C. Rabouille, Extracellular cleavage of E-cadherin promotes epithelial cell extrusion, J Cell Sci 127(Pt 15) (2014) 3331-46.
[339] T. Chiba, E. Ishihara, N. Miyamura, R. Narumi, M. Kajita, Y. Fujita, A. Suzuki, Y. Ogawa, H. Nishina, MDCK cells expressing constitutively active Yes-associated protein (YAP) undergo apical extrusion depending on neighboring cell status, Scientific reports 6 (2016) 28383.
[340] C. Hogan, S. Dupré-Crochet, M. Norman, M. Kajita, C. Zimmermann, A.E. Pelling, E. Piddini, L.A. Baena-López, J.P. Vincent, Y. Itoh, H. Hosoya, F. Pichaud, Y. Fujita, Characterization of the interface between normal and transformed epithelial cells, Nature cell biology 11(4) (2009) 460-7.

[341] S.K. Wu, G.A. Gomez, M. Michael, S. Verma, H.L. Cox, J.G. Lefevre, R.G. Parton, N.A. Hamilton, Z. Neufeld, A.S. Yap, Cortical F-actin stabilization generates apical-lateral patterns of junctional contractility that integrate cells into epithelia, Nature cell biology 16(2) (2014) 167-78.
[342] G. Piedrafita, V. Kostiou, A. Wabik, B. Colom, D. Fernandez-Antoran, A. Herms, K. Murai, B.A. Hall, P.H. Jones, A single-progenitor model as the unifying paradigm of epidermal and esophageal epithelial maintenance in mice, Nature communications 11(1) (2020) 1429.
[343] M.P. Alcolea, P. Greulich, A. Wabik, J. Frede, B.D. Simons, P.H. Jones, Differentiation imbalance in single oesophageal progenitor cells causes clonal immortalization and field change, Nature cell biology 16(6) (2014) 615-22.
[344] B. Colom, M.P. Alcolea, G. Piedrafita, M.W.J. Hall, A. Wabik, S.C. Dentro, J.C. Fowler, A. Herms, C. King, S.H. Ong, R.K. Sood, M. Gerstung, I. Martincorena, B.A. Hall, P.H. Jones, Spatial competition shapes the dynamic mutational landscape of normal esophageal epithelium, Nature genetics 52(6) (2020) 604-614.
[345] S. Lowell, P. Jones, I. Le Roux, J. Dunne, F.M. Watt, Stimulation of human epidermal differentiation by delta-notch signalling at the boundaries of stem-cell clusters, Current Biology : CB 10(9) (2000) 491-500.
[346] O. Shaya, U. Binshtok, M. Hersch, D. Rivkin, S. Weinreb, L. Amir-Zilberstein, B. Khamaisi, O. Oppenheim, R.A. Desai, R.J. Goodyear, G.P. Richardson, C.S. Chen, D. Sprinzak, Cell-Cell Contact Area Affects Notch Signaling and Notch-Dependent Patterning, Dev Cell 40(5) (2017) 505-511.e6.
[347] F. Chowdhury, I.T. Li, T.T. Ngo, B.J. Leslie, B.C. Kim, J.E. Sokoloski, E. Weiland, X. Wang, Y.R. Chemla, T.M. Lohman, T. Ha, Defining Single Molecular Forces Required for Notch Activation Using Nano Yoyo, Nano Lett 16(6) (2016) 3892-7.
[348] T. Yugawa, K. Nishino, S. Ohno, T. Nakahara, M. Fujita, N. Goshima, A. Umezawa, T. Kiyono, Noncanonical NOTCH signaling limits self-renewal of human epithelial and induced pluripotent stem cells through ROCK activation, Mol Cell Biol 33(22) (2013) 4434-47.
[349] J.M. Peng, R. Bera, C.Y. Chiou, M.C. Yu, T.C. Chen, C.W. Chen, T.R. Wang, W.L. Chiang, S.P. Chai, Y. Wei, H. Wang, M.C. Hung, S.Y. Hsieh, Actin cytoskeleton remodeling drives epithelial-mesenchymal transition for hepatoma invasion and metastasis in mice, Hepatology 67(6) (2018) 2226-2243.
[350] G.L. Hunter, L. He, N. Perrimon, G. Charras, E. Giniger, B. Baum, A role for actomyosin contractility in Notch signaling, BMC Biol 17(1) (2019) 12.
[351] C.J. Watson, A.L. Papula, G.Y.P. Poon, W.H. Wong, A.L. Young, T.E. Druley, D.S. Fisher, J.R. Blundell, The evolutionary dynamics and fitness landscape of clonal hematopoiesis, Science 367(6485) (2020) 1449-1454.
[352] L.I. Shlush, S. Zandi, A. Mitchell, W.C. Chen, J.M. Brandwein, V. Gupta, J.A. Kennedy, A.D. Schimmer, A.C. Schuh, K.W. Yee, J.L. McLeod, M. Doedens, J.J. Medeiros, R. Marke, H.J. Kim, K. Lee, J.D. McPherson, T.J. Hudson, A.M. Brown, F. Yousif, Q.M. Trinh, L.D. Stein, M.D. Minden, J.C. Wang, J.E. Dick, Identification of pre-leukaemic haematopoietic stem cells in acute leukaemia, Nature 506(7488) (2014) 328-33.
[353] Q. Li, N. Bohin, T. Wen, V. Ng, J. Magee, S.C. Chen, K. Shannon, S.J. Morrison, Oncogenic Nras has bimodal effects on stem cells that sustainably increase competitiveness, Nature 504(7478) (2013) 143-147.
[354] M.A. Reuss-Borst, H.J. Bühring, G. Klein, C.A. Müller, Adhesion molecules on CD34+ hematopoietic cells in normal human bone marrow and leukemia, Ann Hematol 65(4) (1992) 169-74.

[355] J. Bajaj, T. Konuma, N.K. Lytle, H.Y. Kwon, J.N. Ablack, J.M. Cantor, D. Rizzieri, C. Chuah, V.G. Oehler, E.H. Broome, E.D. Ball, E.H. van der Horst, M.H. Ginsberg, T. Reya, CD98-Mediated Adhesive Signaling Enables the Establishment and Propagation of Acute Myelogenous Leukemia, Cancer Cell 30(5) (2016) 792-805.
[356] Y. Saito, K. Kaneda, A. Suekane, E. Ichihara, S. Nakahata, N. Yamakawa, K. Nagai, N. Mizuno, K. Kogawa, I. Miura, H. Itoh, K. Morishita, Maintenance of the hematopoietic stem cell pool in bone marrow niches by EVI1-regulated GPR56, Leukemia 27(8) (2013) 1637-49.
[357] L. Vermeulen, E. Morrissey, M. van der Heijden, A.M. Nicholson, A. Sottoriva, S. Buczacki, R. Kemp, S. Tavaré, D.J. Winton, Defining stem cell dynamics in models of intestinal tumor initiation, Science 342(6161) (2013) 995-8.
[358] H.J. Snippert, A.G. Schepers, J.H. van Es, B.D. Simons, H. Clevers, Biased competition between Lgr5 intestinal stem cells driven by oncogenic mutation induces clonal expansion, EMBO Rep 15(1) (2014) 62-9.
[359] M.K. Yum, S. Han, J. Fink, S.S. Wu, C. Dabrowska, T. Trendafilova, R. Mustata, L. Chatzeli, R. Azzarelli, I. Pshenichnaya, E. Lee, F. England, J.K. Kim, D.E. Stange, A. Philpott, J.H. Lee, B.K. Koo, B.D. Simons, Tracing oncogene-driven remodelling of the intestinal stem cell niche, Nature 594(7863) (2021) 442-447.
[360] S.M. van Neerven, N.E. de Groot, L.E. Nijman, B.P. Scicluna, M.S. van Driel, M.C. Lecca, D.O. Warmerdam, V. Kakkar, L.F. Moreno, F.A. Vieira Braga, D.R. Sanches, P. Ramesh, S. Ten Hoorn, A.S. Aelvoet, M.F. van Boxel, L. Koens, P.M. Krawczyk, J. Koster, E. Dekker, J.P. Medema, D.J. Winton, M.F. Bijlsma, E. Morrissey, N. Léveillé, L. Vermeulen, Apc-mutant cells act as supercompetitors in intestinal tumour initiation, Nature 594(7863) (2021) 436-441.
[361] D.J. Flanagan, N. Pentinmikko, K. Luopajärvi, N.J. Willis, K. Gilroy, A.P. Raven, L. McGarry, J.I. Englund, A.T. Webb, S. Scharaw, N. Nasreddin, M.C. Hodder, R.A. Ridgway, E. Minnee, N. Sphyris, E. Gilchrist, A.K. Najumudeen, B. Romagnolo, C. Perret, A.C. Williams, H. Clevers, P. Nummela, M. Lähde, K. Alitalo, V. Hietakangas, A. Hedley, W. Clark, C. Nixon, K. Kirschner, E.Y. Jones, A. Ristimäki, S.J. Leedham, P.V. Fish, J.P. Vincent, P. Katajisto, O.J. Sansom, NOTUM from Apc-mutant cells biases clonal competition to initiate cancer, Nature 594(7863) (2021) 430-435.
[362] S.J. Suijkerbuijk, G. Kolahgar, I. Kucinski, E. Piddini, Cell Competition Drives the Growth of Intestinal Adenomas in Drosophila, Curr Biol 26(4) (2016) 428-38.
[363] J.P. Vincent, G. Kolahgar, M. Gagliardi, E. Piddini, Steep differences in wingless signaling trigger Myc-independent competitive cell interactions, Dev Cell 21(2) (2011) 366-74.
[364] A.S. Cleary, T.L. Leonard, S.A. Gestl, E.J. Gunther, Tumour cell heterogeneity maintained by cooperating subclones in Wnt-driven mammary cancers, Nature 508(7494) (2014) 113-117.
[365] M. Janiszewska, D.P. Tabassum, Z. Castaño, S. Cristea, K.N. Yamamoto, N.L. Kingston, K.C. Murphy, S. Shu, N.W. Harper, C.G. Del Alcazar, M. Alečković, M.B. Ekram, O. Cohen, M. Kwak, Y. Qin, T. Laszewski, A. Luoma, A. Marusyk, K.W. Wucherpfennig, N. Wagle, R. Fan, F. Michor, S.S. McAllister, K. Polyak, Subclonal cooperation drives metastasis by modulating local and systemic immune microenvironments, Nat Cell Biol 21(7) (2019) 879-888.
[366] Y.L. Dong, G.P. Vadla, J.J. Lu, V. Ahmad, T.J. Klein, L.F. Liu, P.M. Glazer, T. Xu, C.Y. Chabu, Cooperation between oncogenic Ras and wild-type p53 stimulates STAT non-cell autonomously to promote tumor radioresistance, Commun Biol 4(1) (2021) 374.
[367] P.C. Nowell, The clonal evolution of tumor cell populations, Science 194(4260) (1976) 23-8.
[368] R. Vendramin, K. Litchfield, C. Swanton, Cancer evolution: Darwin and beyond, EMBO J 40(18)

(2021) e108389.
[369] Z. Liu, P.P. Yee, Y. Wei, Z. Liu, Y.I. Kawasawa, W. Li, Differential YAP expression in glioma cells induces cell competition and promotes tumorigenesis, J Cell Sci 132(5) (2019).
[370] C.J. Price, D. Stavish, P.J. Gokhale, B.A. Stevenson, S. Sargeant, J. Lacey, T.A. Rodriguez, I. Barbaric, Genetically variant human pluripotent stem cells selectively eliminate wild-type counterparts through YAP-mediated cell competition, Dev Cell 56(17) (2021) 2455-2470.e10.
[371] R. Nagata, N. Akai, S. Kondo, K. Saito, S. Ohsawa, T. Igaki, Yorkie drives supercompetition by non-autonomous induction of autophagy via bantam microRNA in Drosophila, Curr Biol 32(5) (2022) 1064-1076.e4.
[372] M. Katsukawa, S. Ohsawa, L. Zhang, Y. Yan, T. Igaki, Serpin Facilitates Tumor-Suppressive Cell Competition by Blocking Toll-Mediated Yki Activation in Drosophila, Curr Biol 28(11) (2018) 1756-1767.e6.
[373] J.R. Tse, A.J. Engler, Preparation of hydrogel substrates with tunable mechanical properties, Current protocols in cell biology Chapter 10 (2010) Unit 10.16.
[374] C. Hajal, G.S. Offeddu, Y. Shin, S. Zhang, O. Morozova, D. Hickman, C.G. Knutson, R.D. Kamm, Engineered human blood–brain barrier microfluidic model for vascular permeability analyses, Nature Protocols 17(1) (2022) 95-128.
[375] F. Polleux, A. Ghosh, The slice overlay assay: a versatile tool to study the influence of extracellular signals on neuronal development, Sci STKE 2002(136) (2002) pl9.
[376] V. Panzetta, S. Fusco, P.A. Netti, Cell mechanosensing is regulated by substrate strain energy rather than stiffness, Proc Natl Acad Sci U S A 116(44) (2019) 22004-22013.
[377] S. Taniguchi, A. Elhance, A. Van Duzer, S. Kumar, J.J. Leitenberger, N. Oshimori, Tumor-initiating cells establish an IL-33-TGF-β niche signaling loop to promote cancer progression, Science 369(6501) (2020).
[378] D. Bumann, R.H. Valdivia, Identification of host-induced pathogen genes by differential fluorescence induction reporter systems, Nat Protoc 2(4) (2007) 770-777.
[379] U. Kamensek, G. Sersa, M. Cemazar, Evaluation of p21 promoter for interleukin 12 radiation induced transcriptional targeting in a mouse tumor model, Mol Cancer 12(1) (2013) 136.
[380] L. He, R. Binari, J. Huang, J. Falo-Sanjuan, N. Perrimon, In vivo study of gene expression with an enhanced dual-color fluorescent transcriptional timer, Elife 8 (2019).
[381] A.W. Watson, A.D. Grant, S.S. Parker, S. Hill, M.B. Whalen, J. Chakrabarti, M.W. Harman, M.R. Roman, B.L. Forte, C.C. Gowan, R. Castro-Portuguez, L.K. Stolze, C. Franck, D.A. Cusanovich, Y. Zavros, M. Padi, C.E. Romanoski, G. Mouneimne, Breast tumor stiffness instructs bone metastasis via maintenance of mechanical conditioning, Cell reports 35(13) (2021) 109293.
[382] P. Bardou, J. Mariette, F. Escudié, C. Djemiel, C. Klopp, jvenn: an interactive Venn diagram viewer, BMC bioinformatics 15(1) (2014) 293.
[383] J. Fares, E. Petrosyan, D. Kanojia, C. Dmello, A. Cordero, J.T. Duffy, R. Yeeravalli, M.H. Sahani, P. Zhang, A. Rashidi, V.A. Arrieta, I. Ulasov, A.U. Ahmed, J. Miska, I.V. Balyasnikova, C.D. James, A.M. Sonabend, A.B. Heimberger, M.S. Lesniak, Metixene is an incomplete autophagy inducer in preclinical models of metastatic cancer and brain metastases, The Journal of clinical investigation (2023).
[384] Y. Zou, A. Watters, N. Cheng, C.E. Perry, K. Xu, G.M. Alicea, J.L.D. Parris, E. Baraban, P. Ray, A. Nayak, X. Xu, M. Herlyn, M.E. Murphy, A.T. Weeraratna, Z.T. Schug, Q. Chen, Polyunsaturated Fatty Acids from Astrocytes Activate PPARγ Signaling in Cancer Cells to Promote Brain Metastasis, Cancer Discov 9(12) (2019) 1720-1735.

[385] P. Romani, L. Valcarcel-Jimenez, C. Frezza, S. Dupont, Crosstalk between mechanotransduction and metabolism, Nat Rev Mol Cell Biol 22(1) (2021) 22-38.
[386] K. Onwudiwe, A.A. Burchett, M. Datta, Mechanical and metabolic interplay in the brain metastatic microenvironment, Front Oncol 12 (2022) 932285.
[387] E.S. Villodre, X. Hu, B.L. Eckhardt, R. Larson, L. Huo, E.C. Yoon, Y. Gong, J. Song, S. Liu, N.T. Ueno, S. Krishnamurthy, S. Pusch, D. Tripathy, W.A. Woodward, B.G. Debeb, NDRG1 in Aggressive Breast Cancer Progression and Brain Metastasis, Journal of the National Cancer Institute 114(4) (2022) 579-591.
[388] E.S. Villodre, Y. Gong, X. Hu, L. Huo, E.C. Yoon, N.T. Ueno, W.A. Woodward, D. Tripathy, J. Song, B.G. Debeb, NDRG1 Expression Is an Independent Prognostic Factor in Inflammatory Breast Cancer, Cancers (Basel) 12(12) (2020).
[389] C.J. Sevinsky, F. Khan, L. Kokabee, A. Darehshouri, K.R. Maddipati, D.S. Conklin, NDRG1 regulates neutral lipid metabolism in breast cancer cells, Breast Cancer Res 20(1) (2018) 55.
[390] E.S. Villodre, X. Hu, R. Larson, B.L. Eckhardt, Y. Gong, L. Huo, J. Song, S. Krishnamurthy, N. Ibrahim, N.T. Ueno, D. Tripathy, W.A. Woodward, B.G. Debeb, Abstract P3-01-10: Ndrg1-egfr axis in inflammatory breast cancer tumorigenesis and brain metastasis, Cancer research 80(4_Supplement) (2020) P3-01-10-P3-01-10.
[391] E.S. Villodre, X. Hu, B.L. Eckhardt, R. Larson, L. Huo, E.C. Yoon, Y. Gong, J. Song, S. Liu, N.T. Ueno, S. Krishnamurthy, S. Pusch, D. Tripathy, W.A. Woodward, B.G. Debeb, NDRG1 in Aggressive Breast Cancer Progression and Brain Metastasis, J Natl Cancer Inst 114(4) (2022) 579-591.
[392] C. Yang, M.W. Tibbitt, L. Basta, K.S. Anseth, Mechanical memory and dosing influence stem cell fate, Nat Mater 13(6) (2014) 645-52.
[393] M. Gupta, B.R. Sarangi, J. Deschamps, Y. Nematbakhsh, A. Callan-Jones, F. Margadant, R.-M. Mège, C.T. Lim, R. Voituriez, B. Ladoux, Adaptive rheology and ordering of cell cytoskeleton govern matrix rigidity sensing, Nat Commun 6 (2015) 7525.
[394] B.L. Doss, M. Pan, M. Gupta, G. Grenci, R.-M. Mège, C.T. Lim, M.P. Sheetz, R. Voituriez, B. Ladoux, Cell response to substrate rigidity is regulated by active and passive cytoskeletal stress, Proc Natl Acad Sci U S A 117(23) (2020) 12817-12825.
[395] E. Moreno, L. Valon, F. Levillayer, R. Levayer, Competition for Space Induces Cell Elimination through Compaction-Driven ERK Downregulation, Current Biology : CB 29(1) (2019).
[396] H. Li, X. Shen, M. Ma, W. Liu, W. Yang, P. Wang, Z. Cai, R. Mi, Y. Lu, J. Zhuang, Y. Jiang, Y. Song, Y. Wu, H. Shen, ZIP10 drives osteosarcoma proliferation and chemoresistance through ITGA10-mediated activation of the PI3K/AKT pathway, Journal of experimental & clinical cancer research : CR 40(1) (2021) 340.
[397] T. Okada, A.Y. Lee, L.X. Qin, N. Agaram, T. Mimae, Y. Shen, R. O'Connor, M.A. López-Lago, A. Craig, M.L. Miller, P. Agius, E. Molinelli, N.D. Socci, A.M. Crago, F. Shima, C. Sander, S. Singer, Integrin-α10 Dependency Identifies RAC and RICTOR as Therapeutic Targets in High-Grade Myxofibrosarcoma, Cancer discovery 6(10) (2016) 1148-1165.
[398] W. Tong, J. Li, X. Feng, C. Wang, Y. Xu, C. He, W. Xu, Kaiso regulates osteoblast differentiation and mineralization via the Itga10/PI3K/AKT signaling pathway, International journal of molecular medicine 47(4) (2021).
[399] Y. Song, Z. Meng, S. Zhang, N. Li, W. Hu, H. Li, miR-4739/ITGA10/PI3K signaling regulates differentiation and apoptosis of osteoblast, Regenerative therapy 21 (2022) 342-350.
[400] J. Kempska, L. Oliveira-Ferrer, A. Grottke, M. Qi, M. Alawi, F. Meyer, K. Borgmann, F. Hamester,

K. Eylmann, M. Rossberg, D.J. Smit, M. Jücker, E. Laakmann, I. Witzel, B. Schmalfeldt, V. Müller, K. Legler, Impact of AKT1 on cell invasion and radiosensitivity in a triple negative breast cancer cell line developing brain metastasis, Frontiers in oncology 13 (2023) 1129682.
[401] B. Adamo, A.M. Deal, E. Burrows, J. Geradts, E. Hamilton, K.L. Blackwell, C. Livasy, K. Fritchie, A. Prat, J.C. Harrell, M.G. Ewend, L.A. Carey, C.R. Miller, C.K. Anders, Phosphatidylinositol 3-kinase pathway activation in breast cancer brain metastases, Breast cancer research : BCR 13(6) (2011) R125.
[402] P.F. Peddi, S.A. Hurvitz, PI3K pathway inhibitors for the treatment of brain metastases with a focus on HER2+ breast cancer, Journal of neuro-oncology 117(1) (2014) 7-13.
[403] F. Batalini, S.L. Moulder, E.P. Winer, H.S. Rugo, N.U. Lin, G.M. Wulf, Response of Brain Metastases From PIK3CA-Mutant Breast Cancer to Alpelisib, JCO precision oncology 4 (2020).
[404] F.M. Ippen, J.K. Grosch, M. Subramanian, B.M. Kuter, B.M. Liederer, E.G. Plise, J.L. Mora, N. Nayyar, S.P. Schmidt, A. Giobbie-Hurder, M. Martinez-Lage, S.L. Carter, D.P. Cahill, H. Wakimoto, P.K. Brastianos, Targeting the PI3K/Akt/mTOR pathway with the pan-Akt inhibitor GDC-0068 in PIK3CA-mutant breast cancer brain metastases, Neuro-oncology 21(11) (2019) 1401-1411.
[405] Y. Zhang, L. Sun, H. Li, L. Ai, Q. Ma, X. Qiao, J. Yang, H. Zhang, X. Ou, Y. Wang, G. Chen, J. Xue, X. Zhu, Y. Zhao, Y. Yang, C. Liu, Binding blockade between TLN1 and integrin β1 represses triple-negative breast cancer, eLife 11 (2022).
[406] N. Thapa, X. Tan, S. Choi, T. Wise, R.A. Anderson, PIPKIγ and talin couple phosphoinositide and adhesion signaling to control the epithelial to mesenchymal transition, Oncogene 36(7) (2017) 899-911.
[407] D.J. Kloosterman, J. Erbani, M. Boon, M. Farber, S.M. Handgraaf, M. Ando-Kuri, E. Sánchez-López, B. Fontein, M. Mertz, M. Nieuwland, N.Q. Liu, G. Forn-Cuni, N.N. van der Wel, A.E. Grootemaat, L. Reinalda, S.I. van Kasteren, E. de Wit, B. Ruffell, E. Snaar-Jagalska, K. Petrecca, D. Brandsma, A. Kros, M. Giera, L. Akkari, Macrophage-mediated myelin recycling fuels brain cancer malignancy, Cell 187(19) (2024) 5336-5356.e30.
[408] F. Geng, D. Guo, SREBF1/SREBP-1 concurrently regulates lipid synthesis and lipophagy to maintain lipid homeostasis and tumor growth, Autophagy 20(5) (2024) 1183-1185.
[409] Y. Li, X. Huang, G. Yang, K. Xu, Y. Yin, G. Brecchia, J. Yin, CD36 favours fat sensing and transport to govern lipid metabolism, Prog Lipid Res 88 (2022) 101193.
[410] B.A. Krajina, B.L. LeSavage, J.G. Roth, A.W. Zhu, P.C. Cai, A.J. Spakowitz, S.C. Heilshorn, Microrheology reveals simultaneous cell-mediated matrix stiffening and fluidization that underlie breast cancer invasion, Sci Adv 7(8) (2021).
[411] H.D. Nguyen, C.C. Lin, Viscoelastic stiffening of gelatin hydrogels for dynamic culture of pancreatic cancer spheroids, Acta Biomater 177 (2024) 203-215.
[412] F. Calvo, N. Ege, A. Grande-Garcia, S. Hooper, R.P. Jenkins, S.I. Chaudhry, K. Harrington, P. Williamson, E. Moeendarbary, G. Charras, E. Sahai, Mechanotransduction and YAP-dependent matrix remodelling is required for the generation and maintenance of cancer-associated fibroblasts, Nature cell biology 15(6) (2013) 637-46.
[413] N. Saxena, S. Chakraborty, S. Dutta, G. Bhardwaj, N. Karnik, O. Shetty, S. Jadhav, H. Zafar, S. Sen, Stiffness-dependent MSC homing and differentiation into CAFs - implications for breast cancer invasion, J Cell Sci 137(1) (2024).
[414] S. Ishihara, D.R. Inman, W.J. Li, S.M. Ponik, P.J. Keely, Mechano-Signal Transduction in Mesenchymal Stem Cells Induces Prosaposin Secretion to Drive the Proliferation of Breast Cancer Cells, Cancer research 77(22) (2017) 6179-6189.
[415] E. Sahai, I. Astsaturov, E. Cukierman, D.G. DeNardo, M. Egeblad, R.M. Evans, D. Fearon, F.R.

Greten, S.R. Hingorani, T. Hunter, R.O. Hynes, R.K. Jain, T. Janowitz, C. Jorgensen, A.C. Kimmelman, M.G. Kolonin, R.G. Maki, R.S. Powers, E. Puré, D.C. Ramirez, R. Scherz-Shouval, M.H. Sherman, S. Stewart, T.D. Tlsty, D.A. Tuveson, F.M. Watt, V. Weaver, A.T. Weeraratna, Z. Werb, A framework for advancing our understanding of cancer-associated fibroblasts, Nature reviews. Cancer 20(3) (2020) 174-186.

[416] Y. Jiao, Y. Yu, M. Zheng, M. Yan, J. Wang, Y. Zhang, S. Zhang, Dormant cancer cells and polyploid giant cancer cells: The roots of cancer recurrence and metastasis, Clin Transl Med 14(2) (2024) e1567.

[417] S. Zhang, I. Mercado-Uribe, Z. Xing, B. Sun, J. Kuang, J. Liu, Generation of cancer stem-like cells through the formation of polyploid giant cancer cells, Oncogene 33(1) (2014) 116-28.

[418] M. Fukumoto, T. Ijuin, T. Takenawa, PI(3,4)P(2) plays critical roles in the regulation of focal adhesion dynamics of MDA-MB-231 breast cancer cells, Cancer Sci 108(5) (2017) 941-951.

[419] M.C. Caino, J.C. Ghosh, Y.C. Chae, V. Vaira, D.B. Rivadeneira, A. Faversani, P. Rampini, A.V. Kossenkov, K.M. Aird, R. Zhang, M.R. Webster, A.T. Weeraratna, S. Bosari, L.R. Languino, D.C. Altieri, PI3K therapy reprograms mitochondrial trafficking to fuel tumor cell invasion, Proc Natl Acad Sci U S A 112(28) (2015) 8638-43.